Long-term Performance of Bonded Concrete Overlays Subjected to Differential Shrinkage

Hans-Dieter Beushausen

Thesis Presented for the Degree of
DOCTOR OF PHILOSOPHY
in the Department of Civil Engineering
UNIVERSITY OF CAPE TOWN

February, 2005

ABSTRACT

The performance of bonded concrete overlays relates mainly to the resistance against cracking and debonding. The associated failure mechanisms are largely a result of differential volume changes between substrate and overlay. The objective of this research was to develop analytical tools to facilitate the design of bonded overlays subjected to differential shrinkage.

The experimental programme included the identification of fundamental strain characteristics and bond strength development of composite members in relation to different interface textures and overlay materials. Existing analytical models for the prediction of strains and stresses in bonded overlays were evaluated. Results from the experimental work indicated that existing models, which are based on simple beam theory, are deficient in modelling overlay strains in a realistic manner. The degree of overlay restraint was found to depend far less on relative sectional dimensions of substrate and overlay as commonly assumed. Based on fundamental aspects concerning strain characteristics of bonded overlays identified through experimental tests and numerical simulations, an analytical prediction model was developed based on localised strain conditions at the interface.

The most important material parameters in respect to overlay crack resistance are overlay shrinkage, relaxation properties, elasticity, and tensile strength. Tests on composite specimens revealed that substrate creep is a major component in composite members subjected to differential shrinkage. These parameters were combined in the analytical model to allow prediction of time-dependent overlay stresses.

In fully bonded members, shear bond strength development was found to relate closely to mechanical overlay strength at the interface. Failure patterns and long-term bond strength development indicate that an interface transition zone exists, similarly to that between aggregates and cement paste. Long-term bond strength could be related to the combined influences of macro-mechanical interaction at the interface and overlay shrinkage. Changing environmental conditions were found to have no detrimental influence on interface shear strength.

Bond development depends on a large range of influences that are difficult to control in practice. It therefore appears appropriate to rely on prescriptive design recommendations for interface bond strength, considering substrate surface preparation, overlay materials and application methods. However, in terms of crack resistance, analytical modelling of shrinkage-induced stresses, taking into account the combined influences of various material parameters and the characteristics of the structural system, can greatly facilitate the design for long-term performance.

ACKNOWLEDGEMENTS

I would like to express my gratitude to the following individuals for their assistance in my research and preparation of this dissertation:

- My supervisor Professor M.G. Alexander for his guidance and commitment throughout this research
- Laboratory and workshop staff of the Department of Civil Engineering, especially Eike von Geurard, Charles Nicolas, and Charles May
- Rukshani Heiyantuduwa for continuous help in editing this dissertation
- Thomas Henke for his assistance in site experiments
- Allan Scott for various laboratory activities
- Students for their help in the preparation and testing of specimens during the last 4 years, especially Musikayise Masina, Sibusiso Mwandla, and Mafanelo Sibuyi
- Dr Stefan Mieth for advice and discussions
- And my family and friends for their continuous support and encouragement

TABLE OF CONTENTS

DEVELOPMENT OF AN ANALYTICAL MODEL

CLOSURE

APPENDICES

LIST OF FIGURES

LIST OF TABLES

NOTATION

$d_{O,\varepsilon,r}$	Length of restraint decay in the overlay
$d_{S,\varepsilon}$	Length of strain decay in the substrate
f_t	Concrete tensile strength
f_c	Concrete compressive strength
A	Cross-sectional area
E	Modulus of elasticity
E_{CC}	Modulus of elasticity in compression
RH	Relative humidity
α_T	Thermal coefficient of concrete
σ	Stress
σ^+	Tensile stress
σ^-	Compressive Stress
ε	Strain
$\varepsilon_{O,I}$	Overlay strains at the interface
$\varepsilon_{S,I}$	Substrate strains at the interface
ε_κ	Curvature strain
ε_{FSS}	Free Shrinkage Strain of the overlay
ε^-	Compressive strain
ε^+	Tensile strain
$\varepsilon_{O,I}$	Overlay strain at the interface
$\varepsilon_{O,r,I}$	Restrained overlay strain at the interface = $\varepsilon_{FSS} - \varepsilon_{O,I}$
$\varepsilon_{S,I}$	Substrate strain at the interface
$\varepsilon(d_O)$	Function describing strain pattern and strain values across the overlay depth
$\varepsilon(d_S)$	Function describing strain pattern and strain values across the substrate depth

ε_{creep}	Creep strain
$\varepsilon_{inst.}$	Instantaneous strain, i.e. initial strain before occurrence of visco-elastic effects
τ	Shear stress
φ	Creep function
$\psi(t, t_0)$	Coefficient expressing visco-elastic stress relaxation
$\Psi(t)$	Relaxation function describing the time dependent magnitude of the relaxation coefficient $\psi(t, t_0)$
ΔT	Temperature difference

Indices

C	Concrete
nr	Non-restrained
r	Restrained
t	Time
T	Temperature
O	Overlay
S	Substrate
I	Interface

"Whenever a theory appears to you as the only possible one, take this as a sign that you have neither understood the theory nor the problem which it was intended to solve"

Karl Popper (1902-1994)

CHAPTER 1

INTRODUCTION

1.1 Background and problem statement

For many decades concrete has been one of the most important construction materials for the building industry and for infrastructural projects. The understanding of concrete deterioration mechanisms however has developed at a much slower rate, resulting in a growing number of structures needing to be repaired. In addition, increasing traffic and higher design loads have created a demand to retrofit many existing bridges and roads in order to enlarge their structural capacity. The bonded overlay technique is particularly suitable for needs arising from the above and has been extensively used for repair, lining, and strengthening of concrete structures.

During previous experimental research as well as in practice, bonded concrete overlays have often experienced serious performance problems, which are mainly manifested in overlay cracking and/or debonding. These failure mechanisms are largely a result of differential volume changes between substrate and overlay. The overlay is subjected to shrinkage and thermal movements, while the substrates' deformations are usually completed or negligible. Overlay volume changes are caused at very early ages due to the effects of hydration heat development and plastic shrinkage. At later ages it is the effect of progressing overlay shrinkage that is of major concern for the performance of the composite member. Environmental temperature changes may add to the problem when substrate and overlay have different thermal properties or when the overlay itself experiences a significant temperature gradient through its depth. The restraint of overlay deformations causes direct stresses, bending stresses and interface shear stresses.

Cracking often occurs shortly after overlay placement and may during the first days be controlled by the application of curing techniques. However, depending on material characteristics and environmental influences, cracking might also occur at a later stage during the lifetime of the structure. A cracked overlay is visually not appealing and enables harmful substances to enter the concrete and cause further deterioration. Overlay debonding, which is

of even greater concern for the durability of composite members, commonly starts at free member ends, joints, and cracks and might lead to delamination and spalling and hence result in overlay failure.

The mechanisms of cracking and debonding are complex and mainly depend on material parameters, environmental influences, and the degree of restraint governed by the structural characteristics of the system. The most important overlay material parameters with respect to the above are tensile strength, elastic and visco-elastic properties, and volume changes caused by shrinkage. Development and magnitude of interface bond strength further greatly depend on substrate surface preparation and workmanship during overlay application.

Codes and standards governing bonded concrete overlays can be divided into design recommendations for concrete repair works, and structural design procedures for load-bearing overlays. For concrete repair works, no reliable design is available for the practitioner (Granju, 2004). Design recommendations are commonly very crude and often restricted to mechanical strength and substrate surface preparation methods. Decisions on important material parameters such as shrinkage and thermal properties is often left to the judgement of the design engineer. Visco-elastic material characteristics, which are important for the relaxation of stresses and therefore present a crucial indicator of overlay durability, are generally not covered at all.

The need for more practical design recommendations has been recognised by practitioners and researchers (Vaysburd et al, 2004, Granju, 2004). This resulted in the formation of the RILEM Technical Committee for "Bonded cement-based material overlays for the repair, the lining, and strengthening of slabs or pavements", which will present a state of art report during the year 2005, aiming for practical design procedures (Granju, 2004). Another weakness of existing design recommendations is that they do not cover new materials such as high-performance, self-compacting, and fibre reinforced concretes, which are increasingly gaining importance in the field of concrete repair. The use of these materials for rehabilitation and improvement of structures is currently being investigated in the project SAMARIS (Sustainable and Advanced MAterials for Road InfraStructures), which is steered by the European Community (Žnidaric et al, 2003). The above research efforts indicate the subject's significance for the modern construction industry.

Standards and codes for structural overlays allow the design of composite members as equivalent monolithic sections if sufficient shear strength is provided at the interface between substrate and overlay. Limiting values for design shear strengths of unreinforced interfaces commonly depend on substrate preparation and mechanical overlay strength. In respect of short-term bond strength, which has been widely explored in previous research projects, these limiting values are generally considered as conservative. However, the main reasons for such conservative values are the detrimental effects of overlay shrinkage, which are difficult to

assess and which may lead to bond deterioration with time. It is often pointed out in the literature that these effects have not yet been sufficiently researched.

It is crucial to understand that the performance of bonded overlays is a function not only of its material components but also of how the materials and the system as a whole respond to environmental influences. It therefore appears necessary to develop analytical procedures for the prediction of overlay durability with which overlays can be designed accounting for structural properties of the system, relevant environmental influences and material properties. To date, reliable analytical procedures are not available. A deeper fundamental understanding must therefore be developed for the structural behaviour of bonded concrete overlays, as well as for factors influencing long-term bond properties. The objectives of this research in respect to the above are outlined in the following section.

1.2 Thesis objectives and research strategy

The literature review revealed that differential shrinkage between substrate and overlay is commonly the most crucial aspect for the durability of composite members both in respect to bond strength and cracking resistance. Numerous research projects concerning short-term bond properties between concretes of different ages have been reported in the literature. The effects of long-term material characteristics and environmental influences on the performance of bonded overlays have however not been fully researched yet. Fundamental understanding of time-dependent volume changes in composite members is essential for the correct modelling of overlay stresses. Existing analytical models were found to focus mainly on theoretical background without necessarily relating to real composite behaviour encountered in the structure. Based on the above, the following three main objectives were identified for this research:

- Characterisation of bond mechanisms between substrate and overlay with consideration of short-term and long-term effects
- Identification of fundamental characteristics of overlay strain development
- Development of an analytical model which facilitates the design of bonded concrete overlays based on fundamental strain characteristics

Supported by experimental test results and theoretical background, this research aims for a better understanding of the mechanisms influencing the long-term performance of bonded concrete overlays. Experimental procedures and test parameters were chosen based on the literature review. Fundamental aspects concerning strain characteristics of composite members identified during the experimental programme were verified using the FEM method of analysis. With the above, an analytical model for bonded concrete overlays subjected to differential shrinkage was developed, based on localised restraint at the interface. This model was designed for the prediction of tensile overlay stress development and can be used as an

indicator for crack resistance. The modelling of interface shear stresses is not included in the analytical approach. For long-term bond properties, fundamental mechanisms were identified on an experimental basis.

From the above, recommendations for the design of bonded concrete overlays are given and the need for future research is identified. The strategy adopted for this research is schematically illustrated in **Figure 1.1**.

1.3 Outline of thesis document

From the literature review (Chapter 2), fundamental bond mechanisms and factors influencing bond properties between concretes of different ages are identified. Short- and long-term overlay volume changes and their influences on structural behaviour are discussed, focussing on the characteristics of thermal properties, shrinkage, creep, and relaxation. Existing analytical models for bonded overlays subjected to differential shrinkage are summarized and evaluated in Chapter 3. Based on the above, the need for further research is identified.

Strain characteristics of composite members are investigated using specimens consisting of substrate beams with various interface textures and different overlays (Chapter 4). The influences of mechanical restraint at the interface and overlay shrinkage values on strain development along the length and across the depth of the members are evaluated. Conclusions are drawn on the mechanisms of interface restraint and the characteristics of different strain components such as elastic strain, substrate creep, overlay relaxation, as well as the effects of curvature. Fundamental aspects concerning the mechanisms of overlay shrinkage restraint, as identified during the experimental research, are verified using numerical simulation on a simple FEM model (Chapter 5). Results from the experimental research and the numerical simulation challenge existing analytical models which are based on simple beam theory and which appear to be deficient in predicting actual strains and stresses in composite members on a rational basis.

The development of a new analytical model for overlay strains and stresses is discussed in Chapter 6, based on fundamental aspects concerning the restraint of overlay shrinkage identified in previous sections.

Chapter 7 comprises the development of suitable methods for the testing of parameters influencing long-term bond properties between substrate and overlay. Mechanisms of short-term bond strength development are identified. Long-term bond properties are assessed on specimens with different interface textures and overlay materials after approximately 2 years exposure to various curing regimes. For the evaluation of environmental influences, samples were stored on a number of sites in the Western Cape Province.

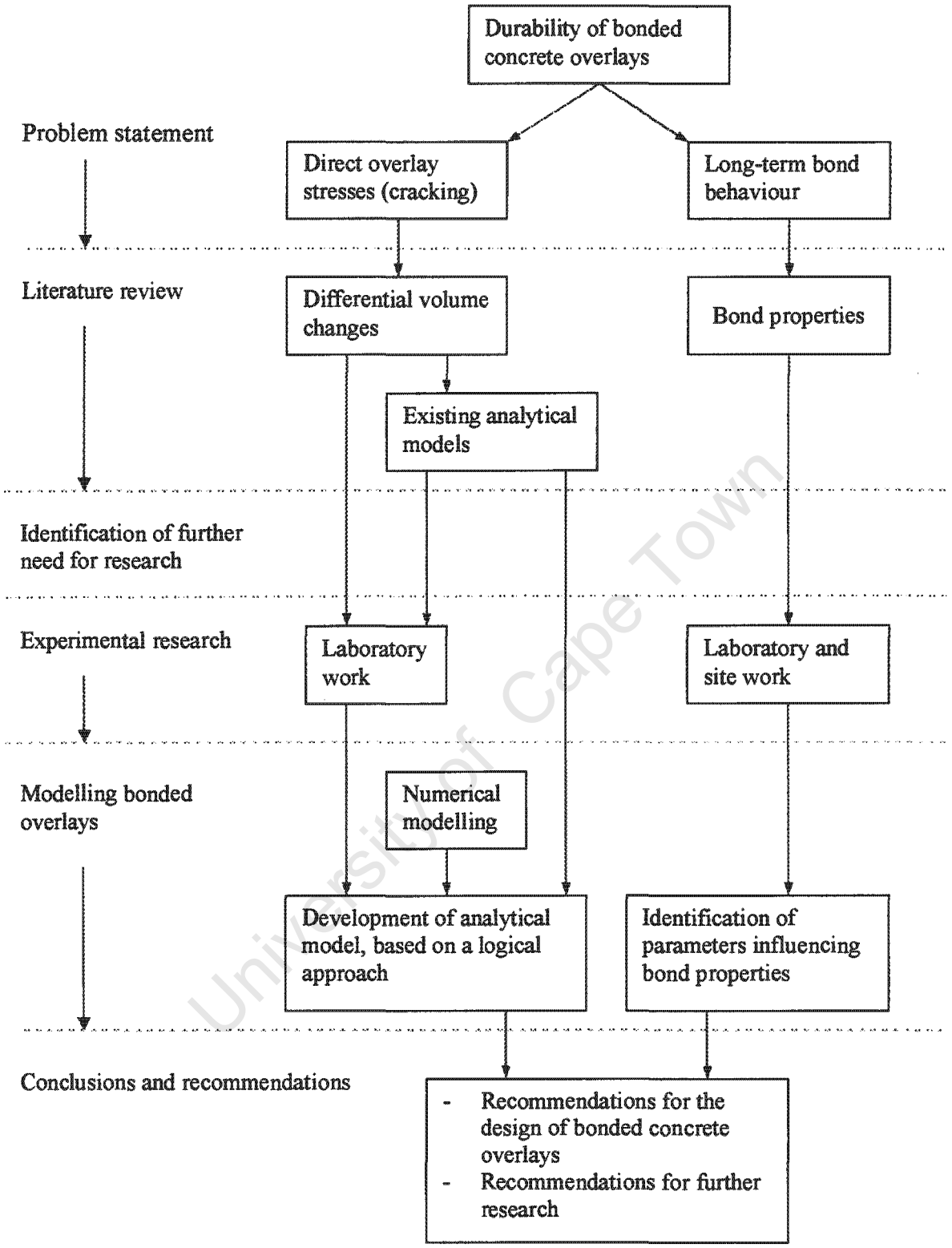

Figure 1.1: Schematic of thesis structure and research methodology

Conclusions on fundamental aspects concerning the durability of bonded concrete overlays subjected to differential shrinkage are summarized in Chapter 8. The applicability of the analytical model for the prediction of overlay strains and stresses is discussed. The need for

further research, especially in the fields of localised shrinkage restraint at the interface, overlay relaxation properties, and bond mechanisms in relation to the transition zone at the interface between substrate and overlay are identified.

1.4 Limitations

The scope of the topic "long-term performance of bonded concrete overlays" is large and not all relevant aspects could be dealt with. The focus of this research lies in the identification of fundamental mechanisms apparent in bonded overlays subjected to differential shrinkage and cracking behaviour and bond strength development resulting therefrom. For the experimental research, different interface textures and various overlay materials were used. However, conclusions drawn from the experimental work should be verified by further tests using a broad range of overlay and substrate materials.

The scope of experimental research was limited to cement-based overlays. Resin-based materials, as well as high-performance, self-compacting and fibre reinforced concretes were not examined.

Shrinkage in concrete is a three-dimensional process. For bonded overlays it is safe to consider shrinkage a 2-dimensional phenomenon, as overlay volume changes in direction perpendicular to the interface are unlikely to affect the performance of the member. However, to facilitate modelling of bonded overlays, shrinkage is commonly treated as a one-dimensional phenomenon, considering the longer axis of the member. This was adapted in this research both for strain measurements on composite specimens and for the development of an analytical model. Two-dimensional effects are not taken into account.

CHAPTER 2

ASPECTS OF THE LONG-TERM PERFORMANCE OF BONDED CONCRETE OVERLAYS

2.1 Introduction

Bonded concrete overlays are widely used for the repair and strengthening of concrete members. The primary purpose of overlays is the extension of the service life of the overlaid structure. This can principally be achieved by providing a protective and visually appealing layer to a damaged substrate, or by increasing the structural strength and stiffness of a structural concrete section. Granju (2004) has summarized further general functions of bonded overlaying slabs and pavements as follows:

- Increasing surface elevation to match an adjacent slab
- Replacement of deteriorated or contaminated concrete and renewed protection of the remaining element
- Provision of a more durable and wear-resistant surface
- Provision of an improved frictional resistance for pavements or bridges
- Provisions of architectural features such as colour or texture

Generally, overlays can be applied to horizontal and vertical substrate surfaces. Despite increasing use of bonded overlays for concrete repair and rehabilitation projects, failure of overlays is often observed in practice, manifesting itself mainly in overlay cracking and debonding. Possible reasons for such failures are numerous and include substrate surface preparation, choice and application of overlay materials, curing procedures, time-dependent material properties and environmental influences. The assessment of individual parameters on the durability of bonded concrete overlays is difficult. Standards and specifications for the design of bonded concrete overlays are generally considered as deficient in scope and detailing.

The mechanisms and characteristics of bond between old and new concretes in respect to various influences have been widely researched in the past decades. The number of ongoing research projects in the field however show that many questions still remain unresolved. In terms of the choice of substrate preparation methods, material parameters, and adequate test methods, opinions vary among individual researchers.

In general it is accepted that poor workmanship and differential shrinkage are the main detrimental influences for the performance of bonded concrete overlays both in terms of cracking resistance and bond strength. The mechanisms of shrinkage in concrete are generally well understood, as are the development of important material parameters like

elastic modulus and tensile strength. It is however often pointed out that knowledge on the important mechanisms of tensile relaxation is still insufficient.

In the following sections, the main aspects concerning the performance of bonded overlays are discussed and evaluated. Based on the literature review, the need for further research is identified. Only the aspects considered as most important are discussed: bond mechanisms, shrinkage and creep. These issues are discussed in relation to fundamental aspects and the more specific case of long-term performance of bonded concrete overlays. Other aspects that are important for design and performance of concrete overlays, e.g. mechanisms and causes of concrete deterioration, substrate condition survey, overlay materials and available repair mortars, repair techniques, and material parameters such as tensile strength and elastic properties, are not discussed in detail. Information on these can be found in the general literature. A good overview on these issues is provided by Granju (2004).

2.2 Design specifications for bonded overlays

Standards and specifications for bonded concrete overlays can basically be divided in design recommendations for concrete repair patches and structural design procedures for load-bearing bonded overlays.

In terms of design specifications for repair patches, the European and American standards can be considered as very limited (Granju, 2004). From all standards investigated in this research, the one proposed by the DAfStb (2001) was found to be the most detailed. It contains recommendations for substrate surface preparation, general rules for the application of repair materials, as well as limiting values for material strength, shrinkage, thermal coefficients and tensile bond strength. Details on the specifications given by DAfStb (2001) are summarized in **Appendix 1**. The minimum required bond strengths, which have to be obtained with pull-off tests, depend on the type of repair material and exposure conditions and range between 1.0 and 2.5 MPa. Shrinkage values are limited according to the repair class and repair material to up to 1200.10^{-6}. The lowest limiting shrinkage value given is 1000.10^{-6}. However, for non-structural surface repairs, no limit for shrinkage values is given. Limiting values for thermal coefficients are only presented for resin-based mortars on industrial floors with high wear resistance. For all other applications and materials, the appropriate thermal coefficient has to be "judged by the design engineer".

The above specifications are fully prescriptive, i.e. they cannot be used for the actual design of overlays for individual projects. Important materials such as high-strength overlays, self-compacting concretes, and fibre-reinforced materials are not covered. These new technologies however are increasingly gaining importance in the field of concrete repair (e.g. Turatsinze et al, 2003, Denarié et al, 2004, Granju et al, 2004).

The recommendations for limiting overlay shrinkage values and thermal coefficients can be considered very crude, which appears problematic especially considering that differential volume changes between substrate and overlay may have a significant influence on the performance of bonded overlays.

For structural applications of bonded overlays, codes commonly define limitations for design shear resistance at the interface between substrate and overlay. If composite members are designed with adequate interface shear strength, they can be modelled following the same procedures as those developed for monolithic members. The design interface shear strength commonly exists of three parts: the strength of adhesion, a term that is dependent on external compressive forces across the interface (accounting for shear friction mechanisms), and a term that is dependent on the amount of reinforcement crossing the interface. For the shear bond strength resulting from adhesion, the following values are given in selected codes:

- CEB-FIP MC 90 (1993): The design shear resistance equals 0.06 times the lower compressive strength of either substrate or overlay. Hence, for example, a 20 MPa overlay (on a higher strength substrate) has a design shear resistance of 1.2 MPa, if the substrate surface is "rough" or "indented".
- The draft Eurocode 2 (2001) states that the design shear resistance at the interface is proportional to the design tensile strength of the weakest concrete. The coefficient of proportionality is 0.45 for "rough" surfaces and 0.5 for "indented" surfaces. Hence, for example, an overlay with a design tensile strength of 1.5 MPa on a rough interface results in a design interface shear resistance is 0.68 MPa.
- The draft of the new DIN 1045-1 (2001) defines design interface shear resistance in terms of interface texture and compressive overlay strength. For example, a 25 MPa overlay on a "rough" surface has a design interface shear strength of 0.58 MPa.
- American code ACI 318-99 (1999): 0.55 MPa for clean surfaces, free of laitance and "intentionally roughened"

In general, design interface shear strength values of the above magnitudes can be considered conservative. Short-term shear bond strength much higher than the above magnitudes is relatively easy to obtain. The main reason for such conservative design values is that the development of long-term material properties such as differential shrinkage might cause considerable bond deterioration with time.

From the above it can be concluded that standards and specifications for concrete repair are rather limited and do not present adequate design aids for bonded concrete overlays. As far as overlay shrinkage is concerned, design recommendations for concrete repair are relatively generous as they hardly present any restrictions to shrinkage values. By contrast, design specifications for structural overlays appear to be conservative, which shows the need for a deeper understanding of the mechanisms of differential shrinkage in composite members.

2.3 Bond properties between substrate and overlay

2.3.1 Introduction

The long-term performance of bonded concrete overlays can be mainly linked to the resistance against cracking and debonding. As discussed in Section 2.2, the scope of existing specifications for bonded overlays is limited. This is mainly due to the need of further understanding of long-term performance under varying environmental influences. A large number of research projects have been documented in the literature, discussing aspects of bond properties in terms of material parameters, interface textures and substrate surface conditions, curing procedures, and environmental influences. However, despite the relatively large pool of theoretical and practical knowledge, overlay debonding is still occasionally observed in actual structures, which explains why existing specifications for structural overlays are fairly conservative in assigning bond strength to unreinforced interfaces.

The objective of this research is to identify fundamental influences on long-term performance of bonded overlays both in terms of crack resistance and bond durability. The main focus lies on the mechanisms of differential shrinkage between substrate and overlay, for which an analytical model is developed, as discussed in Chapter 6. The influence of differential shrinkage on bond strength was tested, as discussed in Chapter 7. The following sections comprise a discussion on fundamental bond mechanisms, the influences of material parameters and environmental conditions on bond properties, and a critical assessment of available bond strength test methods. Based on the above, the need for further research is identified.

2.3.2 Definition and classification

The characteristics of adhesion, or "bond", can be perceived from two different angles (Courard, 1999): firstly, the conditions and kinetics of joining two materials, taking into account different bond mechanisms; secondly, the quantitative measure of the magnitude of adhesion, usually expressed in terms of stress or energy required to separate the two materials. Available information on overlay bond strength commonly refers to the stress required to separate substrate and overlay.

The term "adhesion" describes the condition in the boundary layer between two connecting materials with a common interface. Adhesion mechanisms can be divided basically into mechanical interaction, thermo-dynamic mechanisms, and chemical bonding (Fiebrich 1994).

Mechanical adhesion in repaired concrete members relies on the hardening of the overlay inside the open cavities and asperities of the substrate surface and the physical anchorage resulting therefrom. Capillary absorption plays an important role in the anchorage effect as it

draws overlay paste into small cavities of the substrate. It is dependent on the substrate surface moisture condition. The influences of substrate surface texture and moisture condition on mechanical bond strength are discussed in Section 2.3.4.2.

Mechanical bond may be assisted by contact friction between substrate and overlay in areas where the actual adhesion has been destroyed. This is described by shear friction models as discussed in the literature (e.g. Reinhardt and Walraven, 1982, Walraven et al, 1987, Tassios and Vintzeleou, 1987, Walraven, 1993). Shear friction is an important mechanism especially for interfaces that contain reinforcement and/or are subjected to compressive stress. However, this research focuses on unreinforced interfaces that are not subjected to significant compressive stress. Shear friction is therefore of minor importance in the scope of this research and will not be discussed.

It is important to note that mechanical adhesion in tension differs significantly from that in shear. For example, a high interface roughness may improve shear bond strength, whereas tensile mechanical bond strength primarily depends on vertical anchorage in pores and voids (**Figure 2.1**).

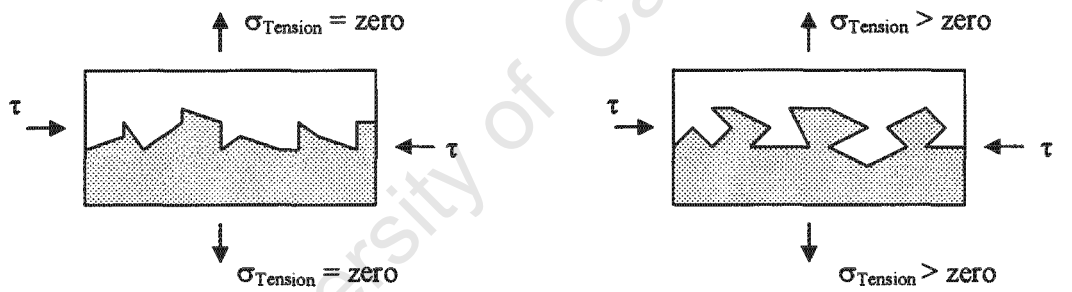

Figure 2.1: Schematics of mechanical shear and tensile bond between substrate and overlay, resulting from interlock mechanisms

The above is important for the correct choice of bond strength test methods for given test parameters. Differential volume changes between substrate and overlay resulting from temperature gradients or overlay shrinkage cause both shear and tensile stresses at the interface. In structural design, tensile stresses perpendicular to the interface are rare. By contrast, interface shear stresses occur frequently in composite elements, e.g. those caused in composite slabs subjected to bending stresses. Standards and specifications for concrete repair define bond strength commonly in relation to tensile strength alone, which, with consideration of the above, appears problematic. Different bond strength test methods are discussed in Section 2.3.3.

All bond mechanisms act on the true surface area, as opposed to the geometric surface area, and the contact surface area, also termed effective surface area (**Figure 2.2**).

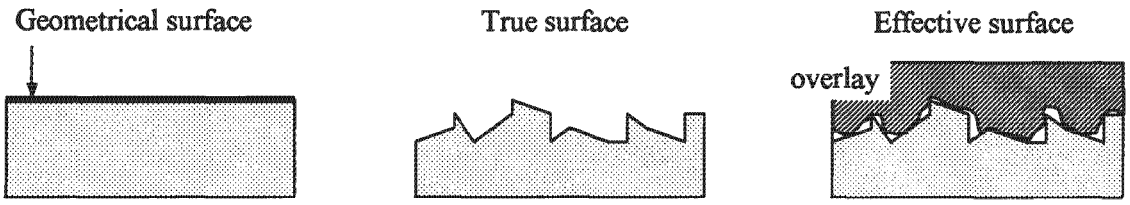

Figure 2.2: Geometrical, true, and effective surface areas between substrate and overlay

A higher degree of roughness increases the true surface area. The effective surface describes the actual covered area and depends to a great extent on the consistency, compaction and thermo-dynamic properties of the fresh concrete overlay. The influences of overlay workability on bond strength are discussed in Section 2.3.4.1. For quantification of bond strength, the failure load is usually divided by the geometric surface area.

Physical adhesion mechanisms on a molecular scale refer to the sub-microscopic interface roughness in the scale of a few nm (**Figure 2.3**), whereas microscopic, technically measurable roughness lies in the scale of μm (Fiebrich, 1994). Bond mechanisms on a microscopic scale are important for the correct modelling of interface shear stresses resulting from differential shrinkage, which is discussed in detail in Chapter 6.

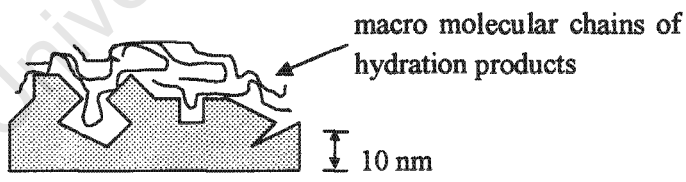

Figure 2.3: Adhesion on a sub microscopic level (Fiebrich, 1994)

Courard (1999 and 2000) described thermo-dynamic mechanisms of adhesion with respect to the relation between contact angle and free energies of liquid and solids (**Figure 2.4**). A lower contact angle θ between the wet overlay and substrate results in better interface contact and adhesion. The contact angle θ depends on the surface energy of both solid substrate and wet overlay. A detailed discussion of thermo-dynamic mechanisms between fluids and solid bodies can be found in (Fiebrich, 1994).

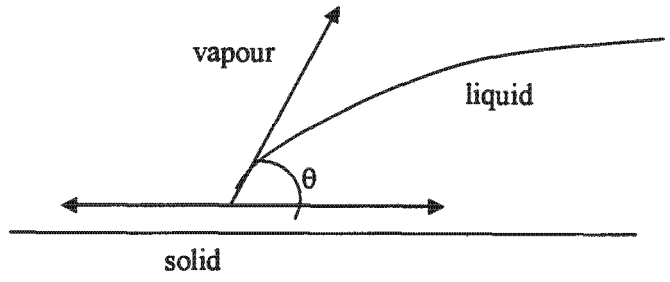

Figure 2.4: Wetting of a solid surface by a liquid (Courard, 2000)

Thermo-dynamic and chemical effects have to date hardly been applied in bond strength characterisation between concrete substrate and overlay. Research on specific bond behaviour of concrete repairs is normally restricted to the testing of adhesion strength. From that, conclusions are commonly drawn on mechanical bond mechanisms.

Pigeon and Saucier (1992) state that the interface between old and new concrete is very similar to bond between aggregates and cement paste. According to their research, a wall effect exists between overlay and substrate, resulting in a transition zone that creates a layer of weakness (**Figure 2.5**).

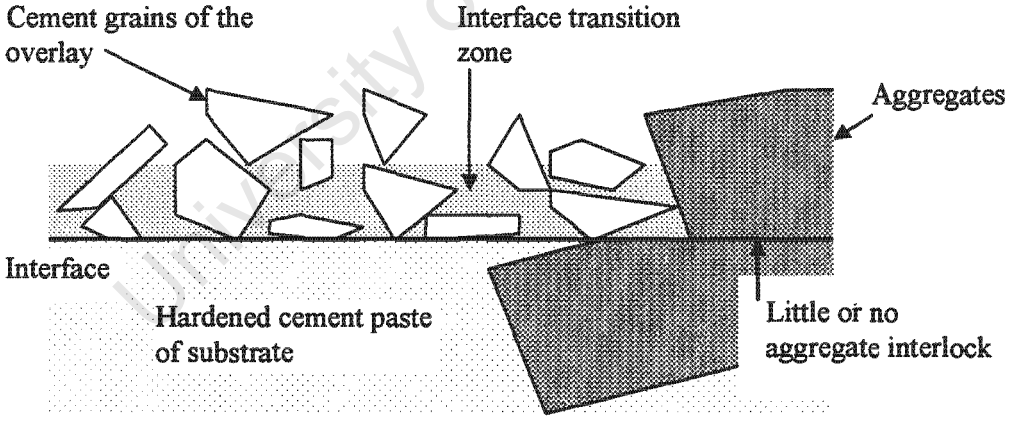

Figure 2.5: Transition zone between substrate and overlay, according to Pigeon and Saucier (1992)

Van Mier (1997) has summarized existing knowledge on interfaces between aggregates and cement matrix. The bond mechanisms between aggregate and cement paste depend largely on the porosity of the aggregate. Generally a thin layer of CH forms at the physical boundary between aggregate and cement matrix, followed by a relatively open layer containing oriented CH crystals, ettringite, and CSH. This so-called contact or transition layer has a very high porosity. Van Mier explains this high porosity with absorption of mixing water at the

surface of aggregate particles, which increases the effective w/c ratio. According to his research, fracture surfaces generally exist not directly at the physical boundary between aggregate and matrix but rather slightly removed from the interface in the porous transition zone. These mechanisms have not yet fully been investigated in relation to interface between concretes of different ages but may be useful for the characterisation of fundamental bond properties in composite members. Misra et al (2001) found a relation between air permeability at the interface and bond strength, which could be linked to the effects described above.

The effects of an interfacial transition zone in bonded overlays is considered important as bond is generally described as "interface" bond strength. During the experimental work of this research it was however revealed that bond failure between substrate and overlay hardly ever failed at the interface as such but commonly in the overlay very close to the interface. These observations are discussed in detail in Chapter 7. The definition of interface bond strength should therefore not concentrate on interface properties alone but also on overlay material characteristics close to the interface.

2.3.3 Bond test methods

The results of interface bond tests depend to a large extent on the test method used, which is often not considered in the interpretation of bond strength measurements. Common bond test methods include interface shear, torsion, and tension tests and a wide range of possible test set-ups have been developed for laboratory testing. Interface shear strength values obtained by different test methods may differ substantially as test results depend on specimen size, test set-up, loading rate, etc. Li et al (1999) investigated the size effect in bond tests and concluded that smaller specimen sizes led to larger bond strength in prism splitting tests. A comparison of test results obtained with different test methods, or even results obtained by different researchers using the same test method, therefore is problematic.

Relating interface shear and tension tests is questionable as both bond mechanisms have substantially different characteristics (compare Section 2.3.2). However, Silfwerbrand (2003) and Delatte et al (2000, a) indicated a correlation between the two test methods. The latter measured a mean ratio (shear bond divided by tension bond) of 2.0. Silfwerbrand found a ratio between torsional shear bond strength and tensile pull-off strength in the range 2 to 3.

An objective approach to prediction of overlay resistance performance based on bond strength tests should entail designing and using a test which causes a single stress type in the failure plane and uniform stress distribution. Once the objective quantification of shear and tensile resistances respectively has been done, the most likely actions which will test the overlay can be studied. Schematics of existing test methods for the evaluation of interface bond strength between concretes of different ages are illustrated in **Figures 2.6**.

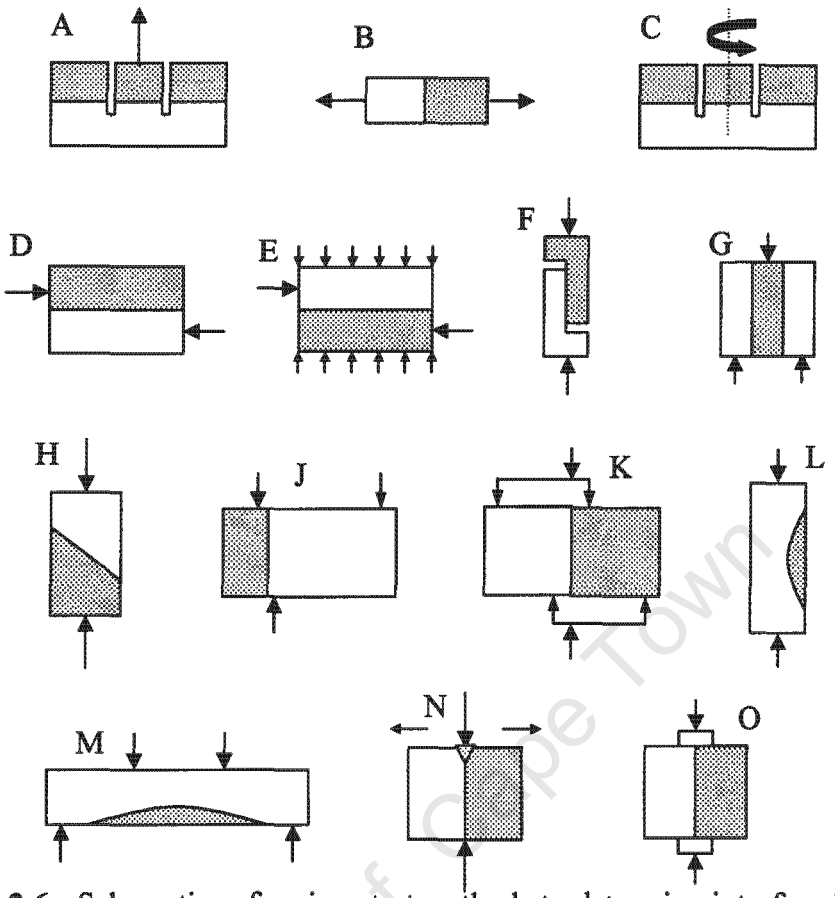

Figures 2.6: Schematics of various test methods to determine interface bond strength between concretes of different ages

In a direct tension test, the specimen is pulled apart by loads applied perpendicular to the bonded interface. The most common test method is the pull-off test, which can be carried out in-situ (Figure 2.6 A) and in the laboratory (Figure 2.6 B). The pull-off test encounters several problems as the test results may be strongly influenced by eccentricity in the load application and damage during coring (Delatte et al 2000, b). Results of pull-off measurements often show a large scatter of results, which makes it difficult to interpret the measurements in relation to the actual test parameter (Vaysburd and McDonald, 1999, USDT, 2000).

Interface pull-off strength is hard to quantify on properly placed overlays, yet easy to quantify in cases where the tensile interface strength is less than the tensile material strength. The results of pull-off tests, therefore, often only give indication of the lower bound of the interface bond strength. The main stress situation at the interface between substrate and overlay is that of a mixed mode of tension and shear, which is discussed in more detail in Section 2.4.1, and bond characterisation by tensile strength alone seems problematic. However, the pull-off test is the only method commonly applied in the testing of bond strength on real structures. Standards and Specifications, as discussed in Section 2.2,

therefore specify bond strength of concrete repairs as tensile bond. RILEM TC 177-MDT (2004) recommended the pull-off test for adhesion bond strength and specified loading rates in relation to the expected adhesive strength. Weber (1971) indicates the usefulness of pull-off bond tests at locations where tensile interface stresses are predominant, for example at the boundaries of a repaired member.

Silfwerbrand (2002) developed an in-situ test for torsional bond strength, which can be equated to interface shear strength (Figure 2.6 C). Common shear bond tests apply a force parallel to the interface (Figure 2.6 D). Pigeon et al (1992) (Figure 2.6 E) and El-Rakib et al (2003) (Figure 2.6 F) used modified shear bond methods. The push-out specimen (Chen et al, 1995, Larralde et al, 2001, Momayez et al, 2004) (Figure 2.6 G) has the disadvantage of having 2 interfaces, which does not represent site conditions and makes the test very impractical. The slant shear test (BS 6319, 1984) (Figure 2.6 H), used by Mainz and Zilch (2002) and Climaco and Regan (2001), measures bond strength under a combination of shear and compression. Several researchers (Emberson and Mays 1990, Austin et al, 1999, Delatte et al 2000 a) indicated shortcomings of this test in respect to unrealistic loading conditions and the vast number of parameters that may affect the test results. The guillotine test (Figure 2.6 J) can be used both on cores and prisms. Delatte et al (2000 a), however, reported difficulties with the alignment of the loading head for use on cores.

The disadvantage of most common shear test methods is the occurrence of an interface bending moment due to force eccentricity. The FIP (1978) developed a test method for interface shear strength, in which the interface is theoretically subjected to pure shear forces (Figure 2.6.K). Robins and Austin (1995) developed different patch tests, which measure interface shear and tensile bond strength under structural loading (Figures 2.2.7 L and M). The wedge splitting test device (Tschegg et al, 2000) characterises bond by fracture mechanical parameters such as crack opening and specific fracture energy, and tensile interface strength in bending (Figure 2.6 N). Li et al (1999) measured interface tensile strength with a prism splitting test device (Figure 2.6 O).

In cases where destructive in-situ bond testing is not appropriate, chain dragging or tapping the surface with a hammer may be used to determine locations of debonding (Carter et al, 2002). Lacombe et al (1999) analysed bond characteristics of different repair materials visually and by a scanning electron microscope. They evaluated the quality of the bond by observation of overlay compaction, cracks and voids at the interface. Cao and Chung (2001) estimated bond strength under cyclic loading by measuring the contact electrical resistance between old and new mortar. With this method, bond degradation could be observed without having to fail the specimen, i.e. without separating substrate and overlay.

As can be seen from the above, test methods for interface bond strength are numerous which highlights the problematic in comparing test results obtained from different researchers. Test values for interface bond strength obtained by different researchers are therefore not

discussed. The influences of material parameters and environmental influences on bond strength are discussed in the following sections, focusing on fundamental characteristics rather than bond strength values.

When evaluating bond strength values it is important to consider the dominant interface stress condition caused by the respective method, which may or may not represent the main stress condition encountered in the actual structure under investigation.

2.3.4 Factors influencing bond strength

2.3.4.1 Repair material properties

Fresh material properties

The fresh repair material properties are important both for early age bond strength development and bond durability. Workability and compaction of the freshly placed overlay influence the ability to fill open cavities and voids on the substrate concrete surface and therefore determine the effective contact area between the two composites (compare Figure 2.2). A relatively fluid overlay further enhances capillary suction in the substrate and therefore improves physical anchorage in substrate surface pores and cavities. Horizontal repairs, for example on pavements or bridge decks, and large application areas on vertical and overhead surfaces may be carried out with concrete of high fluidity. Self-levelling mortar applied for overhead repair using formwork was found to have very good bond properties in terms of its ability to fill cavities at the interface (Lacombe et al, 1999). The fact that good anchorage can be achieved without the effects of gravity implies that capillary suction of the old concrete plays an important role in bonding mechanisms.

By contrast to the above, small repair patches are commonly made with premixed, relatively stiff mortars, which are applied with a trowel. This leads to a smaller contact area between substrate and overlay and lower capillary suction of the substrate, compared to overlays of higher fluidity, thus resulting in lower mechanical and chemical bond strength. For these kinds of mortars, bonding agents might be helpful to improve adhesion. The use of bonding agents is discussed in more detail in Section 2.3.4.3.

Shotcrete, which is economical only for very large repair areas, is applied to the concrete substrate utilizing a high amount of energy. The mixture of fine aggregate and paste is pressed into the open pores and surface texture of the substrate. Following layers add on to this base layer with the coarse aggregate being embedded in the initial thin layer of mortar. Lacombe et al (1999) used a microscope to visually assess the interface between shotcrete and old concrete. The quality of bond appeared so be so good that is was almost impossible to see the difference in microstructure between shotcrete and old concrete. Bond properties

between substrate and shotcrete may depend on the nature of the shotcrete and, most importantly, on workmanship. Talbot et al (1994) performed bond tests on specimens repaired with different types of shotcrete and concluded that mix composition, such as wet or dry shotcrete, has little influence on bond durability.

The above indicates that overlay workability plays an important role for bond strength. However, even with relatively stiff overlays, good bond can be achieved if the overlay is applied with sufficient pressure and workmanship is good.

Hardened material properties

The hardened overlay material property directly influencing bond is the mechanical strength. Of equal importance are material parameters that influence the development of stresses in the overlay and at the interface, such as elastic modulus, shrinkage, thermal coefficient, permeability, additions like fibre reinforcement and admixtures, etc. The combined influence of different material parameters on bond strength is generally difficult to assess. Research has therefore commonly been carried out on the influences of individual material properties on bond strength and bond durability.

The significance of overlay mechanical strength is immediately revealed when the characteristics of the interface transition zone are considered, as discussed in Section 2.3.2. The location of "bond failure", i.e. substrate, interface, or overlay, indicates the zone of weakness in the system. For the case of "bond failure" in the overlay it is important to understand the prevailing mode of fracture. Cracks in concrete commonly develop as a mixture of tension and in-plane shear (Van Mier et al, 1991). It appears reasonable to assume that the same applies to the fracture zone in debonded overlays, which highlights the importance of overlay shear and tensile strength.

Delatte et al (2000a and b) link bond strength to the maturity of the overlay, which in turn relates to the material strength. They found that an increase in early age concrete strength increased both tensile and shear bond strength significantly. The maturity approach appears useful as it allows predicting interface bond strength in terms of overlay strength, which is commonly easy to measure.

The mechanisms of bond failure in connection with failure modes, i.e. the actual location of failure, and mechanical material parameters have however not been fully researched to date.

Tensile strength of the overlay is also important from a practical point of view as it affects crack development and therefore the formation of boundary conditions that may support the initiation of debonding. In relation to the above, Granju (1996) states that fibres enhance bond durability through the control of crack development. Chen et al (1995) measured a

significant increase in shear bond strength with the addition of short carbon fibres to repair mortar and attributed the effect to the decrease in drying shrinkage. However, it appears more accurate to link the beneficial effects of fibre reinforcement to internal overlay restraint, which reduces interface stresses resulting from differential movement between overlay and substrate.

Some researchers established a link between overlay constituents and interface bond strength. The addition of polymers to cementitious repair mortars was found to result in better bond characteristics on specimens subjected to extensive temperature cycles (Atzeni et al, 1993). According to Rizzo and Sobelman (1989), resin-based repair mortars have generally better bond quality than cement-based mortars. Li (2003) states that the addition of Fly Ash to overlay mixes results in lower short-term but higher long-term bond strength, which he links to the effects that the addition of Fly Ash has on the rate of hydration. He further states that Fly Ash or Silica Fume in the overlay can improve the microstructure of the interface transition zone and hence increase bond strength. Similar test results were reported by Kuroda et al (2000) who found significant enhanced bond strength at both 7 and 28 days when a high CaO content fly ash was added to the overlay mix.

Overlay permeability may influence bond durability, for example very impermeable overlays result in stresses at the interface when moisture from the substrate cannot migrate through the overlay (Schrader, 1992). By contrast, relatively permeable overlays might weaken interface bond strength through cyclic swelling and shrinking if the overlay is subjected to frequent changes in ambient humidity.

2.3.4.2 Condition and texture of the interface

General

Surface preparation and cleaning of the concrete substrate is generally considered to be the most crucial step in a concrete repair project. A poorly prepared surface will always be the weak link in a repair, no matter how good the repair material might be. Holl and O'Connor (1997) stress the difference between surface preparation and cleaning. Surface preparation includes the removal of parts of the substrate concrete and previously applied coatings, whereas cleaning commonly refers to the removal of loose particles and contaminants. Surface preparation is important for the removal of deteriorated concrete and the creation of a good interface texture. Surface cleanliness is probably the most crucial factor in concrete repairs, as any loose debris, dirt, grease or other surface contaminants can act as bond breakers. The above highlights the importance of workmanship. All academic research on bond durability appears ineffective unless proper site practice can be ensured.

Methods of roughening the substrate surface

Common surface preparation methods include mechanical roughening and blast methods utilizing abrasive, sand, or water, or a mixture of them. The use of heavy mechanical techniques such as jackhammers, drills and scabblers usually results in the formation of microcracks at the substrate surface, which has a detrimental effect on bond strength (Warner et al, 1998, Silfwerbrand, 1990, Delatte et al, 2000 b). However, sandblasting subsequent to the use of heavy mechanical methods can remove the damaged concrete and provide a sound interface (Talbot et al, 1994, Carter et al, 2002). Wells et al (1999) and Warner et al (1998) achieved good bond strength on surfaces which were sandblasted without prior roughening.

According to Silfwerbrand (2000), water-jetting results in a sound, rough, and clean concrete surface, removing deteriorated concrete and leaving sound concrete. Murray (1989) recommends cleaning with high-pressure water subsequent to surface preparation. Kauw and Dornbusch (1997) discussed the effects of applied pressure during waterjetting on the quality of the concrete surface. They concluded that waterjetting is a good method of concrete removal but has to be specified carefully with consideration of the properties of the concrete to be treated.

Interface texture and roughness

Interface texture can be divided into macroscopic, microscopic, and sub-microscopic texture (**Figure 2.7**).

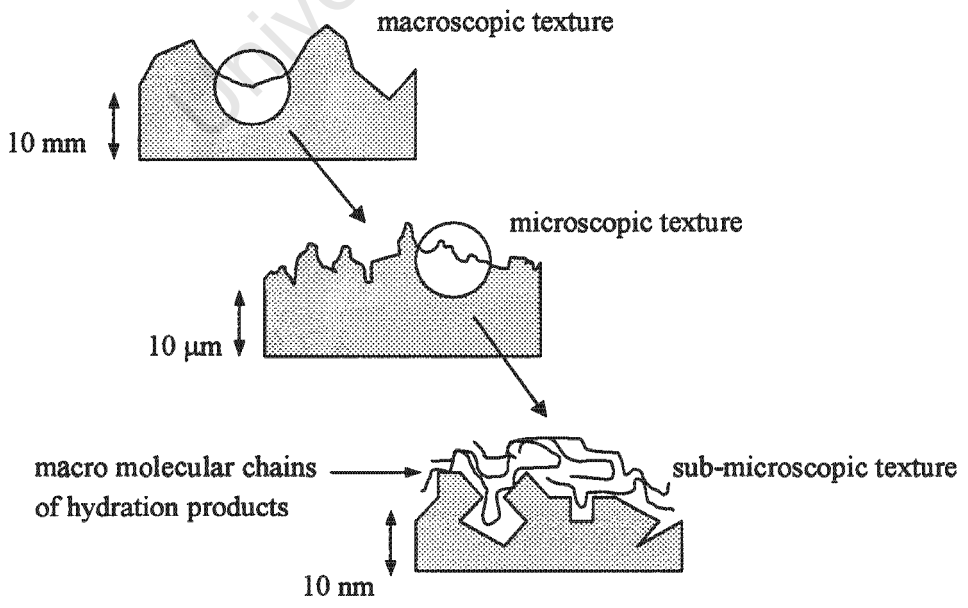

Figure 2.7: Macroscopic, microscopic, and sub-microscopic surface texture

Interface texture is commonly expressed in terms of roughness. Interface roughness depends to a large extent on the method of substrate surface preparation. Mechanical methods of concrete removal normally leave the substrate surface much rougher than blast methods. The magnitude of surface roughness for concrete repairs is commonly measured in mm. The most widespread test method is the sand area method (**Figure 2.8**) (Kaufmann, 1971), in which sand of known volume V is spread over the concrete surface to form a circle until all sand has settled in the surface cavities.

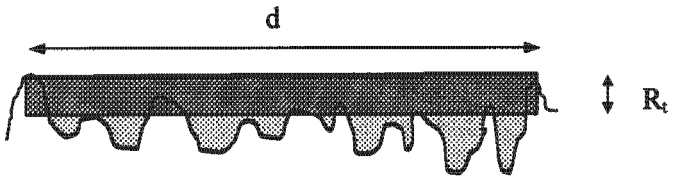

Figure 2.8: Determination of surface roughness using the sand area method (Kaufmann, 1971)

The roughness R_t can be calculated from the diameter d of the circle, using the following equation:

$$R_t\,[\text{mm}] = \frac{40.V[cm^3]}{\pi.d^2[cm^2]} \qquad [2.1]$$

Where V is the volume of the sand. More accurate surface profiles can be assessed electronically using touch-pins (Courard, 1998) or laser techniques (Schäfer et al, 1996).

A number of researchers have linked interface roughness to bond strength. Tschegg et al (2000) compared roughness of 1.75 mm to 0.65 mm on water-jetted surfaces and found better bond characteristics for the rougher interface, using a wedge-splitting test. Mainz and Zilch (2002) achieved high bond strengths on water-jetted surfaces with a roughness of >1 mm and concluded that an increase in roughness did not improve the bond strength significantly. In their study, they measured bond strength with slant shear specimens (compare Figure 2.6 H). It should however be noted that the slant shear method applies a unrealistically high compressive stress to the interface which makes shear friction, which is activated once actual adhesion is destroyed, one of the most important bond mechanisms. The direct influence of interface roughness on adhesion can therefore not be assessed with this method. It therefore appears questionable if the above results can be related to real repair patches.

Silfwerbrand (1990) compared interface strengths resulting from different surface treatments and different roughnesses. Similarly to Mainz and Zilch, he concluded that that the threshold value for tensile bond strength improvement lies in the range of the surface roughness of

sandblasted surfaces. An increase in surface roughness beyond this value did not seem to increase bond strength. However, the tensile pull-off method is hardly susceptible for the effects of surface roughness, as discussed in Section 2.3.2. Similarly to results presented by Mainz and Zilch, as discussed above, it appears that conclusions were drawn from a test method that is ineffective for the test parameter under consideration.

Generally it appears reasonable to assume that interface roughness has an influence on shear bond strength while it is of minor importance for tensile bond mechanisms. The actual influence of interface roughness on bond strength however also depends on a range of other parameters such as mechanical material strength and effective surface area. The interpretation of bond properties in terms of individual parameters therefore appears problematic and should be done with caution.

Temperature

The substrate temperature at the time of overlay placing was found to have a significant effect on shear bond strength development (Delatte et al, 2000 b). Cold substrates (4 °C) resulted in lower initial bond strength but higher long-term bond strength, compared to substrates of higher temperature (21 or 38°C). This effect probably relates to the effects of hydration of the cement paste. Low temperatures generally slow down the hydration rate. At slow hydration rates the hydration products have sufficient time to diffuse uniformly throughout the cement paste, which consequently positively affects later age strength. The influence of mechanical material strength on interface bond is discussed in Section 2.3.4.1.

Carbonation

According to Schrader (1992), carbonation of the substrate can result in a soft surface and dusting, which may result in poor bond strength if an overlay is applied. Similar test results were obtained by Gulyas et al (1995) who found that substrate carbonation can decrease bond significantly. By contrast, Block and Porth (1989) found that substrate carbonation does not affect pull-off bond strength. These contradicting results show the problematic in interpreting bond tests in terms of a single test parameter.

Moisture condition

The substrate moisture condition may have a significant influence on bond strength. A dry, "thirsty" concrete surface tends to suck water from the overlay, which may result in a weak interfacial repair layer and low bond strength (**Figure 2.9 A**). A surface, which is too wet, tends to dilute the repair material at the interface and increases the water/cement ratio and

hence leads to low material strength, increased shrinkage and low bond strength. Water in open pores further prevents the interlocking effect (**Figure 2.9 B**). The substrate concrete should, therefore, be saturated but surface dry (**Figure 2.9 C**).

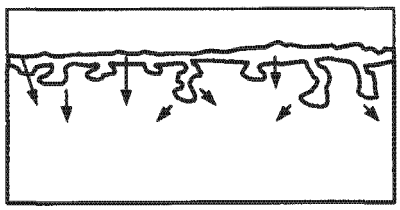

weak overlay layer

A: The dry substrate sucks water from the freshly placed overlay

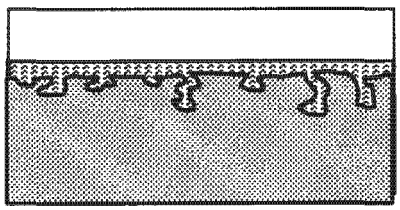

B: Surface water prevents the interlocking effect and dilutes the overlay near the interface

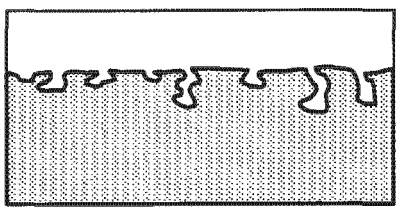

C: A saturated and surface-dry substrate prevents suction and provides open cavities for interlocking

Figure 2.9: Critical moisture conditions of the substrate surface

The influence of the substrate surface moisture condition on bond strength has been investigated in many studies. In general the opinions on the effects of substrate moisture differ significantly between individual researchers and engineers (Pigeon and Saucier, 1992). Li et al (1999) and Geissert et al (1999) measured the bond strength of repaired specimens after freeze-thaw cycles and found that different repair materials correspond to different optimum interface moisture conditions at the time of casting. Zhu (1992) has found experimental signs of optimal moisture, but the effects were so insignificant that it was difficult to discern between the actual test parameter and the scatter of test results.

2.3.4.3 Bonding agents

The use of bonding agents has been intensively investigated by many researchers, resulting in a broad range of opinions. However it is generally accepted that bonding agents cannot compensate for bad substrate surface preparation and may act as a bond breaker when used inappropriately (Pigeon et al 1992, Schrader 1992). By contrast, bonding agents may improve

bond strength for certain materials, especially stiff repair mortars that cannot properly fill open pores and cavities, as discussed in Section 2.3.4.1. The efficiency of bonding agents further depends on the interface texture (Wells et al, 1999).

Different types of bonding agents are available, the main types being cement-based slurries, epoxies, and latex emulsions. Cement-based slurries were found to result in high bond strengths (Knutson, 1990, Pigeon et al, 1992, Hartl, 2000). El-Rakib et al (2003) measured improved shear bond strength with the use of an epoxy bonding agent. Montani (1995) states that the reasons bonding agents have gained a bad reputation lie in poor workmanship during their application.

2.3.4.4 Curing procedures

Cracks resulting from shrinkage may initiate debonding due to the formation of boundary conditions at free edges, as discussed in Section 2.3.4.1. Curing prevents rapid moisture loss to the environment and thus controls the development of overlay and interface stresses by reducing shrinkage at early ages when bond strength may be low.

Paulsson and Silfwerbrand (1998) recommend a minimum of 5 days water curing on bridge deck overlays. Exposure to direct sunlight was found to have a detrimental effect on shear bond strength even under proper curing conditions which included wet burlap and plastic (Delatte et al, 2000a). Schrader (1992), on the contrary, states that curing mainly affects the surface of a concrete repair, but has little influence on the material or bond properties at a depth of more than 25 mm.

2.3.5 Short-term bond properties

The development of early age bond strength is important for the structure's ability to withstand interface stresses induced by early age differential movement between substrate and overlay. For pavement and bridge deck overlays high early bond strength is usually required due to traffic and live loads.

According to Delatte et al (2000 a and b), bond strength develops rapidly after placement, similar to concrete compressive strength development. In their studies they suggest a concrete maturity approach, which characterises bond strength development in relation to the concrete's rate of hydration rather than it's age. Similarly, Silfwerbrand (1992) concluded from pull-off tests that bond strength development at early ages is rapid. Carter et al (2002) state that bond strength develops more fully in the centre of an overlay as the boundaries are especially subjected to cyclic stresses related to differential temperature and moisture content.

In general, short-term bond strength can be used as an indication of the quality of workmanship, i.e. surface preparation, material selection, overlay application, and curing. Long-term bond strength however can significantly be influenced by environmental influences as discussed in the following.

2.3.6 Long-term bond properties

Most studies documented in the literature concern the quality of bond at early ages. However, factors influencing long-term bond strength are most important for the performance of composite members.

Pigeon and Saucier (1992) state that although the durability of bond between old and new concrete is influenced by many factors, differential shrinkage is the most important aspect. In their study, they subjected composite specimens to a range of ageing treatments and found that simple air-drying was the main cause of deterioration. By contrast, freezing and thawing had a positive effect, which was accounted to the effects of ongoing hydration that was facilitated by water used in the test procedure. Li et al (1999) found specimens that had been subjected to 300 freeze-thaw cycles to have similar bond strength as air cured specimens.

A common way to assess bond durability is to test long-term bond strength in actual structures. Carter et al (2002) state that well designed bridge deck overlays can be expected to provide more than 30 years of service life if they are placed and cured correctly. Paulsson and Silfwerbrand (1998) tested repaired concrete bridge decks, which had been overlaid with fibre reinforced concrete, and found a slight increase in bond strength after a period of 9 years. Langlois et al (1994) tested pull-off strength on a road repair overlay and concluded that as long as good quality concrete is used and workmanship is good, bond durability can be achieved regardless of the type of repair mortar or surface preparation. Repaired beams and columns with well-bonded overlays were shown to have structural capacities similar to those of monolithic members (Silfwerbrand, 1986, Souza and Appleton, 2003). Okada et al (1970) found that differential shrinkage greatly affects cracking behaviour but does not influence flexural strength of composite beams, indicating that bond strength is not necessarily affected even if restrained shrinkage exceeds tensile overlay strength.

Talbot et al (1994) investigated the influence of different interface textures and concluded that smooth surfaces as well as sandblasted surfaces experienced a significant loss of bond strength with time. On the contrary, surfaces that were roughened mechanically and subsequently sandblasted had good bond durability. The reason for this lies in the circumstance that high interface roughness, as is commonly achieved with mechanical methods, improves the resistance against interface shear stresses resulting from differential shrinkage.

2.3.7 Mechanisms of debonding

The term 'debonding' implies that bonding had previously developed but then declined to zero. Bond failure may occur at the interface, in the substrate, in the overlay, or in a combination thereof. However, reports on bond tests in the literature commonly do not include the location of failure but merely state the values for bond strength. It therefore appears necessary to investigate the mechanisms of debonding in relation to the actual failure plane to conclude on fundamental bond mechanisms.

Most cracks in concrete develop under combined modes, of which the mixed mode (1 (tension) and 2 (in-plane shear)) is the most common. According to Van Mier et al (1991), most interface shear tests will initiate in mode 1 and true mode 2 failures are very difficult to obtain. Robins and Austin (1995) proposed a bond failure envelope for concrete repairs based on the Mohr circle and related it to interface shear and tension test results.

According to Carter et al (2002), debonding usually causes the overlay to fail slowly, similar to concrete crack propagation. This may be divided into 3 different stages, namely, initiation, propagation and disintegration. According to Knutson (1990) and Carter et al (2002), debonding in areas within the center of an overlay is usually caused by poor surface preparation or weak substrate surface concrete. Debonding usually starts at the overlay boundaries, at the edges, joints and cracks (Carter et al, 2002, Silfwerbrand, 1997). The main reason for this is the development of interface stresses due to differential shrinkage, which are commonly believed to have maximum values at the boundaries of an overlay. All existing analytical models for the prediction of interface stresses due to differential shrinkage assume that interface shear stress only exists at the end of an overlay, which is discussed in more detail in Chapter 3. However, this aspect was challenged in this research, as discussed in detail in Sections 4 and 6. The main reason why debonding commonly occurs at the member ends is that the mechanism of debonding is connected to overlay slip. The latter can only develop fully at the member ends where the overlay is not attached to a restraining "neighbour" (**Figure 2.10**).

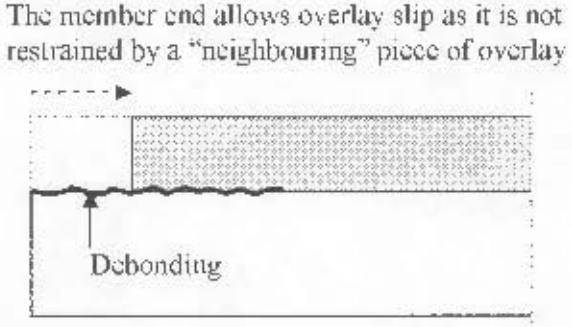

Figure 2.10: Mechanisms of debonding at the end of composite members (neglecting peeling effects)

Member end conditions can also exist at cracks. Granju (1996) identified cracking perpendicular to the interface as one of the main causes of bond deterioration and states that fibre reinforcement can effectively increase crack resistance and therefore enhance bond durability. However, Laurence et al (2001) studied the field performance of different concrete overlays and concluded that extensive cracking had no detrimental influence on bond strength. Shrinkage stresses at the overlay boundaries occur in a mixed form of shear and tensile stress, which is discussed in more detail in Section 2.4.1. Structural and thermal loadings induce cyclic stresses, which may lead to debonding from fatigue effects.

2.3.8 Summary, conclusions and identification of further research

Many researchers have investigated bond properties between concrete substrates and overlays. A large range of material parameters and environmental conditions can influence the quality of bond and in general it appears difficult to interpret bond strength measurements in terms of individual test parameters. This is revealed in the often contradicting opinions reported in the literature regarding the influences of substrate surface preparation, the use of bonding agents, curing procedures and material properties.

It is generally accepted that adequate short-term bond strength can be achieved if the quality of workmanship is good and overlay materials are carefully selected. In the literature it is however often emphasized that the *mechanisms of bond under long-term influences* have not yet been fully researched. Available information on bond durability indicates that differential shrinkage between substrate and overlay is the main mechanism affecting the long-term performance of bonded overlays.

Most studies define bond strength as the stress required to separate substrate and overlay and provide information on the overall location of failure, i.e. substrate, interface, or overlay failure. In case of "interface failure" however, the actual location of fracture is often not exploited. Considering mechanical and chemical bond mechanisms it appears unlikely that bond failure occurs at the interface as such, i.e. without fracture in substrate or overlay. Fundamental understanding of adhesion between concretes of different ages must base on information on the weakest link in the composite member. Only with such information, bond mechanisms can be identified. In respect to the above it appears important to exploit the characteristics of the interface transition zone, which may exist at the interface between substrate and overlay similarly to the interface between aggregate and cement paste, in more detail.

The importance of mechanical overlay strength is revealed in the assumption that the interface transition zone is likely to be the dominant zone of fracture. A maturity approach that links bond strength to overlay hydration, as suggested by Delatte et al (2000), appears useful as it facilitates the design of bonded overlays. However, as stated above, the durability

of bond is subjected to a large range of influences and the characterisation of bond strength in terms of single parameters is not practical.

Test methods for bond strength presented in the literature are numerous, which makes it difficult to compare results obtained from different researchers. In general it is important to use a method that represents the most significant stress condition in the type of structure under investigation. From the literature it appears that at occasions conclusions were drawn from test results that did not relate to the actual test parameter. This highlights the importance of the right choice of test method.

This research focuses on the long-term performance of bonded overlays under the influence of differential shrinkage. Experimental research on bond properties between substrate and overlay is discussed in Chapter 7. The parameters identified from literature review are:

- Short-term bond strength development in relation to mechanical overlay strength and the location of fracture
- Long-term bond properties in relation to different overlay materials, environmental conditions and interface textures.

Bond strength values were compared to strain measurements on composite beams. Test methods were designed that represent main stress conditions encountered in bonded overlays subjected to differential shrinkage. With the above, fundamental bond mechanisms in terms of mechanical overlay properties and long-term overlay shrinkage were investigated.

2.4 Overlay volume changes

2.4.1 Introduction

Differential volume changes between substrate and overlay are commonly considered as the most critical aspects influencing the durability of composite members. The focus of this research lies in the development of an analytical model for the prediction of overlay stresses induced by differential shrinkage. To develop a fundamental understanding of the important mechanisms involved, relevant material properties as well as the specific case of differential volume changes in bonded overlays are discussed in the following.

In general, the mechanisms of volume changes can be divided into short-term and long-term effects. During the early processes of setting and hardening, concrete may experience significant temperature and volume changes. The interaction between overlay and substrate and the restraint of overlay deformations resulting thereof may lead to early failure of the overlay while tensile overlay strength and interface bond strength are low. Continuous

overlay deformation resulting from ongoing drying shrinkage and cyclic temperature changes may further affect the long-term performance of the system.

Stresses due to temperature and volume change are normally not constant throughout the overlay depth and can be divided into restraint stresses and intrinsic stresses. Restraint stresses result from bond mechanisms at the interface between substrate and overlay and as such they are caused by an external restraining mechanism. They are related to the restraint of expansion or shortening parallel to the interface and primarily take the form of direct stresses. Intrinsic stresses, on the contrary, are caused by internal restraining mechanisms. The overlay surface tends to cool down and shrink faster than the inner sections, which results in temperature and shrinkage gradients throughout the overlay thickness. These gradients generate intrinsic stresses due to internal restraint from one depth increment to the next. In the case of reducing temperature or increasing shrinkage in bonded overlays, they can practically be considered as the stresses that correspond to restrained curling deformations (**Figure 2.11**).

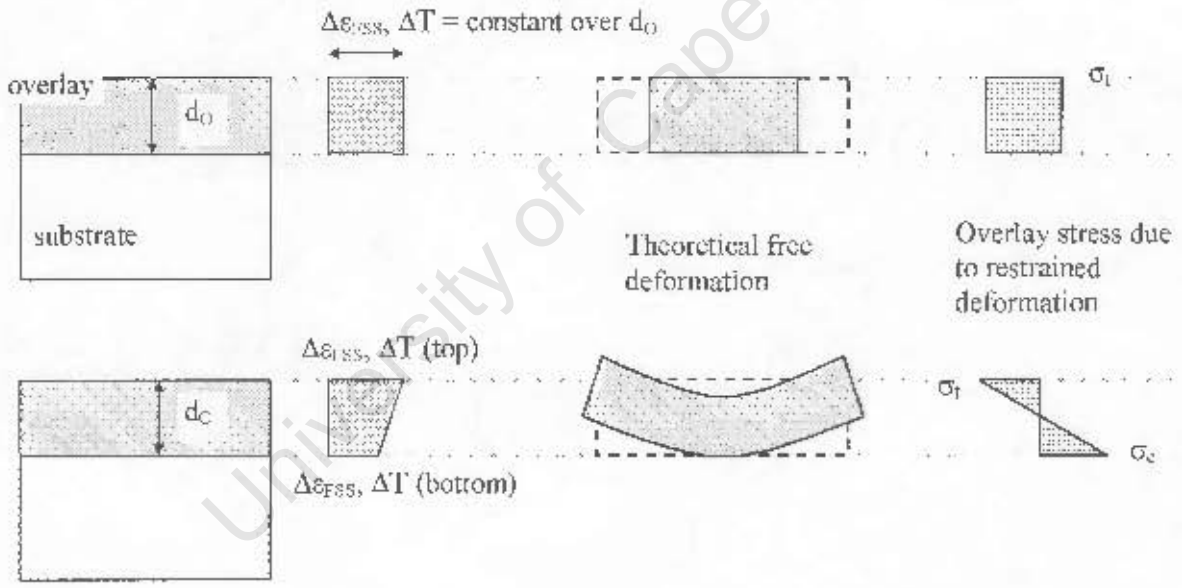

Figure 2.11: Simplified schematic of the main components of restraint stress and intrinsic stress in a bonded concrete overlays due to shrinkage and temperature change (cooling)

The evaluation of stresses resulting from differential shrinkage or temperature gradients is complex, as rate and magnitude of stress generation depend on the development of material properties. The material properties in turn depend on the rate of hydration and environmental conditions. Relevant parameters like shrinkage, tensile strength, elastic modulus, creep, and the degree of restraint develop at different rates and interact with each other, which makes it difficult to predict stresses, especially at an early age.

2.4.2 Temperature effects at an early age

Cement hydration is an exothermic process, causing temperature increase in the fresh concrete, which results in thermal expansion. The amount and rate of heat energy generation is primarily governed by the type and amount of cement used (Taylor et al, 1994). The concrete heats up until the heat loss on the surface exceeds the internal heat generation.

In a restrained concrete overlay, thermal expansion and contraction produce compressive and tensile stresses respectively. Springenschmidt (1984) illustrated early age temperature stresses in bonded overlay schematically (**Figure 2.12**).

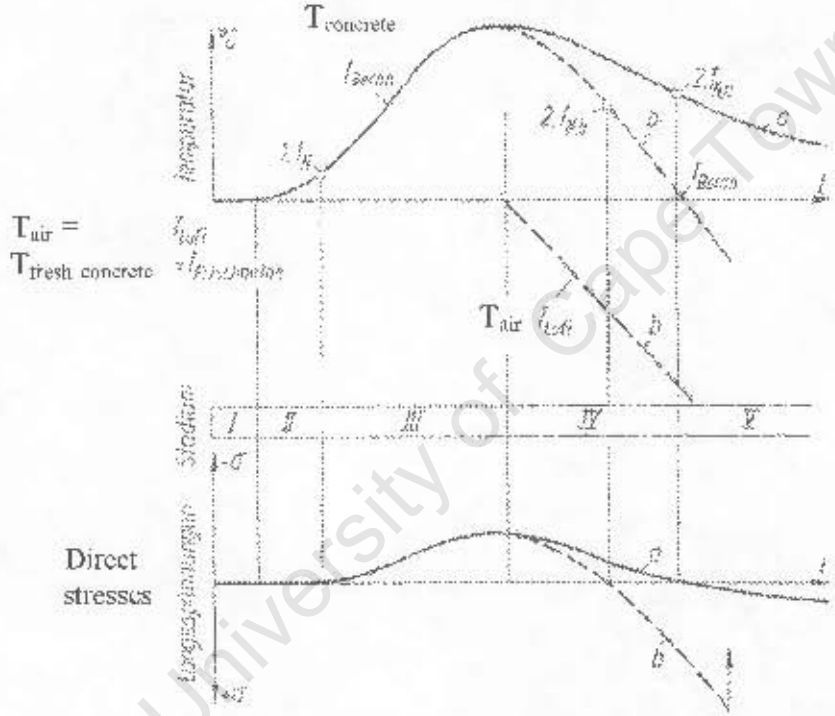

Figure 2.12: Stages of temperature development during hardening and the resulting stresses a) due to loss of hydration heat and b) due to drop in air temperature (Springenschmidt, 1984)

In the first few hours after placement, the concrete is still plastic and stress development only starts after a period of approximately 5 to 7 hours ($1.T_N$). Until the maximum temperature is reached, the concrete experiences high compressive creep relaxation. The so-called zero-stress temperature of the hardening concrete is reached during the cooling process, approximately 1 to 4 K below the maximum hydration temperature ($2.T_N$). Differences from the zero-stress temperature result in stresses due to thermal deformations during the lifetime of the structure. Following the maximum hydration temperature the concrete cools and attempts to contract. The concrete, however, has hardened at this stage and the imposed

contraction is restrained at the substrate interface. This restraint generates tensile stresses that may exceed the early age tensile strength and hence cause cracking in the first few days after the repair. A drop in the surrounding temperature subsequent to hardening may accelerate this stress generation.

However, for thin overlays which have a large surface-area to volume ratio a major part of the hydration temperature can be expected to be lost rapidly to the environment. The zero-stress temperature should therefore not be much higher than the surrounding air temperature during hardening.

Letsch (1995) measured stresses in restrained concrete specimens and concluded that lower temperatures during placement and the first few days after hardening lead to lower stresses, compared to higher temperatures. Lange und Shin (2001) developed a prediction model for overlay stresses due to temperature changes and concluded that thermal contraction is likely to cause cracking within the first 24 hours, but thermal stresses become less significant hereafter. Eierle and Schikora (2000) evaluated existing models for the calculation of early age temperature stresses in concrete slabs. They concluded that creep parameters, which are difficult to assess accurately at an early age, are the main uncertainty for the estimation of stress evaluation.

A model presented by Brühwiler et al (2000) indicates that a reduction in cement content of 50 kg/m^3 leads to a similar decrease of early age tensile stress in a concrete overlay as would a reduction in fresh concrete temperature of 5 °C. However, reducing the cement content also leads to a decrease in tensile strength and the overall effect of the cement content on structural performance at early ages is therefore of minor importance. As a practical solution for the control of hydration heat development, Brühwiler et al suggested the use of cooling systems, for which they developed a numerical prediction model for overlay stresses.

Emberson (1990) measured early age temperature development of different repair mortars, most of which had considerably low peak temperatures in the range of 21 to 24°C, compared to an ambient temperature of 20 °C. This indicates that for these materials, early age temperature development was possibly of minor importance compared to the effects of shrinkage.

2.4.3 Early age shrinkage

Very early age shrinkage, also termed capillary or plastic shrinkage is caused in fresh concrete due to surface moisture loss and is often accompanied by surface cracking. Plastic shrinkage involves the transfer of moisture from the surface to the environment by evaporation and a simultaneous mass transfer from inside the concrete to the surface. Environmental conditions such as high wind velocity, high air temperature and low relative

humidity lead to an increase in plastic shrinkage. Suction of water by the substrate may add to the effect of surface evaporation. According to Radocea (1994), total plastic shrinkage deformation depends on the rate of evaporation and the development of capillary pressure, which are controlled by the pore structure near the surface exposed to the environment. High early age volume changes may cause significant intrinsic stresses. For the quantification of shrinkage microcracking in concretes at early ages, different microscopy techniques can be used, e.g. fluorescence light microscopy and Environmental Scanning Electron Microscopy (Bisschop and Van Mier, 1999).

Early age shrinkage, which is commonly measured as the 0-24 hour curing shrinkage, can be of significant magnitude. Emberson (1990) measured early age shrinkage of 11 common repair mortars, and found it to be in the range of 80.10^{-6} to 2400.10^{-6}. According to Emmons and Vaysburd (1995) cracks caused by plastic shrinkage occur commonly shortly after setting and can most effectively be controlled by keeping the repair surface moist during this period. Mueller et al (2002) claim that plastic shrinkage can be completely avoided through mix design and curing procedures.

2.4.4 Long-term temperature effects

During the service life of a concrete member any temperature rise in the overlay above the zero-stress temperature leads to expansion and any drop in temperature leads to contraction (compare Figure 2.12). The origins of the resulting temperature stresses can be divided into differences in thermal coefficients between substrate and overlay and temperature gradients through the depth of the member. Different thermal coefficients cause restraint stresses only if the temperature change reaches the interface. The stresses increase linearly with increasing difference in thermal coefficients and are not affected by their absolute value (Sodeikat 2002). Temperature gradients throughout the member, on the contrary, cause instant intrinsic stresses, which depend on the absolute values of thermal coefficients.

Direct sunlight can heat concrete surfaces considerably. At an air temperature of 27 °C, for example, black and white concrete surfaces can reach temperatures of 65 °C and 38 °C respectively (Springenschmidt et al, 1978). Sudden cooling, such as that caused by a cold rain shower, leads to distinct temperature gradients (**Figure 2.13**) and the generation of high tensile stresses at the overlay surface.

With significant temperature changes and a large difference in thermal coefficients between substrate and overlay, excessive interface shear stresses may be produced. This might cause bond failure or, in the case of high bond strength, failure within the lower strength material (Emmons and Vaysburd, 1995). Sodeikat (2002) recommends limiting the difference in thermal coefficient to 2.10^{-6}/K for thin overlays of less than 40 mm, and $2,5.10^{-6}$/K for thicker overlays.

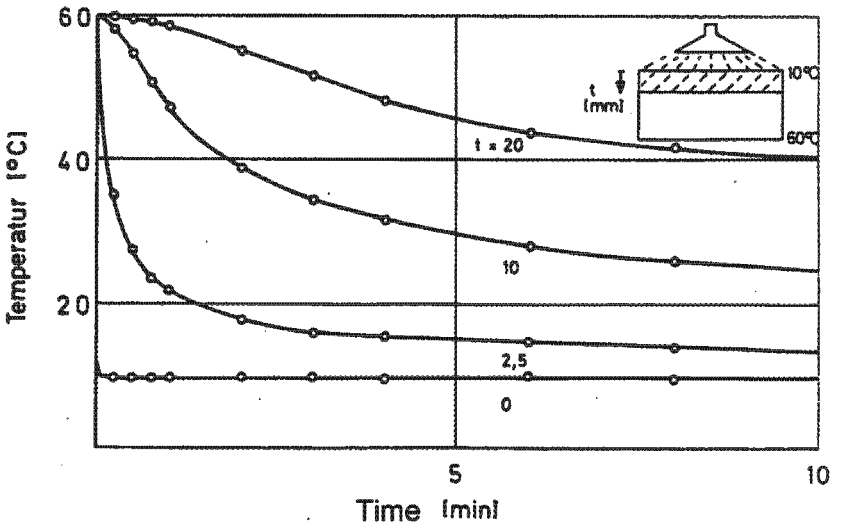

Figure 2.13: Temperature gradients in a concrete overlay, heated to 60 °C and subjected to a simulation of heavy rainfall of 10 °C (Haardt and Hilsdorf,1988)

The major factors influencing the thermal coefficient of concrete are the type of aggregate used, the moisture content of the concrete and the volume concentration of aggregate in the mix. The effects of other factors such as type of cement, strength and age of concrete and curing methods are of less importance (Alexander, 2001). Concrete and cement paste generally have coefficients of thermal expansion ranging from $5{,}5.10^{-6}$/K to 14.10^{-6}/K and 10.10^{-6}/K to 23.10^{-6}/K respectively (Hilsdorf, 1995). A study by Emmons and Vaysburd (1995) indicated that resin-based repair materials have significantly higher coefficients of thermal expansion ($18{,}7.10^{-6}$/K to $23{,}1.10^{-6}$/K) compared to unmodified or polymer modified materials ($7{,}3.10^{-6}$/K to $12{,}1x10^{-6}$/K). Non-resin-based repair materials were found to have values similar to that of many unmodified concretes. The German standard on concrete repair (DAfStb, 2001) limits the thermal coefficient of resin-based mortars to 25.10^{-6}/K, whereas no limitations are made for non-resin-based mortars. Atzeni et al (1993) measured thermal expansion of polymer-modified mortars to be in the same order of magnitude as plain cement mortars.

The thermal coefficient of cement paste is mainly affected by the moisture content and is low for saturated and very dry paste and reaches its maximum at approximately 65% to 70% RH. Partially moist concretes, therefore, have coefficients of expansion higher than those in the completely dry or saturated state. Continued temperature changes combined with wetting-drying cycles consequently represent the most crucial thermally induced volume change of concrete overlays.

The assumption that stresses due to changes in temperature develop linearly with the restrained expansion or contraction results in the following equation:

$$\sigma_T = (\varepsilon_{nr} - \alpha_T \times \Delta T) \times E \qquad [2.2]$$

where σ_T = Stress due to temperature change [MPa]
ε_{nr} = non-restrained part of the deformation
ΔT = change in temperature [K]
E = elastic modulus [MPa]

Springenschmidt et al (1978) measured compressive stresses of approximately 5.3 MPa in restrained concrete specimens resulting from a temperature rise of 41 K. Stress values calculated using equation 2.2 were 40 % higher, which can be related to the mechanisms of creep. Letsch (1991) calculated relaxation of tensile stresses in restrained concrete specimens subjected to a temperature change of 60K to be approximately 50%. Walraven and Shoukani (1993) point out that relaxation of stresses due to thermal expansion increases with concrete temperature and decreases with concrete age. The mechanisms of creep and relaxation are discussed in more detail in Section 2.5.

2.4.5 Long-term shrinkage

2.4.5.1 Introduction

The generation of stresses associated with differential shrinkage between concrete overlay and existing base concrete has long been recognized as the main problem for the durability of repaired concrete structures. The relaxation of such stresses plays a key role for durable structural performance and depends on the total deformability of the overlay, which combines the influences of elastic strain, stress relaxation, and the strain related to microcracking of the cement matrix.

In the following sections fundamental mechanisms of shrinkage in concrete and models for the prediction of shrinkage strains are briefly summarized. Previous research on repair material shrinkage characteristics and the effects of shrinkage restraint on the performance of bonded overlays is discussed.

2.4.5.2 Fundamental mechanisms of shrinkage in concrete

Shrinkage in concrete can be divided into different components, all of which have different characteristics and are subjected to different influences. The mechanisms of early-age shrinkage are discussed in Section 2.4.3.

Drying shrinkage

Total shrinkage deformations is a sum of different components. Drying shrinkage is the factor of most concern in structural performance of normal strength concrete repairs, and is associated with a net outflow of moisture from the repair concrete to the environment. A large portion of the first drying shrinkage cannot be recovered if the concrete is later re-wetted. On subsequent wetting and drying cycles, however, a portion of the original shrinkage movement is recovered with each wetting. Shrinkage therefore consists of reversible and irreversible components (**Figure 2.14**).

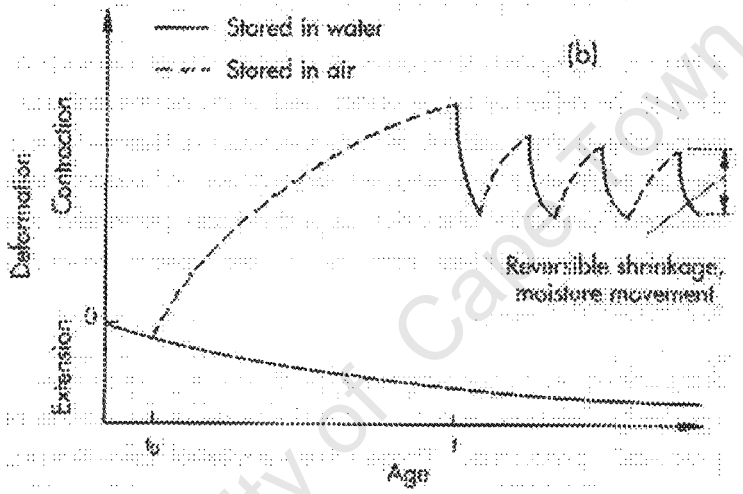

Figure 2.14: Basic characteristics of reversible and irreversible drying shrinkage (Neville, 2002)

Total drying shrinkage decreases with an increase of member thickness, and is a function of the volume/surface area ratio of the member. Drying shrinkage of repair patches, which are relatively thin, develops at a considerably higher rate than that of massive concrete members.

The major factors influencing shrinkage of concrete can be divided into material properties and environmental conditions. The paste is the source of shrinkage in concrete as its porosity determines the rate of water transport and diffusion. Irreversible shrinkage in normal strength concrete increases linearly with porosity, which decreases with a decrease in W/C and an increase in the degree of hydration. The paste holds water at different bonding energies, with the interlayer and gel pore water being much more tightly held than the free capillary water. The early days of drying represent the removal of free water, and shrinkage tends to be similar for different W/C since only capillary water is being lost (Alexander, 2001).

Subsequently, gel water begins to be removed, causing a larger component of shrinkage as contraction forces are generated.

Shrinkage is little influenced by the use of common cement extenders and deformations tend to be similar to those of plain OPC concrete. Testing the influence of different cement composition and fineness has led to conflicting results (Springenschmidt and Fleischer, 1993). The effect of admixtures is variable and depends on the specific admixture and cement, and the exposure conditions (Alexander, 2001). Aggregates have the effects of dilution and restraint of paste shrinkage. Dilution refers to a decrease in shrinkage with increasing aggregate concentration, while restraint refers to decreasing shrinkage with increasing aggregate stiffness.

The concrete's environment comprises the type and extent of curing and the subsequent drying conditions, i.e. the ambient relative humidity, temperature, and wind conditions. The duration of curing, and hence the onset of initial drying, mainly affects the rate at which shrinkage strains are generated. The influence on total long-term shrinkage deformations is however of minor significance. Curing controls the tensile strength development versus shrinkage strains, and thus helps to prevent early age cracking of overlays. However, it should be noted that extensive curing results in a comparatively high elastic modulus and low creep factor at the onset of shrinkage, which can have a detrimental effect on crack behaviour. The net curing effect depends on the material used, the type and duration of curing, and environmental conditions. The drying condition has a major influence on shrinkage strain development and therefore on the long term structural performance of the repair patch. In general, shrinkage strains increase with increasing temperature and decreasing humidity. Baroghel-Bouny and Godin (2001) found a linear relationship between shrinkage strains and relative humidity for a large range of concrete mixes. Strong winds can further accelerate drying shrinkage at the concrete surface, which is of significance for concrete overlays exposed to the environment.

Carbonation shrinkage

Carbonation shrinkage is caused by the reaction between the carbon dioxide of the atmosphere and the constituents of hardened cement paste. The volume reduction caused by carbonation shrinkage is slow and occurs over a long period, but in some cases may exceed the drying shrinkage in magnitude (Alexander, 2001). This is particularly important for concretes exposed to atmospheres of intermediate relative humidities and possessing small cross-sectional dimensions, such as conventional repair patches.

Autogenous shrinkage

Autogenous shrinkage, also called basic shrinkage, is a volume reduction caused by cement hydration and the internal consumption of water. It explains the shrinkage of concrete in sealed condition, without moisture exchange between concrete and environment. For normal strength concrete, autogenous volume changes are usually small compared with carbonation and drying shrinkage. However, concrete with a W/C of less than 0.4 has a much higher consumption of mixing water and therefore a high autogenous shrinkage component. Baroghel-Bouny and Godin (2001) measured autogenous shrinkage for a large set of Portland cement pastes and concluded that the magnitude of shrinkage increases linearly with decreasing w/c ratio. Recent developments in high performance concrete have shown that autogenous shrinkage in such materials cannot be modelled accurately with existing prediction models which were designed for normal strength concretes (Miyazawa and Tazawa, 2001, Mueller and Kvitsel, 2002).

Approximately 40% of autogenous shrinkage occurs within the first 24 hours, during which the tensile strain capacity is low, resulting in a high risk of early cracking (Alexander, 2001). Being an internal process, autogenous shrinkage cannot be controlled by curing procedures. It develops rapidly after setting and tends to reach its limiting value after approximately 10 weeks (Dilger et al, 1996).

2.4.5.3 Development and magnitude of shrinkage strains

Shrinkage may continue for years depending on size, shape, and material properties of the member. A literature review carried out by Emmons and Vaysburd (1995) revealed conflicting results as to when actual shrinkage strains reach a maximum. In general it seems to be accepted that approximately 50% of the total shrinkage occurs between 10 and 25 days. According to Emmons et al (1983), approximately 70% of the total shrinkage strain of a concrete repair material occurs in the first 30 days. Hartl (1983) measured free shrinkage on concrete repair materials to nearly reach the total shrinkage strain after 28 days and concluded that overlays are mainly at risk to fail in this period. However, Silfwerbrand (1997) measured overlay shrinkage strain on composite specimens and noted that this process continues significantly for a period of more than 300 days.

The development of shrinkage strains was tested for a range of common South African repair materials. Test results and discussions are presented in **Appendix 2**. The results of the experiments indicated that shrinkage continued to increase considerably for more than 3 months, with approximately 40% to 60% of the long-term strain occurring in the first 4 weeks (**Figure 2.15**).

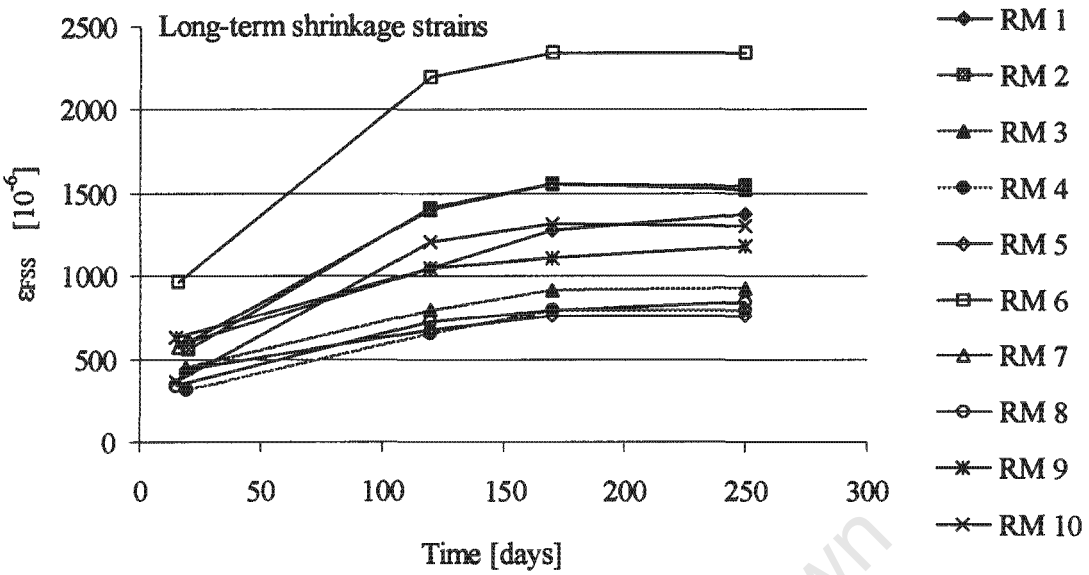

Figure 2.15: Long-term shrinkage of common South African repair materials (RM), measured on 200x100x100 mm prisms under laboratory conditions (details are given in Appendix 2)

Different models for the prediction of shrinkage strain development can be found in the literature. Prediction models are usually based on the product of estimated ultimate shrinkage strain and a function describing the development of shrinkage with time. For example, the CEB-FIP Model Code 1990 (1990) and ACI Committee 209 (1992) express time-dependent shrinkage strain as follows:

$$\varepsilon_s(t,t_0) = \varepsilon_s(t_\infty)\cdot\beta_s(t,t_0) = \varepsilon_s(t_\infty)\cdot\left(\frac{t-t_0}{350\left(h_0/h_{ref}\right)^2 + t - t_0}\right)^{0.5} \quad \text{(CEB-FIP, 1990)} \quad [2.3]$$

where ε_s (t, t_0) = shrinkage strain at time t

t_0 = time when curing is stopped

ε_s (t_∞) = ultimate shrinkage strain

β_s = time depended shrinkage function

h_0 = notional member thickness = 2.A_C/u, A_C = cross-section, u = perimeter

h_{ref} = 100 mm

$$\varepsilon_s(t,t_0) = \frac{t-t_0}{35+(t-t_0)}\cdot\varepsilon_s(t_\infty) \qquad \text{(ACI 1993)} \qquad [2.4]$$

where t_0 = end of moist curing period at 7 days

Mueller and Kvitsel (2002) presented an improved shrinkage prediction model. This model includes autogenous shrinkage of high strength concrete and is the base for the analysis of time dependant stress-strain behaviour in the new DIN 1045.

The variables influencing shrinkage are numerous and estimation of shrinkage strains from material and environmental data is difficult. The literature gives a wide range of shrinkage strains for different cementitious composites. In general, cement paste has a long-term shrinkage strain of 2000.10^{-6} to 4000.10^{-6}, mortar 1000.10^{-6} to 2000.10^{-6}, and concrete 200.10^{-6} to 800.10^{-6}.

Tests on free shrinkage strains of common repair materials show that the type of repair mortar in general has no significant influence on maximum strain values (Emberson and Mays, 1990, Emmons et al, 1983, Chen et al, 1995). For all different types of repair mortars (cementitious, polymer modified, and epoxy) a large range of shrinkage strains with maximum values of more than 2000.10^{-6} were measured, independent of the type of material. Similar observations were made with South African repair materials during this research, as discussed in Appendix 2.

Emmons and Vaysburd (1995) classified concrete repair materials based on 28-day drying shrinkage (**Table 2.1**) and found that a minority of repair materials tested could be labelled as low shrinkage, despite the fact that manufacturers classify them as expansive, non-shrinking or shrinkage compensating.

Table 2.1: Classification of repair material based on drying shrinkage (Emmons and Vaysburd, 1995)

Classification	Range of free shrinkage strains at 28 days [10^{-6}]
Very low shrinkage	0 – 250
Low shrinkage	250 – 500
Moderate shrinkage	500 – 1000
High shrinkage	> 1000

For the characterization of shrinkage properties, measurements of free shrinkage strains on concrete prisms or cylinders are normally utilized by the standards and specifications. The specimens are subjected to specified curing conditions, such as relative humidity and temperature. Measurements of shrinkage strains commonly start at day 1, without accounting for 24-hour plastic shrinkage, and continue for a period of 28 days or longer. Specimen measurements and conditions vary according to the different standards of different countries. Charron et al (2001) state that linear shrinkage tests tend to underestimate actual, i.e.

volumetric deformations. However, for practical purposes it appears reasonable to measure shrinkage as a one-dimensional parameter.

2.4.6 Shrinkage restraint

Differences in shrinkage through the overlay depth generate stresses, which, due to restrained curling, are mainly tensile near the surface and compressive near the interface (compare Figure 2.11). Ambroise et al (2002) developed a numerical model for the prediction of curling stresses in cement-based screeds due to moisture gradients within the thickness of the screed. However, for relatively thin overlays the major concern is the restraint of shrinkage at the interface to the substrate and direct stresses resulting thereof. The free shrinkage strain of most repair materials is far higher than their tensile strain capacity of 100.10^{-6} to 200.10^{-6} (Pigeon and Bissonette, 1999). Restrained shrinkage stresses therefore often exceed tensile overlay strength and cause cracking. Further, the restraint of shrinkage generates interface shear stresses, which may lead to local delamination or complete debonding.

The generation of restrained shrinkage stresses depends on a number of time-dependent factors such as shrinkage and creep strains, elastic modulus and the degree of restraint, as well as on cross sectional dimensions, surface area, substrate properties, and environmental conditions.

Weber (1971) investigated the cracking behaviour of restrained concrete overlays and concluded that overlays either crack at regular and small distances, or completely resist cracking through elastic and plastic deformation. Laurence et al (2001) monitored different overlay materials in field tests and found long-term crack density, i.e. the number of cracks over a certain area, to be inversely proportional to the overlay thickness. Another interesting observation of their study was that crack density continued to increase over a period of one year, which was attributed to long-term drying shrinkage.

Hartl (2000) conducted a study on the influences of selected parameters on the development of tensile stress in the overlay at the interface. According to his research, the most significant influences are those of shrinkage strain and elastic modulus of the overlay. Thin overlays reach the maximum tensile stress at an earlier stage than thicker overlays. They also experience higher peak stress values. Relaxation however leads to similar long-term stress values of thin and thick overlays.

Restrained shrinkage tests

For the evaluation of the effects of restrained shrinkage, a number of restrained shrinkage tests are available, the 3 basic types being the linear, plate, and ring test. The mechanisms,

advantages and disadvantages of available tests have been documented in detail (e.g. Emmons and Vaysburd, 1995, Bentur, 2001). In the following, a short overview on common test methods is provided.

In the linear restrained shrinkage test, restraint of deformations is provided either internally by axially embedded bars, externally by a steel mould or frame, or by a combination thereof. A common linear restrained shrinkage test, which is often used in conjunction with the observation of relaxation characteristics, is the use of a prismatic, "dog-bone"-shaped specimen, which is clamped at both ends (**Figure 2.16 A**). Other tests use linear restraint in connection with regular-shaped prisms and member-end restraint (**Figure 2.16 B**) (e.g. Banthia et al, 1993). The German standard on concrete repairs (DAfStb, 2001) recommends a free shrinkage test for resin-based repair mortars using a steel angle mould (**Figure 2.16 C**). The ring test (ASTM, 2003) is a common method for testing the cracking behaviour of mortars and concretes and has been used for over 60 years. In this test, the material is cast around a ring of steel which provides restraint during setting and hardening (**Figure 2.16 D**). The relative effects of material variations on induced tensile stresses and cracking potential can be estimated. The test appears very useful especially for the direct comparison of different mix ingredients, e.g. it can give an indication of the increase in crack resistance resulting from the addition of fibres (Corinaldesi et al, 2003). The ring test may be carried out with a large number of different sample sizes, as listed in a literature study by Emmons et al (2000), ranging from external diameters of 40 mm to 660 mm.

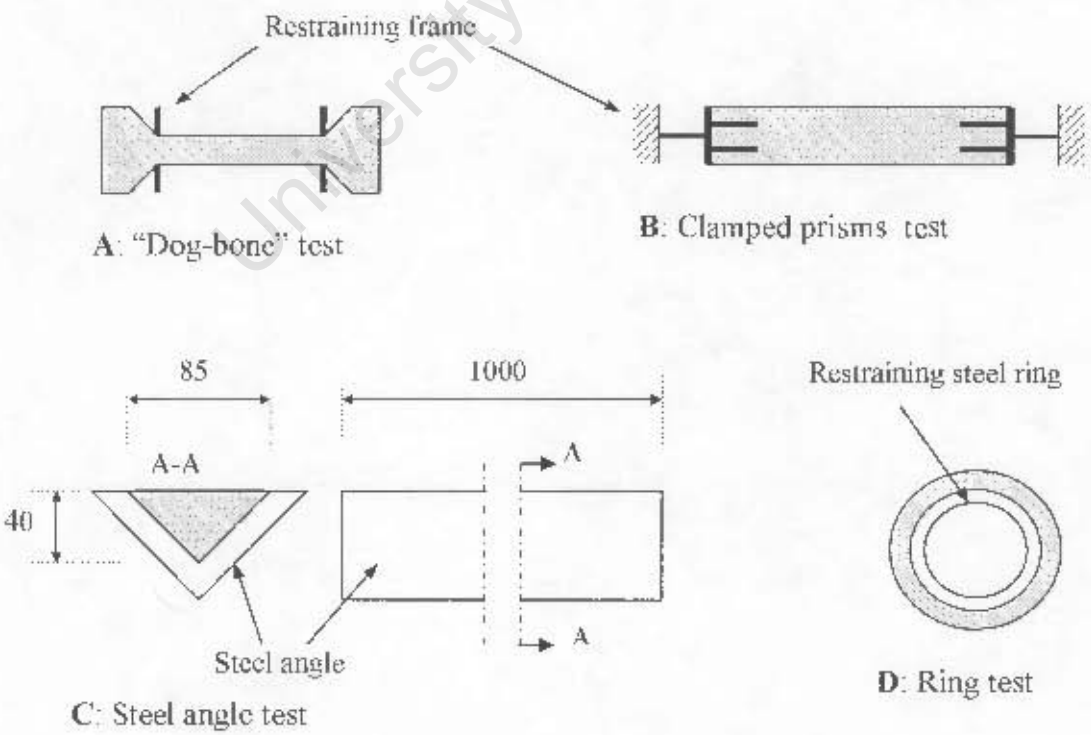

Figures 2.16: Common restrained shrinkage test methods

The above test methods have been used extensively for the prediction of cracking in restrained concrete and mortar specimens. In general they provide a good estimation of the influences of different material properties on the developments of tensile stress and stress relaxation. Letsch (1991) states that the comparison between stresses measured in restrained specimens and stresses computed from free shrinkage strains and elastic modulus gives a good indication of the materials' relaxation properties.

However, the common test methods discussed above may not always represent the degree of restraint experienced in actual composite members. Bentur (2001) stresses the need to resort to tests which provide information which is of physical relevance both in terms of material parameters and the nature of the structural system with respect to the restraint it produces.

To test the effects of overlay shrinkage restraint in real composite specimens, Vaysburd et al (2000) conducted a series of restrained shrinkage tests under site conditions, utilizing 3 different environments in North America. The program included the application of 12 selected cementitious repair materials in cavities on prefabricated concrete slabs (**Figure 2.17**), and the visual monitoring of the repair surfaces for a period of 18 months. The 12 repair materials tested showed a higher resistance to cracking than was originally anticipated. This was accounted to the workmanship and quality control during the project. In respect to environmental influences, it was concluded that a dry and hot climate in general has a detrimental effect on specimen performance.

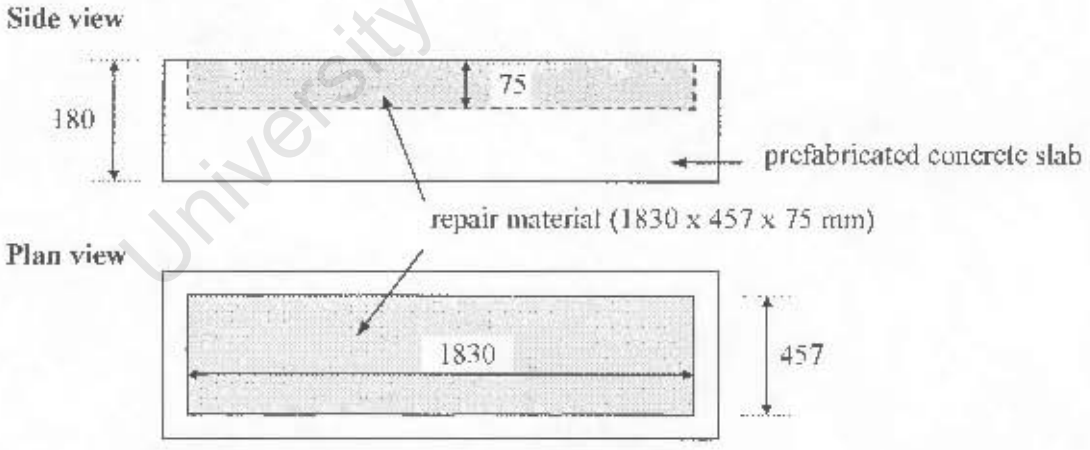

Figure 2.17: Restrained shrinkage specimens for site monitoring (Vaysburd et al, 2000)

Testing effects of differential shrinkage may be investigated with any kind of composite substrate-overlay specimen that is assumed to represent realistic conditions in terms of its measurement and exposure conditions.

Emmons et al (2000) developed a test for the estimation of strains and stresses due to restrained shrinkage in the form of a composite steel to concrete specimen. In this test, the concrete is cast on to a thin, 1300 x 100 mm steel plate, and the whole specimen clamped at its one end after the concrete has hardened (**Figure 2.18**). By measuring the curling deflection at the free end of the specimen, the time-depended stresses can be calculated.

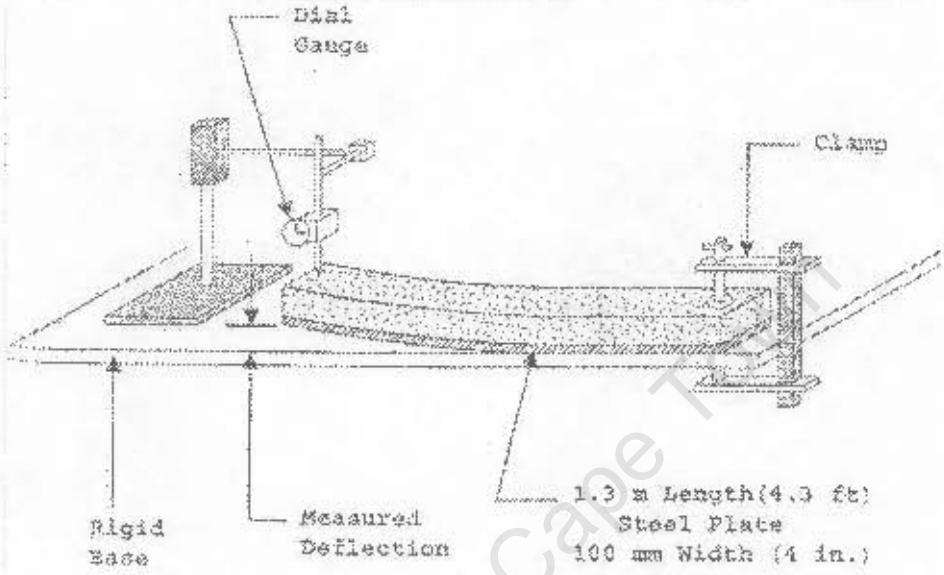

Figure 2.18: "SPS Plate Test" (restrained volume change strain/stress indicator) (Emmons et al, 2000)

2.4.7 Summary

Stresses due to differential volume changes have long been recognised as the main problem for the performance of bonded concrete overlays. Direct overlay stresses are caused by the restraint of expansion or contraction parallel to the interface, whereby tensile stresses resulting from constrained contraction are the most critical and can result in extensive overlay cracking. Bending stresses exist if curling, resulting from temperature or shrinkage gradients through the overly depth, is restrained. Bending stresses can result in considerable interface tension at the overlay boundaries and may thus initiate debonding.

Early age shrinkage and temperature effects may lead to cracking or debonding in the early days after overlay placement and are difficult to predict as overlay material properties are changing rapidly. Long-term temperature effects are problematic especially in thin overlays if substrate and overlay have significantly different coefficients of thermal expansion.

Differential shrinkage is generally considered to be the most critical influence on the long-term performance of composite members. The mechanisms of diverse shrinkage components

are well known. The effects of differential shrinkage on the performance of bonded overlays have however not been fully clarified yet. This is mainly due to the large number of influences on differential shrinkage stresses, which are difficult to assess individually and which include time-dependent material characteristics, environmental conditions, structural properties of the system, and the effects of workmanship. In a number of studies, common repair mortars were found to have excessive free shrinkage strains, which explains the general tendency of such materials to crack or debond. A number of test methods have been developed to investigate the development of stresses under restraint conditions. These methods generally serve as a valuable indicator of relaxation properties and can be used to estimate the influences of different mix constituents. For prediction of stresses in actual composite members however, these methods may not be practical as they commonly do not represent the degree of restraint experienced in real structures.

Research on structural effects of thermal volume changes and shrinkage has shown that creep and relaxation properties of the overlay have a major effect on the performance of composite members. Mechanisms of creep and relaxation are discussed in the following section.

2.5 Creep and relaxation characteristics

2.5.1 Introduction

Creep is defined as the time dependent deformation of concrete under sustained loading. It may also be manifested as a relaxation of stress under a constant deformation, which is the most important form of creep for concrete overlays subjected to differential shrinkage stress.

Creep terminology differentiates between basic creep and drying creep. Basic creep is defined as the creep that occurs when there is no drying shrinkage or moisture movement between concrete and the ambient environment. Drying creep is the additional creep that occurs when the concrete is also drying while being under stress. The distinction between the two is, however, commonly ignored for practical purposes and creep is simply considered as the deformation under load in excess of elastic strain and free shrinkage strain. Total creep strain is a sum of two components: reversible creep, which acts as time-delayed elastic strain under stress, and irreversible, or 'plastic' creep. Reversible creep reaches its maximum after a relatively short period of time and can simply be taken as 0.4 times the elastic strain, whereas plastic creep continues to increase for many years (Illston, 1979). Since for most design purposes only long-term creep is of importance, it is generally only the total creep strain that is considered in the design of concrete structures.

At service stress levels, creep strain in concrete is generally treated as a linear phenomenon and is thus proportional to applied elastic strain and elastic stress. On this basis, creep strain at a certain time t may be expressed as

$$\varepsilon_{creep}(t) = \frac{\sigma(t_0)}{E(t_0)} \cdot \varphi(t, t_0) = \varepsilon_{elastic}(t_0) \cdot \varphi(t, t_0) \quad [2.5]$$

where $\sigma(t_0)$ is the applied stress at age t_0, $E(t_0)$ is the elastic modulus at age t_0, and φ is a non-dimensional creep coefficient depending on the age of loading t_0 and the time t for which the strain is calculated. The coefficient φ represents the ratio of creep to instantaneous strain and its value increases with the decrease of age of loading t_0 and the increase of the length of the period $(t-t_0)$. The total strain due to elastic and creep deformations under constant stress applied at t_0 is

$$\varepsilon(t) = \frac{\sigma(t_0)}{E(t_0)} \cdot (1 + \varphi(t, t_o)) \quad [2.6]$$

Creep in concrete is affected by many external and internal factors such as temperature, humidity, mix composition, materials used, and the geometry of the member. The complexity of the factors influencing creep makes it very difficult to develop an approach which is applicable to all situations. The estimation of creep strains is therefore at best imperfect. Many publications are available in which empirical methods for the estimation of creep are presented (e.g. CEB, 1993a, EC2, 1991, ACI, 1992). Bangash (1991) presented a comprehensive summary of creep prediction models developed by national institutions and individual researchers.

Only the method proposed by ACI (1993) will be discussed here since it will be used at a later stage for the estimation of substrate creep strains in composite specimens. This method was chosen, as it is straightforward and hence easy to apply. According to the ACI (1992) method, the coefficient of creep at time t for age at loading t_0 can be estimated from the following hyperbolic function:

$$\varphi(t, t_0) = \frac{(t - t_0)^{0.6}}{10 + (t - t_0)^{0.6}} \cdot \varphi_u \quad [2.7]$$

The coefficient φ_u is the final creep after a very long time for an age of loading t_0 and is expressed as

$$\varphi_u = \varphi(t_\infty, t_0) = 2.35\,\gamma = 2.35\ \gamma_1\ \gamma_2\ \gamma_3\ \gamma_4\ \gamma_5\ \gamma_6 \quad [2.8]$$

The correction factors γ_1 to γ_6 account for the most important parameters which affect the magnitude of creep. A detailed description of these factors may be found in (ACI 1992). As stated above, creep prediction is at best imperfect. Alexander (2001) compared different creep prediction models with test results gained on South African concretes and concluded that the ACI method tends to underestimate creep strains.

The effects of creep on structural performance are generally manifested in a re-distribution of stress and an associated increase in deflections. In bonded concrete overlays, the beneficial effects of creep are the relief of tensile stresses induced by differential shrinkage or thermal strains.

Walraven and Shkoukani (1993) tested compressive creep and relaxation characteristics of concrete mixes subjected to restrained temperature deformations. They found stress relaxation to be approximately 30% and 10% in specimens which were 2 months and 5 years old respectively. They proposed stress- and temperature-dependent prediction models and concluded that creep increases significantly with increasing temperature. However, for bonded overlays, the first weeks after placement are the most important period for stresses resulting from restrained deformations. Relaxation in concrete members less than 2 months old is probably considerably higher than that measured in the above study.

2.5.2 Creep and relaxation under tensile stress

Most research on creep has been carried out for members under compressive loading. However, for stress relief in concrete overlays, it is mainly tensile creep relaxation that is of concern for the performance of the composite system. Rostàsy et al (2002) state that creep in tension is approximately equal to creep in compression. Kordina et al (2000) found creep in tension to be approximately 20% higher than creep in compression under similar stress conditions. Alexander (2001) states that creep in tension at a given tensile stress-strength ratio is of the same order of magnitude as compressive creep at a corresponding compressive stress-strength ratio. The initial rate of creep, however, may be higher in tension. Yuan and Marsszeky (1994) base the analysis of shrinkage-induced stresses on the assumption that the magnitude and rate of development of tensile creep are similar to those of compressive creep at low stress levels involved. Bissonnette and Pigeon (1995) conclude from their literature review that tensile creep is proportional to the applied stress if stress levels are kept below approximately 50-60% of the tensile strength. Similarly, Kordina et al (2000) tested a constant creep/stress ratio with loads up to 70% of direct tensile strength.

However, it should be noted that bonded concrete overlays often experience tensile stress that exceeds tensile strength, which commonly results in extensive cracking. The assumption that the specific creep does not depend on the stress/strength ratio might, therefore, be inaccurate for bonded concrete overlays that experience very high stress levels when subjected to differential shrinkage or thermal deformation. According to Kordina et al (2000), tensile stress relaxation, in contrast to compressive stress relaxation, increases if the concrete member has experienced a certain degree of pre-cracking. According to their research, tensile stress caused by restrained shortening always causes micro-cracking if it reaches magnitudes close to the tensile strength.

Pigeon and Bissonnette (1999) found a constant ratio between specific tensile creep and free shrinkage strain and used this value as an indication of the relaxation capacity of the material under restrained shrinkage. Since tensile creep can determine the performance of concrete overlays to a large extent, they suggest the use of the ratio between specific creep (i.e. creep under sealed conditions) and free shrinkage as a dimensional compatibility index for concrete repair materials. For the particular concrete mix they tested, the ratio between specific tensile creep and free shrinkage was 0.25.

Estimation of relaxation is usually based on creep strain characteristics. However, the relaxation of stress under applied strain might be different to creep strain under applied stress. For a more accurate prediction, a direct relaxation function may be used. Horimoto and Koyanagi (1994), and Gutsch and Rostásy (1994) proposed relaxation functions for concrete under tensile stress due to restrained thermal movement. According to Horimoto and Koyanagi (1994), the ultimate tensile creep relaxation of specimens loaded after 1 and 3 days is approximately 25% and 15% of the initial stress respectively. In their tests, it took only 2-3 hours to reach the ultimate values of tensile relaxation. Both ultimate relaxation values and time to ultimate relaxation were measured irrespective of the stress-strength ratio which ranged from 0% to 60%.

Tests carried out by Gutsch and Rostásy (1994) also showed that the initial stress-strength ratio has no significant influence on tensile creep relaxation. However, contrary to Horimoto and Koyangani, they found continuous relaxation for more than 100 hours of testing and proposed a time dependent relaxation function:

$$\Psi(t-t_1,\alpha_1)=\frac{\sigma(t,t_1)}{\sigma(t_1)}=\exp\left[-P_1(\alpha_1)\left(\frac{(t-t_1)}{t_k}\right)^{P_2(\alpha_1)}\right] \qquad [2.9]$$

where α_1 is the degree of hydration at time t_1, t_1 denotes the time of first loading, t_k is a constant (t_k = 1h), and P_1 and P_2 are empirical functions of the degree of hydration α_1 and can be derived from relaxation tests. Gutsch and Rostásy used 2 concrete mixes for their tests and found that approximately 10-20% and 15-25% of initial tensile stress were released after 1 and 10 hours respectively. Relaxation after 100 hours was found to be 35-50%. Kordina et al (2000) tested different concrete mixes for tensile relaxation and found that maximum relaxation values were reached after 2 days. In their tests, relaxation reduced tensile stress to approximately 40-50% of initial tensile stress.

2.5.3 Creep under incremental loading

In most research projects, experimental work on the evaluation of creep characteristics has been done under constant stress situations and the results are not necessarily applicable for

the evaluation of creep under incremental load conditions such as differential shrinkage in composite members. The linear relationship between creep and stress at low stress levels allows the *Boltzmann* superposition principle to be applied to concrete subjected to incremental loading. According to this viscoelastic law, the total creep ε_{creep} at the time t can be estimated by summing the creep strains of the individual stress increments applied at different ages during the preceding stress history (Illston, 1979, Walraven and Shkoukani, 1993, Müller and Kvitsel, 2002). Numerically this may be expressed as

$$\varepsilon_{creep}(t) = \sum_{i=1}^{n} \frac{\Delta\sigma_i}{E_i} \varphi(t, t_i) \qquad [2.10]$$

for n increments of stress, where $\Delta\sigma_i$ is the stress increment applied at time t_i, E_i is the elastic modulus at time t_i, and $\varphi(t, t_i)$ is the creep factor for the time period $(t-t_i)$. More generally, for a continuous variation in stress, as is for the case of ongoing differential shrinkage, the creep at time t for a first age of loading of t_1 is given by:

$$\varepsilon_{creep}(t) = \int_{\tau_1}^{t} \frac{d\sigma(\tau)}{d\tau} \cdot \frac{\varphi(t,\tau)}{E} \cdot d\tau \qquad [2.11]$$

(Illston, 1979). For calculation of creep in a young concrete overlay, the change in elastic modulus with time would have to be considered in the above formula. For practical design purposes, Trost (1967) developed a simplistic form of equations [2.10] and [2.11]:

$$\varepsilon_{creep}(t) = \frac{\sigma_0}{E} \cdot \varphi(t, t_0) + \frac{\sigma_t - \sigma_0}{E} \rho\varphi\ (t, t_0) \qquad [2.12]$$

where ρ is an aging coefficient that considers that the stress $(\sigma_t - \sigma_0)$ has been applied in increments during the period $(t - t_0)$. The aging coefficient ρ commonly ranges between $0.5 < \rho < 1.0$ (Müller and Kvitsel, 2002). According to Walraven and Shkoukani (1993), the value of ρ varies very little between different practical conditions and may be taken as 0.8 for all concretes under "normal" load conditions with creep factors of $1.5 < \varphi(t, t_0) < 4$. More accurate values for ρ were presented by CEB (1993 b).

2.5.4 Summary

Creep mechanisms play an important role for the performance of bonded concrete overlays. Various creep prediction models have been developed. However, estimation of creep is at best imperfect as the development of creep strains and stress relaxation depends on a large range of complex influences.

Most information available deals with creep under compression. However, for bonded overlays, tensile relaxation of stress is of much greater significance. Various research projects have shown that creep in tension can generally be considered to be similar to that under compression. In a number of studies, tensile relaxation was found to develop rapidly after loading, with relaxation decreasing stress levels to approximately 40-60% of initial stress.

CAPTER 3

EXISTING ANALYTICAL MODELS FOR CALCULATING SHRINKAGE-INDUCED STRESSES IN BONDED CONCRETE OVERLAYS

3.1 General

Models for the analysis of differential shrinkage stresses in composite members can basically be divided into analytical and numerical approaches. Numerical approaches are difficult to find in the literature since they normally consist of computer programmes which cannot easily be presented in the form of papers. Publications on numerical models usually concern results gained from a certain computer programme that was used in conjunction with specific input parameters. In that respect, they do not present an analytical tool that can be used in engineering practice unless the actual programme is made available. By contrast, analytical models usually consist of one or more equations with which composite behaviour can be computed. Refinement of analytical models can be carried out by FEM programmes, using the same, or more, relevant input parameters. The focus of this section rests on existing analytical approaches. In addition, a numerical approach based on FEM analysis is discussed in Section 3.6.

A number of analytical approaches for the modelling overlay stresses due to shrinkage restraint have been developed. In the following sections, the basic theories of these models are presented and discussed. For clarity, the models are discussed individually. The order in which these models are presented was chosen to facilitate the understanding of structural issues related to differential shrinkage stresses. This chapter therefore presents a stepwise introduction into existing tools for the analysis of composite members, starting with the discussion of the simplest models to aid the reader to familiarize him- or herself with the topic. However, during the individual discussion of each model, reference may be made to other analytical approaches to highlight important aspects. Similarities and differences between the models are discussed and summarized in Section 3.9. Models presented by different researchers which are based on the same principles are summarized in each respective section. The sections are named after the researcher who first introduced the model under consideration.

3.2 Evans and Parker (1955)

Evans and Parker (1955) model the effects of differential shrinkage through tensile and compressive forces (F_t and F_c) of equal magnitude acting on the overlay and substrate respectively. Considering that the interface is the location of restraint, both F_t and F_c are assumed to act at the vertical boundaries of the member at the interface. To facilitate analysis

of stresses and strains, overlay and substrate are imagined to be unbonded. F_t and F_c produce direct stresses and bending moments in overlay and substrate respectively. Interface strains can be calculated using the respective sections properties of overlay ($Z_{O,i}$) and substrate ($Z_{S,i}$) at the interface. The magnitudes of F_t and F_c are then evaluated from the compatibility of direct strains at the interface **(Figure 3.1)**.

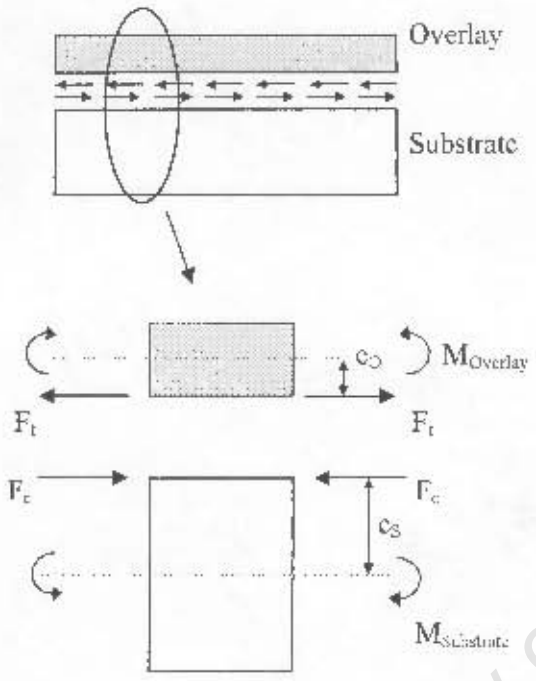

Bending moments due to F_t and F_c:

$$M_{Overlay} = F_t.e_O$$
$$M_{Substrate} = F_c.e_S$$

Tensile overlay strain at the interface $\varepsilon_{O,i}$:

$$\varepsilon_{O,i} = \frac{\frac{F_t}{A_O} + \frac{F_t.e_O}{Z_{O,i}}}{E_O}$$

Compressive substrate strain at the interface $\varepsilon_{S,i}$:

$$\varepsilon_{S,i} = \frac{\frac{F_c}{A_S} + \frac{F_c.e_S}{Z_{S,i}}}{E_S}$$

Compatibility of interface strains in the bonded section $\Rightarrow \varepsilon_{O,i} - \varepsilon_{S,i}$

Figure 3.1: Evaluation of differential shrinkage stresses, according to Evans and Parker (1955)

"Partial restraint" of overlay shrinkage refers to the situation where the overlay is allowed to undergo a portion of its shrinkage deformations, as opposed to full shrinkage restraint where the overlay does not undergo any deformation at all. Evans and Parker consider partial restraint of overlay shrinkage based on relative member stiffnesses of substrate and overlay. Modelling the resulting stresses through a force acting at the interface appears reasonable as the interface is the location of restraint and hence the location of stress initiation in both substrate and overlay. However, the above analytical approach solely depends on compatibility of interface strains, whereas full bond also corresponds to the compatibility of interface curvature. The latter is not taken into account in the model, as overlay and substrate are imagined to deform independently from each other. Saha (1998) tried to improve the model by incorporating equations that account for curvature resulting from both differential shrinkage and self-weight of the members. However, the suggested improvements cannot

account for compatibility of interface curvature either, which shows the difficulties in using the above approach.

3.3 Birkeland (1960) and the prestress analogy

A model developed by Birkeland (1960) applies a compressive force F_c to a bonded composite beam section, which is of magnitude equal to the tensile force F_t needed to cancel free shrinkage strain ε_{FSS} on an unbonded overlay (**Figure 3.2**).

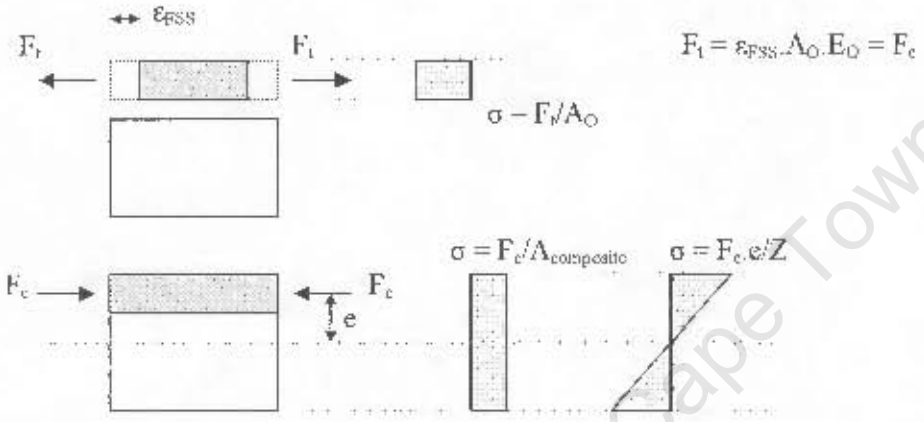

Figure 3.2: Modelling differential shrinkage stresses according to Birkeland (1960)

The model's analytical procedure can be divided into 3 stages: firstly, the overlay is imagined to be separated from the substrate beam and allowed to shrink freely. A tensile force F_t is then applied in the centre of the overlay cross-section to cancel free shrinkage strain. Secondly, overlay and substrate are now bonded together and F_t is cancelled through a compressive force F_c of equal magnitude, acting on the whole member. F_t and F_c act in the same line. Thirdly, stresses from the first 2 stages are superimposed.

The sum of stresses generally leads to tension in the overlay and bottom of the substrate, and compression at the top of the substrate. Curvature induced by restrained shrinkage generally causes contraction in the overlay, and relieves some of the tensile stress. A stiff substrate element, e.g. large section properties, results in the minimisation of curvature and hence in maximum overlay stress.

The external load applied to the boundaries of the composite member, i.e. the beam ends, causes a constant moment and hence constant direct stress along the member length. According to conventional beam analogy, shear stress along the member is created through the change in direct stress, which in turn corresponds to a change in bending moment (**Figure 3.3**). Constant direct stress results in the non-existence of shear. Conventional beam

analogy in connection with the assumption of constant direct stress can, therefore, not account for interface shear stress due to restrained overlay shrinkage.

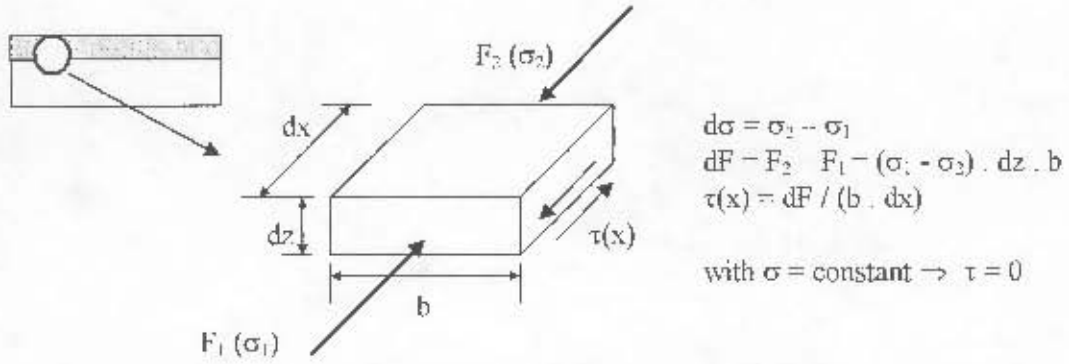

Figure 3.3: Relation between restrained normal stress and shear stress in conventional beam analogy

Birkeland applies essentially the same theory as that used in the structural analysis of bonded prestressed members. The fabrication of prestressed concrete members includes the elongation of the prestress strand by an outside force F_t, which is transferred to the beam as a compressive force F_c by cutting the ends of the strand once the concrete has hardened (**Figure 3.4**).

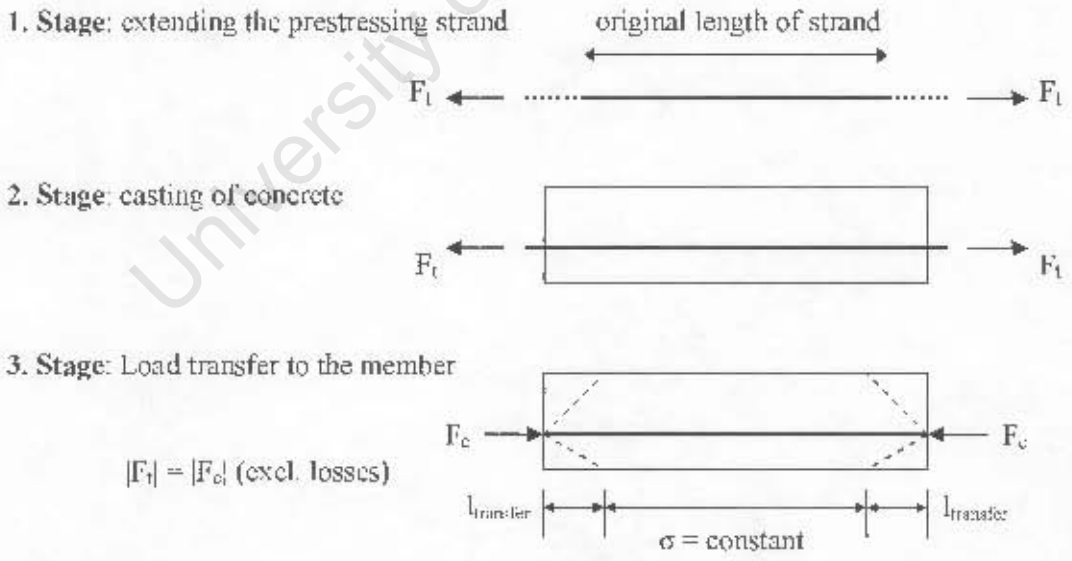

$l_{transfer}$ – length of prestress transfer through interface bond between steel and concrete

Figure 3.4: Load transfer in bonded prestressed members

Compressive stress in the section develops in the member end zones through interfacial bond between steel and concrete. Interface shear bond stress, therefore, develops only at the ends

of the strand over the length that is needed to establish a constant direct stress (e.g. Thomsing, 1998). This is rational and easy to agree with, as the location of initiation of compressive stress, and thus the activation of bond stress between steel and concrete, is the end of the member. By cutting the ends of the strand, the strand tends to slip into the hardened concrete, starting from the ends, which makes the restraint of slip a local phenomenon at the member ends.

Birkeland's analytical model has the advantage of being based on a simple and (apparently) logical theory. At first sight it seems reasonable to apply the prestress analogy to the problem of bonded overlays subjected to differential shrinkage. However, Birkeland's illustration of force application at the ends of the beam misjudges the location of stress initiation. Overlay shrinkage is restrained at the interface along the whole length of the member, and can thus not be transformed into a single external force acting only on the member ends. The analogy to prestressed concrete members thus fails in modelling the actual stress initiation. The issue of the location of stress initiation is very important. During the development of a new analytical model, as discussed in Chapter 6, this issue will be dealt with in detail. At this stage it should be noted that all existing analytical approaches model differential shrinkage through forces applied at the member ends, irrespective of the circumstance that differential shrinkage is restrained along the whole interface between substrate and overlay.

The basic ideas of Birkeland's analytical approach have been used in a number of numerical models developed at a later stage. Evans and Chung (1967) extended Birkeland's model to account for the effect of eccentrically placed overlay reinforcement and the bending stresses resulting therefrom. It is interesting to note that Evans, by adopting Birkeland's theory, seems to have discarded his own analytical model (Evans and Parker, 1955), which was presented in Section 3.2. Yuan and Marsszeky (1994) and Yuan et al (2003) directly adopted Birkeland's approach, which was originally developed for precast concrete elements with in-situ overlay, to model stress in repaired concrete members. Other modifications and adoptions of this method are discussed in more detail the following sections.

3.4 Alonso Junghanns (1997)

When estimating stresses due to differential shrinkage, the first, and one of the most important, classifications to be made is that of the degree of restraint from the substrate. Partial restraint infers that overlay shrinkage directly causes a certain degree of substrate contraction, allowing the overlay to undergo a portion of its free shrinkage deformation.

Alonso Junghanns (1997) analysed differential shrinkage tresses in concrete repair patches and considered the degree of shrinkage restraint to depend on the ratio of substrate and overlay stiffness:

$$\varepsilon_O = \varepsilon_S = \frac{\varepsilon_{FSS}}{1 + \frac{A_S \cdot E_S}{A_C \cdot E_C}} \qquad [3.1]$$

The above equation is based on the assumption that the deformations of the overlay (ε_O) and the substrate (ε_S) are equal and constant across the whole member depth. The whole member, therefore, undergoes the same linear deformation and curvature is not considered. This theory can be related to a resultant force F_{res} acting in the centroid of the whole member. **Figure 3.5** shows the attempt to schematically present the above theory.

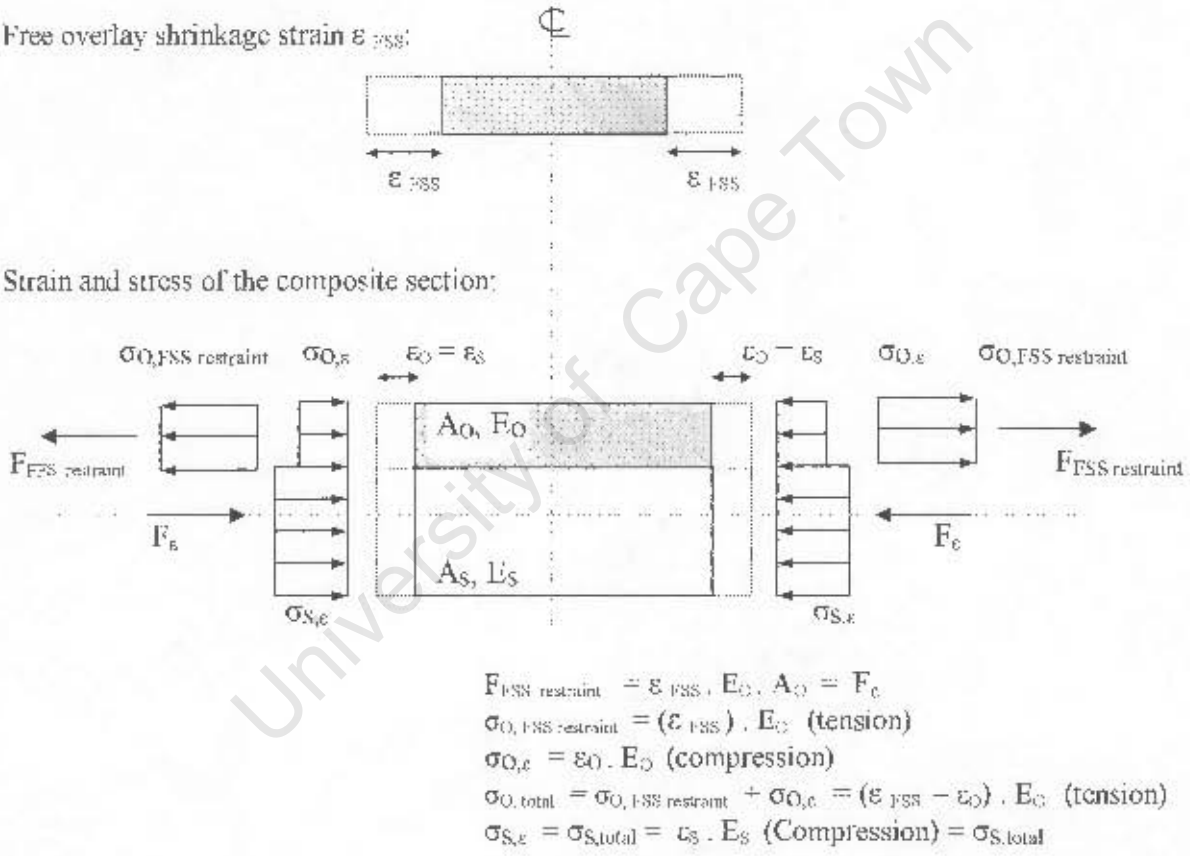

Figure 3.5: Stresses and strains due to differential shrinkage, schematic based on the model presented by Alonso Junghanns (1997)

The overlay experiences tensile stress due to the full restraint of free shrinkage deformations. The resulting tensile force of the overlay is counteracted by a compressive force of equal magnitude acting at the centre of gravity of the composite member. The compressive stress induced in the whole cross section relieves parts of the tensile overlay stress. Resultant overlay and substrate stresses are dependent on the stiffness ratio, and hence on the elastic properties and cross-sectional areas of both overlay and substrate. A substrate of infinite

stiffness would result in total restraint of overlay shrinkage and maximum overlay stress, while equal stiffness of overlay and substrate, i.e. equal cross-sections and elastic properties, would result in 50% - restraint of overlay shrinkage.

Consideration of partial restraint, based on elastic properties of the composites seems logical and reasonable. However, the consideration of member stiffness through conversion of restraint overlay shrinkage into a linear deformation of the whole member as shown in Figure 3.5 is not realistic, as this does not respect the circumstance that differential shrinkage stresses are initiated at the interface. The assumption that the centroid of the composite member can be considered as the point of load application is too simplistic to yield reasonable results in the analysis of stresses and strains.

The analytical approach used by Alonso Junghanns is essentially the same as that presented by Birkeland (see Section 3.3), however with the difference that the force from overlay shrinkage is considered to act at the centre of gravity of the composite member, which does not account for possible curvature due to eccentric load application.

Alonso Junghanns used the above analytical model to estimate shrinkage stresses in repair mortars bonded to stiff substrates, i.e. repair mortars experiencing full restraint of shrinkage. Practical laboratory work was carried out using fully restrained mortar specimens clamped into rigid steel frames (**Figure 3.6**).

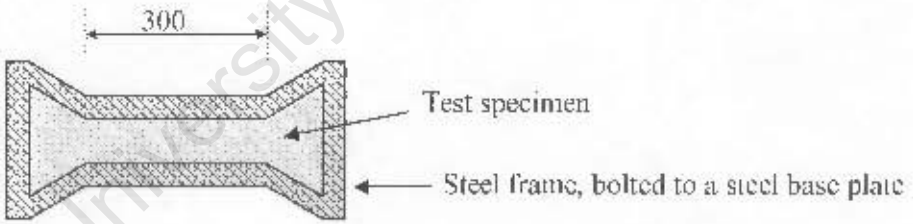

Figure 3.6: Test frame for the evaluation of stresses resulting from complete shrinkage restraint (Alonso Junghanns, 1997)

The development of time-dependent tensile stresses measured on the specimens presented in Figure 3.6 conformed relatively closely to the above theory. However, full restraint of shrinkage does not represent real-life conditions, where the elasticity of the substrate material will always allow a certain deformation at the interface. The test set-up was, therefore, designed to fit the theoretical model, irrespective of the actual applicability of the model to practical situations.

3.5 Bernard (2000)

Denarié presented a model to calculate normal stresses due to differential shrinkage in composite beams with complete bond. This model was part of a publication prepared by Denarié and Silfwerbrand (2004) and is based on an approach first developed by Bernard (2000). The model is based on the assumption that overlay shrinkage restraint is related to the amounts of axial and flexural "freedom" of the composite section, where "freedom" is defined as a lack of deformational restraint. Axial freedom is calculated following the same principles as those used by Alonso Junghanns, as discussed in Section 3.4 (compare equation 3.1). Flexural freedom is based on the ability of the member to deflect under an applied bending moment. The principle of the analysis consists in balancing the tensile force in the overlay in the composite member by a compressive force and a bending moment acting at the centroid of the composite section. Therefore, the method used by Denarié corresponds to the method introduced by Birkeland (1960), as discussed in Section 3.3, using the same assumptions and the same calculations. Denarié associates the degree of overlay shrinkage restraint to the effect of release of the stress for each degree of freedom:

$$\mu = \frac{\sigma_{full} - \sigma_N - \sigma_M}{\sigma_{full}} = 1 - \mu_N - \mu_M \qquad [3.2]$$

where

μ = degree of restraint

σ_{full} = tensile overlay stress at the interface, assuming full restraint of overlay shrinkage

σ_N = stress relief due to axial deformation of the composite member

σ_M = stress relief due to flexural deformation of the composite member

μ_N = factor accounting for shrinkage restraint resulting from axial deformation of the composite member "axial release"

μ_M = factor accounting for shrinkage restraint resulting from flexural deformation of the composite member "flexural release"

Figure 3.7 shows a graphical representation of the method used by Denarié (Denarié and Silfwerbrand, 2004) for a rectangular beam with E_O = 25 GPa and E_S = 35 GPa. Axial release of overlay stress increases in a monotonic way when the overlay thickness increases. The flexural release first increases with increasing overlay depth, passes a maximum and then decreases to below zero. The decrease to below zero relates to the case where the overlay is thicker that the substrate, which results in negative curvature strain in the overlay, i.e. tensile strain, hence increasing tensile overlay stress. For the chosen set of parameters, the global restraint varies significantly for overlay depths smaller than approximately 30% of

the substrate depth. However, for overlays with depths greater than approximately 30% of the substrate depth, the overall degree of restraint is relatively constant at 0.5 – 0.6.

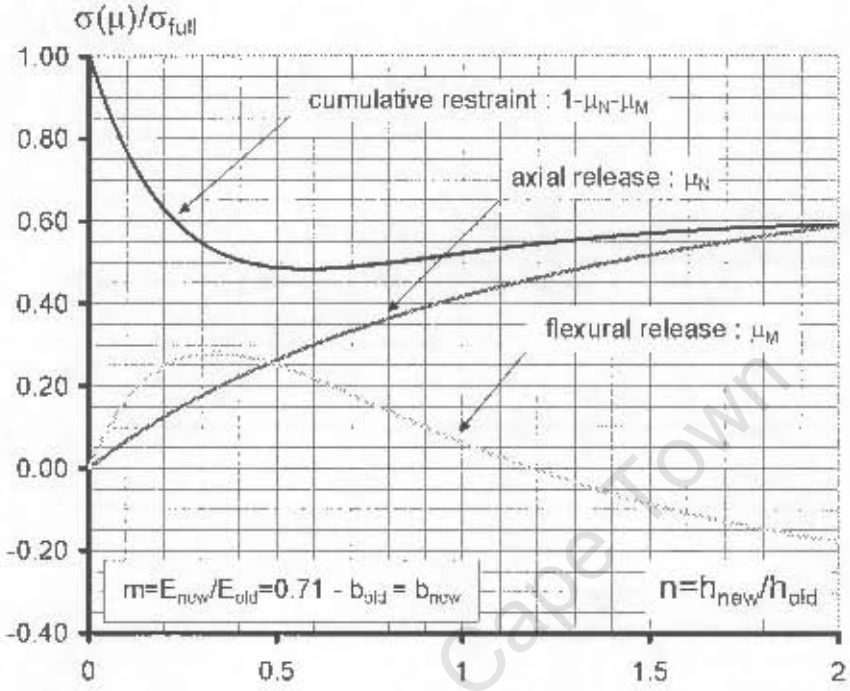

Figure 3.7*: Principle of restraint of overlay shrinkage as a function of axial and flexural freedom of the composite member (Denarié and Silfwerbrand, 2004)

* In Figure 3.7 are:

σ_μ = actual tensile overlay stress at the interface, taking into account axial and flexural degrees of freedom

Notation "new" refers to the overlay, notation "old" refers to the substrate

The method presented by Denarié represents a useful and illustrative tool for the practical application of the theory originally introduced by Birkeland (1960). However, as stated previously, Birkeland's theory is too simplistic to model strains and stresses in composite members realistically. The assumption that stresses due to differential shrinkage can be modelled through forces applied at the member ends does not account for the real location of load application, which is the interface. This point will be discussed in detail in Chapter 6.

3.6 Hartl (1983)

Hartl (1983) assumed that restrained overlay shrinkage stress is transferred to the substrate only at the boundaries, i.e. the ends and sides, of the composite member. This is also reflected in later models presented by Klopfer (1987), Haardt and Hilsdorf (1988), and Haardt (1991). Haardt and Hilsdorf extended Hartl's theory by differentiating between two types of overlay boundary conditions, namely free member ends and vertically bonded member ends (**Figure 3.8**).

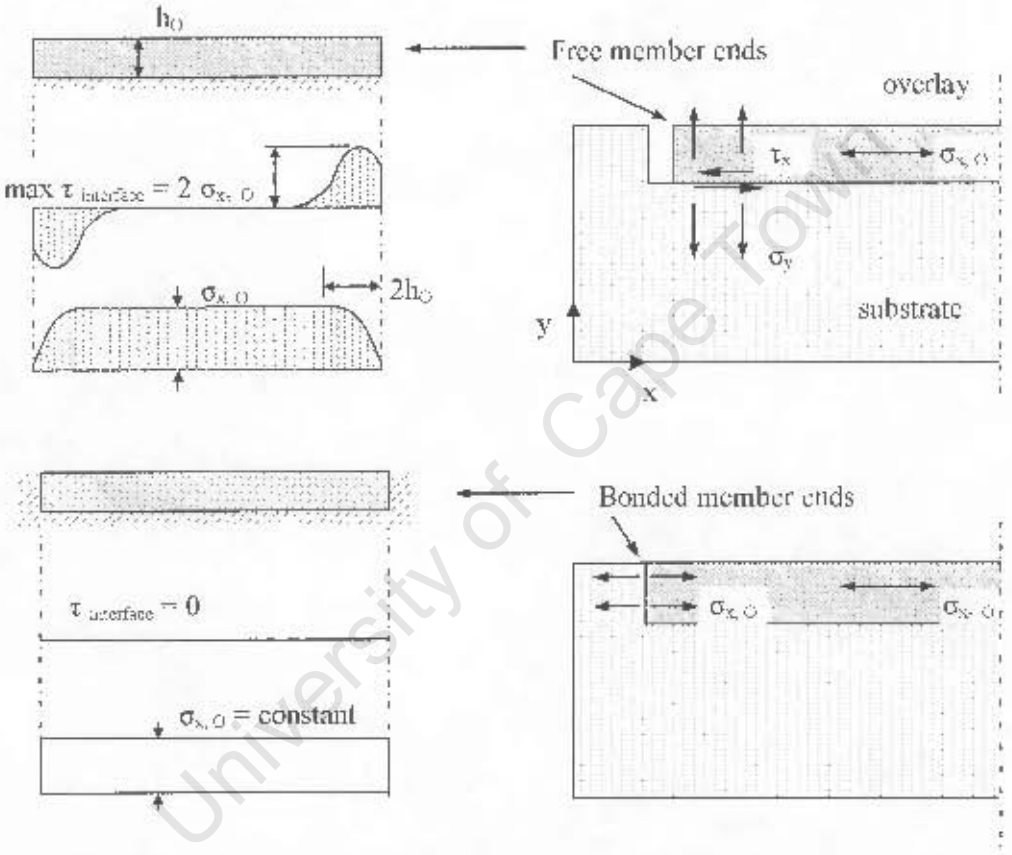

Figure 3.8: Systems with bonded and unbonded (free) vertical overlay perimeters. Transmission of restrained overlay shrinkage forces into the substrate, and overlay stresses (direct stress: $\sigma_{x,O}$) and interface shear stress ($\tau_{interface}$) according to Haardt and Hilsdorf (1988).

According to this theory, free member ends result in a horizontal zone of force transmission between overlay and substrate. Analogous to the induction of concentrated forces into a concrete member, e.g. columns resting on concrete foundations, the slope of force transmission is assumed to be 2:1, which results in a force transmission zone length of twice the overlay depth. The force transmission zone is needed to establish constant direct stress conditions. Following the same relationship between direct stress and shear stress as presented in Section 3.3, this zone of changing direct stress is the only location where

interface shear occurs. Vertically bonded overlay ends, on the other hand, result in constant direct stress along the whole length of the overlay, which eliminates any interface shear stresses.

As discussed in Section 3.3, from a logical point of view it seems unlikely that stresses due to differential shrinkage are only transmitted at the ends of the member, considering that every increment of the overlay is experiencing shrinkage and the overlay is bonded to the substrate along its full length. This misconception of stress transfer is in particular apparent in the case of vertically bonded overlay boundaries as presented in Figure 3.8. In that respect, the above model represents a purely academic attempt to analyse stresses from differential shrinkage without correlation to what actually happens in the member.

In 2000, Hartl presented a parameter study on the influences of different overlay and substrate material properties on direct stresses in the overlay fibre at the interface. The study was based on the theory discussed above, i.e. it was assumed that stresses due to differential shrinkage are transferred at the member ends only. With that assumption, stresses and strains in the member can be calculated using common structural analysis, e.g. using Birkeland's theory, as discussed in Section 3.3. In his parameter study, Hartl accounted for the influences of overlay shrinkage, overlay relaxation, overlay thickness, and elastic moduli of overlay and substrate. Results were expressed in relation to a reference concrete member with an overlay depth of 20 mm. The results of this study are presented in **Figures 3.9 A to E**.

According to the above parameter study, the most significant influences are those of shrinkage strain and elastic modulus of the overlay. The influences of overlay thickness and elastic modulus of the substrate refer to the influence of the relative stiffnesses of overlay and substrate. A thicker overlay, as well as a substrate of lower elastic modulus, result in a lower ratio between overlay and substrate stiffness and hence in a lower degree of shrinkage restraint. The above parameter study was conducted for a substrate member of finite thickness, however without stating the substrate thickness used in the study. On a substrate beam of infinite thickness, the influences of overlay thickness and elastic modulus of the substrate should be negligible as an infinite substrate thickness, according to Hartl, results in full restraint of overlay shrinkage.

As stated earlier, the assumption that stresses are only transferred at the member ends leads to unrealistic results. The above parameter study is therefore believed to not represent realistic stress conditions in the overlay. However, Hartl's approach to present the influences of different parameters separately in graphic form seems very useful as it gives a good overview and indicates the main assumptions that the model is based on.

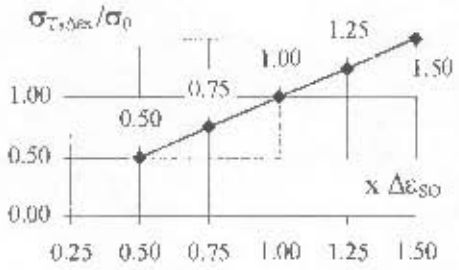

A: Overlay shrinkage strain ε_s

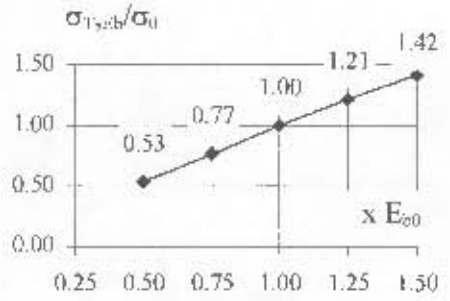

B: Elastic modulus of the overlay E_b

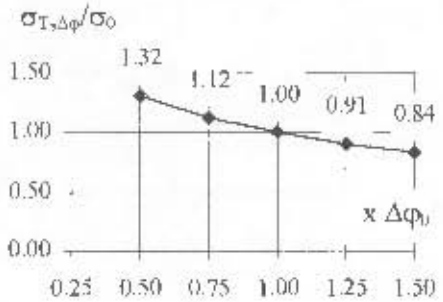

C: Overlay relaxation φ

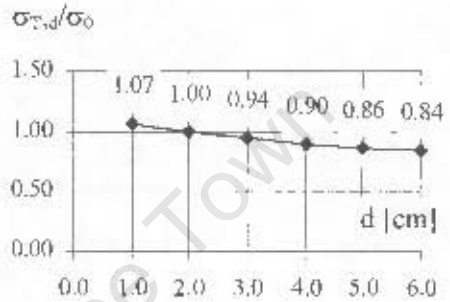

D: Overlay thickness d

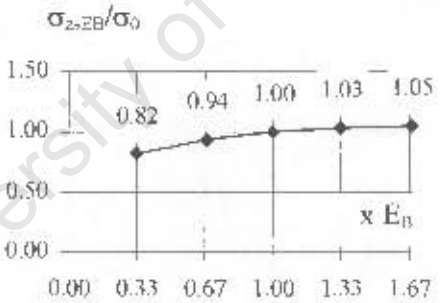

E: Elastic modulus of the substrate E_s

Figures 3.9 4 A to E*: Selected parameter influences on restrained shrinkage stresses in a concrete overlay. Figures redrawn from Hartl (2000).

* In Figures 3.9 are:

σ_T = Tensile stress due to shrinkage, influenced by the change in magnitude of the relevant parameter

σ_0 = Tensile stress due to shrinkage for the initial magnitude of the relevant parameter

$_0$ = index: initial magnitude

3.7 Haardt and Hilsdorf (1988)

In respect to the degree of substrate restraint, i.e. the ability of the substrate to restrain overlay shrinkage deformations, Haardt and Hilsdorf (1988) linked the ratio between overlay and substrate stiffnesses to overlay stress. Their findings were based on FEM analysis. They considered that the substrate allows the overlay to undergo a portion of its shrinkage deformation. In comparison to full restraint, this results in lower overlay stress. Haardt (1991) presented a more detailed version of these findings, which are summarized in **Figure 3.10**.

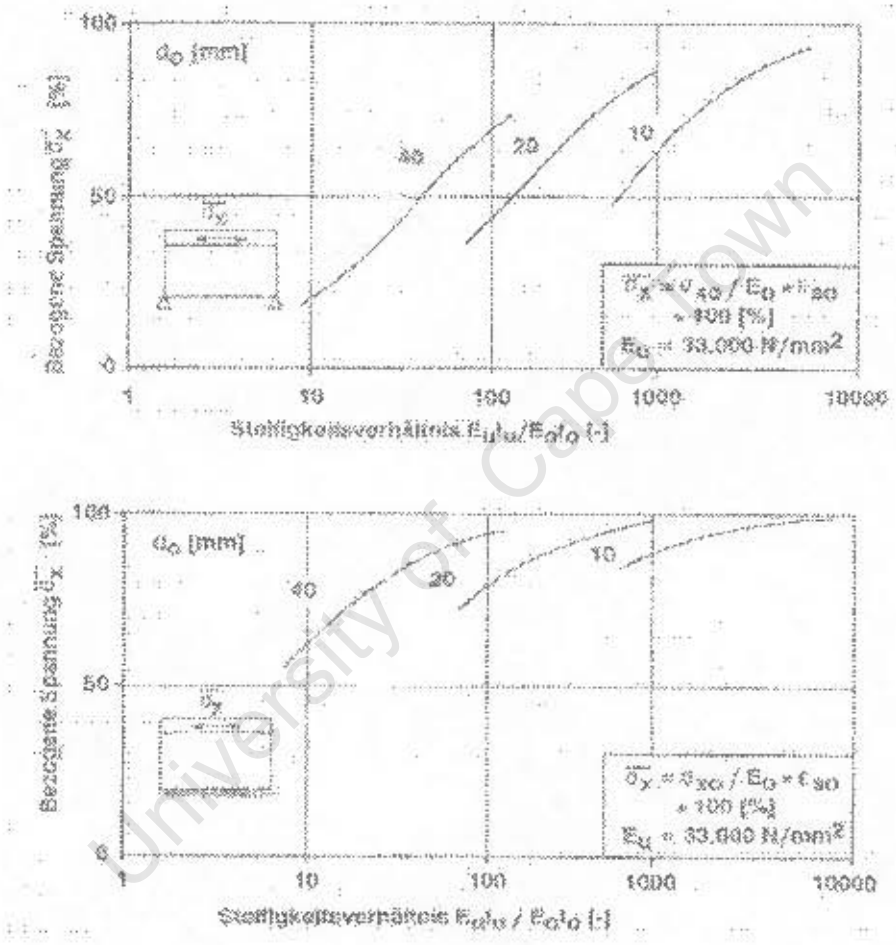

Figure 3.10*: Direct overlay stress due to restraint shrinkage in relation to stiffness ratio between substrate and overlay. Top: the substrate is free to deform, bottom: the substrate cannot deform (Haardt, 1991)

*In Figure 3.10 are:

σ_{XO} = mean overlay stress due to shrinkage restraint

E_O = modulus of elasticity of the overlay

E_U = modulus of elasticity of the substrate

$E_U I_U / E_O I_O$ = Stiffness ratio between substrate and overlay

ε_{SO} = overlay shrinkage strain

d_O = overlay thickness

According to Haardt, the degree of shrinkage restraint depends to a large extent on the deformability of the composite member, i.e. on the freedom to curve (compare top and bottom graph of Figure 3.10). Curvature results in additional compressive strain in the overlay and hence in a relief of tensile stress. Haardt's findings show that the ratio between substrate and overlay stiffnesses is not the only parameter in determining the degree of restraint. This stands in contrast to models based on the prestress analogy (Sections 3.3 to 3.6).

However, Haardt's results as presented in Figure 3.10 seem to be somewhat unrealistic. For example, it is startling that a stiffness ratio $E_U I_U / E_O I_O$ of 100 leads to much lower stress than a stiffness ratio of 1000 (Figure 3.10 - top, overlay depth d_0 = 10 mm). In practice, a stiffness ratio of 100 could be considered exceptionally high and any value beyond 100 should not influence the stresses to such a significant extent. Further, on composite sections with relatively high stiffness ratios, the difference between elements that are free to deform (Figure 3.10 - top) and those that are not (3.10 - bottom), should be less pronounced. For example, an overlay of 10 mm depth, whose stiffness is 1000 times less than that of the substrate, should not cause major deformations of the composite member even if the composite member was free to curve. However, Haardt's model concludes that in such an element, when compared to a composite member that cannot curve, overlay stresses are much less.

In that respect, Haardt's findings may merely be considered to qualitatively indicate certain trends. The use of the numerical values in the analysis of composite members would not yield reasonable results.

3.8 Silfwerbrand

Silfwerbrand (1997) developed a model for restrained overlay shrinkage stresses and strains in simply supported beams, which is very different to any other analytical approach that can be found in the literature. The model is based on a linear relationship between slip and shear stress at the interface, and uses the following assumptions:

- Shrinkage restraint causes overlay slip at the interface and curvature of the whole member
- Overlay slip and curvature of the composite member determine stress development in the overlay
- Interface shear stress is directly proportional to overlay slip at the interface. Without slip, there is no shear stress.
- Direct stresses and curvature are variable along the length of the member, with a maximum at mid-span of the beam (**Figure 3.11**)

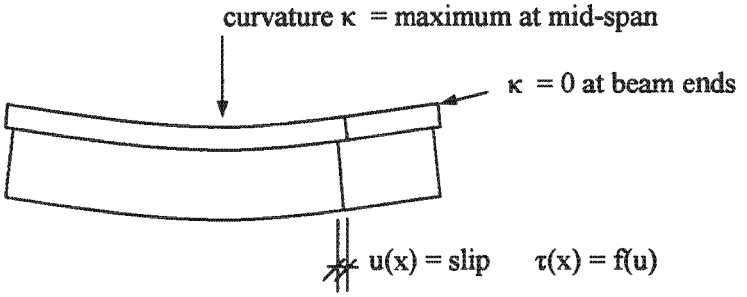

Figure 3.11: Curvature and interface slip due to restrained overlay shrinkage in a simply supported beam, according to Silfwerbrand (1997)

Slip, curvature, and direct stress are estimated using an empirical bond constant λL that describes the effectiveness of interfacial bond. Silfwerbrand explains the linear relationship between slip and interface shear with mechanical friction between overlay and base. However, interfacial bond between substrate and overlay consists of mechanical, chemical, and physical adhesion, cohesion, and interlock mechanisms (compare Section 2.3.2). Mechanical friction can only be activated once these bond mechanisms have been partly, or completely, destroyed. In practical terms, therefore, interface slip corresponds to a loss of bond, and should at best be avoided in modelling the behaviour of fully bonded overlays.

Silfwerbrand's approach differs significantly from most other analytical models in that it assumes a change in normal stress along the member (**Figure 3.12**), which, in addition to slip at the interface, is the second origin of interface shear stress. However, his calculated interface shear values have a high peak at the beam end and approach zero in inner regions of the member (**Figure 3.13**), which corresponds to the shear stress distribution suggested by the models discussed previously (Sections 3.2 to 3.6).

A disadvantage of Silfwerbrand's theory lies in the complexity of the suggested analytical equations, which makes the model rather cumbersome and user-unfriendly. Further, the verification of the analytical model was done using a very limited number of test results which were interpreted in strong favour of the model. The outcome of the analysis depends to a major extent on the bond constant λL. This bond constant has to be determined empirically, i.e., through strain measurements on composite beams, which was done for a single interface texture only. It was not questioned or tested if different interfaces would in fact result in different strain values and hence in different bond constants. The practical tests carried out to verify the model were, therefore, insufficient to allow any conclusions on the applicability of the model.

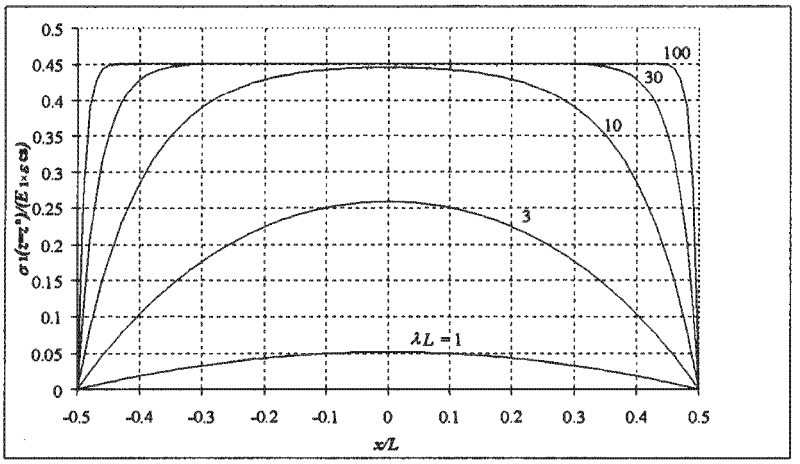

Figure 3.12: Example of restrained normal stress at the bottom of the overlay as a function of the bond constant λL (Silfwerbrand 1997).

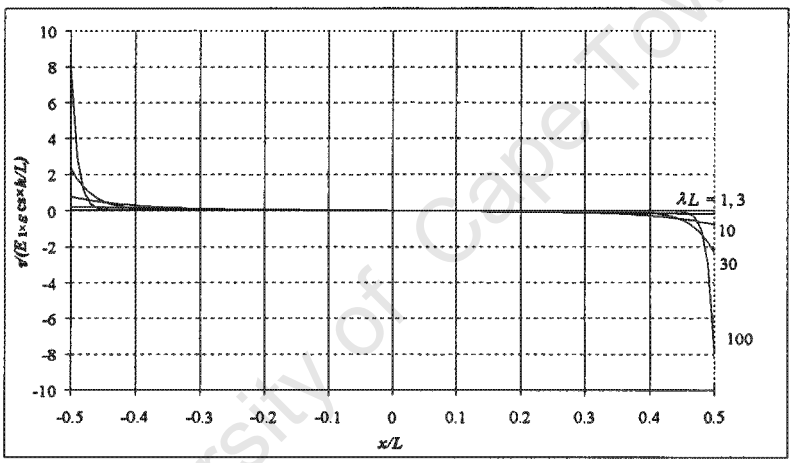

Figure 3.13: Example of interface shear stress as a function of the bond constant λL (Silfwerbrand 1997).

3.9 Summary and discussion

The existing analytical models for bonded concrete overlays discussed in Sections 3.2 to 3.8 are based on common beam theory, and as such they attempt to model stresses through externally applied forces. However, differential shrinkage between substrate and overlay takes place inside the member and the location of stress initiation is the interface. Common beam theory first converts internal stresses into outside forces to then calculate internal stresses, which in itself is problematic. This point is probably the biggest shortcoming of existing analytical models. None of the analytical approaches discussed in Sections 3.2 to 3.8 takes the internal stress development into account accurately.

In essence, there are 2 internationally accepted analytical theories for the modelling of bonded concrete overlays. These are the theories presented by Birkeland (1960, compare

Section 3.3) and Silfwerbrand (1997, compare Section 3.8). The model presented by Evans and Parker (1955), as discussed in Section 3.2, can be considered as inadequate as it fails to apply both logic and sound analytical procedures. The models presented by Alonso-Junghanns (1997), Denarié (2004), and Hartl (1983 and 2000) (Sections 3.4 to 3.6) are essentially adaptations and modifications of Birkeland's theory.

The prestress analogy, which is applied in the models based on Birkeland's theory, is convenient to use, especially because it is easy to understand and easy to apply. However, it fails in formulating the correct force application to the composite member, with the result that stresses are computed in an unrealistic manner. Considering the characteristics of shrinkage strain development it appears to be illogical to assume that stresses can be modelled through member end forces. In Chapter 6, which contains the development of a new analytical model, these issues are discussed in detail.

Another shortcoming of existing analytical procedures is that they commonly simply superimpose the effects of direct strain and curvature, which leads to an overestimation of tensile stress release resulting from bending stresses. The force resulting from overlay restraint produces secondary effects, i.e. bending stresses in the composite section. Since curvature is linked to compressive strain in the overlay, it leads to reduction in tensile stress. Direct and bending stresses in concrete members are commonly calculated individually and subsequently superimposed to compute total stress. Moments induced by restrained shrinkage are internal moments and as such they depend on internal deformations. The force that produces bending moments and thus curvature in the composite section results from restrained overlay shrinkage, i.e. it results from restrained shortening of the overlay. Curvature causes additional shortening in the overlay and thus reduces the force that initially caused the curvature. Bending moments and curvature must, therefore, be computed with the total overlay stress resulting from elastic strain including curvature. This principle is discussed in more detail in Chapter 6.

Silfwerbrand's model represents an approach that is very different from the other existing models. The problem with this approach is that its applicability was not tested sufficiently through experimental research. Strains and stresses in this model depend to a major extent on an empirical "bond constant", which, in absence of test values, can be chosen arbitrarily to suit any desired analytical result. The model is based on the theory that stresses are proportional to overlay slip at the interface. However, it is questionable if interface slip does in fact commonly occur in composite members. Tests carried out on composite beam specimens, as discussed in Chapter 4, indicated that slip did not occur in any of the tested specimens, regardless of interface texture or overlay shrinkage. The theoretical basis of Silfwerbrand's approach, therefore, seems to be somewhat unrealistic. Further, the complexity of the model's equations makes it a very cumbersome tool to use. This is especially unsatisfying considering that the equations are based on empirical parameters.

An important aspect to notice is that all analytical models discussed in Section 3 agree in the following 3 fundamental aspects:

- Composite sections correspond to Bernoulli's principle that plane sections remain plane after being stressed
- A substrate of in infinite depth in connection with an overlay of finite depth results in complete restraint of overlay shrinkage
- Interface shear stresses only develop at the member ends, i.e. there is a zone at the member ends over which the full stress resulting from restrained overlay shrinkage is transferred to the composite section

The above 3 aspects are critically discussed and evaluated in detail in Chapter 6.

A shortcoming of most of the existing analytical models is that they are not supported by sufficient practical experiments. Alonso Junghanns (3.3) utilized a laboratory test set-up that corresponded to the assumptions on which she based her theoretical model. Even though she could support her analytical approach with her tests, neither analytical approach nor test set-up relate to the circumstances actually encountered in composite members. In general, practical tests are often insufficient in number and sometimes do not include the most important parameters that should have been tested to support the theoretical approach.

Based on the review of existing analytical approaches it appears necessary to develop a new model with which stresses due to differential shrinkage can be computed in a more logical manner. As an engineering tool for the design of bonded overlays, the model should be based on relatively simple formulae that can be applied easily. However, the formulae must be based on a sound theoretical background that incorporates both logic and reason without deviating from the basic principles of structural analysis. Since differential shrinkage between substrate and overlay is a very complex problem, the verification of the analytical approach must be supported through extensive practical research. For a comprehensive investigation, practical work must include the important parameters of overlay material characteristics, interface texture, and member dimensions. Since stresses can be related to strain, strain measurements on composite specimens appear to be a suitable method in determining stress development. The number of tests must allow a sound statistical evaluation of the results, and the chosen parameters should relate to real composite members.

CHAPTER 4

STRAIN CHARACTERISTICS OF COMPOSITE SPECIMENS SUBJECTED TO DIFFERENTIAL SHRINKAGE

4.1 Introduction

Differential shrinkage between substrate and overlay has a significant influence on the serviceability and durability of the composite system. Existing analytical models for the analysis of stresses resulting from differential shrinkage are based on simple beam theory and may not represent real strains, and thus real stresses, of the member.

Composite specimens consisting of substrate concrete beams with bonded concrete overlays were tested for their short-term and long-term strain characteristics. At the time of overlay casting, the substrate beams were at least 9 months old to ensure that most of the substrate shrinkage had taken place before the overlay was applied. Measured strain on the members was therefore fully accounted to the effects of overlay shrinkage.

Based on literature and the evaluation of existing analytical models, the following main test parameters were identified:

- Strain distribution along the length of the overlay
- Strain distribution across the depth of the overlay
- Strain distribution across the interface between substrate and overlay
- Strain distribution across the depth of the whole member
- Influence of the interface texture on strain and stress development
- Influence of overlay shrinkage characteristics (different overlay materials)
- Influence of overlay and substrate depths, and hence, in connection with elastic material properties, the influence of the relative member dimension of substrate and overlay

The analysis of strain measurements in composite members is complex. In general, strain values can be interpreted in a number of different ways, analysing a large range of different aspects both in respect to numerical strain values and fundamental strain characteristics. In this research, a large number of specimens with different properties were tested, which offered the possibility to research many important aspects in detail. However, to not exceed the scope of this section it was decided to concentrate on the identification of fundamental aspects of strain characteristics. The combined influence of different strain components on the behaviour of bonded overlays can be analysed with the prediction model discussed in Chapter 6. This model was based on fundamental strain characteristics of bonded overlays

discussed in this section. The strategy adopted in this research for the development of an analytical model and detailed analysis of experimental work is illustrated in **Figure 4.1**.

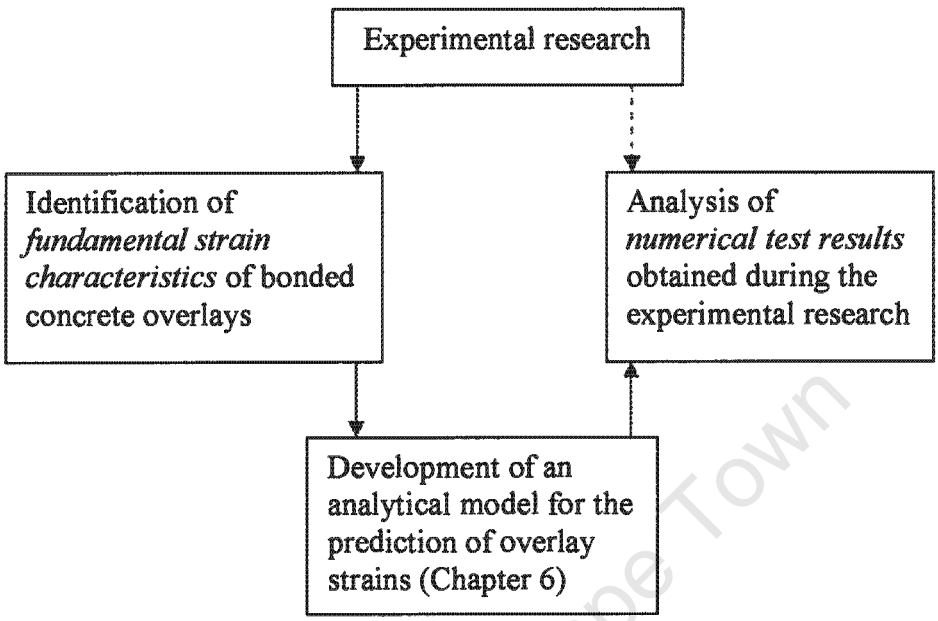

Figure 4.1: Research strategy for detailed interpretation of experimental results and the development of an analytical model

4.2 Test specimens

4.2.1 General

Shrinkage in concrete members is a 3-dimensional phenomenon, i.e., concrete members shrink in all directions. However, analytical models for shrinkage stresses in composite members generally only consider shrinkage strains parallel to the longer axis of the member. This is a reasonable simplification, as it allows for stresses in the most critical direction and facilitates analysis. Therefore, shrinkage measurements on the test specimens were taken along one axis only, treating overlay shrinkage as a one-dimensional phenomenon.

4.2.2 Substrate concrete

For the duration of this work, the same concrete mix design was used for all substrate concrete specimens. A concrete mix with a target strength of 40 MPa was designed using conventional, locally available materials in order to simulate common concrete repair and concrete strengthening situations. Crushed Greywacke of 19 mm nominal maximum size, typically used for concrete construction in the Cape Peninsula in South Africa, was chosen as

the coarse aggregate. From the two commonly utilised local sands, Klipheuwel sand, which is a siliceous pit sand with good particle shape and continuous grading, was chosen because of its relatively high content of coarse aggregate particles. The latter provided a sound and rough interface texture using sandblasting for interface preparation.

Procedures for the testing of material parameters are described in Section 4.3. Mix design and relevant fresh and hardened properties of the substrate concrete are presented in **Table 4.1**.

Table 4.1: Substrate concrete: Mix design and material properties

Cement CEM I 42.5	[kg/m^3]	350
Water	[kg/m^3]	175
19 mm Greywacke	[kg/m^3]	1025
Klipheuwel sand	[kg/m^3]	875
W/C ratio	[-]	0.50
Slump	[mm]	90±20
28d Compr. Strength	[MPa]	48.4
28d Elastic modulus	[GPa]	28.1

4.2.3 Interface texture and substrate surface condition

The substrate concrete of all composite test specimens was least 9 months old at the time of overlay placement to make sure that most of its drying shrinkage had taken place. Different substrate surface preparations, and hence different interface textures between substrate and overlay, were selected to study the effects of micro- and macro-roughness and the resulting degree of restraint at the interface.

4.2.3.1 Sandblasted interface

Sandblasting the concrete substrate is one of the most common methods for provision of a sound and rough interface for concrete repair works and was, therefore, adopted as the main interface texture in this project. The original surface of the freshly cast beams was made smooth using a trowel. The beams were sandblasted at an age of approximately 3 months, leaving fine aggregates and, at random intervals, coarse aggregates exposed. Due to the originally smooth surface of the beams the sandblasted interfaces had virtually no macro-roughness, i.e. the overall surface texture of the substrate beams was relatively smooth. The average surface roughness of all specimens, measured with the Sand-Area Method (Kaufmann, 1971), was 0.7 mm. **Figure 4.2** shows a typical sandblasted surface.

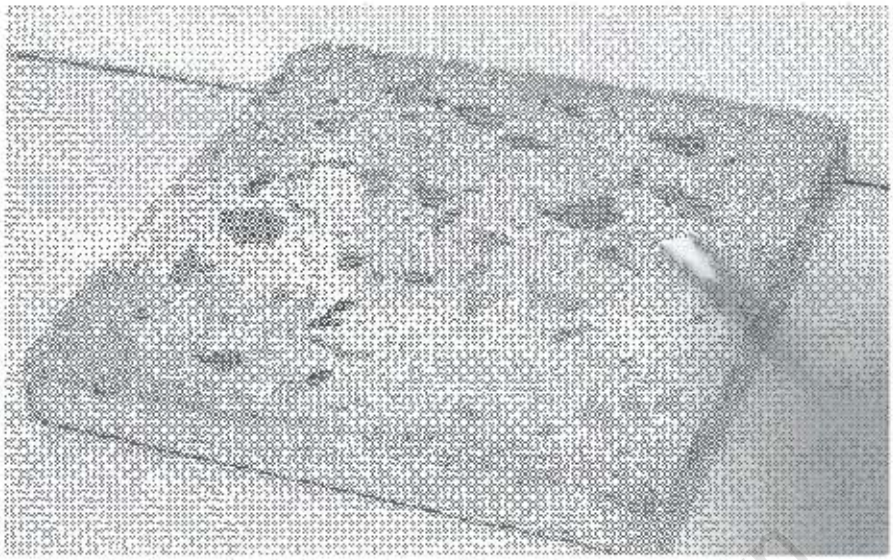

Figure 4.2: Photograph of a typical sandblasted concrete surface

4.2.3.2 Smooth interface

Specimens with smooth substrate surfaces were used to study differential shrinkage of composite members with relatively little mechanical restraint at the interface. Smooth surfaces were cast against steel formwork and, except for surface pores, had a roughness only on microscopic scale. Very little formwork oil was used for the casting of specimens in order to prevent deterioration of the interface. **Figure 4.3** shows substrate beams with a smooth surface.

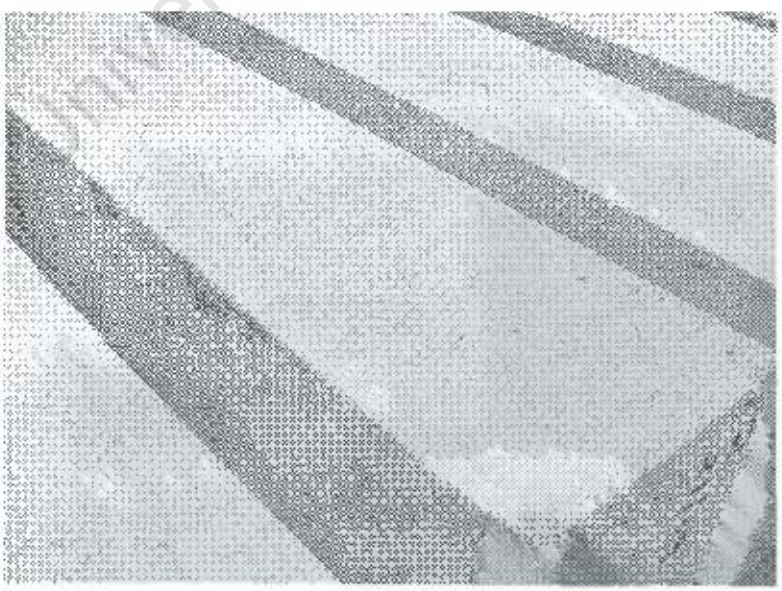

Figure 4.3: Photograph of substrate beams with a smooth surface

4.2.3.3 Notched interface

Substrate members with notched surfaces were prepared to represent interfaces with well-defined macro roughness and minimum of micro roughness. To study the effect of macro-roughness in more detail, notches were applied with a different spacing, in the following named *notched interface 1* and *notched interface 2* with a spacing of 110 and 220 mm respectively (**Figure 4.4**).

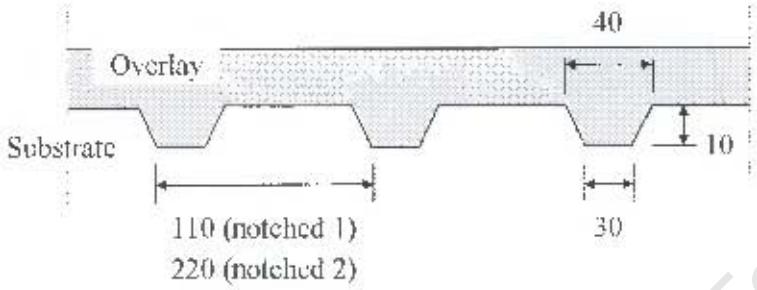

Figure 4.4: Schematic of notched interface texture

A *notched 1* interface provided more regular mechanical interaction between substrate and overlay, compared to a *notched 2* interface. A photograph of the notched interfaces is shown in **Figure 4.5**.

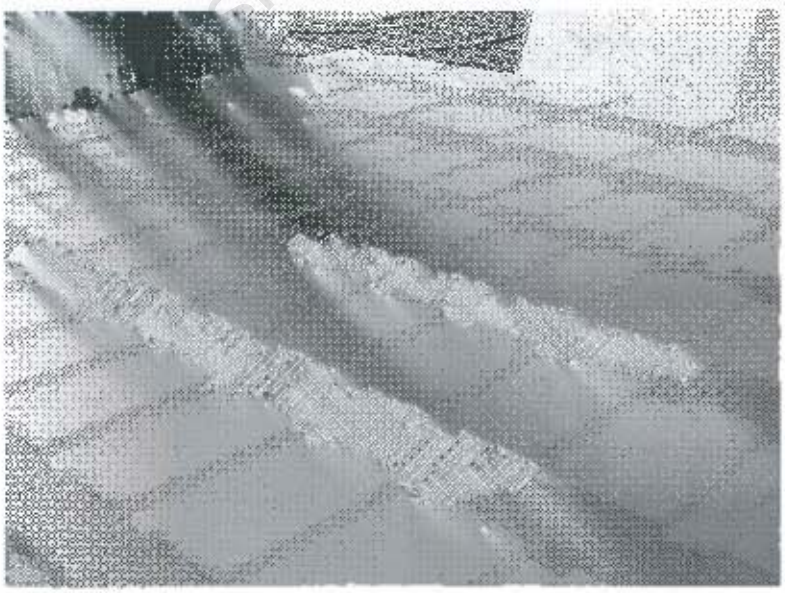

Figure 4.5. Photograph of substrate beams with notched surfaces (*notched 1* in the front and *notched 2* at the rear)

4.2.3.4 Substrate moisture condition

All substrate surfaces were kept moist for 24 hours, using wet burlap and plastic sheets, and left to dry for approximately 30 – 60 minutes prior to overlay application. This was done to prepare a saturated, surface-dry substrate, which represents optimum moisture conditions for bonding (compare Section 2.3.4.2).

4.2.4 Overlay materials

Overlay mixes were designed to suit different shrinkage characteristics. In general, overlays with high free shrinkage strain (ε_{FSS}) were designed with high paste content as a mortar without coarse aggregates, whereas those with low ε_{FSS} were designed as concretes with crushed granite of 9 mm nominal maximum size as coarse aggregates. The consistency of fresh overlays can have a major influence on interface bond strength. In general, higher fluidity leads to better bond properties as it facilitates the penetration of open surface pores and thus improves anchorage to the substrate. In order to achieve high bond strengths, all overlays were designed with a high slump. This was done by means of relatively high water contents. No admixtures were used. Concrete mix proportions and selected material properties are presented in **Table 4.2**.

Table 4.2: Overlays 1 – 3: Mix proportions and selected material properties

		Overlay 1	Overlay 2	Overlay 3
Designation*		LS	HS	MS
Cement CEM I	[kg/m^3]	394	640	510
Water	[kg/m^3]	217	300	235
9 mm Greywacke	[kg/m^3]	985	-	940
Klipheuwel sand	[kg/m^3]	750	1300	660
W/C ratio	[-]	0.55	0.47	0.46
Slump**	[mm]	110±20	collapse	80±20
28-d Compressive Strength	[MPa]	54.1	50.9	53.3
28-d Tensile split strength	[MPa]	3.4	2.1	3.0
28-d Elastic modulus	[GPa]	25.1	22.1	29.6
28-d ε_{FSS}	[10^{-6}]	140	540	290

* For this research the following designations were given to Overlays 1-3:
Overlay 1: LS = low shrinkage
Overlay 2: HS = high shrinkage
Overlay 3: MS = medium shrinkage

** The slump was measured according to BS 1881:Part 102:1983.

4.2.5 Specimen dimensions and test parameters

4.2.5.1 Overview of specimens and main test parameters

For testing shrinkage-induced strain characteristics of composite members, specimens comprising substrate concrete beams with a concrete overlay were prepared. Initially, the influence of different interface textures on overlay strain along the length of the member was tested (Specimens A). Two different overlay material compositions were used for this (Overlays 1 and 2, see Table 4.2). Specimens with Overlay 2 showed extensive cracking, which was due to the high rate of shrinkage strain development at early ages. By contrast, using Overlay 1, cracking was avoided.

The analysis of test results and ongoing research revealed the necessity to also test strains across the interface, i.e. strains close to the interface in both substrate and overlay (Specimens B). Based on the performance of Overlays 1 and 2 on Specimens A, Overlay 3 was designed for Specimens B with shrinkage strains intermediate between Overlay 1 and Overlay 2.

On identifying substrate strains at the interface it was apparent that information on strains across the whole member depth was also needed in order to complete the information on strain characteristics (Specimens C which were unable to curve, and Specimens D which were free to curve). For these specimens, Overlay 3 was utilised as it had proved to lead to conclusive results on Specimens B.

Therefore, specimens were made and tested over a 3-year period with a casting sequence of approximately one year between Specimens A, B and C/D. The different types of specimens are described separately in Sections 4.2.4.2 – 4.2.4.5. **Table 4.3** presents an overview of the specimens and the main test parameters.

Strain measurements were taken by 2 different operators. Comparison of experimental data obtained from the 2 operators showed that the variability between their measurements was insignificant and did not inflict on the accuracy of test results.

4.2.5.2 Overlay strain distribution along the length of the member – Specimens A

Strains along the length of the overlay were measured on beam specimens consisting of a substrate concrete beam (1600 x 155 x 200 mm) with a 40 mm overlay. Strain-measuring discs were applied on the overlay at 100-mm gauge length both at the interface, as close to the substrate as possible, and on top along the centre-line of the overlay. The measurement locations were numbered according to their position on the specimen. Due to symmetry of the beams, most positions were presented twice on the same member (**Figure 4.6**).

Table 4.3: Overview of specimens and main test parameters

Specimen	Interface texture	Overlay		Main test parameter
		Type	depth [mm]	
A1	sandblasted	1 (LS)	40	Overlay strain development at different locations along the interface and the top of the member
A2	sandblasted	2 (HS)	40	
A3	smooth	2 (HS)	40	
A4	notched 1	2 (HS)	40	
A5	notched 2	2 (HS)	40	
B1	sandblasted	3 (MS)	40	Strains across the interface
B2	smooth	3 (MS)	40	
C1	sandblasted	3 (MS)	20	Strains across the depth of the whole member. Influence of relative cross-sectional areas of substrate and overlay
C2		3 (MS)	40	
C3		3 (MS)	80	
D1	sandblasted	3 (MS)	20	
D2		3 (MS)	40	
D3		3 (MS)	80	

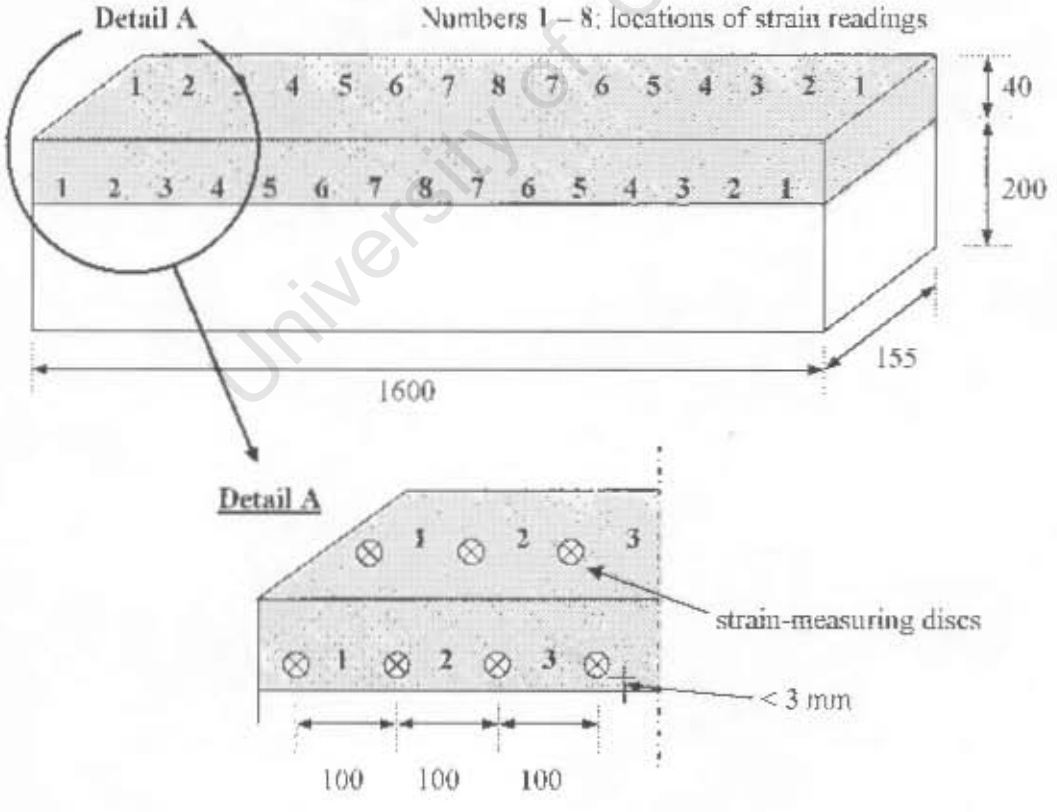

Figure 4.6: Specimens A: specimen dimensions and location of strain-measuring discs

Shrinkage readings were taken with a BAM strain-measuring extensometer, PFENDER type, rated measuring length 100 mm, Measuring resolution: 0.001 mm. Developed by the Federal Institute for Material Research BAM, Berlin, Germany (**Figure 4.7**).

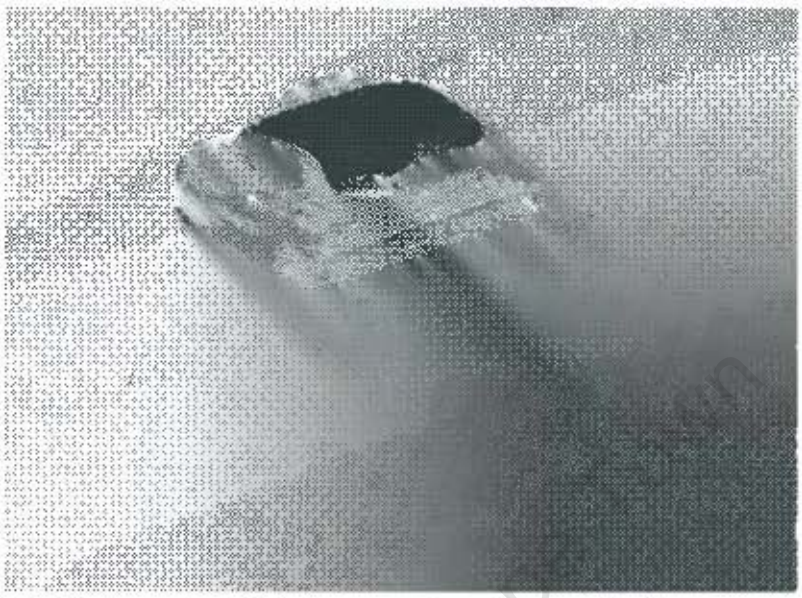

Figure 4.7: Photograph of strain-measuring discs applied to the overlay and strain-measuring extensometer

Strain readings along the interface were taken on only one side of the specimen. Prior to the test programme, composite specimens with the same dimensions as shown in Figure 4.6 were tested for differences in overlay strain between both sides of the member. Different overlay materials were tested over a period of approximately 8 weeks. In all cases, strain values on opposite sides were very similar, with measurements on the two sides in most cases not differing more than 20.10^{-6}. This was observed along the whole length of the members. This led to the conclusion that specimens undergo a deformation that is uniform across the member width. Hence, strain measurements taken on only one side were taken as representative of the deformation of the specimens.

2 beams were cast per test parameter in order to allow statistical evaluation of strain measurements. Consequently, measurements were usually taken at 4 different positions per strain location along the members.

In addition to the measurement of shrinkage strains, the specimens were used for the observation of overlay cracking. Cracks were identified visually with a magnifying glass.

Different interface textures and different overlay mixes were tested. **Table 4.4** summarizes the specimens.

Table 4.4: Summary of Specimens A

Specimen	Interface texture	Overlay
A1	sandblasted	1 (LS)
A2	sandblasted	2 (HS)
A3	smooth	2 (HS)
A4	notched 1	2 (HS)
A5	notched 2	2 (HS)

4.2.5.3 Strains across the interface – Specimens B

After evaluation of strain results on Specimens A, it was apparent that additional information on strains across the interface would be needed in order to characterise the restraining action of the substrate. Specimens B were cast with strain targets applied close to the interface on both substrate and overlay (**Figure 4.8**).

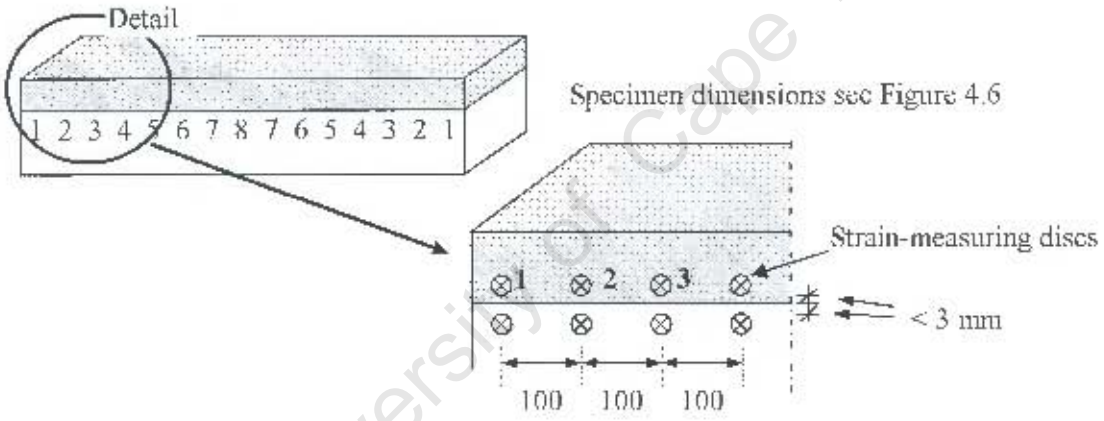

Figure 4.8: Specimens B: Location of strain-measuring discs along the interface

Specimens B had the same dimensions as Specimens A, i.e., the same substrate beam dimensions and a 40 mm overlay. To compare the influence of the different degrees of mechanical bond between overlay and substrate, both sandblasted and smooth interface textures were used. The overlay (Overlay 3) was designed to have higher crack resistance than Overlay 2 and higher shrinkage strain than Overlay 1. Only one specimen was cast per test parameter. **Table 4.5** summarizes the specimens.

Table 4.5: Summary of Specimens B

Specimen	Interface texture	Overlay
Beam B1	sandblasted	3 (MS)
Beam B2	smooth	3 (MS)

4.2.5.4 Strain across the member depth, members that cannot curve - Specimens C

Specimens C were designed with the aim to isolate the effects of overlay shrinkage strains from curvature strains (**Figure 4.9**).

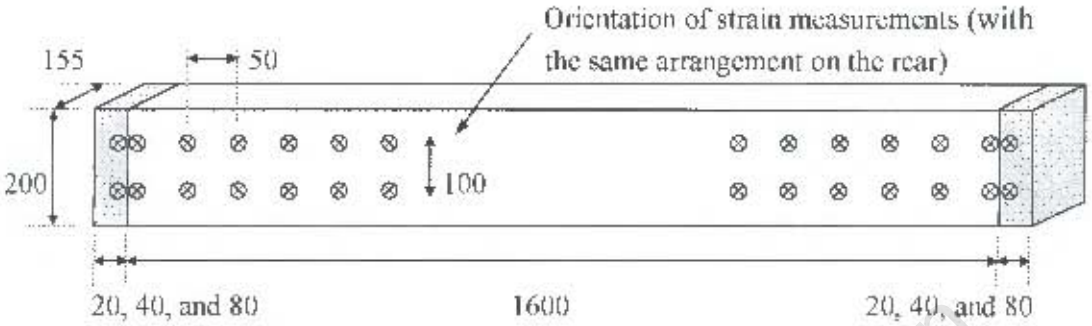

Figure 4.9: Specimens C: Specimen dimensions and location of strain-measuring discs

Overlays were cast at 3 different depths, 20, 40, and 80 mm. Strain-measuring discs were applied on the overlay at the interface, and across the substrate with a spacing of 50 mm. Substrate strains were measured at 6 different heights. One specimen was cast per overlay depth. Measurements were taken at 2 ends and 2 sides of the specimens, resulting in 4 measurements per test location. Test results for each level therefore commonly represent the mean value of 4 measurements. The interface was sandblasted. **Table 4.6** summarizes the specimens.

Table 4.6: Summary of Specimens C

Specimen	Interface texture	Overlay
Beam C1	sandblasted	3 (MS), 20 mm
Beam C2	sandblasted	3 (MS), 40 mm
Beam C3	sandblasted	3 (MS), 80 mm

4.2.5.5 Strain across the member depth, members that are free to curve – Specimens D

Specimens D were cast in order to evaluate the influence of relative substrate and overlay dimensions on strain characteristics of the whole member if the member is free to curve (**Figure 4.10**).

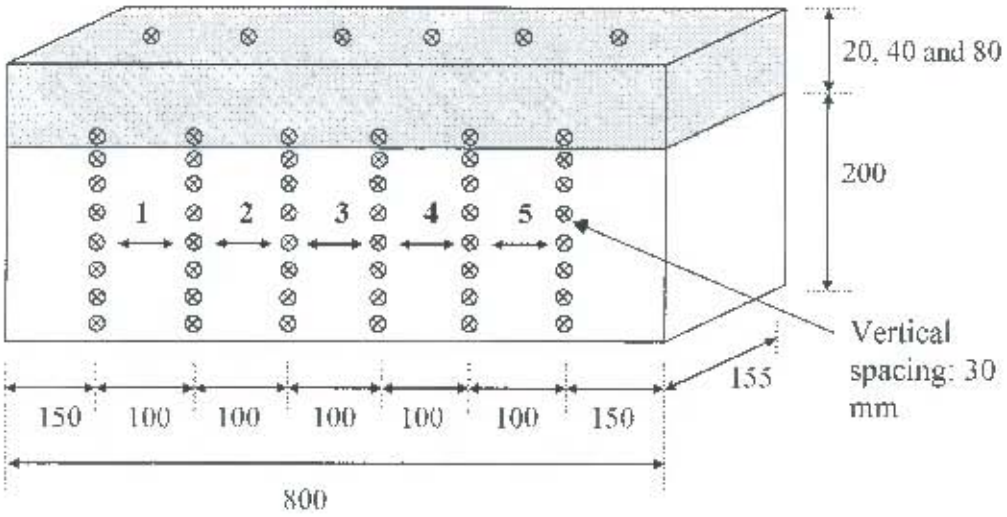

Figure 4.10: Specimens D: Specimen dimensions and location of strain-measuring discs

Strain-measuring discs were applied on the overlay on top of the beam and at the interface, and across the whole depth of the substrate with a vertical spacing of 30 mm. In total, substrate strains were measured at 7 different heights. On each horizontal level, 5 measurements were taken as shown in Figure 4.10. Test results for each level therefore represent the mean value of 5 measurements. Overlays were cast at 3 different depths, 20, 40, and 80 mm. **Table 4.7** summarizes the specimens.

Table 4.7: Summary of Specimens D

Specimen	Interface texture	Overlay
Beam D1	sandblasted	3 (MS), 20 mm
Beam D2	sandblasted	3 (MS), 40 mm
Beam D3	sandblasted	3 (MS), 80 mm

4.2.6 Curing

All overlays were moist cured for a period of 7 days after casting, using wet burlap and plastic sheets. Subsequently, the test specimens were left uncovered in the laboratory where they were exposed to seasonal changes in temperature and relative humidity ranging from 16 to 23 °C and 55 to 75 % RH respectively. All overlays were cast in autumn or winter in order to prevent rapid shrinkage development.

The strain results presented in the following sections represent measured values, i.e., values that were not adjusted for changes in temperature or humidity. This was based on the

condition that overlay strains were always interpreted in comparison to free shrinkage strains. Since these were measured on specimens exposed to the same curing conditions as the overlays, the influences of temperature and humidity on the analysis of overlay strain readings were considered to be of minor importance.

4.2.7 Statistical analysis and presentation of strain measurements

Strain values of the composite specimens were related to the position of the measurement along the length or across the depth of the member. Due to the number of test specimens and symmetry of specimens, between two and four readings were available for most measurement locations. **Table 4.8** presents an example of the analysis of strain measurements. Rows "1" and "2" in the above table refer to the first beam, and rows 3 and 4 to the second beam tested for Specimens A3 (**Figure 4.11**).

Table 4.8: Specimens A3, Location 1 at the interface: example of analysis of strain measurements

Measurement	Day						
number	3	6	14	22	37	83	149
1	100	**30**	190	150	160	260	560
2	160	190	230	310	290	270	580
3	160	170	320	350	330	460	630
4	190	180	290	**-50**	350	470	610
mean	153	143	257	190	282	330	595

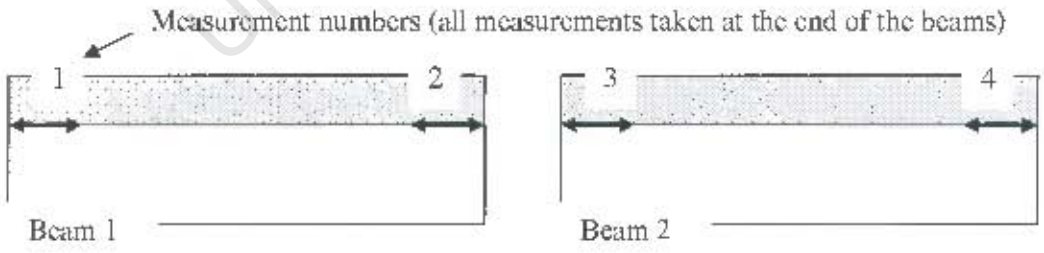

Figure 4.11: Schematic of strain measurements on composite members as an illustration of the values given in Table 4.8

The analysis of strains was done with a focus on the identification of trends in relation to the defined locations on the members. The mean strain values were therefore commonly used in the analysis. At instances a whole row of values was very different from the other rows, i.e. measurements at the same defined location were very different between different beams or

different sides of the same beam. At such occasions, the "outlying row" of measurements was presented separately in the graphical analysis of overlay strain values along the member length (Section 4.5). A row of measurements was only considered to be an "outlying row" if it was consistently different from the other measurements at that location. For example, the strain value at day 6 in row "1" in the above table represents a single outlying value. However, for most of the other days, values of row "1" cannot be considered as outlying values. For consistency, the whole row "1" was therefore considered in the analysis.

Single readings were omitted in the analysis only if they clearly represented a measurement error, which was commonly identified by comparing the respective value to previous and subsequent values at the same position. The value in row 4, day 22 (Table 4.8) is an example. In Appendix 4, all omitted single values are pointed out.

Statistical evaluation of strain measurements was carried out for all specified locations along the specimens. Details are provided in Appendix 4 for all measurements. The mean standard deviation for measurements along specified locations of Specimens A and B (i.e. Locations 1-8, as illustrated in Figure 4.8) ranged between 26% and 34%, which is in an acceptable range, considering the many factors influencing overlay strain readings.

The time-dependent development of strains could usually be related to trend lines, typically in the form of power functions. However, measured values were more valuable for the analysis of strain characteristics. Trend lines were not used.

4.3 Testing material parameters

4.3.1 Concrete compressive strength

Concrete compressive strength was tested in accordance with BS 1881:115 (1983) on 100 mm cubes. 28 day compressive strengths of Overlays 1-3 are presented in Table 4.2.

4.3.2 Concrete tensile strength

Concrete tensile strength was evaluated as tensile splitting strength on 100 mm cubes, according to BS 1881 - 117 (1983). Test results for Overlays 1-3 are presented in **Figure 4.12**. For the composite specimens, day 7 in Figure 4.12 represents the end of the overlay curing period and hence the onset of overlay drying shrinkage. Overlay 3, having similar compressive strength as Overlays 1 and 2, had comparatively low tensile strength. This was due to relatively large inherent surface stresses resulting from high paste content (Overlay 3 had no coarse aggregate) in connection with high shrinkage strains and air-drying.

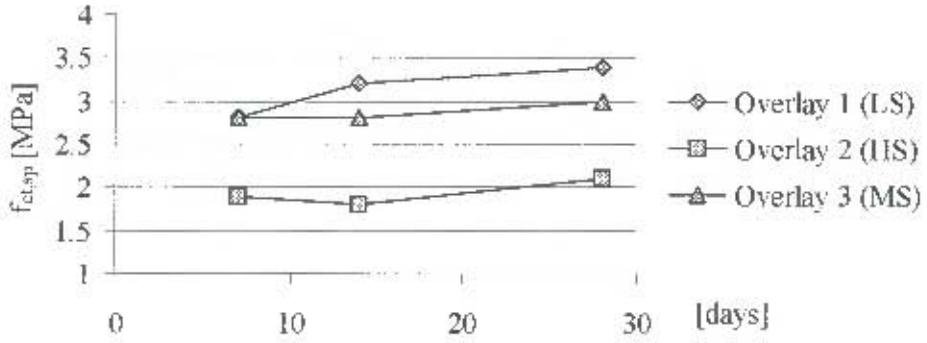

Figure 4.12: Development of tensile splitting strength f_{ctLsp} of Overlays 1-3

Stresses due to restrained shrinkage in bonded overlays can mainly be considered as direct tensile stresses. According to Neville (2002), the tensile splitting strength is generally believed to be close to the direct tensile strength of concrete, being 5 to 12 percent higher. The values presented in Figure 4.12 were therefore representative for the direct tensile strength of the tested overlays.

4.3.3 Elastic Modulus

Elastic Modulus in compression was tested on 200x100x100 mm prisms, using a compressometer device (**Figure 4.13**) in connection with electronic data aquisition. Test results are presented in **Figure 4.14**.

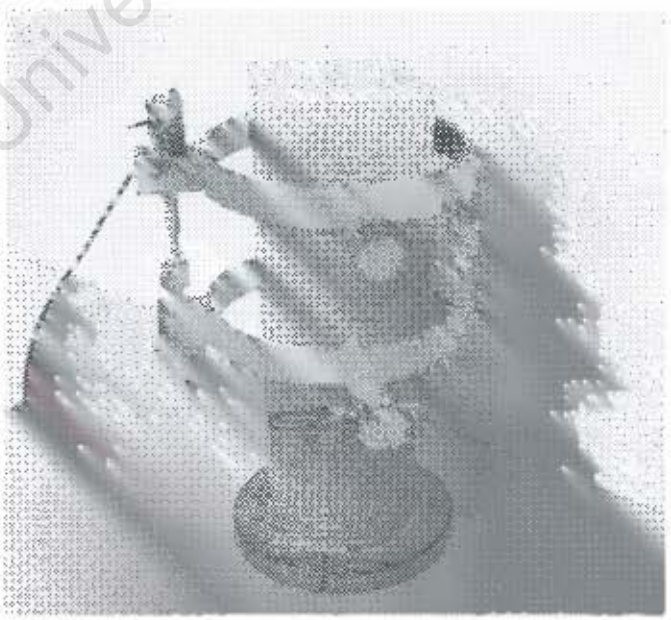

Figure 4.13: Testing of elastic modulus - Photograph of test equipment and specimen (hydraulic compression machine not shown)

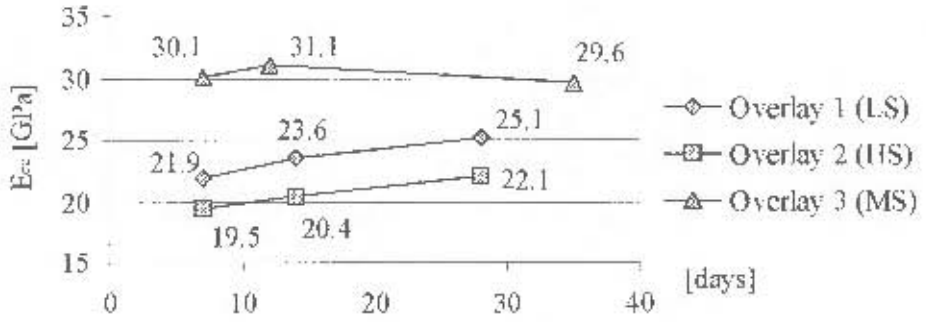

Figure 4.14: Development of the modulus of elasticity in compression E_{cc} of Overlays 1-3

Overlay 3 showed a unique development of elastic modulus, as the measured modulus of elasticity had already reached its 28-day value after 7 days and remained relatively constant thereafter, which could not be explained.

Since bonded overlays subjected to differential shrinkage commonly experience tensile stress, the modulus in tension is of greater significance than that in compression. However, the two can generally be considered to be very similar (Neville, 1995) and the measured modulus of elasticity in compression was therefore used in the analysis of tensile overlay stress.

4.4 Free overlay shrinkage strains

4.4.1 Test specimens

Strains on bonded overlays resulting from overlay shrinkage can be analysed only in relation to free overlay shrinkage strain, i.e., the strain the overlay would have experienced had it not been bonded to the substrate.

Free shrinkage strains (ε_{FSS}) were measured on specimens made from the same batch of concrete as the overlays. Differences in free shrinkage strains between Specimens with the same overlay material are a result of different casting dates. Measurements were taken over the whole test period under the same curing conditions as the composite specimens. The cross sectional dimensions of the test specimens were the same as those of the tested overlays (**Figure 4.15**).

Two specimens were tested per mix. Test results therefore commonly represent a mean of four measurements. All specimens were moist cured during the first 7 days after casting and did not show any strain during this time.

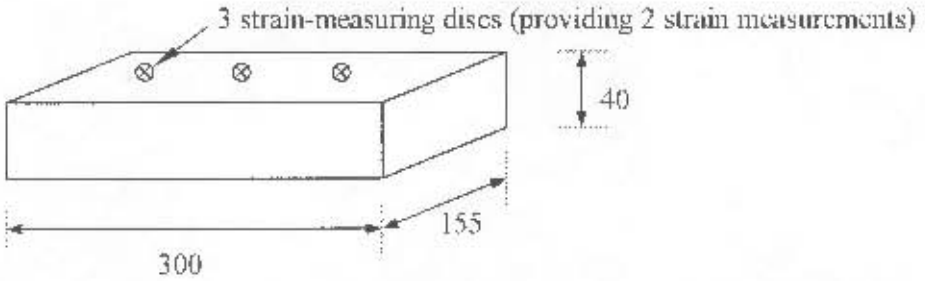

Figure 4.15: Specimens for the testing of free shrinkage strain of a 40 mm overlay

4.4.2 Test results and analysis

4.4.2.1 Short-term results

Most important for the serviceability and durability of bonded concrete overlays is the shrinkage strain during the first days and weeks, as this is the time period where restrained shrinkage often exceeds the tensile strain capacity of the material, thus causing cracking and/or debonding. **Figure 4.16** shows the short-term free shrinkage strains of overlays 1 – 3 (40 mm depth), where "day 0" denotes the end of the moist curing period at 7 days.

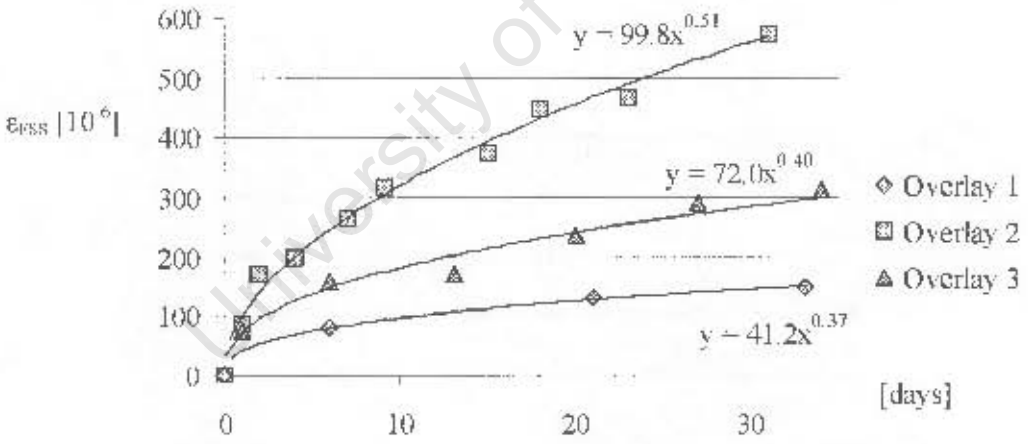

Figure 4.16: Free shrinkage strains of Overlays 1 – 3 (40 mm depth), short term results and trend lines

The trend lines shown in Figure 4.16 are calculated by *Microsoft-Windows-EXCEL* and show a close correlation of the test results to power functions. The exponents of the trend line equations are always smaller than 1, showing that the rate at which shrinkage develops is larger at earlier ages. 7-day shrinkage strains reach approximately 50-60% of the 28-day values. This relatively rapid shrinkage strain development in early days explains the high risk of early age failure of bonded concrete overlays. At young ages, concrete stress relaxation is

high and the elastic modulus is low, which is of benefit for the development of lower restrained shrinkage stresses. However, rapid stress increase due to high early age shrinkage in connection with low early age strength often leads to overlay cracking shortly after the end of the curing period.

4.4.2.2 Long-term results

Long-term shrinkage strains of Overlays 1 - 3 are presented in **Figure 4.17**.

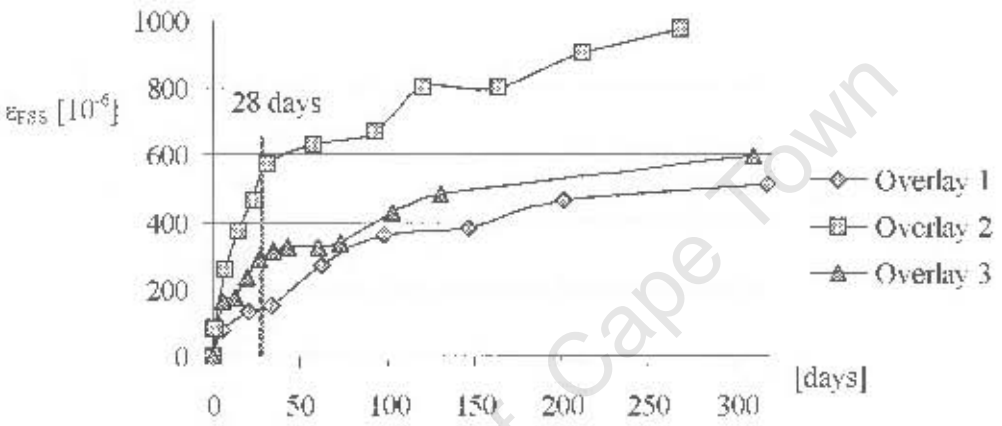

Figure 4.17: Free shrinkage strains of Overlays 1 – 3 (40 mm depth), long-term results

As presented in the above figure, considerable shrinkage strain develops for much longer than 28 days. CEB-FIP (1990) and ACI (1993) (compare Section 2.4.5.3) estimate 28-day shrinkage strains to be 49% and 44% of the ultimate shrinkage strains respectively. This, in comparison to test results of Overlays 1 – 3, seems reasonable.

4.4.2.3 The influence of the overlay depth

Member dimensions influence the rate at which shrinkage develops, as thin members tend to dry out quicker than thick members. The influence of member dimensions is commonly expressed by the notional member thickness h_0 (e.g. compare CEB-FIP, 1990, shrinkage prediction model, equation 2.3).

Specimens C and D were cast with overlays of 20, 40, and 80 mm. Free shrinkage strains for these overlays were measured on specimens of the same cross-sectional dimensions as the overlays (**Figure 4.18**). Test results are presented in **Figure 4.19**.

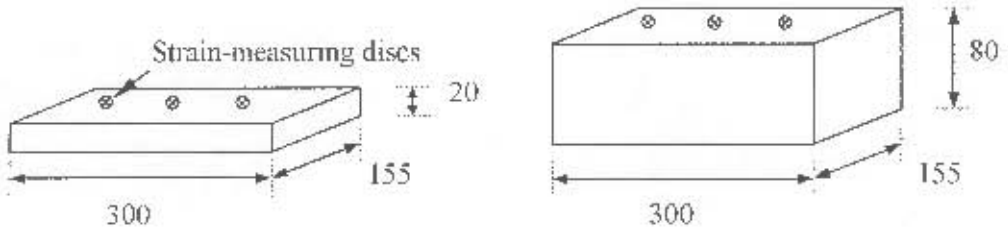

Figure 4.18: Specimens for the testing of free shrinkage strain of 20 and 80 mm overlays

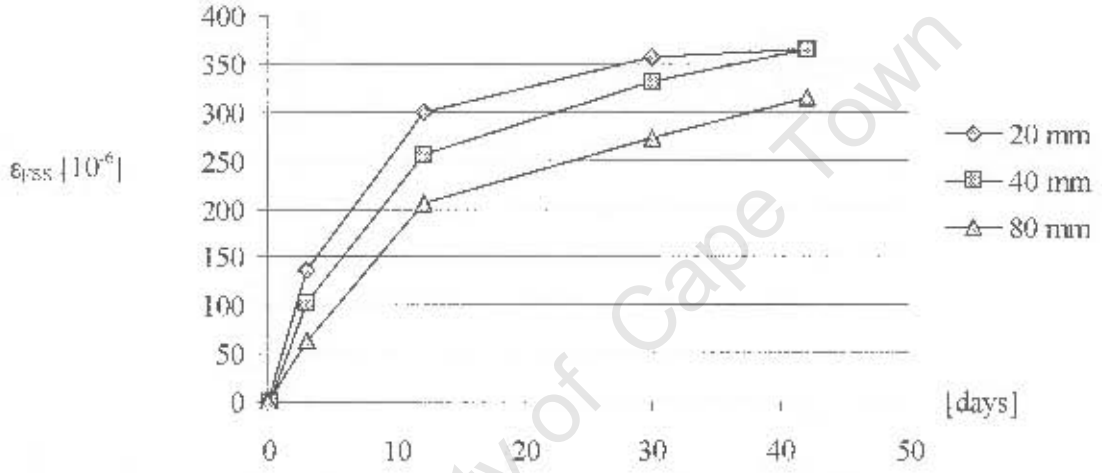

Figure 4.19: Free shrinkage strains of Overlay 3, test results in relation to overlay thickness

Thin overlays have a higher rate of shrinkage development and higher shrinkage values at early ages. The difference in shrinkage strain between different overlay thicknesses becomes less pronounced as time proceeds. The overlay thickness therefore has a significant influence on the rate of shrinkage strain development, which has to be considered in the analysis of strains on composite members.

Specimens for the testing of free overlay shrinkage were exposed to the environment at all sides. However, at the interface to the substrate, bonded overlays are not exposed to the environment. This effect was neglected as generally overlays also loose moisture to the substrate, resulting from the substrate's capillary suction.

4.5 Overlay strain distribution along the length of the member

4.5.1 Introduction

For the analysis of overlay strain distribution along the length of the member, Specimens A1-A5 and B1 (compare Sections 4.2.4.2 and 4.2.4.3) were used.

Due to high overlay shrinkage strains, all members with Overlay 2 (IIS) (Specimens A2 – A5) cracked extensively during the first 2 weeks after casting, which split the overlays into separate parts. Overlay strain measured across cracks was considered not to represent the test parameter under consideration. Therefore, for the analysis of overlay strain distribution along the member, only sections situated between cracks were utilized (**Figure 4.20**).

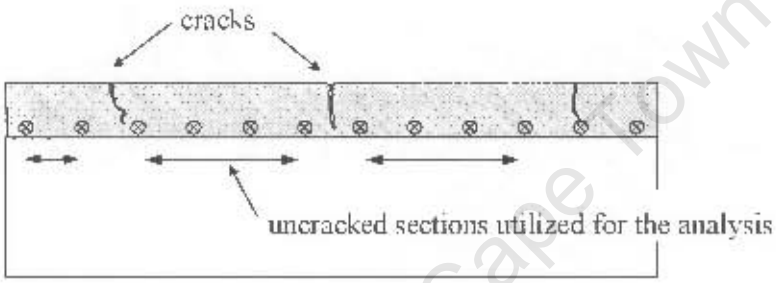

Figure 4.20: Cracked overlays: only uncracked locations were used for the analysis of the magnitude of overlay strain

The influence of cracks on overlay strain characteristics is discussed separately in Section 4.11. Specimens A1 and B1, which were made with overlays of "low" and "medium" shrinkage strain, did not crack during the test period and were therefore taken as the most conclusive specimens for the analysis of strain distribution along the length of the member.

Sections 4.5.2 and 4.5.3 comprise the presentation of test results. Discussion and analysis of the test results is presented in Section 4.5.4.

4.5.2 Overlay strain at the interface – test results

Figures 4.21 to 4.26 show the time-dependent overlay strain distributions along the interfaces of the specimens with respect to different overlays and different interface textures. The figures show free shrinkage strains (ε_{fSS}), overlay strains at the interface ($\varepsilon_{O,I}$) at uncracked locations along the member, and the mean value of overlay strains. For the specification of different locations along the member, see Figure 4.6. The focus of this section lies solely on the strain distribution along the specimens. The numerical magnitude of overlay strains will be discussed separately in Section 4.7. Test results presented do not

include measurements taken at the ends of the beams (Location 1). The member ends showed significantly higher strain values than the inner parts of the member, which will be discussed in Section 4.10. Specimens B2, on which overlay debonding occurred, are discussed separately in Section 4.11.3.

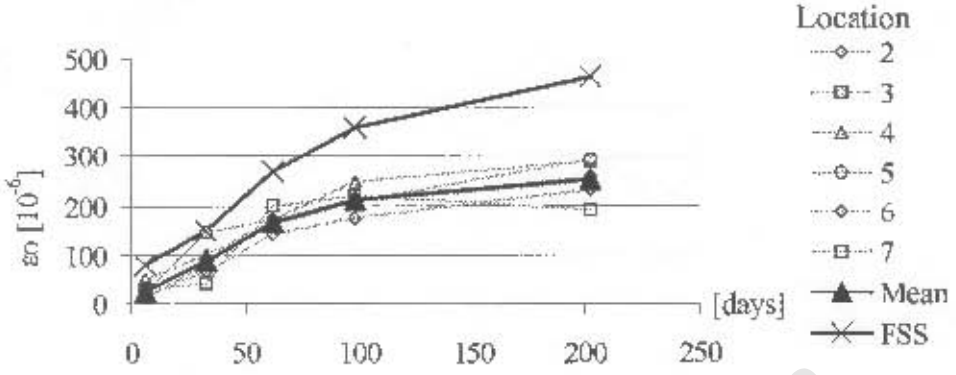

Figure 4.21: Overlay strains at the interface: Specimens A1 (sandblasted interface, Overlay 1 (LS))

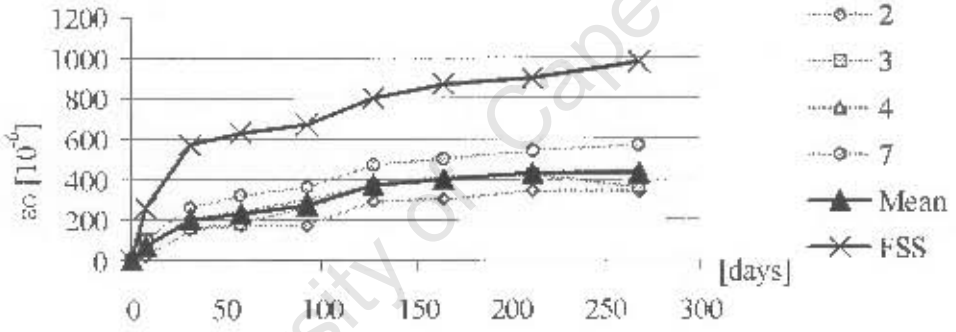

Figure 4.22: Overlay strains at the interface: Specimens A2 (sandblasted interface, Overlay 2 (HS))

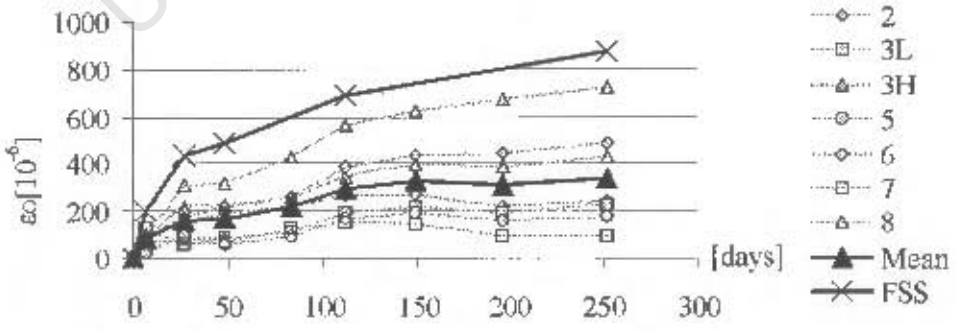

Figure 4.23: Overlay strains at the interface: Specimens A3 (smooth interface, Overlay 2 (HS))[1]

[1] Locations "3L" and "3H" represent the lowest and highest strain measured at Location 3 respectively. Due to the large difference between the two, the mean value was considered not to be representative for the representation of trends. In Figure 4.23, the two locations were therefore presented separately.

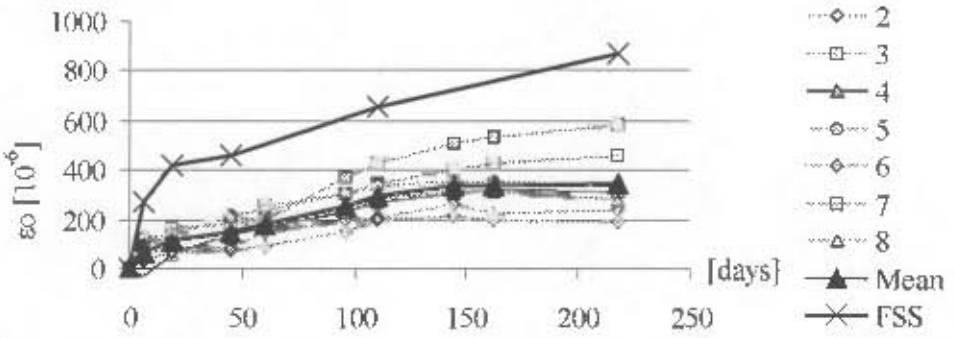

Figure 4.24: Overlay strains at the interface: Specimens A4 (notched interface A, Overlay 2 (HS))

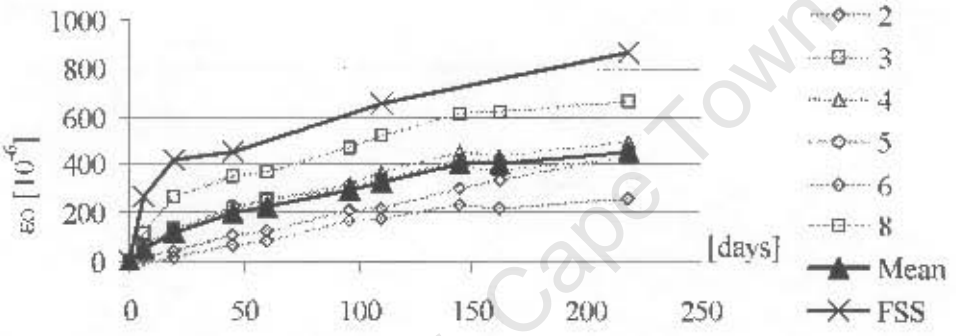

Figure 4.25: Overlay strains at the interface: Specimens A5 (notched interface B, Overlay 2(HS))

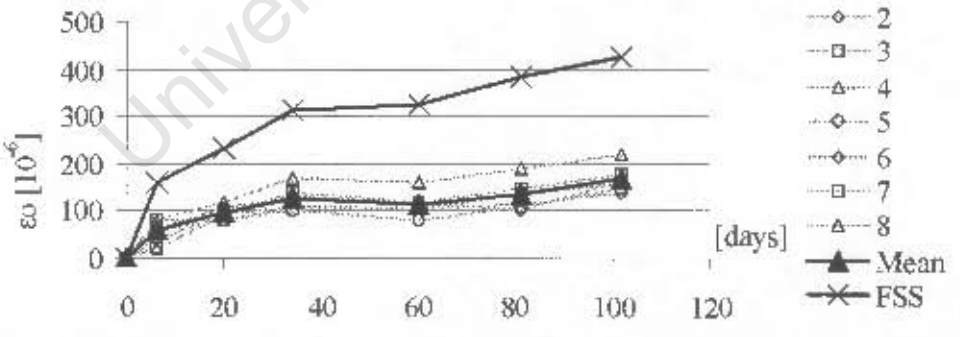

Figure 4.26: Overlay strains at the interface: Specimens B1 (sandblasted interface, Overlay 3 (MS))

4.5.3 Strain on top of the overlay – test results

Figures 4.27 to 4.31 show the time-dependent strain distributions along the top of the overlay with respect to different overlays and different interface textures.

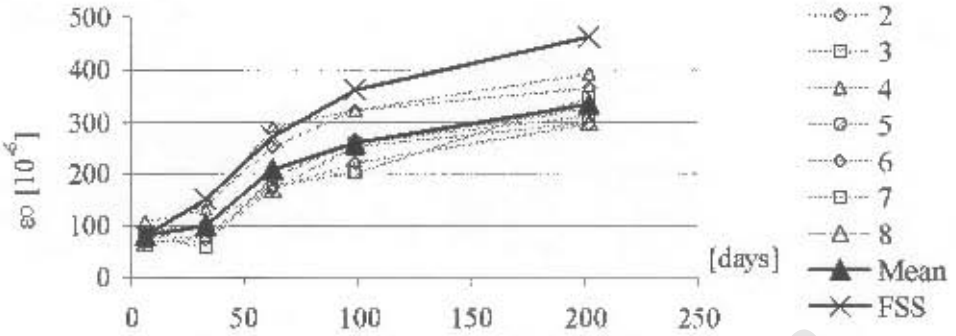

Figure 4.27: Strains on top of the overlay: Specimens A1 (sandblasted interface, Overlay 1 (LS))

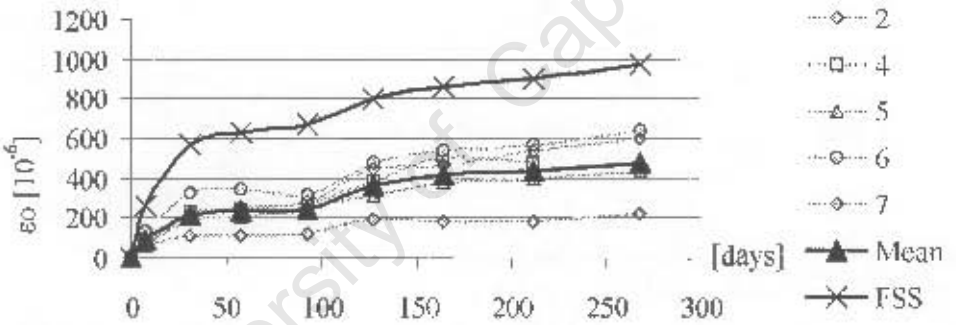

Figure 4.28: Strains on top of the overlay: Specimens A2 (sandblasted interface, Overlay 2 (HS))

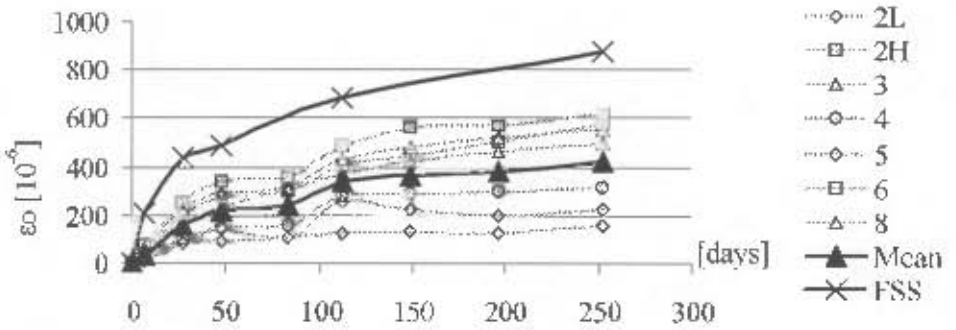

Figure 4.29: Strains on top of the overlay: Specimens A3 (smooth interface, Overlay 2 (HS))[2]

[2] For locations 2L and 2H, see footnote 1 on page 88

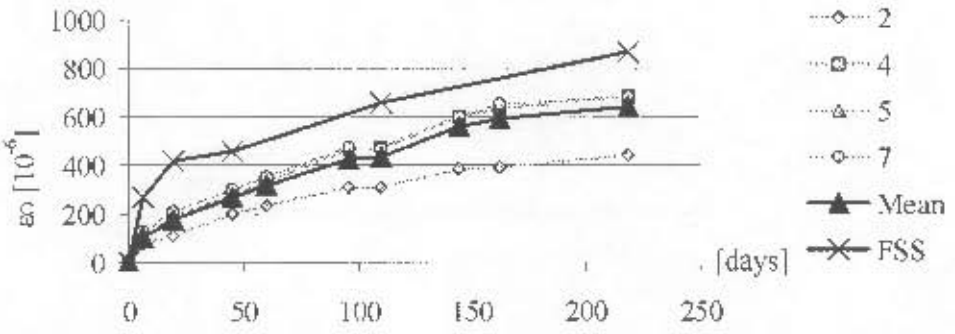

Figure 4.30: Strains on top of the overlay: Specimens A4 (notched interface A, Overlay 2 (HS))

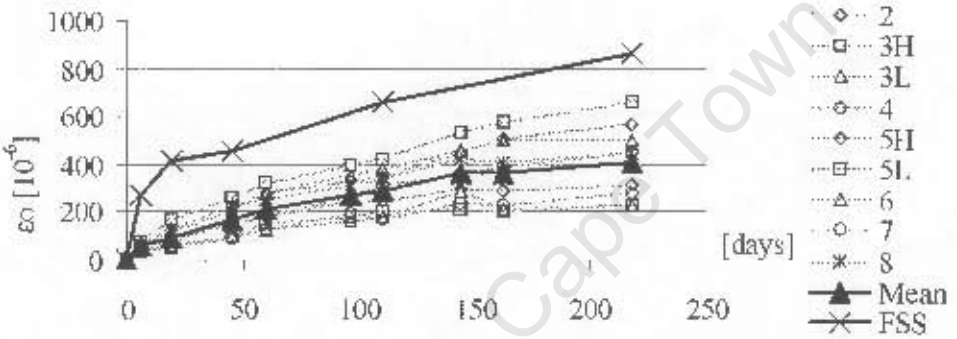

Figure 4.31: Strains on top of the overlay: Specimens A5 (notched interface B, Overlay 2 (HS))[3]

4.5.4 Discussion of test results

Specimens A2-A5 showed very large scatter of test results, which are a result of the formation of overlay patches along the member, separated by cracks. The evaluation of strain characteristics on continuous, "long" overlays was not possible with these specimens. The position of strain-measuring discs in respect to cracks might have influenced the measured strain. However, no strain trends related to the distance to cracks could be established, i.e., some positions next to cracks showed relatively high, others relatively low strain.

Specimens A1 and B1 did not crack and were the most conclusive in terms of strain distribution along the member length. It was evident that the location along the specimens at the interface or on top of the overlay had no influence on overlay strain values. Maximum and minimum strains occurred arbitrarily across different locations along the beams, with the scatter of test results being relatively small. Typical variation of strains along the length of the member is presented in **Figure 4.32**, using interface strains of Specimens A1, measured 98 days after the completion of curing, as an example.

[3] For locations 3 and 5, see footnote 1 on page 88

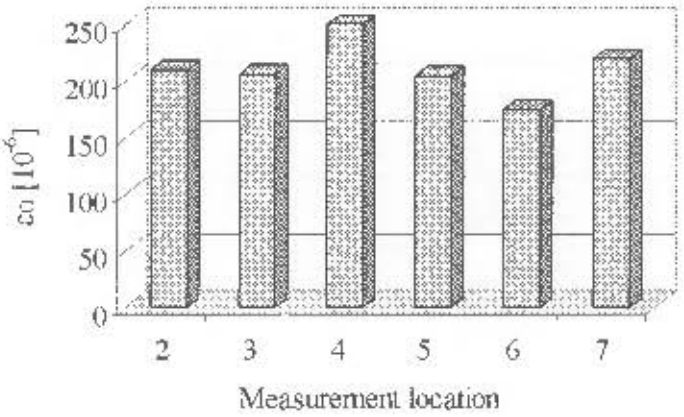

Figure 4.32: Variation of strains along the interface of Specimens A1, measured 98 days after completion of curing

The substrate beam provided constant restraint to overlay shrinkage along its whole length. The only exceptions to this observation were the member ends, which will be discussed separately in Section 4.10.

4.6 Strain across the overlay depth

Drying shrinkage in concrete members has a maximum value at the surfaces exposed to the environment, which causes strain gradients throughout the member thickness. In bonded overlays, drying might also take place at the interface to the substrate, depending on the pore structure and moisture condition of the substrate surface region. Overlays therefore experience a non-linear shrinkage profile across their depth. However, existing analytical models for bonded concrete overlays usually assume a constant shrinkage profile, and hence constant direct strain, across the overlay depth (Chapter 3). In such models, the only differences in strain across the overlay depth are those resulting from curvature. The simplified assumption of constant strain facilitates the analytical modelling and is generally believed to be applicable for relatively thin overlays. On Specimens A1-A5, overlay strains were measured at the interface and on top of the composite member, in order to test if the assumption of constant strain throughout the overlay depth is realistic.

Overlay strains of Specimens A1-A5 are summarized in **Figures 4.33**. The strain values in the figures represent the mean value of all locations along the member, with exception of member end locations.

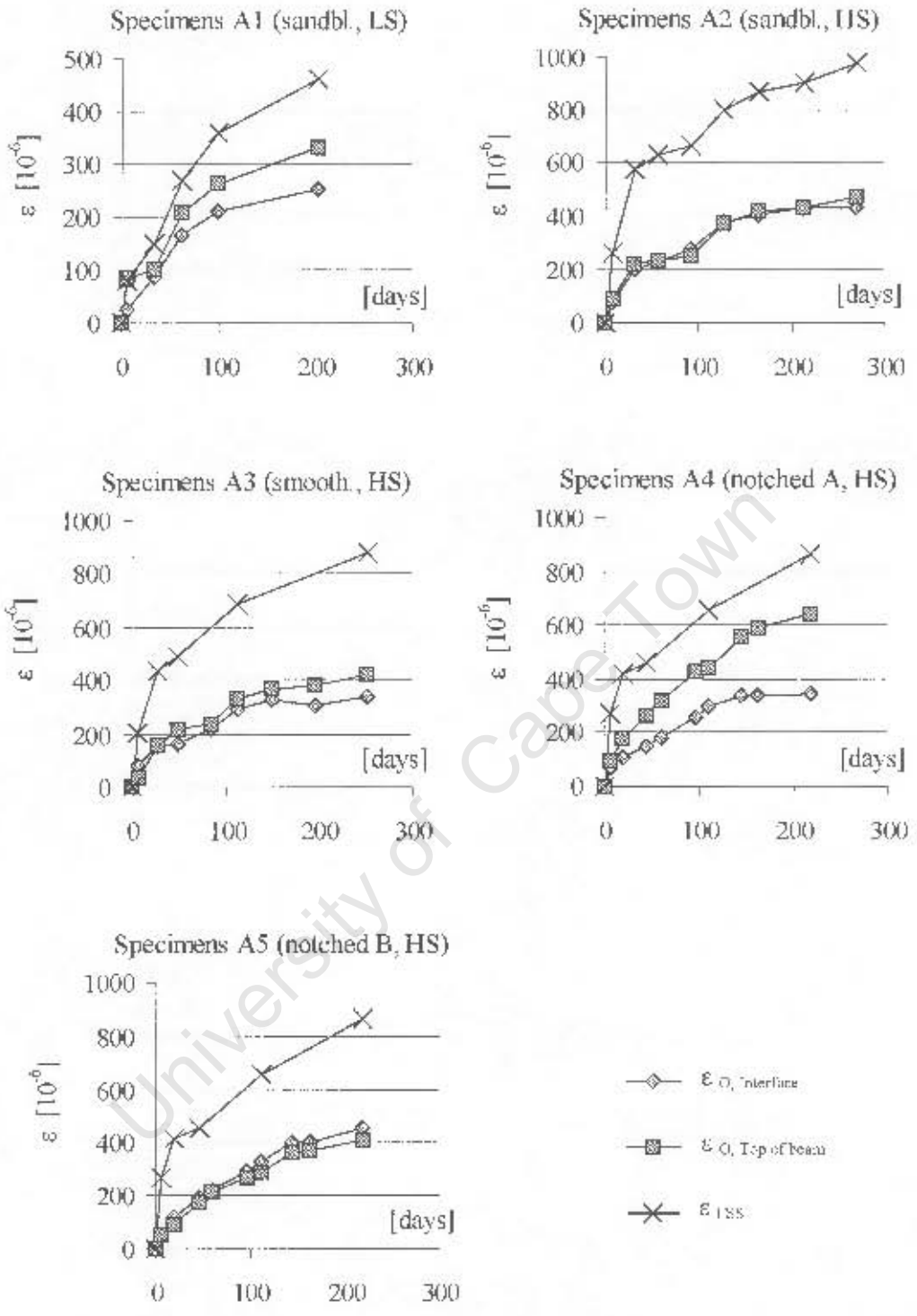

Figures 4.33: Summary of test results of Specimens A1-5, overlay shrinkage strain ε_O and free shrinkage strain ε_{FSS}

Specimens A2 experienced very similar overlay strains at the interface and on top of the beams. In Specimens A1 and A3, overlay strains on top of the composite member were slightly higher than at the interface. Specimens A4 showed a unique and unusual strain

distribution across the overlay depth with the top of the member experiencing substantially larger strain than the interface. By contrast, Specimens A5 experienced slightly larger overlay strain at the interface, compared to the top of the member. Strains on Specimens A2-A5 might have been influenced by the crack pattern in the overlay, which could explain the strain profiles in Specimens A4 and A5.

The strain distributions across the overlay depth of Specimens A1 – A5, expressed as the ratio between overlay strains on top of the member and overlay strains at the interface, are presented in **Figure 4.34**.

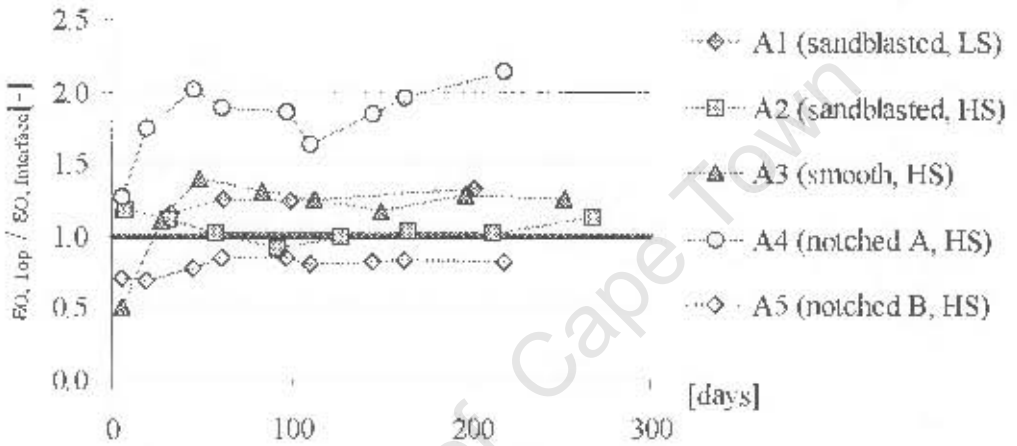

Figure 4.34: Strain distribution across the overlay depth of Specimens A1 – A5: ratio between strains on top of the member and interface strains

Figure 4.34 shows that using Specimens A1-5 it is difficult to generalize the strain distribution across the overlay depth. However, it appears that strains on top of the member have the tendency to be somewhat higher than interface strains. This was expected due to the influences of restraint decay in regions distant from the restraining substrate, and curvature. On overlays with depths considerably greater than 40 mm, the difference between interface strain and strain on top of the member would be expected to increase with increasing overlay depth. However, for the computation of tensile stress in relatively thin overlays, i.e. overlays up to approximately 40 mm depth, it seems reasonable to make the simplified assumption of constant strain, and hence, constant stress across the overlay depth. If interface strain values are utilised for this, the computation of stresses is conservative.

4.7 Magnitude and development of overlay strains

4.7.1 Introduction

This section comprises the analysis of overlay strain magnitudes of Specimens A1-A5 and B1, with an emphasis on the complex interaction between different strain and stress components. A method for the analysis of overlay strains is introduced, including a critical assessment of the practical limitations of this method. Fundamental strain characteristics are identified and discussed.

4.7.2 Sign convention

Free shrinkage strain, i.e., contraction, is considered as positive strain. Compressive strain in structural members, however, is generally considered as negative strain. For the evaluation of strain measurements, compressive strain on the composite members, as well as free shrinkage strain is defined as positive.

4.7.3 Different strain components

Overlay strain measurements on composite members represent the sum of different strain components. These can be divided into the following:

- Direct elastic strain
- Curvature strain
- Strain reduction due to overlay stress relaxation
- Substrate creep strains
- Interface slip

Direct elastic strain results from the interaction between overlay and substrate. The overlay attempts to contract, which is partly counteracted by the restraining action of the substrate. Overlay shrinkage induces compressive stress into the substrate, which is coupled to compressive strain, i.e. contraction. The substrate does not restrain overlay shrinkage completely and, depending on the magnitude, of restraint, both overlay and substrate undergo elastic strain, i.e. shortening. Direct elastic strain is a positive strain component (compressive strain).

Curvature is caused in members that are free to deform, with the overlay commonly experiencing compressive bending strain. Curvature strain in the overlay is therefore a positive strain component.

The partial restraint of overlay shrinkage induces tensile stress into the overlay. The tensile stress is the result of an imposed deformation, or, in actual fact, it is the result of the prevention of an attempted deformation, which, in principle, is the same phenomenon.

Concrete members under constant imposed deformation experience stress relaxation with time, i.e., a time dependent reduction in stress. The effect of stress relaxation is generally not associated with strain. However, overlay stress relaxation reduces tensile overlay stress, which leads to a redistribution of forces in the composite member. The redistribution of forces, in turn, has an influence on overlay and substrate strains. Stress relaxation can be divided into short-term and long-term effects. As stated in Section 2.5.2, a large component of tensile stress relaxation in concrete occurs in the early hours after stress induction. Short-term overlay relaxation has therefore a more direct influence on strain of the composite member as rapid relaxation of overlay tensile stress could possibly prevent the development of direct elastic strain. Therefore, overlay stress relaxation causes a reduction of positive strain components.

Substrate creep strains result from sustained elastic stress related to the restraining action described above. Substrate creep strain is a positive strain component. It has commonly not been considered in the modelling of bonded concrete overlays, however it proved to be significant for the tested specimens.

Interface slip could be caused by localised debonding, leading to overlay movement relative to the substrate. Slip is a positive strain component.

The accurate estimation of the magnitudes of individual strain components from overlay strain measurements is difficult as all the above components interact with each other and depend on the time-dependent material characteristics of substrate and overlay (**Figure 4.35**). However, the trends in strain development observed on the composite specimens allow a reasonable estimation of the influence of different strain components, as well as an estimation of overlay stress relaxation, which will be discussed in the following sections.

4.7.4 Method of analysis

In order to evaluate the magnitude of overlay strain (ε_O), it has to be compared to the free shrinkage strain (ε_{FSS}), i.e. the strain the overlay would have experienced had it not been restrained by the substrate. The difference between free shrinkage strain and overlay strain measured on the composite member indicates the degree of restraint. The degree of restraint, in turn, can be related to stress.

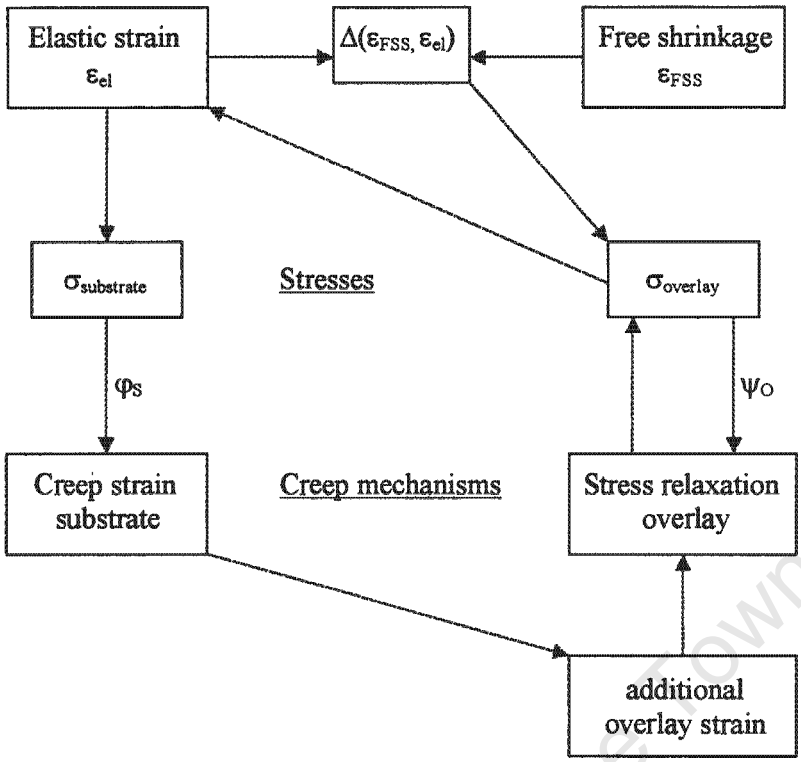

Figure 4.35: Schematic of the interaction between different strain and stress components in a bonded concrete overlay

In order to facilitate the analysis of the test results, the graphical presentation of overlay strain measurements (both at the interface and on top of the specimens) was divided into 2 different parts:

- Strain ratio between ε_O and $\varepsilon_{FSS} = \dfrac{\varepsilon_O(t)}{\varepsilon_{FSS}(t)}$
- Numerical strain difference between ε_O and $\varepsilon_{FSS} = \varepsilon_{FSS}(t) - \varepsilon_O(t)$

The ratio between ε_O and ε_{FSS} at any time can be used as an indicator of the combined influences of different strain components over the total test period under consideration (**Figure 4.36**). A relatively low initial ratio can best be interpreted by high early age overlay relaxation as discussed in Section 4.7.3. An increasing ratio between ε_O and ε_{FSS} with time indicates a decrease in the magnitude of overlay shrinkage restraint. As time proceeds, the overlay experiences an additional component of strain to what would be expected on the basis of pure elastic interaction between overlay and substrate. This can be related to substrate creep deformations. Another influence on an increasing ratio between ε_O and ε_{FSS} is that of decreasing overlay relaxation, i.e. the more mature overlay experiences less total relaxation and lower early age relaxation (early age relaxation denoting the relaxation shortly after shrinkage-induced stress). By contrast, a constant ratio between ε_O and ε_{FSS} over a certain

period of time corresponds to constant restraint. The latter, in connection with increasing strain values, theoretically leads to a constant increase in elastic overlay tensile stress. In practice however, overlay relaxation would prevent such a steady increase in stress.

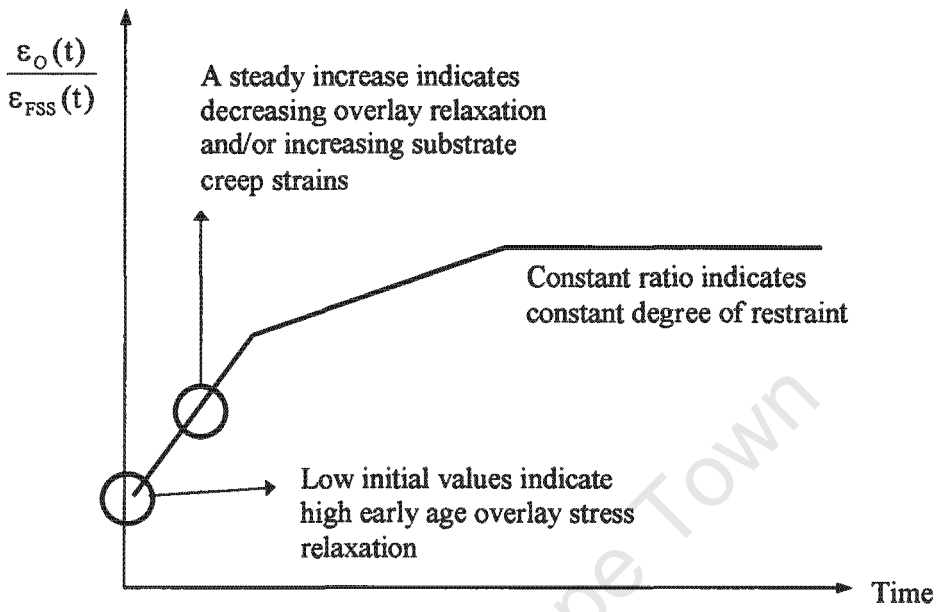

Figure 4.36: Schematic of graphical analysis of overlay strain values: ratio between overlay strains and free shrinkage strains

The numerical strain difference between ε_O and ε_{FSS} denotes the magnitude of restrained overlay shrinkage, i.e., the strain the overlay was not "allowed" to undergo (**Figure 4.37**). It is therefore directly related to the tensile stress development. Under purely elastic conditions, tensile overlay stress would correspond to:

$$\sigma_O = (\varepsilon_{FSS}(t) - \varepsilon_O(t)) \cdot E_O \qquad [4.1]$$

However, overlay stress relaxation reduces the elastic stresses substantially.

A large increase in ($\varepsilon_{FSS}(t)$ - $\varepsilon_O(t)$) over a given period of time generally corresponds to a low ratio between ε_O and ε_{FSS} in connection with a steady increase in elastic stress. As stated in Section 2.4.6, the tensile strain capacity of concrete is approximately 100 to 200.10^{-6}. In the absence of overlay stress relaxation, a numerical difference between ε_O and ε_{FSS} larger than this value would result in overlay failure, i.e. cracking or debonding. On sound overlays, ($\varepsilon_{FSS}(t)$ - $\varepsilon_O(t)$) can therefore serve as an indicator for overlay stress relaxation.

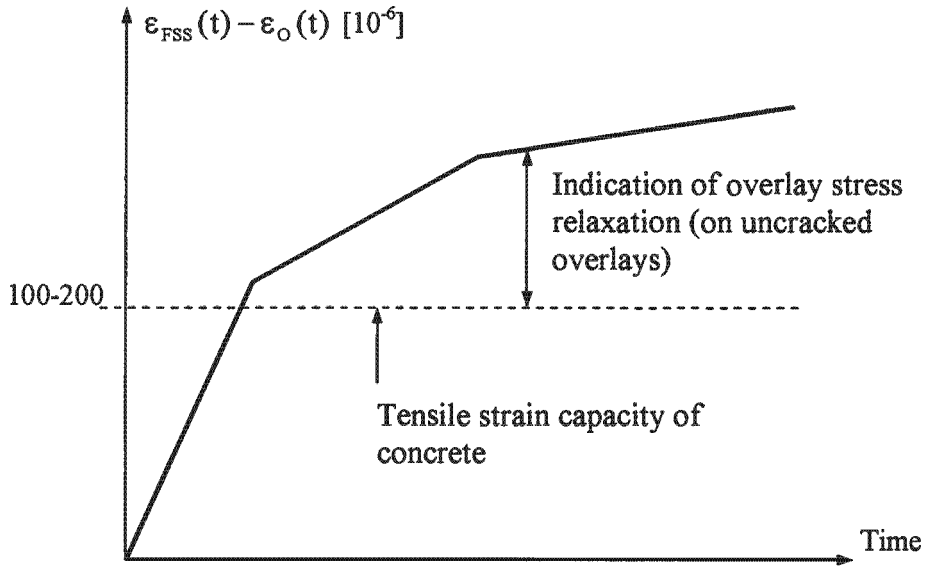

Figure 4.37: Schematic of graphical analysis of overlay strain values: numerical difference between overlay strains and free shrinkage strains

With the above, different strain components as well as overlay tensile stress can be estimated. However, correct estimation of different strain and stress components from overlay strain measurements is difficult. **Table 4.9** gives an overview of the influence that different strain components and overlay relaxation have on the development of the ratio between ε_O and ε_{FSS}.

Table 4.9: Influence of different strain and stress components on the time-dependent development of the ratio between ε_O and ε_{FSS}

Strain/stress component	Time-dependent ratio ε_O / ε_{FSS}
Elastic strain	constant
Curvature	constant
Substrate creep	increase
Overlay slip	increase
Overlay stress relaxation	decrease

Substrate creep, overlay slip, and overlay relaxation all lead to a reduction of tensile overlay stress. However, while the former two lead to an increase in the ratio between ε_O and ε_{FSS} with time, the latter leads to a decrease. As can be seen, the interpretation of overlay strain measurements in terms of different strain components is complex. The emphasis during interpretation of test results should therefore rest on the identification of trends rather than the analysis of isolated measurements.

4.7.5 Test results

4.7.5.1 Introduction

In the following sections, overlay strains are expressed as the mean of all measurement locations along the respective specimens. Mean values of overlay strains at individual locations along the members were presented in Figures 4.21 to 4.31. Strain at the member ends are excluded at this stage and are discussed separately in Section 4.10.

The restraint of differential shrinkage takes place at the interface between substrate and overlay. Interface strains are therefore the most indicative parameter of overlay shrinkage restraint. For this reason, the analysis of overlay strain values as discussed in the following sections is done for interface strains only. Strain gradients across the overlay depth were discussed in Section 4.6.

Analysis of test results was carried out for overlay strains that occurred during the first approximately 8-12 months after fabrication of the composite members. Strains during this period were believed to be of importance for two reasons. Firstly, they can be used for the identification of the time-dependent development of different overlay strain components. Secondly, the first 8-12 months represent approximately the period where significant shrinkage strains occur. Short-term overlay strains, i.e. strains during the first weeks after the onset of drying shrinkage, are discussed in connection with overlay failure in Section 4.11.

In Section 4.7.5.2, test results are presented and briefly discussed. Detailed analysis of overlay strains in terms of the following parameters is done in Sections 4.7.6 to 4.7.9:

- Magnitude and development of overlay strains
- Influence of interface texture on overlay strains
- Substrate creep deformations
- Overlay stress relaxation

The main findings are summarized in Section 4.7.10.

4.7.5.2 Presentation and discussion of test results

Strain test results of Specimens A1 (sandblasted interface, Overlay 1 (LS)) are presented in **Figures 4.38**.

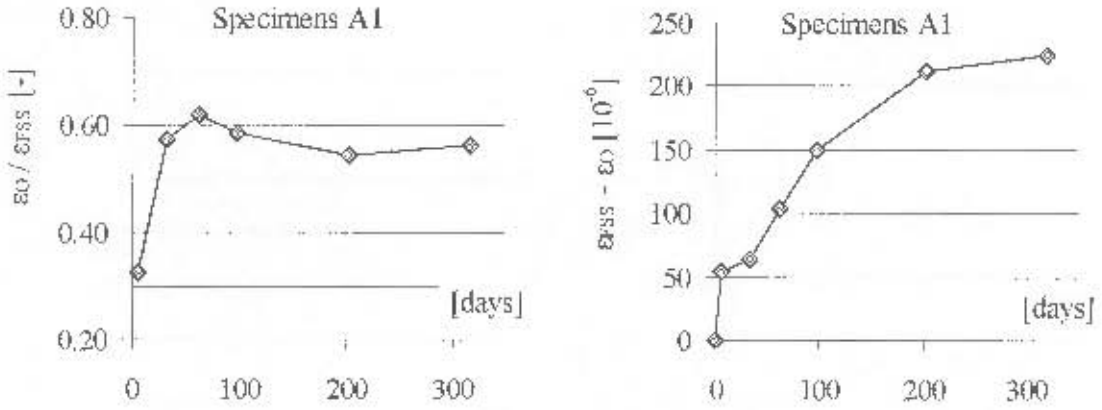

Figures 4.38: Specimens A1 (sandblasted interface, Overlay 1(LS)): Summary of test results

The initial ratio between ε_O and ε_{fss} on Specimens A1 was relatively low, compared to the rest of the test period (Figure 4.38, left). This indicates high early age overlay relaxation as discussed in Section 4.7.4. Considering the remaining test period, the ratios between ε_O and ε_{fss} were relatively constant at between 0.55 and 0.61. This was related to a relatively steady increase in numerical strain difference between ε_{fss} and ε_O (Figure 4.38, right). However, the critical value of the tensile strain capacity of concrete of roughly 100-200.10^{-6} was only reached after approximately 100 days. During this time, overlay relaxation should have reduced overlay tensile stress substantially, which explains the absence of cracks on Specimens A1.

Specimens B1, which were made with a "medium shrink" overlay (Overlay 3) and sandblasted interface, showed essentially similar strain characteristics compared to Specimens A1. However, overlay strain as a ratio of free shrinkage was considerable lower on Specimens B1 (**Figures 4. 39**).

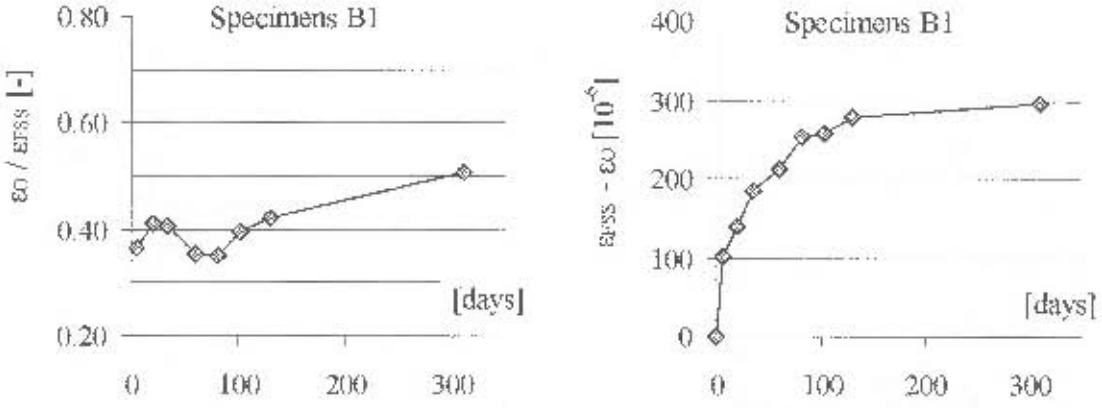

Figures 4.39: Specimens B1 (sandblasted interface, Overlay 3 (MS)). Summary of test results

During the first approximately 150 days, the ratio between ε_O and ε_{FSS} on specimens B1 was relatively constant at between 0.35 and 0.42. This was connected to a steadily increasing numerical difference between ε_O and ε_{FSS}. Similarly to Specimens A1, strains developed at a rate slow enough for relaxation to reduce tensile overlay stress and prevent cracking. After a period of approximately 150 days, overlay strains, compared to free shrinkage strains, developed at an increasing rate, which can probably be related to the increasing influence of substrate creep strains.

The relatively high overlay strains of Specimens A1, in comparison to free shrinkage, seem somewhat startling. However, absolute overlay strains of Specimens A1, in comparison to the other specimens, were low. Positive strain components, such as substrate creep, might have therefore had a relatively large impact on total strain values, which could explain the relatively high overlay strains.

As stated earlier, due to the complexity of overlay strain components, the focus of this section rests on the identification of general trends. Specimens A2-A5, which were made with the same overlay (Overlay 2 (HS)) but different interface textures, and all of which showed extensive cracking during the first 10 days, are therefore discussed concurrently. Results of Specimens A2-A5 are presented in **Figures 4.40 to 4.43**.

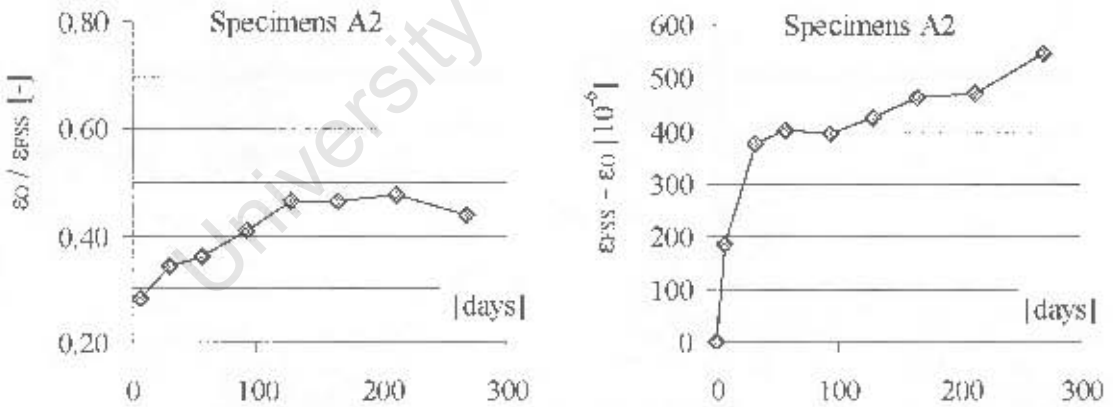

Figures 4.40: Specimens A2 (sandblasted interface, Overlay 2 (HS)): Summary of test results

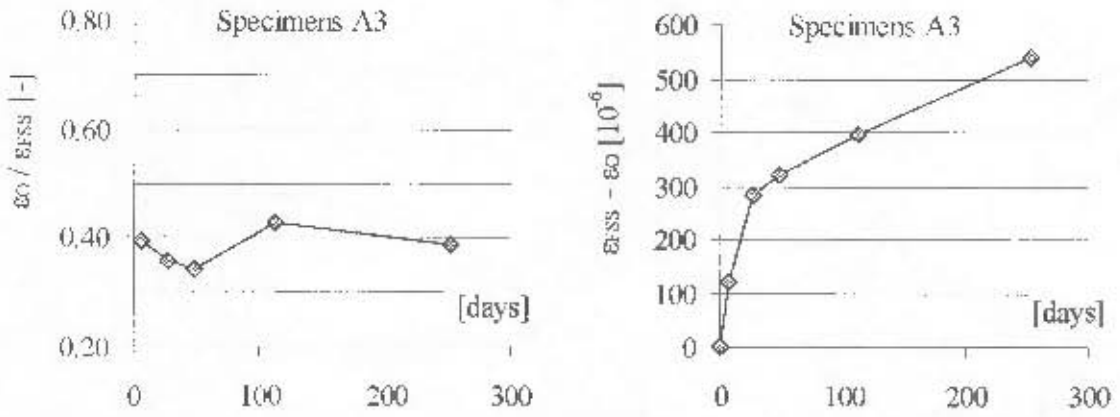

Figures 4.41: Specimens A3 (smooth interface, Overlay 2 (HS)): Summary of test results

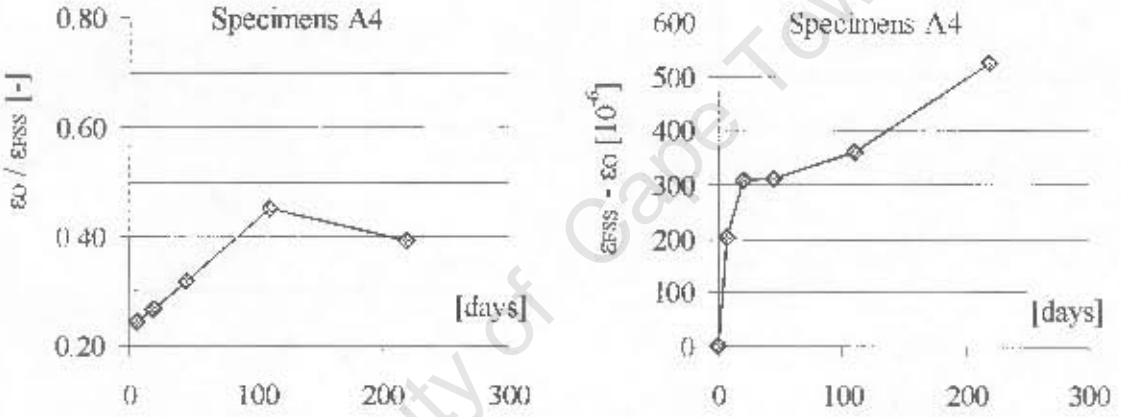

Figures 4.42: Specimens A4 (notched interface A, Overlay 2 (HS)): Summary of test results

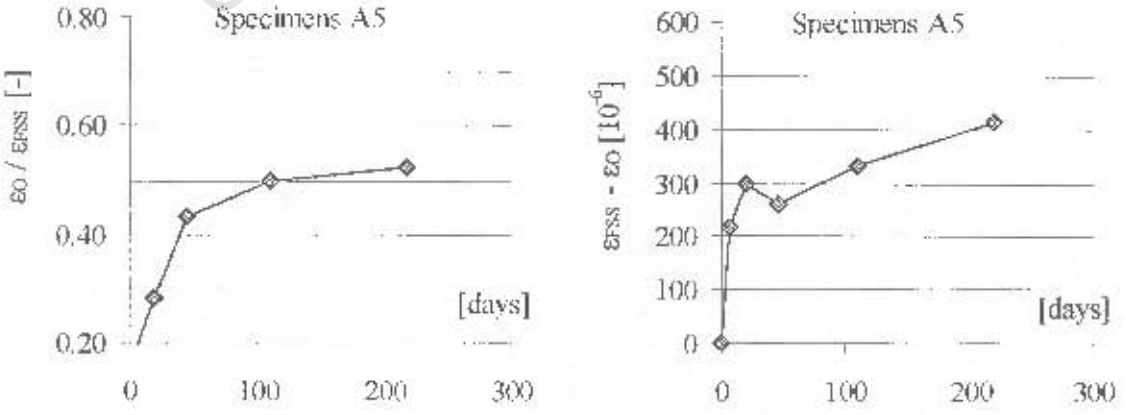

Figures 4.43: Specimens A5 (notched interface B, Overlay 2 (HS)): Summary of test results

Specimens A2-A5 showed a rapid increase in ($\varepsilon_{FSS} - \varepsilon_O$) during the first approximately 30-50 days, which resulted in overlay cracking at early ages. The characteristics of cracking are discussed in detail in Section 4.11. Subsequently, (ε_{FSS} - ε_O) generally showed a relatively constant increase at a slower rate. This was initially related to a relatively steady increase in the ratio between ε_O and ε_{FSS}, indicating a decreasing degree of restraint while the overlay was able to increasingly undergo more of its "desired" deformation. This effect can probably best be related to the dominant influence of substrate creep strains, as discussed in Section 4.7.4. At a later stage (after approximately 100 days), the ratio between ε_O and ε_{FSS} remained relatively constant as overlay strain and free shrinkage now developed at a similar rate. This indicated that none of the visco-elastic strain components had a significantly dominant influence as both substrate creep and overlay relaxation developed at relatively slow rates.

The above results on overlay strains in Specimens A1-5 and B1 allow conclusions on important strain characteristics in bonded concrete overlays, which is discussed in detail in the following sections.

4.7.6 The magnitude and development of overlay strain

All specimens experienced initial interface strain of approximately 25-35% of free overlay shrinkage strain. Subsequently, they showed the trend of an increasing ratio between ε_O and ε_{FSS} with time. The increase in interface strain can mainly be related to the following aspects:

- High early age stress relaxation in the overlay (initially low ε_O)
- Reducing relaxation in the overlay with time (increase in $\varepsilon_O/\varepsilon_{FSS}$)
- Increasing substrate creep deformations with time (increase in $\varepsilon_O/\varepsilon_{FSS}$)

Stress relaxation in concrete is higher at younger ages. The overlay therefore had a relatively high relaxation capacity during the first days of loading, i.e. during the first days after the onset of drying shrinkage. A substantial part of overlay stress was therefore released shortly after it was transmitted to the substrate. Due to redistribution of forces, this resulted in reduction of elastic strain shortly after elastic strains were induced, which explains the relatively low initial strain values. At later ages, relaxation in relation to applied load would have been less, which is one explanation of the increasing ratio between ε_O and ε_{FSS}. The overlay now had more "power" to cause elastic deformations at the interface as less of its stress was released. The other major influence is that of increasing substrate creep deformations under sustained imposed strain. This effect is discussed in more detail in Section 4.7.8.

Comparing all specimens, overlay strains in relation to free overlay shrinkage showed a relatively large range of results. In general, the overlay was able to experience approximately 25 to 50% of its free shrinkage strain during the test period. Specimens A1 were an exception

with relatively large long-term overlay strains of approximately 60% of free shrinkage. With information on overlay relaxation capacities, these numbers serve as an indicator for tensile overlay stress, which is discussed in Section 4.7.9.

4.7.7 The influence of interface texture on overlay strains and stresses

Specimens A2 – A5 were made with the same overlay (Overlay 2 (HS)) but different interface textures. The aim of these specimens was to investigate the influence of interface texture on overlay strain characteristics. The ratios between overlay strains at the interface and free shrinkage strains of Specimens A2 – A5 are summarized in **Figure 4.44**.

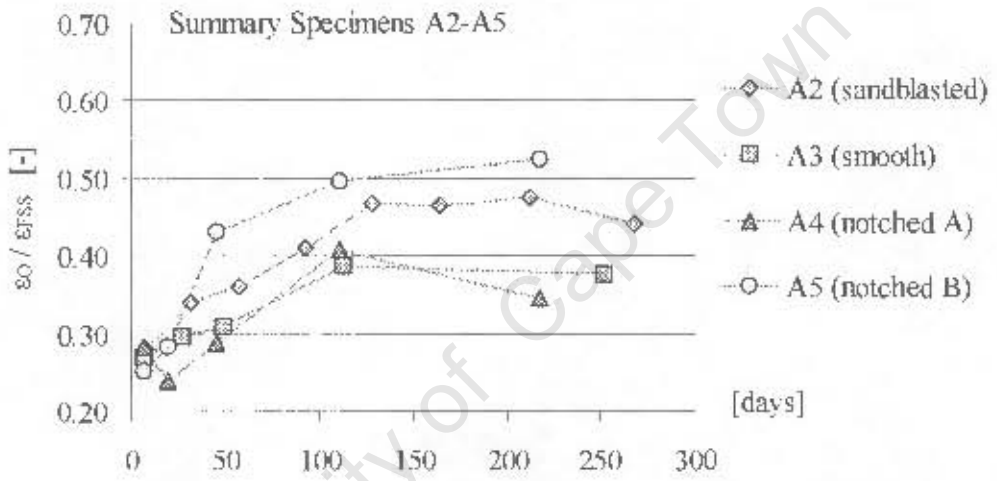

Figure 4.44: Specimens A2-A5 (Overlay 2, (HS)), summary of ratios $\varepsilon_O / \varepsilon_{FSS}$

All interface textures offered a different type of mechanical restraint. The sandblasted interface of Specimens A2 had a relatively uniform micro-roughness along the whole length of the member. The mechanical restraint of Specimens A3 (smooth interface) was theoretically restricted to anchorage of overlay concrete in open pores on the substrate surface. The notched interfaces of Specimens A4 and A5 provided good macro-roughness, with Specimen A4, providing notches in smaller intervals, producing more constant mechanical interaction. Rating the degree of mechanical restraint, it was assumed that Specimens A2 would have offered the highest restraint, followed by Specimens A4, A5, and A3. However, Figure 4.44 shows that the differences in the ratios $\varepsilon_O / \varepsilon_{FSS}$ were not connected to the degree of mechanical restraint as rated above. Overlay strains at the interface could, therefore, not conclusively be related to interface texture. It seems that the degree of mechanical bond at the interface was not a relevant factor for shrinkage restraint on Specimens A2 – A5.

By contrast, as discussed in Section 7.4.3.1, interface shear bond strengths were significantly different for specimens with different interface textures. Differences in shear bond strengths could mainly be related to differences in mechanical interaction between substrate and overlay, interfaces with a higher macro-roughness having higher bond strength. Interface shear bond strengths essentially conformed to the rating of mechanical interaction as described above. Hence, in fully bonded overlays, shrinkage restraint appears to exist independently from interface texture and macro-mechanical bond strength. The significance of this observation is that, in fully bonded overlays, stresses due to differential shrinkage can be modelled without consideration of interface texture.

4.7.8 The characteristics of substrate creep deformations

Compared to the initial magnitudes, all specimens experienced an increase in the ratio between ε_O and ε_{FSS} with time (compare Figures 4.38 to 4.43). An increase of the ratio between ε_O and ε_{FSS} with time indicates a decreasing degree of restraint as the overlay can gradually undergo more of its "desired" deformation. As stated in Section 4.7.4, this phenomenon can in theory be explained by the mechanisms of interface slip or substrate creep. Measurements of strains across the interface, as discussed in Section 4.8, indicated that slip did not occur in the tested specimens. Substrate creep is therefore considered to be the main mechanism causing the decrease in overlay shrinkage restraint. This can be explained by looking at the magnitudes of interface strain.

For example, Specimens A2 – A5 had overlay strains at the interface of approximately 200.10^{-6} after roughly 50 days, which further increased with time. Assuming full bond, overlay and substrate had the same interface strain at any time (results discussed in Section 4.8 show that this assumption is reasonable). The substrate was therefore subjected to considerable sustained compressive stress:

$$\sigma_S = \varepsilon_I \cdot E_S \approx 200.10^{-6} \cdot 30 = 6 \text{ MPa}$$

The above was calculated with the simplifying assumption that the full amount of substrate interface strain after 50 days caused elastic stress. Actual substrate stress would be lower since a portion of measured interface strains consists of substrate creep strains. However, the above numbers show that the substrate experienced relatively high compressive stress at the interface, which necessarily resulted in considerable creep deformations. Using the ACI (1992) method for the estimation of creep strains in the tested specimens, long-term substrate creep strains could be estimated to be approximately 130% of imposed elastic strain (compare Section 6.10). This shows that substrate creep was a major strain component in the composite members.

The influence of substrate creep would be less pronounced on composite members with relatively old substrate sections. However, even old concrete members experience considerable creep deformations under sustained load, which can be estimated using conventional models for the prediction of creep strain (compare Section 2.5.1).

Substrate creep strains are commonly not included in the modelling of bonded overlays. However, test results indicated that they represent a major strain component that should be considered if overlays are to be modelled realistically. The mechanisms of substrate creep in respect to other strain components are discussed in detail in Chapter 6.

4.7.9 Stress relaxation in uncracked overlays

Specimens A2-A5 cracked extensively during the first 10 days. Overlay stress relaxation of these specimens is discussed in Section 4.11.4. By contrast, Specimens A1 (sandblasted interface, Overlay 1) and B1 (sandblasted interface, Overlay 3) did not crack during the test period. The critical magnitude of shrinkage restraint, which is approximately $100\text{-}200.10^{-6}$, was only reached after roughly 100 and 50 days for Specimens A1 and B1 respectively (compare Figures 4.38 and 4.39). During this time, sufficient overlay relaxation developed to prevent tensile stress exceeding tensile strength.

The strain measurements taken on these specimens allow an insight into overlay relaxation characteristics. The estimation of overlay stress relaxation in the following is carried out for Specimens B1 (Overlay 3). Elastic modulus E_O and tensile strength f_t of Overlay 3 at 28 days were approximately 30 GPa and 3 MPa respectively (compare Section 4.3). Restrained overlay shrinkage strain at 28 days, expressed by the numerical difference between ε_{rss} and ε_O (Figure 4.37), was 140.10^{-6}. In the absence of stress relaxation, the restrained shrinkage would have corresponded to elastic stress of

$$\sigma_{O,\,elastic} = \varepsilon_{O,\,restrained\ shrinkage} \cdot E_O = 140.10^{-6} \cdot 30.10^{3}\ MPa = 4.2\ MPa$$

Therefore, at 28 days, tensile stress relaxation can be computed to a factor ψ_O:

$$\psi_O >= f_t / \sigma_{O,\,elastic} = 3.0 / 4.2 = 0.71$$

The factor 0.71 implies that tensile relaxation reduced the actual stress to 71% or less of the elastic stress, thus releasing at least about 29% of the elastic stress. Repeating the above calculations for days 50 and 100 computes relaxation factors of no less than 0.50 and 0.43 respectively. These substantial stress relaxation values explain the absence of overlay cracking on Specimens B1.

Specimens A1 had comparatively low free shrinkage strains and high overlay strain. The computed relaxation factor at 150 days, following the above method, was no more than 0.82, which indicated the large remaining strain capacity.

4.7.10 Summary of main findings

Modelling bonded concrete overlays in a realistic way requires information on different strain components. The development of strain on the test specimens discussed in the previous sections gave an insight into the main strain components experienced in bonded overlays. The influences of substrate creep and overlay stress relaxation were identified. In Section 6, these strain components are incorporated in an analytical model, based on strain characteristics discussed in the previous sections. The influences of other strain components such as slip and curvature are discussed in the following sections.

The influence of interface textures on overlay strains was established. For the design of fully bonded overlays it is important to note that the interface texture does not influence overlay strains and stresses.

Time-dependent magnitudes of overlay strains discussed in the previous sections were used to develop and verify a new analytical model for bonded concrete overlays, as discussed in detail in Section 6. Important information gained from the testing of composite specimens, including the above aspects, which was used for the development of the analytical model is summarized in Section 4.12.

4.8 Strains across the interface between substrate and overlay

Overlay strain characteristics were discussed in the previous sections. This section investigates the characteristics of shrinkage restraint in relation to substrate strains at the interface.

Specimens B1 and B2 were cast for the measurement of strains across the interface, i.e., the comparison of overlay and substrate strains at the interface. Specimen dimensions and strain measurement locations were presented in Section 4.2.4.3. The overlay of Specimen B2 (smooth interface) debonded after a few weeks. Therefore, no test results in relation to the actual test parameter could be gained from this Specimen. The mechanisms of debonding observed on Specimen B2 are discussed in Section 4.11.3.

Test results of Specimen B1 (sandblasted interface) are presented in **Figure 4.45**.

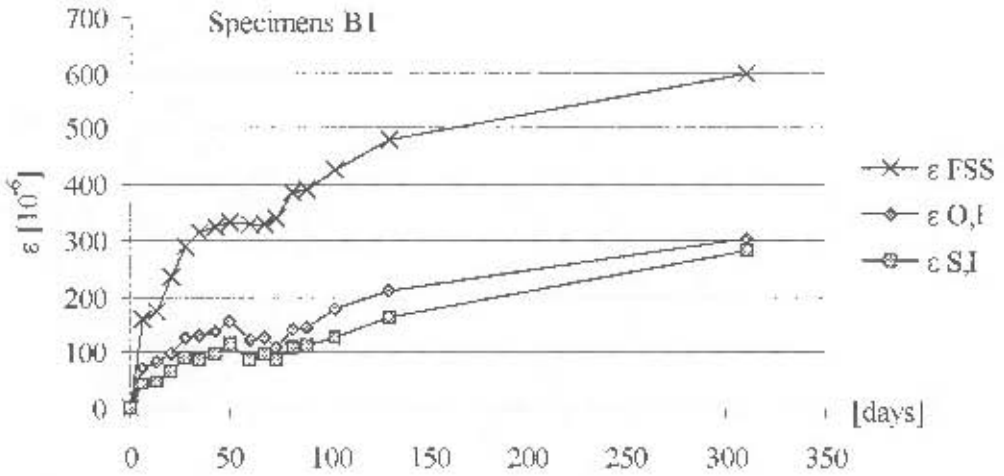

Figure 4.45: Specimen B1: Overlay and substrate strains at the interface in comparison to free shrinkage strains

Strains in the above figure represent the mean value of all test locations along the specimen. The magnitude of overlay strains at the interface of Specimen B1 was discussed in Section 4.7.5. The above figure shows that at the interface, substrate strains were very similar to overlay strains. In the first 7 days, the overlay showed a higher strain rate compared to the substrate. This resulted in an early difference in strain values of approximately 30.10^{-6}, which remained relatively constant throughout the test period. Very similar observations were made on Specimens C and D, as discussed in Section 4.9.

This initial overlay contraction relative to the substrate is probably the result of overlay relaxation, i.e. the overlay released a portion of its strain energy before it caused lasting strain in the substrate. Another possible explanation is overlay slip at the interface. However, overlay slip should have had a maximum value at the member ends, but very similar initial strain differences were observed along the whole length of the member. Overlay stress relaxation, therefore, was probably the main mechanism causing this phenomenon. More important however is that, except for this initial "head-start" of overlay strain, both substrate and overlay strains of Specimens B1 progressed at virtually the same rates, which indicates that overlay and substrate were fully bonded.

The above allows conclusions on the mechanisms of interface slip and interface shear stress. Interface slip, which was used by Silfwerbrand (1997) to model overlay deformations (compare Section 3.8), was shown not to be a factor responsible for overlay strain. Assuming adequate bond, it therefore appears appropriate to model composite members with the assumption substrate and overlay are fully bonded.

Another important aspect related to substrate strains is that of interface shear stress along the member. Substrate strains at the interface of Specimen B1 were relatively constant along the

length of the member. Likewise overlay strains at the interface (see Section 4.5) were sensibly independent of the measurement locations along the specimens. The only exceptions were the beam ends which showed slightly higher strains than the rest of the member (**Figure 4.46**).

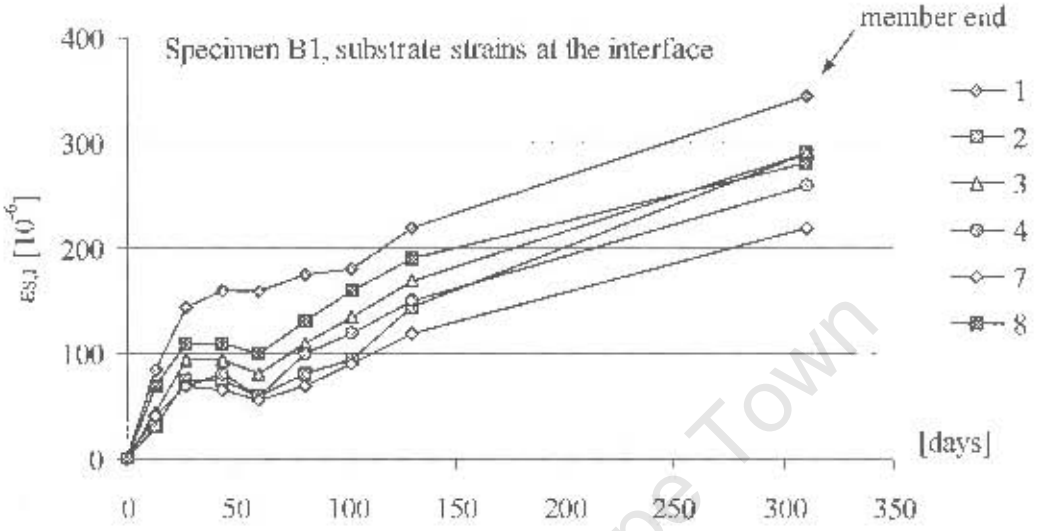

Figure 4.46: Specimen B1, distribution of substrate strains along the interface. (For the definition of strain locations 1-8, see Section 4.2.4.3)[4]

The section to follow (Section 4.9) shows that strains "fade out" into the depth of the substrate to reach a point of zero strain. This indicates that shrinkage restraint is a localised phenomenon at the interface. In connection with constant substrate strain along the whole length of the interface this means that interface shear, which is the mechanism of restraint, must be constant along the whole length of the interface. The only exceptions to this are the member end locations that showed slightly higher interface strain, indicating higher shear stress values.

The above stands in contrast to existing analytical models for bonded concrete overlays, which assume that interface shear stresses due to differential shrinkage exist only at the member ends (compare Chapter 3). For the correct modelling of bonded overlays it is very important to identify the mechanisms of shrinkage restraint in respect to the above aspects. The following sections investigate the restraining action of the substrate in more detail.

[4] Strain measuring discs of locations 5 and 6 detached from the specimen during the test period. No long-term results are available for these locations.

4.9 Strains across the substrate depth

4.9.1 Introduction

The characteristics of overlay strains as well as substrate strains along the interface were discussed in the previous sections. Substrate strains at the interface were found to be relatively constant along the whole length of the member, indicating constant restraint of overlay shrinkage along the interface. Test results on Specimens C and D, discussed in this section, were used to characterise the restraining action of the substrate in more detail. This was done by measuring strains across the substrate depth. The restraint of differential shrinkage causes direct strains in the substrate and, in members that are free to deform, secondary strains due to bending. Specimens C were not free to curve and were used for the assessment of direct strains in the substrate. In addition, Specimens D were used for the assessment of the combined influence of direct strains and curvature. Specimens with different overlay depths were tested to assess the influence of the relative dimensions of substrate and overlay.

Test results of Specimens C and D are presented and discussed separately in Sections 4.9.2 and 4.9.3 respectively. In addition to the above aspects, test results on Specimens D could be used for the quantitative estimation of substrate creep strains as discussed in Section 4.9.4. A summary of the main findings concludes this section.

4.9.2 Members not free to curve - Specimens C

Specimens C were prepared for testing the direct influence that differential shrinkage has on substrate strains, excluding secondary effects from curvature. Specimens C are not intended to represent the most common restraint characteristics experienced in composite members. In common members, the substrate concrete usually provides longitudinal restraint. Specimens C were designed to fundamentally discuss the question of strain localisation. Specimen dimensions were presented in Section 4.2.4.2 (compare Figure 4.9, page 78). Strains across the overlay depth were not measured on Specimens C as these were discussed in the previous sections. Measurements on Specimens C were taken during a period of approximately 50 days, as the early weeks are the most important period for the development of overlay stresses in composite members. **Figure 4.47** presents the development of interface strains in the overlay and strains across the substrate depth. The magnitudes of substrate interface strains are used to compare the substrate's restraining action in respect to different overlay depths. In all specimens, substrate strains had a maximum value at the interface and showed the tendency to approach zero strain in regions away from the interface. Interface strains increased with decreasing overlay depth, which can be ascribed to the circumstance that thinner overlays have a higher rate of shrinkage strain development compared to thicker overlays.

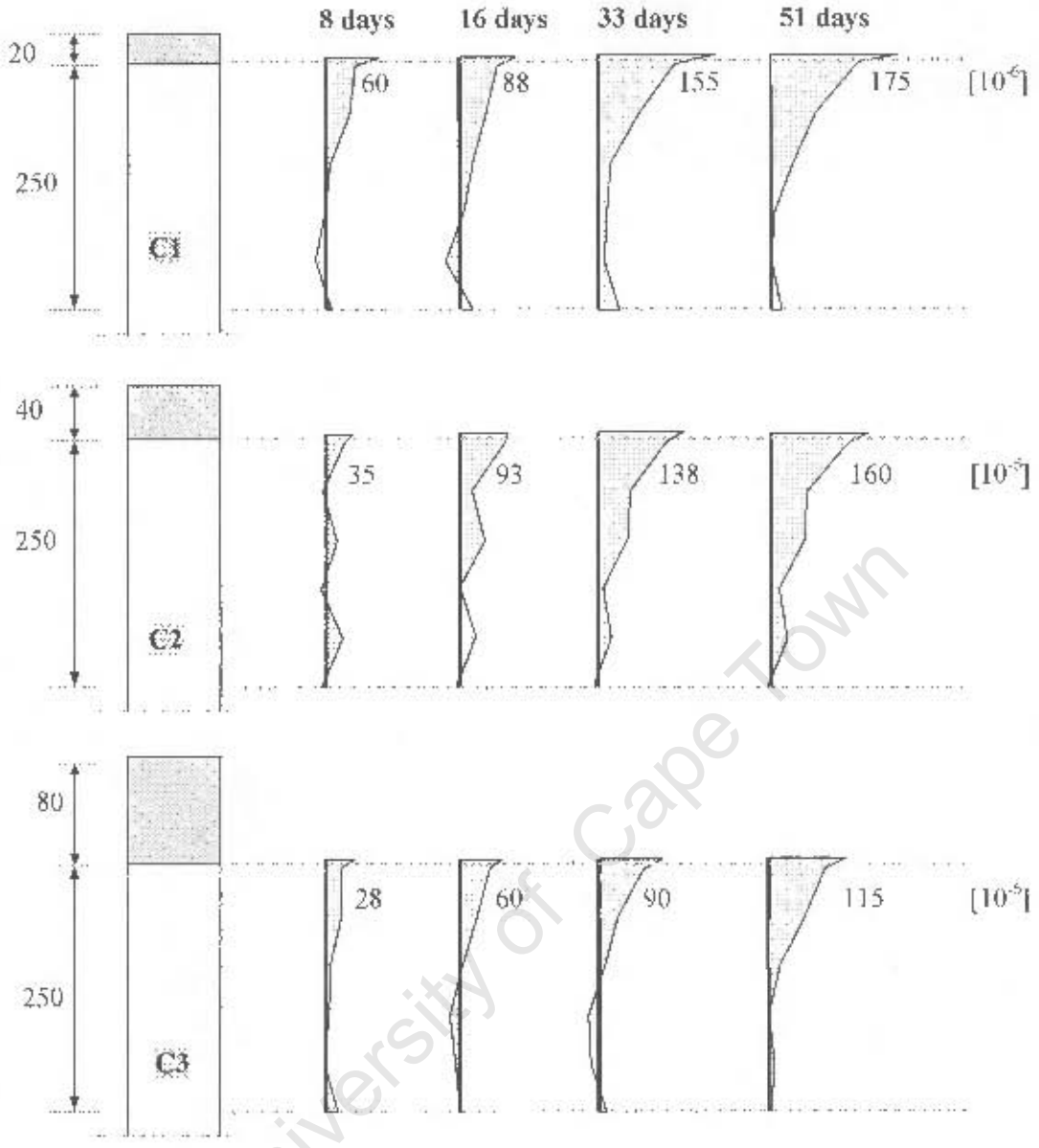

Figure 4.47: Specimens C, schematic of strain development across the substrate

On all specimens, interface strains in the overlay were found to be slightly higher than those in the substrate. This effect was also observed on Specimens B1, as discussed in Section 4.8.

The above test results allow important conclusions on the applicability of the following 2 main assumptions on which existing analytical models (compare Chapter 3) are based:

- Bernoulli's hypothesis of plane sections remaining plane after being stressed applies to members subjected to differential shrinkage, i.e. strain profiles across the sections are linear
- Shrinkage restraint is directly related to the relative member dimensions of substrate and overlay

Strains measured across the substrates of Specimens C indicate that the above two assumptions do not apply for specimens subjected to differential shrinkage. By contrast to the above assumptions, strain profiles across the sections of Specimens C, approaching a point of zero strain, were non-linear and strain magnitudes appeared to be independent of overlay dimensions. The restraint of differential overlay shrinkage appears to be a localised phenomenon at the interface that cannot be modelled using conventional beam theory. This shows the need for an analytical approach with which bonded overlays can be modelled in a more realistic way. The magnitudes of substrate interface strains indicate the influence that the relative member dimensions have on the degree of shrinkage restraint. As discussed in Section 4.4.2.3, thin overlays experience a higher rate of shrinkage development, compared to thick overlays. Interface strains of Specimens C must therefore be interpreted in relation to the respective free shrinkage strain of the overlay. Free overlay shrinkage strains of Specimens C are presented in Figure 4.19. Substrate interface strains in relation to free overlay shrinkage are presented in **Figure 4.48**.

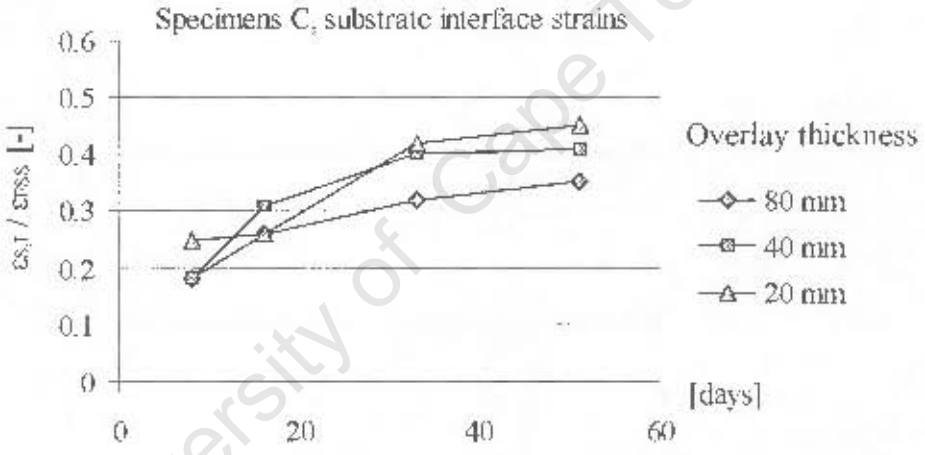

Figure 4.48: Specimens C, ratio between substrate strains at the interface and free overlay shrinkage strains

The ratios between ε_0 and ε_{fss} and the development of interface strains of Specimens C were very similar to those of Specimens A and B. For the interpretation of strain magnitudes, reference is therefore made to Section 4.7.

Specimens C1 to C3 experienced similar substrate interface strains in relation to the respective free overlay shrinkage. Thus, overlay dimensions (here presented by overlay thickness) had little practical influence on shrinkage restraint. Therefore, as stated above, restraint of overlay shrinkage appears to be a localised phenomenon at the interface.

However, the observation that Specimens C1 (overlay depth 20 mm) had the highest interface strain in relation to its free shrinkage, is of considerable interest and further research is necessary to conclude on the effects of overlay thickness on interface strains.

4.9.3 Members free to curve – Specimens D

Specimens D, in contrast to Specimens C, were free to deform and the resulting strains across the composite sections were a combination of direct strains and curvature. On these specimens, strains were measured across the whole substrate depth as well as across the overlay. Specimen dimensions are discussed in Section 4.2.4.5 (compare Figure 4.10, page 79).

The development of strains across the members are presented in **Figure 4.49**. Numerical substrate interface strains are presented as an indicator for the degree of restraint in respect to different overlay depths.

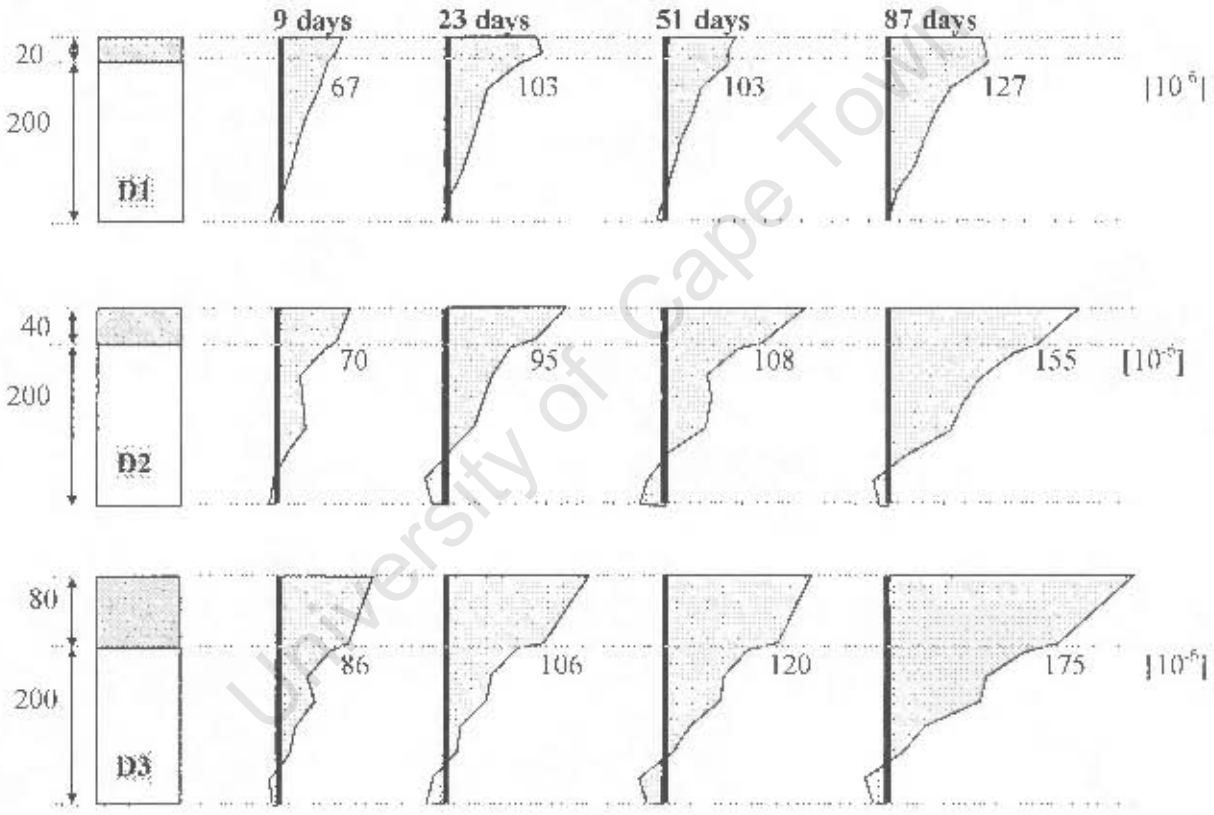

Figure 4.49: Specimens D, schematic of strain development across the member depths

Interface strains in Specimens D were very similar during the first approximately 50 days. Subsequently, the specimens clearly showed increasing interface strains with increasing overlay depth. This development can be related to the circumstance that thin overlays initially experience a higher rate of shrinkage development and therefore a lower rate at later ages, compared to thicker overlays.

The influence of curvature on interface strains in relation to overlay thickness is difficult to assess from the above measurements. Curvature is linked to the overlay force resulting from restrained shrinkage (**Figure 4.50**).

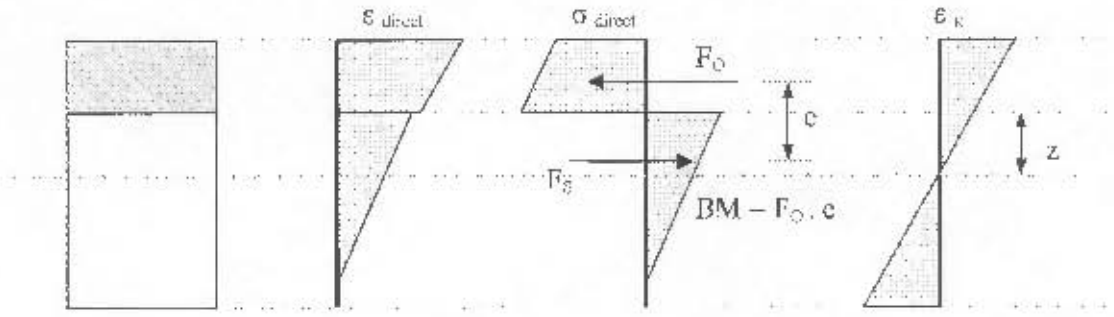

ε_{direct} = Direct strains across the member (assuming simplified strain profile, based on localised strain discussed in Section 4.9.2)
σ_{direct} = Direct stress (in the overlay resulting from restrained shrinkage)
F_O, F_S – Resulting forces in overlay and substrate
c = Lever arm of internal forces
BM = Bending moment
ε_κ = Curvature strain resulting from BM and member stiffness
z – Distance between centroid of the composite section and interface

Figure 4.50: Schematic of strains and stresses in a composite member that is free to curve, assuming simplified strain patterns (the principle of curvature strain was discussed in Section 3.6 on page 66)

As illustrated in Figure 4.50, curvature strain at the interface ($\varepsilon_{\kappa,i}$) is dependent on the force F_O, which combines the influences of shrinkage restraint and overlay dimensions, the lever arm of internal forces, the stiffness of the composite section, and the distance z between the centroid of the composite section and the interface. An increase in overlay thickness has the following effects on curvature strain at the interface:

- Increase in F_O (increase in curvature, hence increase in $\varepsilon_{\kappa,i}$)
- Increase in c (increase in curvature, hence increase in $\varepsilon_{\kappa,i}$)
- Increase in member stiffness (decrease in curvature, hence decrease in $\varepsilon_{\kappa,i}$)
- Decrease in z (decrease in $\varepsilon_{\kappa,i}$)

As can be seen from the above, the relation between overlay thickness and interface curvature strains is complex. It is interesting to note that interface strains, resulting from the combined influence of direct strains and curvature, were initially very similar in members with different overlay depths. This is a result of the contradicting influences that a change in overlay

thickness has on overlay curvature strains, as stated above. The influence of overlay thickness on curvature strains can be estimated under purely elastic conditions when direct strain profiles are known. However, strain measurements on Specimens D combine direct and curvature strains under visco-elastic conditions, which makes it difficult to interpret the measurements in terms of different strain components. This is important to note as the strain profiles of Specimens D seem to correspond to Bernoulli's hypothesis of plane sections remaining plane. The test results presented in Figure 4.49 could therefore be mistaken as a confirmation of existing analytical models. In Section 4.9.2 however it was shown that Bernoulli's hypothesis is not applicable. This shows that strain measurements taken on members that are free to curve are difficult to interpret in terms of overlay shrinkage restraint.

Two main conclusions can be drawn from Specimens D. Firstly, in members that are free to curve shrinkage restraint at the interface appears to be independent of overlay dimensions, which is linked to the aspects discussed above. Denarié et al (2004) included this phenomenon in his model for bonded overlays, as discussed in Section 3.5. Secondly, strain measurements on members that are free to deform are difficult to interpret in terms of different influences on total strain values, i.e. direct strain and curvature. The characteristics of shrinkage restraint are therefore at best examined on specimens that cannot curve, as discussed in Section 4.9.2 (Specimens C).

4.9.4 Substrate creep strains

Specimens D were used to measure strain profiles across the whole member depth. Strains across the distance between measurements locations were assumed to vary linearly with depth (compare Figure 4.49). The strain profiles measured on specimens D allow an estimation of the magnitude of substrate creep strains. Since no external forces or moments were applied to the members, the sum of internal compressive forces in the substrate must be equal to the sum of internal tensile forces in the overlay, the latter resulting from the partial restraint of overlay shrinkage.

The tensile force in the overlay at time t resulting from the restraint of shrinkage, using a unit width for force integration, can be written as:

$$F_O(t) = \psi_O(t, t_0) \int_{\text{interface}}^{d_{\text{overlay}}} E_O\left(\varepsilon_{FSS}(t) - \varepsilon(t, d_O)\right) dd_O \qquad [4.2]$$

where t_0 = time at which overlay shrinkage commenced
ψ_O = factor accounting for the influence of overlay stress relaxation
$\varepsilon(d_O)$ = strain across the overlay depth

The compressive force in the substrate at time t resulting from the imposed strain can be written as:

$$F_S(t) = \frac{1}{1+\varphi_S(t,t_0)} \int_{d_S}^{\text{int erface}} E_S\,\varepsilon(t,d_S)\,dd_S \qquad [4.3]$$

where φ_S = factor accounting for the magnitude of substrate creep strain
$\varepsilon(d_S)$ = strain across the substrate depth

The sum of forces across the section must be zero:

$$F_O(t) = F_S(t) \quad \therefore \quad \varphi_S(t,t_0) = \frac{\int_{d_S}^{\text{int erface}} E_S\,\varepsilon(t,d_S)\,dd_S}{\psi(t,t_0)\int_{\text{int erface}}^{d_{\text{overlay}}} E_O\left(\varepsilon_{FSS}(t)-\varepsilon(t,d_O)\right)dd_O} - 1 \qquad [4.4]$$

The above represents a simplified approach. The actual relation between strain profiles across the member, substrate creep strains, and overlay relaxation is complex. However, in the current context, equation 4.4 can be used for an estimate of substrate creep.

Specimens D were made with overlay 3 (MS). On Specimens B, the relaxation factor for overlay 3 at 50 days was estimated as being no more than 0.5 (compare Section 4.7.9). For the estimation of substrate creep strains in equation 4.4 therefore an overlay relaxation factor of $\psi_O = 0.5$ was applied. Substrate creep factors $\varphi_S(t,t_0)$ were computed using the simplified strain profiles illustrated in Figure 4.49. Test results are presented graphically in **Figure 4.51**.

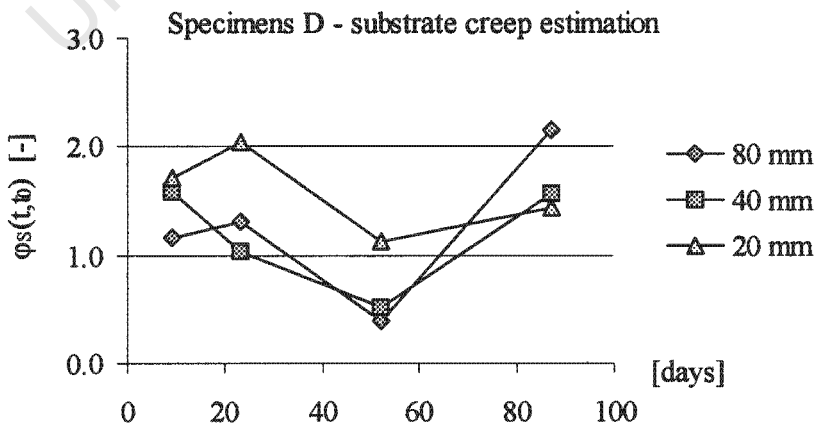

Figure 4.51: Estimation of the substrate creep factor $\varphi_S(t,t_0)$, using test results obtained with Specimens D

The estimation of $\varphi_S(t,t_0)$ as presented in Figure 4.51 shows a relatively large variation between specimens with different overlay depths. However, as stated previously, the above presents an estimate of substrate creep strains using simplified assumptions. The observed variation could thus be expected. The creep factors $\varphi_S(t,t_0)$ of Specimens with 80, 40, and 20 mm, averaged over the test period, were 1.3, 1.2, and 1.6 respectively. This implies that creep strains were somewhat higher than elastic strains. Using the ACI (1992) method for the estimation of substrate creep in the tested specimens, substrate creep factors could be estimated to be approximately 0.9 and 1.0 at 50 and 80 days respectively (compare Section 6.10). Considering that the ACI method represents a relatively rough estimation of creep strains and that the interpretation of overlay strain values is complex, as stated before, it can be concluded that predicted and measured values related to each other sensibly.

Specimens D showed that substrate creep plays a major role in the behaviour of bonded concrete overlays. This must be considered for the analysis of strain measurements on composite specimens and the modelling of bonded overlays. Substrate creep is however commonly not considered in existing analytical models.

4.9.5 Conclusions and main findings

Specimens C and D were cast to investigate the restraining behaviour of the substrate in more detail. The restraining action of the substrate at the interface was characterised through substrate interface strains which appeared to be independent of the overlay thickness both in specimens that were free to curve and in those that were not. However, due to the complex interaction between direct strain and curvature in members with different overlay depths it was concluded that strains measured on specimens that cannot curve are a better indicator of the restraining behaviour of the substrate than those measured on specimens that are free to deform.

Strains measured across the substrate depth of Specimens C (no curvature) indicated that Bernoulli's hypothesis of strain sections remaining plane does not apply for composite members subjected to differential shrinkage. Overlay shrinkage restraint was found to be a localised phenomenon at the interface, resulting in non-linear strain profiles across the members. Overlay dimensions appeared to have no practical influence on substrate interface strains. This indicated that existing analytical models, which link the degree of shrinkage restraint to the relative sectional dimensions of substrate and overlay, are deficient in predicting actual stresses in the member.

Specimens D were used to estimate the magnitude of substrate creep, using the principle of internal equilibrium of forces. Substrate creep strains were found to play a significant role in the behaviour of composite members. A realistic analytical model for bonded concrete overlays should therefore consider the effects of substrate creep.

4.10 Strain at the member ends

4.10.1 Introduction

Specimens A and B were also used for the analysis of strain distribution along the length of the members. Member end strains were found to be considerably higher than strains in inner regions and are therefore discussed separately. In general, member end strains can be used for the characterisation of stress initiation at overlay boundaries. For the correct analysis of member end strains it is however necessary to first identify characteristics of shrinkage restraint at the interface. Existing analytical models assume full transfer of overlay shrinkage stress at the member ends (compare Chapter 3). High member end strains, when analysed on their own, i.e. without consideration of strain profiles across the member sections, could be falsely interpreted as an indication that the above assumption is correct. In this section, high member end strains are analysed in connection with test results discussed in previous sections to obtain a more realistic insight into the strain and stress characteristics at the member ends.

The discussion of strain characteristics in previous sections showed that interface strains are a useful indicator of overlay shrinkage restraint. For the analysis of member end conditions, interface strains were therefore used.

On Specimens A and B, member ends were defined as being in the region of the first measurement location at the ends of the beam (**Figure 4.52**).

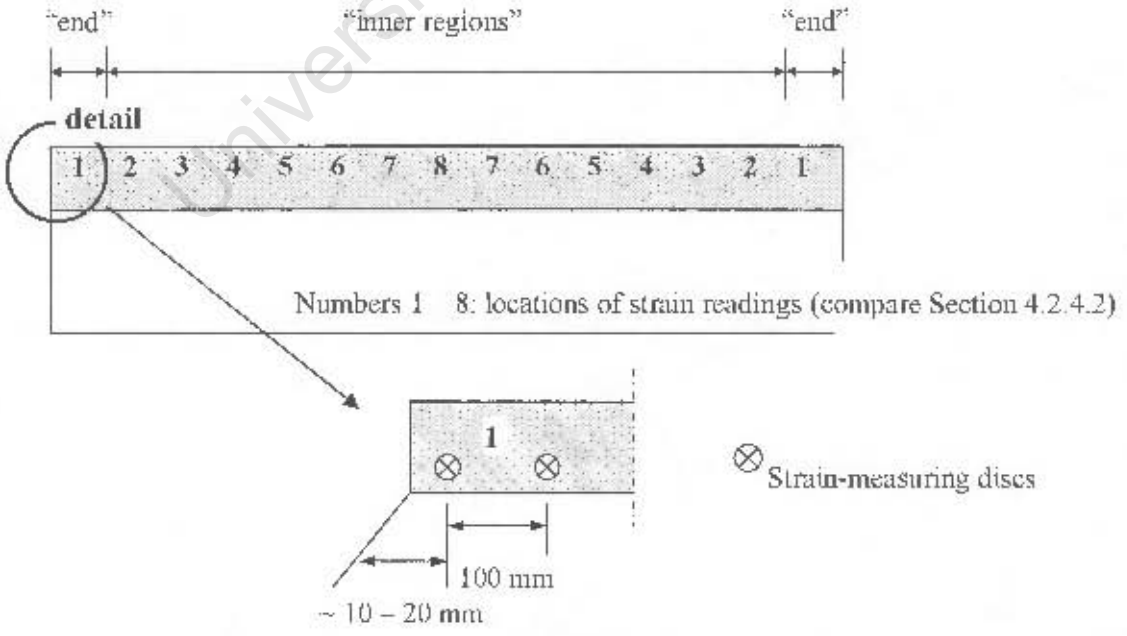

Figure 4.52: Test locations along the composite members: Definition of member end locations on Specimens A and B

Locations 2 along the beam, i.e., the locations adjacent to the member ends, showed the same strain as the rest of the inner regions along the members. High member end strains only occurred in the region of Location 1. However, due to the distance of 100 mm between the strain measuring discs, it could not be established if these maximum strains were in fact distributed over the whole length of the 100 mm, or possibly only occurred closer to the actual member ends.

4.10.2 Test results and discussion

Figures 4.53 show strains at the member ends in comparison to the mean strains along inner regions of the member (for strains in inner regions, compare Section 4.5). Strains are expressed as the ratio between overlay strain and free shrinkage strain.

In general, the specimens experienced notably higher strains at the member ends compared to inner regions of the member. Specimens A5 were the only exception. The comparatively low member end strains of Specimens A5 could not be explained. However, since all other specimens showed significantly higher member end strains, Specimens A5 were believed not to be representative of practical strain characteristics and are therefore excluded in the following discussion. Further research is necessary to identify if the difference in strain of Specimens A5 was actually anomalous or merely a result of the expected scatter of test results.

The ratios between member end strains and strains in inner regions of the member are summarized for Specimens A1-4 and B1 (**Figure 4.54**). During the first approximately 50 days, a large variation between the different specimens was observed. At a later stage, member end strains were generally approximately 50% higher compared to inner regions of the members. However, in Specimens A3 (smooth interface), member end strains were approximately twice as high as in inner regions. This could be an indicator of interface slip, and hence partial or full debonding, at the ends of Specimens A3. This assumption was confirmed through the hammer-tapping method with which a hollow sound was identified at the member ends of Specimens A3, indicating that a portion of interface bond strength had been destroyed. By contrast, debonding could not be identified on any of the other specimens.

Despite high values, member end strains of Specimens A1, A2, A4, and B1 were still considerably smaller than free shrinkage strains, with the mean ratio between $\varepsilon_{o,1\,(\text{member end})}$ and ε_{fss} being in the region of 0.60, indicating that even at member ends there was considerable restraint of overlay shrinkage. The practical explanation of high strain values is the absence of a restraining "neighbour" in both overlay and substrate and hence a discontinuity effect at the member ends. The beam end, which has no "neighbouring piece" attached to it, is relatively free to deform (**Figure 4.55**).

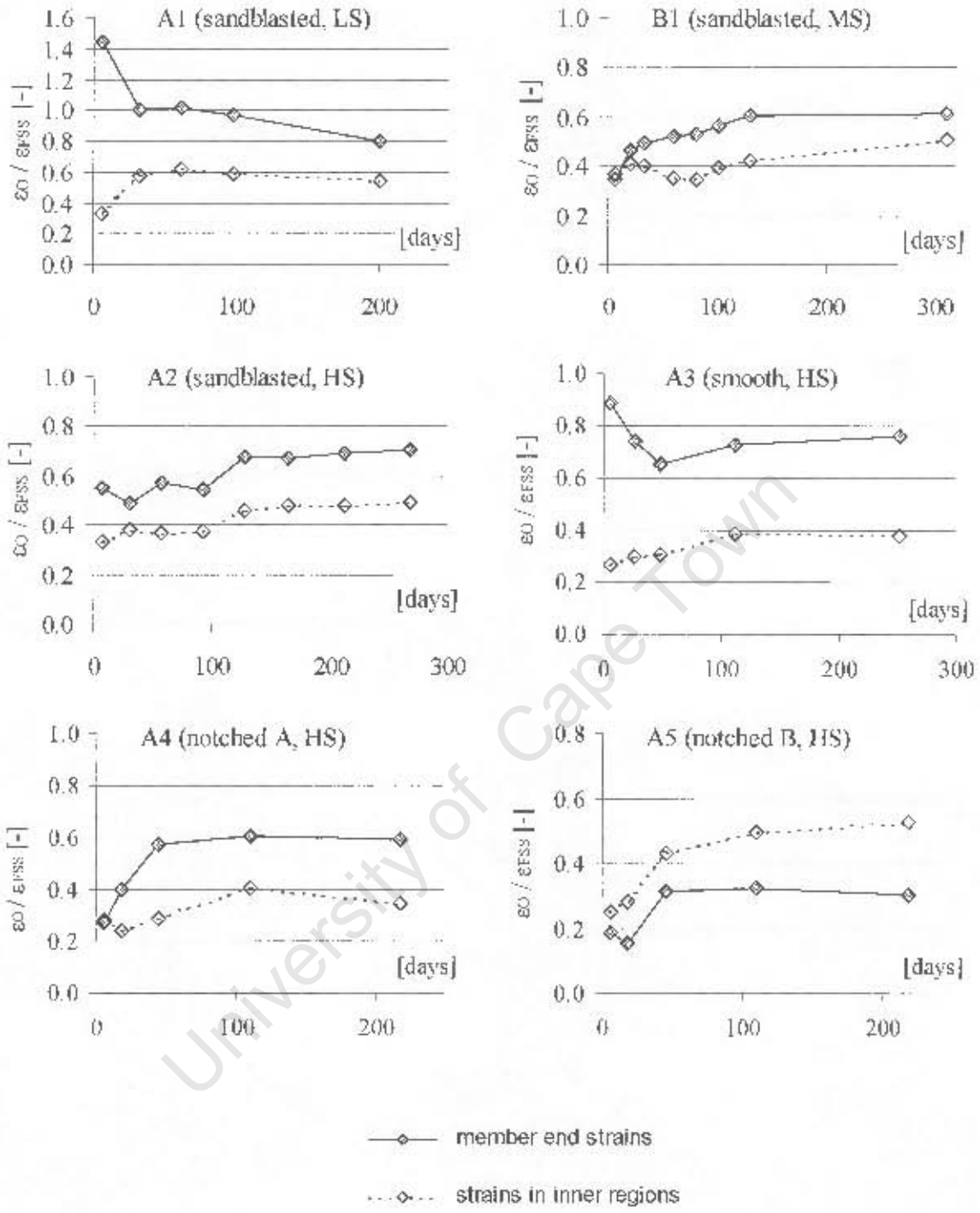

Figures 4.53: Specimens A1 – A5 and B: ratio between ε_o and ε_{FSS} at the member ends in comparison to inner regions of the member. (Average strains from all locations in inner regions of the member were used).

Observations on Specimen B1 showed that overlay and substrate experience the same strain at the member ends, conforming to complete bond. Details are provided in Appendix 4.

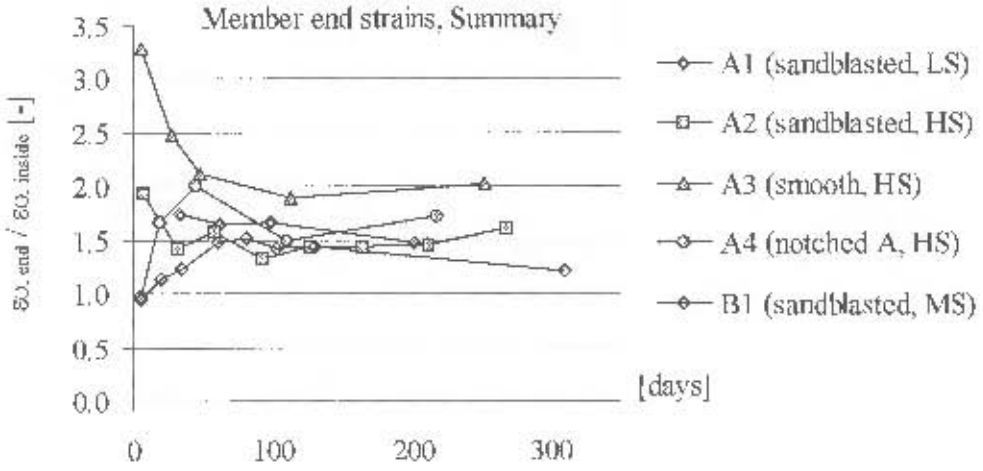

Figure 4.54: Specimens A1-A4 and B2: ratio between member end strains and strains in inner regions of the members

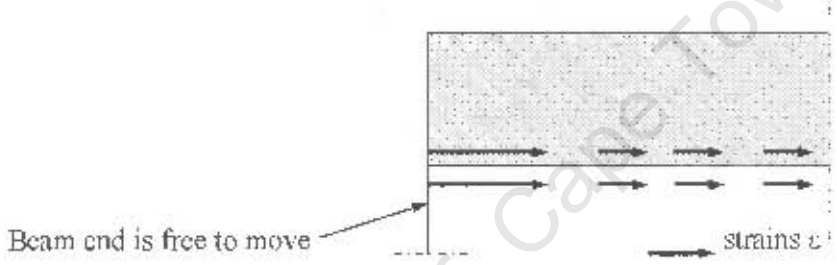

Figure 4.55: Members with free ends: schematic of strains at the member ends

The above observations allow conclusions on stress transfer at the member ends. Silfwerbrand (1997) measured a similar phenomenon, i.e. comparatively high member end strains, in similar types of specimens. From this he concluded that stresses due to differential shrinkage are transferred at the member ends only, i.e. interface shear forces in inner regions of the member are zero. This implies that restraint of overlay shrinkage is a localised phenomenon at the member ends. However, test results discussed in previous sections indicate that mechanisms of shrinkage restraint exist along the whole interface, from which it can be concluded that stresses are transferred along the whole interface. Since the mechanisms of restraint at the interface can be modelled through interface shear stress, this implies that the whole interface experiences shear stress. High member end strains merely indicate that interface shear forces have a maximum value at the member ends and are constant in inner regions of the member. The difference between the 2 approaches is schematically illustrated in **Figure 4.56**.

It should be noted that the mechanisms of shrinkage restraint and interface shear stress at overlay boundaries might be different in members that have fixed ends, i.e. in which the member ends are not free to deform (**Figure 4.57**).

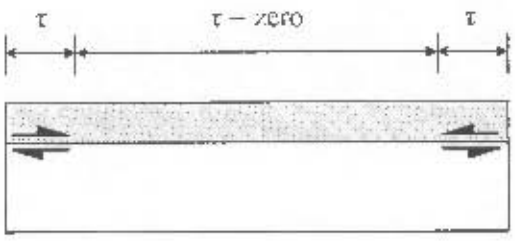

Transfer of forces only at the member ends (existing analytical approaches)

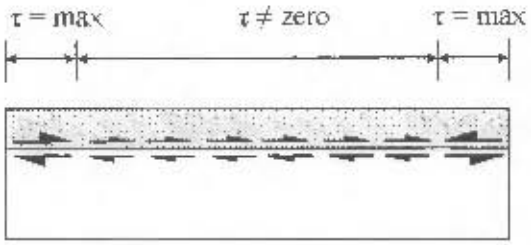

Maximum transfer of forces at the member ends, constant stress in inner regions of the member (conclusion drawn from this research)

Figure 4.56: Schematics of mechanisms of shrinkage restraint in relation to interface shear stress, existing analytical models and conclusions drawn from this research

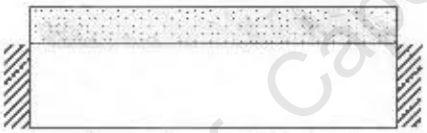

Member ends fixed

Figure 4.57: Schematic of members with fixed substrate ends

In the above-illustrated member, the substrate concrete at the member ends is not free to move under the compressive stress that is imposed by overlay shrinkage. The restraint of shrinkage in this region should therefore be higher compared to members with free ends. However, this case was not examined during this research.

4.10.3 Conclusions

High member end strains measured on Specimens A1-4 and B1 were used as an identification of the mechanisms of stress transfer at member ends. Existing analytical models assume that overlay shrinkage is restraint through interface shear forces at the member ends only. Test results obtained during this research indicate that this assumption is not accurate. High member end strains in connection with constant strain along inner regions of the member indicate that interface shear stresses have a maximum at the member ends and are of constant magnitude in inner regions of the member. This observation is considered very important as it directly relates to the mechanisms of overlay shrinkage restraint at the interface. Only with realistic assumptions of the mechanisms of shrinkage restraint can overlay stresses be modelled in a reasonable way.

4.11 Characteristics of overlay failure

4.11.1 Introduction

The characteristics of overlay and substrate strains along crack-free regions were discussed in the previous sections. Differential overlay shrinkage might cause overlay failure, i.e. cracking or debonding or both. A comprehensive understanding of the behaviour of bonded overlays must include aspects of overlay failure. Specimens A2-A5 showed extensive cracking at early ages. From visual observations and strain measurements on these specimens, fundamental characteristics of overlay crack development could be identified (Section 4.11.2). The mechanisms of debonding are discussed using observations and strain readings of Specimen B2 (Section 4.11.3).

Strain measurements prior and subsequent to the occurrence of overlay failure allowed an estimation of the magnitude of overlay stress relaxation, as discussed in Section 4.11.4.

4.11.2 Overlay cracking

4.11.2.1 Discussion of general observations and overlay strain values

The overlays of Specimens A2 – A5 (Overlay 2 (HS), different interface textures) cracked extensively during the first weeks. This was the result of the combined influences of a high rate of shrinkage development at early ages (compare Section 4.4.2.1) and low tensile strength (compare Section 4.3.2).

Cracks were identified visually using a magnifying glass and were found to occur, independent from interface texture, at relatively regular spacing of 100 to 200 mm. The first cracks along the members were commonly situated approximately 150 to 250 mm from the beam ends. The majority of cracks traversed the whole width and depth of the overlay. Visual observations were analysed in connection with strain measurements across the cracks (**Figure 4.58**).

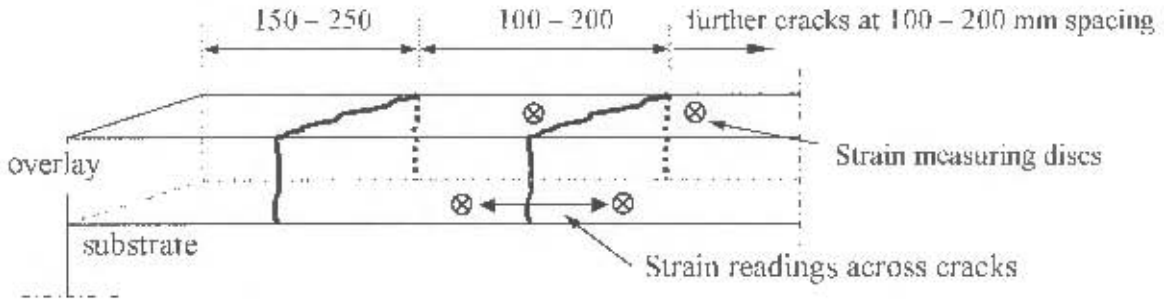

Figure 4.58: Typical overlay crack pattern on Specimens A2-A5

Strain values at different cracked locations along the members showed a fairly large scatter of results, indicating that some cracks opened wider than others. A typical scatter of test results is presented in **Figure 4.59**.

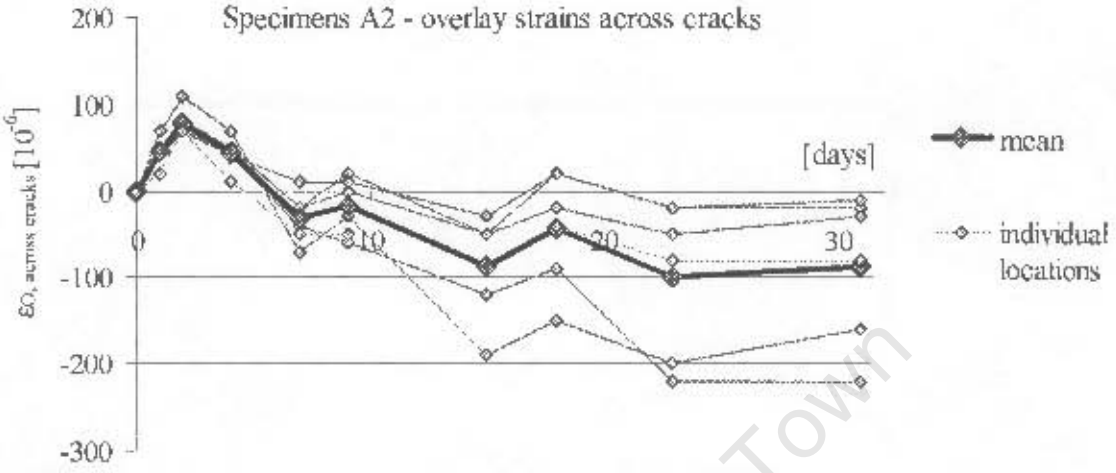

Figure 4.59: Specimens A2, overlay strains on top of the beam, measured across cracks, as an example of the scatter of test results

To facilitate the analysis of strain measurements, the mean values of all strains measured across the cracks of each specimen were used in the following discussion. However, considering the large scatter of test results across cracks, the focus of this section lies on the identification of fundamental mechanisms and not on the interpretation of absolute test values. The short-term strain development of Specimens A2-A5 is presented in **Figure 4.60**. Strain values of uncracked locations are presented as a comparison.

Specimens A2 (sandblasted interface) and A3 (smooth interface) showed similar strain characteristics. The majority of cracks on both specimens appeared between 6 and 10 days after completion of curing. Locations that were going to crack showed lower initial strain, compared to the locations that would not crack. These lesser values were a sign of incipient cracks, indicating that the locations of major cracks were somewhat predestined.

Compared to Specimens A2 and A3, Specimens A4 and A5 (notched interfaces A and B) were different in respect to strain characteristics prior to cracking. Cracked locations showed negative strain values from the beginning of the test period. Cracks were only identified visually after approximately 7 days but the strain values indicate that cracks probably developed earlier, which could have been a result of the high mechanical restraint provided by the notches.

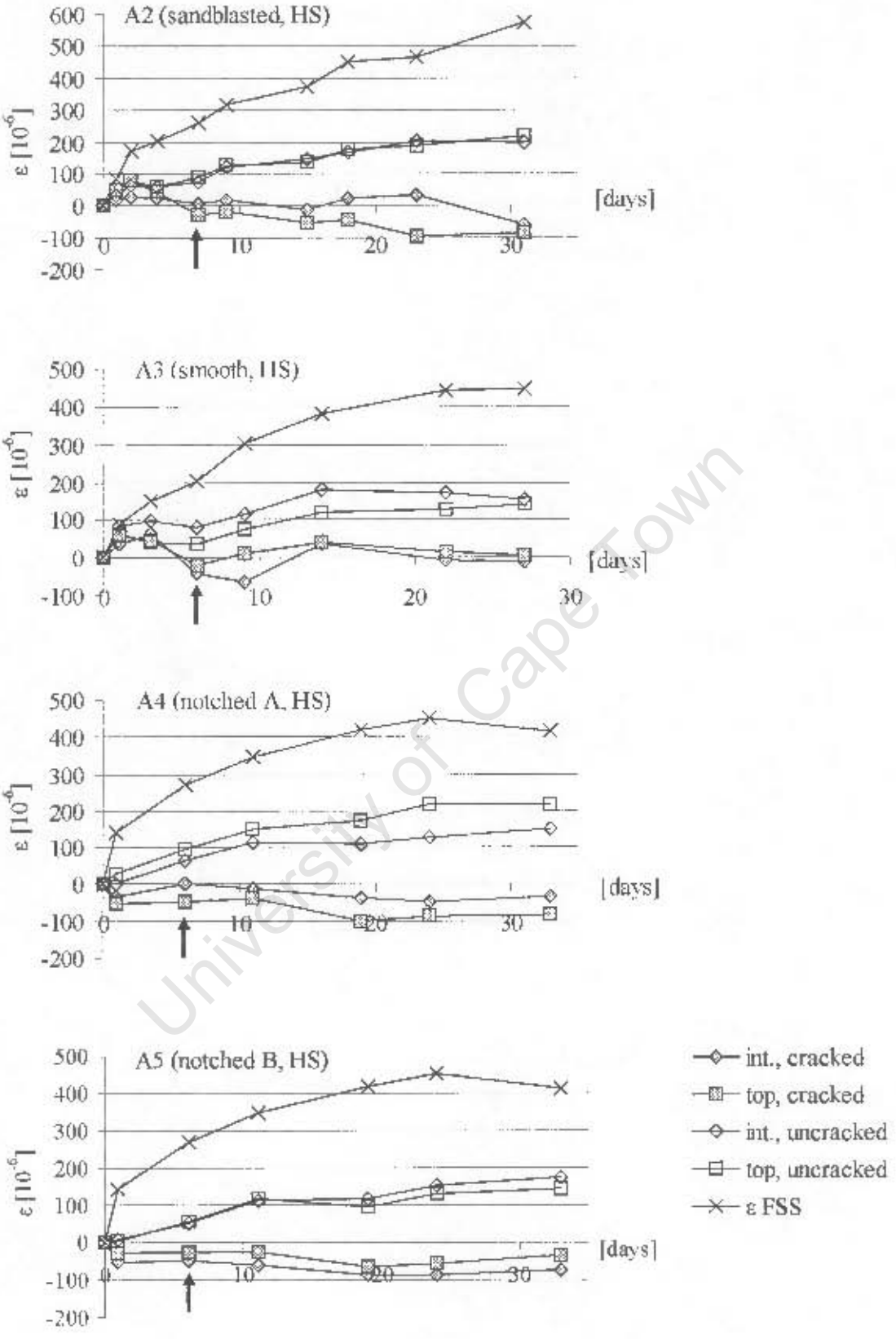

Figures 4.60: Specimens A2-A5, overlay strain development at cracked and uncracked locations (mean values). The arrows indicate the time of first visual crack identification

Subsequent to the onset of cracking uncracked locations showed a temporarily lower rate of strain development, indicating release of overlay strain energy. Strain at the cracked locations generally followed a negatively increasing trend, indicating further opening of cracks. However, this increase in negative strain was relatively small. An increase in crack width at the interface would have been connected to local debonding at the cracked locations. The relatively constant strain values at cracked locations at the interface indicated that major debonding probably did not occur.

Strain values across cracks at the interface and on top of the members were generally very similar, hence crack widths seemed to be relatively constant throughout the overlay depth. Actual crack widths were however not measured on the specimens.

The long-term strain development of Specimens A2-A5 is presented in **Figure 4.61**.

Over most of the test period, cracked locations on Specimens A2 showed higher negative strain on top of the member compared to the interface. This can be related to larger crack widths on top of the member. By contrast, Specimens A3, A4 and A5 showed similar strain both at the interface and on top.

Cracks separate adjacent parts of the overlay from each other, thus creating isolated overlay "patches" along the member. As mentioned earlier, increasingly negative values at cracked locations would have been an indicator for debonding, but were not measured. In general, strains across cracks were either relatively constant over the test period or slightly increasing towards more positive values. This increase in positive strain could theoretically indicate a decrease in crack width. From a practical point of view, however, it seems unlikely that cracks closed up again. Therefore, despite the formation of single overlay patches there was a global effect along the whole member, resulting in compressive substrate creep strains along the length of the interface.

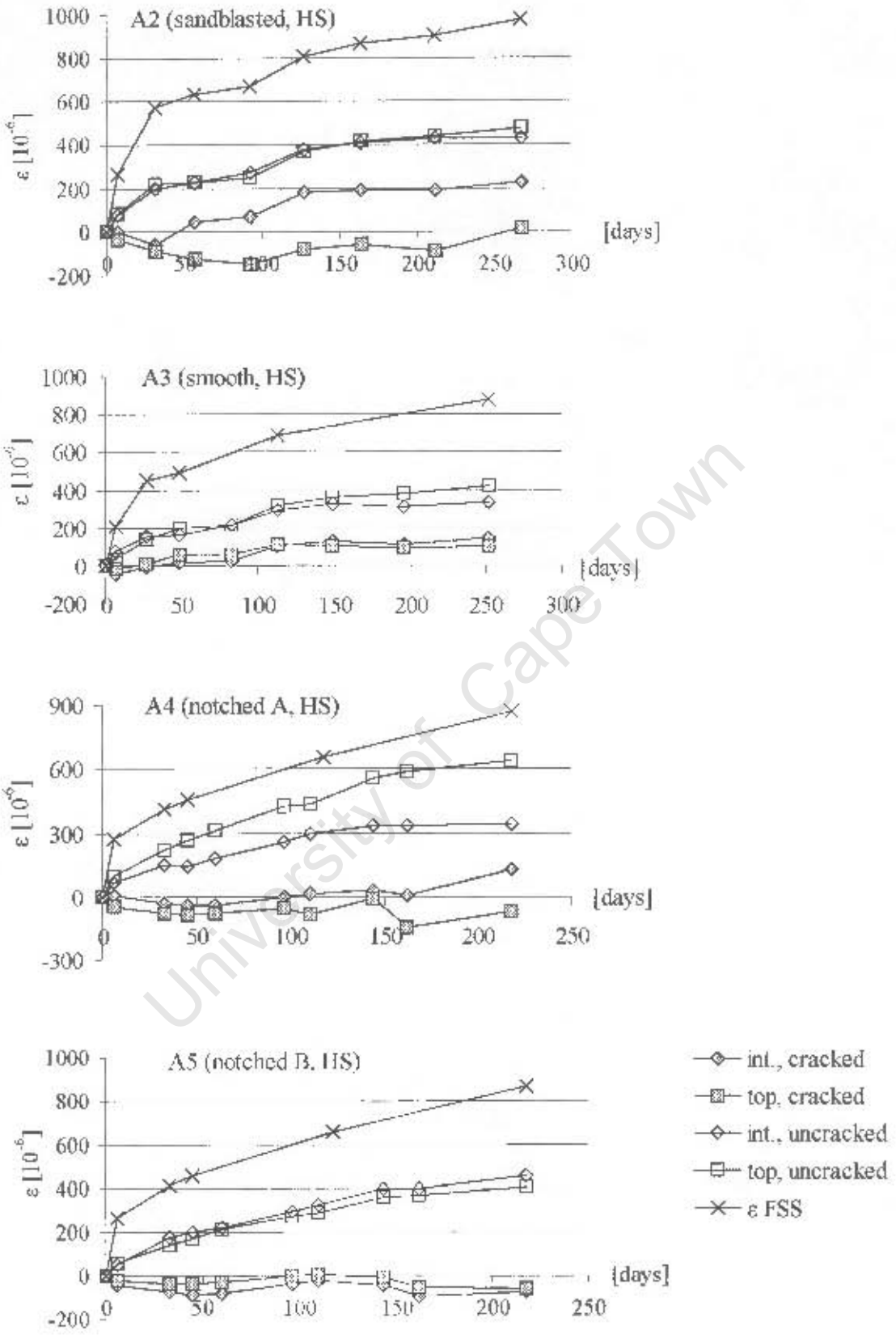

Figures 4.61: Specimens A2-A5, long-term overlay strain development at cracked and uncracked locations.

4.11.2.2 Discussion of the main findings

The visual observation of cracking behaviour in connection with strain measurements on the cracked specimens allowed conclusions on fundamental cracking characteristics of bonded concrete overlays.

It is commonly accepted that overlays either crack at early ages or do not crack at all, which was confirmed by the specimens investigated during this research. Cracks on Specimens A2-5 occurred at regular small distances, while uncracked specimens (Specimens A1, B1, C and D) did not show any sign of failure. This confirms observations made by Weber (1971) who stated that bonded overlays either crack at regular and small distances, or completely resist cracking through plastic and elastic deformations.

Strain measurements indicated that overlays did not move away from cracks, i.e. the bond between substrate and overlay was not affected by the occurrence of cracks, even though the overlays had high shrinkage strains. This is noteworthy especially for the smooth interfaces of Specimens A3, which offered low mechanical restraint of overlay slip. Bond failure, which is sometimes observed in actual composite members next to cracks, can therefore probably be related to the influences of poor interface preparation or cyclic loading due to temperature changes rather than the influences of differential shrinkage.

With strain measurements of Specimens A2-A5, tensile overlay stress relaxation can be estimated, as discussed in Section 4.11.4.

4.11.3 Overlay debonding

The overlay of Specimen B2 (smooth interface, Overlay 3 (MS)) debonded from the substrate after approximately 4 weeks. No cracks developed in the overlay and debonding was thus the sole mechanism of stress release. Debonding was observed visually as the overlay had clearly separated from the substrate over approximately 80% of the member length. Debonding started on one end only while the other end remained bonded to the substrate over the whole test period (**Figure 4.62**).

Overlay and substrate strains at the interface, in comparison to free overlay shrinkage strains, are presented in **Figure 4.63**.

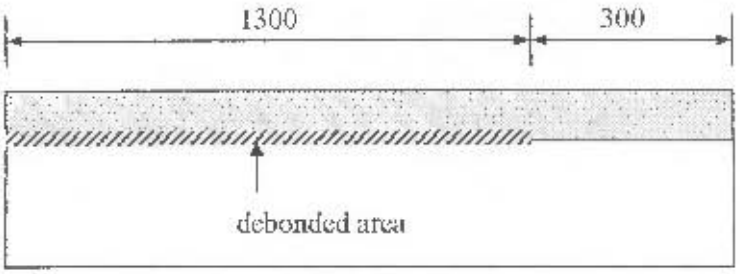

Figure 4.62: Specimens B2: Schematics of overlay debonding

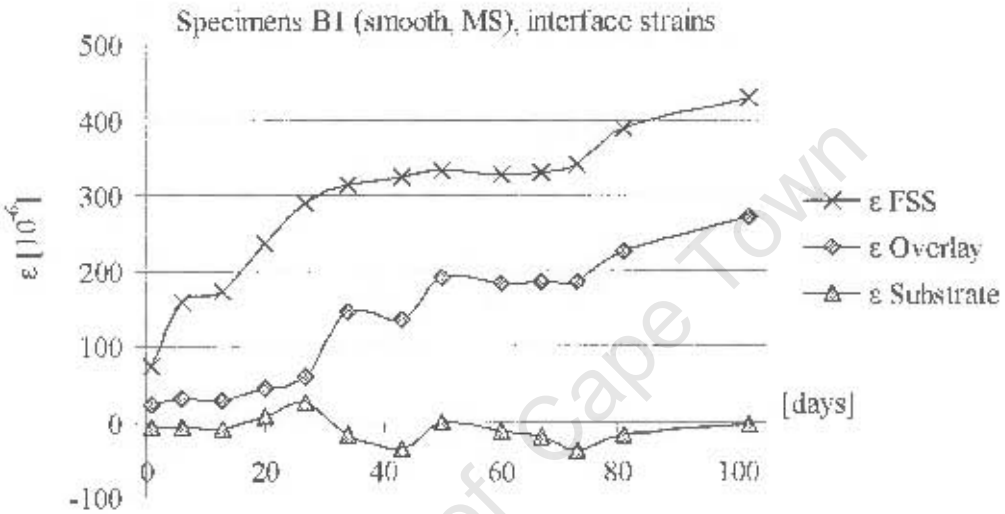

Figure 4.63: Specimens B2: Strain values at the interface compared to free overlay shrinkage strain

During the first approximately 2 weeks, overlay strain developed at a fairly low rate. No substantial substrate strain was measured during this period. This confirmed the previously discussed observation of an initial relative movement between overlay and substrate. After approximately 2 weeks, substrate and overlay strain at the interface began to develop at a similar rate. In Figure 4.63, debonding is indicated through the sudden jump of overlay strain towards higher values after approximately 4 weeks. In the same moment, i.e. in the moment of debonding, substrate compressive strain and stress were released, as indicated by the jump of substrate strain towards lower values.

Subsequently to the onset of debonding, overlay strain developed at a much faster rate than free shrinkage strain. Thereafter, overlay and free shrinkage strains increased at virtually the same rates, indicating that the overlay was now able to shrink freely. The step in the overlay strain curve between days 28 and 42 suggests that the bond was destroyed in stages.

The above observations are significant as they can be used for the estimation of tensile stress relaxation, which is discussed in the following section.

4.11.4 Overlay stress relaxation through failure

4.11.4.1 Stress relaxation through cracking

The strain development of Specimens A2 and A3 clearly indicated the time of overlay cracking, as discussed in Section 4.11.2.1. The estimation of overlay creep relaxation is therefore based on Specimens A2 and A3.

Elastic modulus E_O and tensile strength f_t of Overlay 2 at the time of cracking were approximately 22.5 GPa and 2.0 MPa respectively (compare Section 4.3). On Specimens A2, the majority of cracks were detected after 7 days when free shrinkage strains were $\varepsilon_{fss,7d} = 260.10^{-6}$. Free shrinkage strains measured before cracking was detected were $\varepsilon_{fss,4d} = 200.10^{-6}$ at 4 days. It is therefore assumed that overlay cracking on Specimens A2 occurred between 4 and 7 days, with the free shrinkage strain at the time just before cracking being approximately $\varepsilon_{fss,cracking} = 230.10^{-6}$.

The average overlay strain at locations that were going to crack, measured after 4 days, was $\varepsilon_{O,4d} = 40.10^{-6}$. Therefore, the restrained shrinkage at the time just before cracking occurred can be estimated to be

$$\varepsilon_{O,\text{ restrained shrinkage}} = (230 \quad 40).10^{-6} = 190.10^{-6},$$

which, in the absence of relaxation, would correspond to elastic stress of

$$\sigma_O = \varepsilon_{O,\text{ restrained shrinkage}} \cdot E_O = 190.10^{-6} \cdot 22.5.10^{3}\ \text{MPa} = 4.3\ \text{MPa}$$

At the time of cracking, tensile strength was f_t = 2.0 MPa, from which the short-term relaxation factor for Specimens A2 can be estimated as

$$\psi_O = 2.0 / 4.3 = 0.47$$

The factor 0.47 implies that relaxation reduced tensile stress to 47% of the elastic stress. Repeating the above calculations for Specimens A3 results in a short-term relaxation factor of 0.63. Overlay relaxation therefore led to a reduction in tensile stress of roughly 40-50%.

4.11.4.2 Stress relaxation through debonding

Similarly to the cracked overlays of Specimens A2 and A3, strain development of Specimens B2 can be used to estimate the magnitude of tensile creep relaxation. The ratio between overlay strain at the interface and free shrinkage strain of Specimen B2 is presented in **Figure 4.64**.

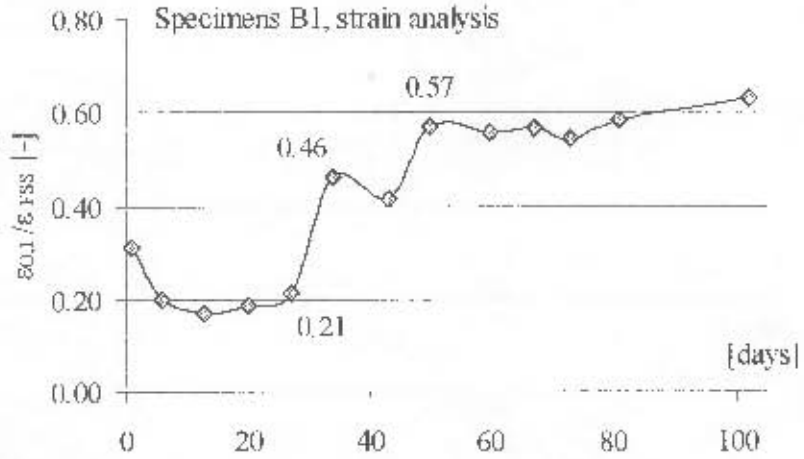

Figure 4.64: Specimens B2: Ratio between overlay strain at the interface and free shrinkage strain

The low ratio between overlay shrinkage and free shrinkage of roughly 0.2 during the first 4 weeks indicates high initial restraint. The onset of debonding led to a sudden increase in the ratio of up to 0.47 and after approximately 6 weeks, when debonding was completed, the ratio reached a value of 0.57.

The difference in overlay strain between the onset and completion of debonding denotes the elastic component of restrained shrinkage, i.e. the component that could be recovered after the restraining action was eliminated. The inelastic component of restrained shrinkage, i.e. the component that could not be recovered after debonding, is expressed through the difference between free shrinkage strain and overlay strain at the completion of debonding. This strain difference corresponds to the stress released. In that respect, the ratio between overlay shrinkage and free shrinkage of 0.57 at the completion of debonding corresponds to the relaxation factor ψ. Therefore, during the first 6 weeks, overlay relaxation led to a reduction of restrained shrinkage stress of approximately 43%.

4.11.4.3 Summary and discussion

Tensile stress relaxation is a crucial mechanism for durability and serviceability of bonded concrete overlays. The magnitude of restrained shrinkage often exceeds the tensile strain capacity of the overlay. This would lead to failure in form of cracking and/or debonding if these stresses were not partly released through overlay relaxation. The importance of tensile stress relaxation for bonded overlays has long been recognised (compare Section 2.5.2). However, detailed information on actual relaxation values is rare and information on stress relaxation measured on composite members subjected to differential shrinkage was not found

in the literature. The results of Specimens A2-A5 and B1 therefore serve as a valuable indication of relaxation characteristics in bonded concrete overlays.

Test results of Specimens A2-A5 and B2 showed that significant overlay relaxation occurs in the early ages of loading. In general, relaxation reduced tensile overlay stress by approximately 40-50%. These values were used to confirm the validity of the analytical model discussed in Chapter 6.

However, overlay relaxation may be very different for different materials and it is necessary to examine the relaxation characteristics of common overlay materials, including concrete repair mortars.

4.12 Summary and conclusions

The experimental research discussed in the previous sections allows conclusions on the parameters identified in Section 4.1 and reveals shortcomings of existing analytical models for the design of bonded concrete overlays subjected to differential shrinkage.

Existing models are based on simple beam theory and apply Bernoulli's hypothesis of plane sections remaining plane after being stressed. Consequences of this assumption are that stresses resulting from differential shrinkage are only transferred at the member ends, i.e. interface shear forces only exist at the member ends, and the degree of overlay shrinkage restraint is related to relative member dimensions of substrate and overlay. Strain measurements discussed in the previous sections reveal that Bernoulli's assumption does not apply for the case of differential shrinkage in composite members. The restraint of overlay shrinkage appeared to be a localised phenomenon at the interface that cannot be modelled realistically if simple beam theory is applied.

Comparison of test results taken from different specimens revealed the importance of critical interpretation of strain measurements. While the behaviour of some of the tested specimens could theoretically be linked to existing analytical approaches, others indicated that existing approaches are based on unrealistic assumptions. It is therefore crucial to identify not only relevant test parameters but also adequate specimen properties to draw correct conclusions. In this research, combined test results from different specimens were analysed to identify fundamental characteristics of bonded concrete overlays.

The interpretation of strain measurements on composite members subjected to differential shrinkage is complex as many time-dependent material properties influence the test results. Measured strains combine elastic and visco-elastic effects and in general it is difficult to draw conclusions on individual strain components. However, the range of test specimens and the methods of analysis discussed in the previous sections allow an estimation of the influence of

different strain and stress components in composite members. Results of the experimental work were used for the development of an analytical model that is based on localised strain initiation at the interface between substrate and overlay. The development of the model is discussed in Chapter 6.

For clear presentation, important findings of the experimental work are summarized individually in the following, concentrating on the main aspects used for the development of a new analytical model. For a detailed discussion of these findings, reference is made to previous sections.

Bernoulli's hypothesis

Existing analytical approaches generally assume that Bernoulli's hypothesis, which states that plane sections remain plane after being stressed, applies for the case of bonded concrete overlays. Test results indicated that this assumption is not correct for the case of differential shrinkage. In substrates of large depth, strains have a maximum at the interface and fade to a point of zero strain in regions away from the interface. The composite member is therefore subjected to localised strain effects at the interface.

Relative sectional dimensions of substrate and overlay

Existing analytical models assume that overlay shrinkage restraint is related to the relative member dimensions of overlay and substrate, concluding that relatively thin overlays on large substrates experience complete restraint and hence maximum stress. Test results indicated that the relative section dimensions have little influence on interface strains. Due to localised effects at the interface, even thin overlays experience considerable strain and hence release of tensile stress.

Force transfer length at the member ends

All existing models are based on the assumption that forces from restrained overlay shrinkage are fully transferred at the member ends. This assumption facilitates the modelling of composite members using conventional analytical approaches. The member ends of the tested specimens showed considerably higher strains compared to inner regions, which was mainly due to the absence of a restraining "neighbour". Member ends experienced higher restraining action compared to inner regions, which is probably connected to a maximum of interface shear stresses. However, overlay shrinkage appeared to be restrained locally along the whole interface. Inner regions of the member experienced similar levels strain and hence the same restraining action along the whole interface, indicating that interface shear stresses exist and are uniform along this region. A force-transfer length at the member ends over which the full amount of force is transferred to the member does therefore not exist.

Interface slip

In some models, interface slip has been considered in the analysis of bonded overlays (e.g. Silfwerbrand 1997). However, results obtained on Specimens B and C indicate that overlay and substrate, if fully bonded, experience the same strain at the interface. For fully bonded overlays, interface slip may be ignored in the computation of strains and stresses.

Strain distribution across the overlay depth

Strain gradients across the overlay depth were detected on Specimens D3 with an overlay of 80 mm depth. This might have been a result of curvature and/or decreasing restraining action, i.e. increasing freedom to deform, towards the top of the overlay. On thinner overlays, i.e. overlays of 20 and 40 mm depth, strain gradients were less pronounced. For thin overlays with a depth of up to approximately 40 mm, it therefore appears appropriate to assume a constant strain profile throughout the overlay, as is commonly suggested in existing analytical models.

Substrate creep strains

Existing analytical approaches do not consider substrate creep for the modelling of bonded overlays. However, for all specimens tested, substrate creep proved to be a major mechanism for strain and stress development in the overlay. Substrate creep strains were found to increase overlay strains, and therefore relax overlay stress, considerably. For the correct modelling of bonded overlays it therefore essential to account for substrate creep. The influence of substrate age on creep strains is discussed in Section 6.10.

Overlay creep relaxation

Tensile stress relaxation has long been recognised as being one of the most important factors for stress development in overlays subjected to restrained shrinkage. However, information on tensile stress relaxation is limited and no information on relaxation values directly measured on bonded overlays was found in the literature. Specimens A and B allowed an estimation of the tensile stress relaxation factors of overlays 2 and 3, which were computed to be approximately 0.5 – 0.6. This implies that on these specimens roughly 40-50 % of tensile overlay stress was released through relaxation. Specimens A further indicated that considerable relaxation occurs shortly after loading. More research is however necessary to find relaxation factors for different types of overlays.

Curvature

Differential shrinkage is generally considered to induce curvature into composite members, with the overlay experiencing compressive curvature strain. Specimens C, which could not curve, showed overlay strains similar to specimens that were free to curve. Curvature strains are generally difficult to assess from strain measurements as the effects of overlay thickness on curvature are complex, especially in members that are subjected to both elastic and viso-elastic strain components, as discussed in Section 4.9.3. The influence of curvature could

therefore not clearly be identified. Generally, it would be conservative to design bonded overlays without accounting for the effects of curvature.

Influence of interface texture and mechanical bond strength on overlay strains and stresses

Specimens A2-A5 were made with the same overlay but different interface textures. The interface texture was found to have no significant influence on overlay strains. By contrast, different interface textures resulted in significantly different shear bond strengths between substrate and overlay, which is discussed in Chapter 7. Mechanical interface bond strength on a macro scale therefore had no notable influence on overlay stresses due to restrained shrinkage. This observation is significant as it allows to model overlay stresses irrespectively of interface texture as long as full bond is assured.

Overlay failure in general

Specimens A2-A5 cracked extensively at early ages, releasing overlay stress resulting from restrained shrinkage. Strain readings on these specimens indicated that during the test period significant debonding did not occur on these specimens despite high overlay shrinkage strains. By contrast, Specimen B2 completely debonded along nearly the whole length of the member but did not show any cracks. It appears that a mixed mode of failure, i.e. a combination of debonding and cracking, did not occur in the specimens. Tensile overlay strength seems to govern the mode of overlay failure in cases where stresses due to differential shrinkage exceed overlay strain capacity.

Overlay cracking characteristics

Specimens that developed cracks did so in the first days after completion of curing, which confirmed observations made by Weber (1971) who concluded that cracks develop at early ages or do not develop at all. Cracks occurred at small, relatively regular intervals. This coincides with observations made on patch repairs which often crack extensively even if they cover small areas.

Comparison of existing analytical models to experimental results

Existing models were not tested against the numerical overlay strain values obtained during the experimental research as this was thought not to be necessary for the following reasons. Existing analytical models assume that stresses resulting from differential shrinkage are transferred at the member ends only. Localised effects at the interface are not considered. The models base on Bernoulli's hypothesis that plane sections remain plane after being stressed and apply common beam theory for the computation of strains and stresses in the member. The above two assumptions were challenged by the test results obtained during the experimental research. Considering that an estimation of overlay strains is difficult due to the numerous elastic and visco-elastic influences, existing models could in fact be interpreted as to conform to strains measured on Specimens A and B and D. In other words, test results from these specimens could be interpreted in favour of the existing models discussed in

Chapter 3. However, interpreting the above specimens in conjunction with Specimens C (members that were unable to curve) shows that existing models apply impractical assumptions. Existing models may thus be useful for the prediction of overlay strains in members that are free to curve and that have relatively small substrate depths. By contrast, these models cannot predict strains and stresses in members that have large substrate depths, which for some applications of bonded overlays, e.g. concrete repair, present the most common cases. This shows how crucial it is to test theoretical assumptions against relevant test results. Testing existing analytical models against the combined results obtained on Specimens A,B,C and D shows that these models apply unrealistic theories. A comparison between existing analytical approaches and numerical test results is therefore considered unnecessary.

The experimental research allowed conclusions on fundamental characteristics of bonded concrete overlays as summarized above. The need for the development of a new analytical approach with which strains and stresses in bonded overlays can be modelled realistically was identified. In Chapter 6, the development of an analytical model that is based on localised effects at the interface between substrate and overlay is discussed. In this section, the above aspects are dealt with in detail from a theoretical point of view.

CHAPTER 5

NUMERICAL SIMULATION OF STRAINS IN COMPOSITE MEMBER SUBJECTED TO DIFFERENTIAL SHRINKAGE

5.1 Introduction

For identification of fundamental strain characteristics of bonded overlays subjected to differential shrinkage, a parameter study was carried out using the Finite Element Method of analysis. The results were used to confirm important observations from the experimental research. The following parameters were investigated:

- Characteristics of localised restraint at the interface between substrate and overlay
- The applicability of Bernoulli's theory that plane sections remain plane
- Influence of overlay thickness on interface strains
- Strain profiles across the member depth
- Influence of elastic overlay properties

Overlay and substrate strains resulting from overlay shrinkage were modelled using overlays of different thicknesses and different elastic properties. Overlays were defined as being fully bonded to the substrate. Only elastic behaviour was examined, visco-elastic effects were not considered. A simplified structural system was used, allowing for one-dimensional deformations in a plane strain analysis, i.e. a 2-dimensional member was used to model strains parallel to the interface and vertical strain components were not considered.

Results of the numerical simulation do not represent actual strain values of bonded overlays subjected to differential shrinkage. They merely serve as an indicator of fundamental characteristics of the behaviour of bonded overlays. The main aim of the numerical simulation was to confirm the observation that restrained overlay shrinkage is a localised effect at the interface.

In general, numerical simulations using FEM analysis can assist in the identification of strain characteristics in bonded overlays, considering important aspects such as visco-elastic material behaviour. However, the focus of this dissertation rests on the development of an analytical model for the prediction of stresses in bonded overlays. The development of the analytical model is discussed in Chapter 6. Results from the numerical simulation were merely used to help identify and confirm important parameters for the development of the analytical model. A detailed numerical simulation of the behaviour of bonded overlays exceeded the scope of this research.

5.2 System and models used

5.2.1 General

The software used for the FEM analysis was ABAQUS Version 6.4-3. The basic structural system chosen for the analysis comprised the following:

- 2-D continuum element
- Plane strain analysis
- One-dimensional strain effects (no vertical displacement)

Overlay and substrate were modelled as being fully bonded, i.e. slip between the composites was not considered, which corresponds to results from the experimental research as discussed in Section 4.8. The direct modelling of differential overlay shrinkage was not possible with the software used. Overlay deformation was thus simulated by applying a decrease in temperature to the overlay, which led to shortening and therefore to an equivalent effect to shrinkage. The change in temperature was applied as a constant throughout the overlay depth and width (**Figure 5.1**). A decrease in temperature was chosen that corresponded to a free shortening of 300.10^{-6}.

5.2.2 Specimen dimensions and material properties

Strains were modelled on members of 1 m width. Initially, substrate depths of 5 m were used in the analysis. However, substrate depths in excess of 2 m were found to have no practical influence on the restraint of overlay shrinkage at the interface. A substrate depth of 2 m was therefore used in the numerical simulation. Overlays were modelled with varying depths (**Figure 5.1**).

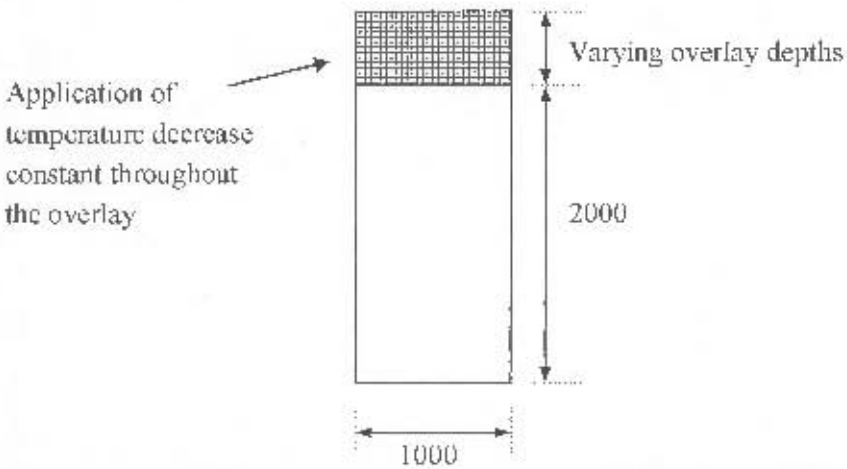

Figure 5.1: Basic member dimensions used in the numerical simulation

Substrate properties were kept the same for all simulations. The influence of the overlay stiffness was tested for a range of overlay thicknesses and elastic properties. For clarity, all specimen parameters, i.e. dimensions and elastic properties, are described in the following sections in combination with the results of the numerical simulation.

5.3 Results of the numerical simulation

5.3.1 General

The results of the numerical simulation were analysed in terms of the following parameters:

- Strain profiles across the member depth
- Strain values at the interface at the centre line of the member (**Figure 5.2**).

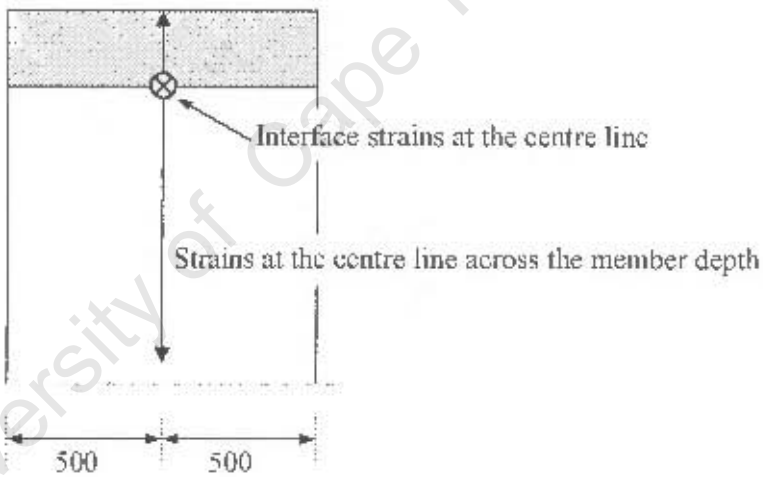

Figure 5.2: Schematic of analysed parameters

As stated previously, the numerical simulation of restrained overlays with FEM analysis was used to identify fundamental strain characteristics. Therefore, a detailed investigation on strain values across the whole member depth and strain distribution along the interface were not carried out as this would have exceeded the scope of this section. However, it is interesting to notice that strains at the edges of the member were generally higher than in inner regions.

High member end strains were also identified during the experimental research and are a result of the absence of a restraining "neighbour" at free edges. The analytical model developed in Section 6 concentrates on inner regions of the member, i.e. regions distant from the influence of member end effects. These are commonly the regions of most importance for

tensile stress development and hence cracking behaviour of the overlay. Therefore, only centre line strains as illustrated in Figure 5.2 are analysed in the scope of this section.

5.3.2 Strains in a member with "infinite" substrate and overlay depths

The basic applicability of Bernoulli's theory of plane sections remaining plane after being stressed was tested on a composite member with infinite substrate and overlay depths. Overlay and substrate depths exceeding 2 m were found to have no noticeable influence on the characteristics of restraint at the interface. Therefore, overlay and substrate depths used in the simulation were 2 m (**Figure 5.3**).

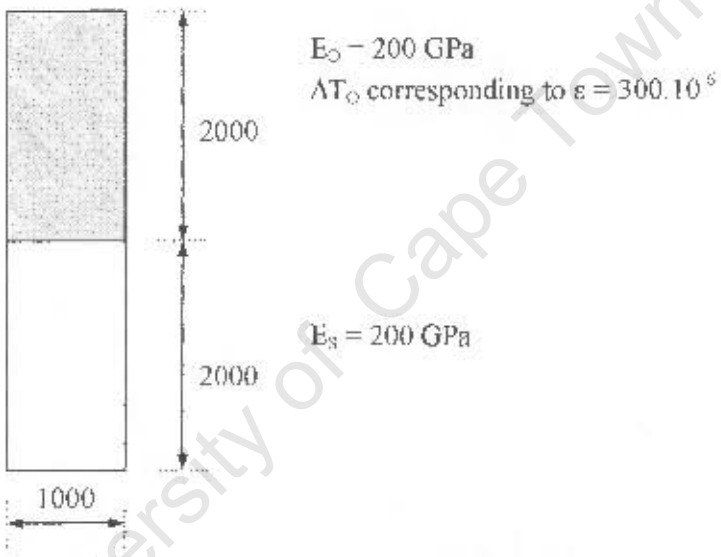

Figure 5.3: Simulation of a composite member with "infinite" substrate and overlay depths: member dimensions and properties

Both overlay and substrate were modelled with the same material properties, i.e. the same elastic properties. To model perfectly elastic conditions, the composite member was defined as a steel section with an elastic modulus of 200 GPa. However, it should be noted that the choice of material, i.e. concrete or steel, was found to have no influence on the results of the numerical simulation of the above member. The overlay was subjected to a temperature drop corresponding to a free contraction of 300.10^{-6}. Strains across the centre line of the member, resulting from the restraint of the differential contraction, are presented in **Figure 5.4**.

The strains illustrated in Figure 5.4 correspond to a deformed member shape as shown in **Figure 5.5**.

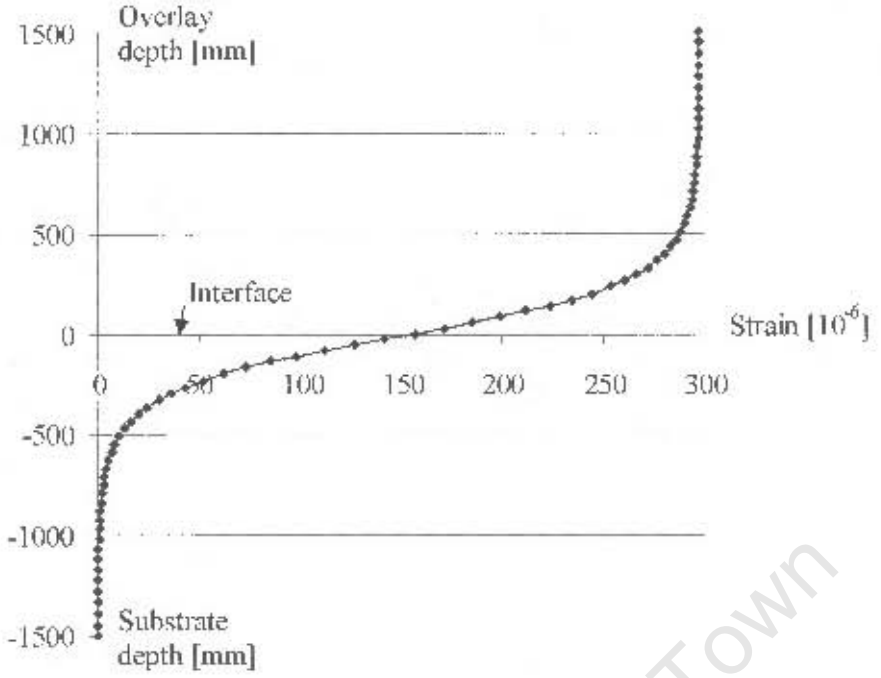

Figure 5.4: Specimen with "infinite" substrate and overlay depths, strain values in the centre line across the member depth

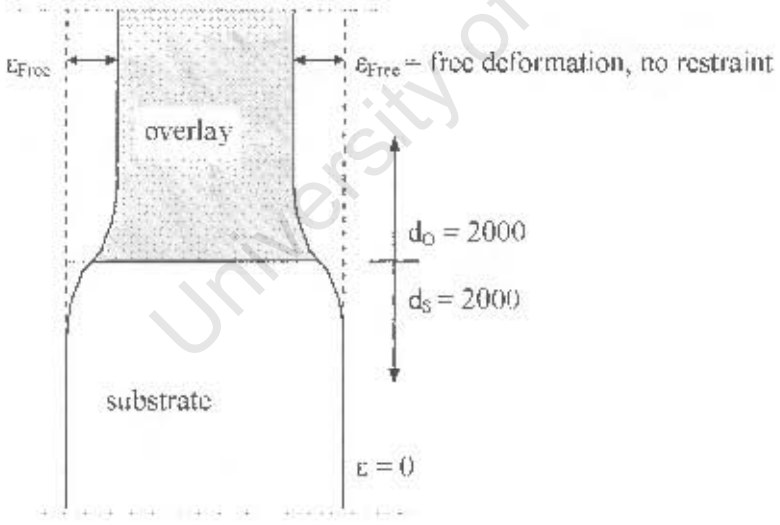

Figure 5.5: Member with "infinite" substrate and overlay depths, deformed member shape resulting from restraint of overlay contraction.

As can be seen in Figures 5.4 and 5.5, according to the numerical simulation, Bernoulli's hypothesis of plane sections remaining plane does not apply to the case of differential shrinkage in bonded concrete overlays. At the interface, overlay and substrate respectively experience maximum restraint and strain. In the simulation, the top of the overlay was too far

removed from the interface to experience appreciable restraint and could deform freely. Similarly, the bottom of the substrate was too far removed from the interface to experience noticeable strain. The depth of strain decay, i.e. the depth after which a reasonably constant strain was reached and where the restraining action at the interface ceased to influence the behaviour of the sections, was approximately 800 mm for both overlay and substrate. Strain profiles in overlay and substrate were parabolic.

At the interface, 50% of the free overlay deformation was restrained (150.10^{-6}), i.e. the overlay was in effect pulled back by 150.10^{-6}. Simultaneously, the substrate was forced to undergo a compressive deformation of 150.10^{-6} at the interface. At the interface, therefore, due to the same elastic properties of overlay and substrate, tensile stress in the overlay was of the same magnitude as compressive stress in the substrate. This phenomenon of equal but opposite overlay and substrate stresses at the interface was discovered to not exist in members with overlay depths of less than approximately 300 mm, as discussed in the following section.

5.3.3 Strains in relation to overlay depth

The influence of overlay thickness on interface strains was simulated using substrate members of 2 m depth and overlays with depths ranging from 1 to 1000 mm (**Figure 5.6**). Material parameters such as elastic properties of overlays and substrate were the same as those discussed in Section 5.3.2.

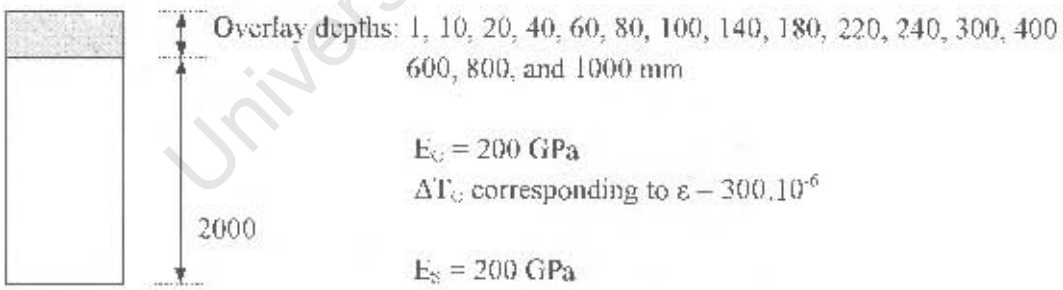

Figure 5.6: Simulation of composite members with different overlay depths: member dimensions and properties

As shown in **Figure 5.7**, in members with overlays of up to approximately 300 mm thickness, interface strains were decreasing with decreasing overlay thickness. An increase in overlay thickness above approximately 300 mm did not result in significantly higher interface strain. It is interesting to note that even an overlay of 1 mm thickness causes notable interface strain on a 2 m thick substrate.

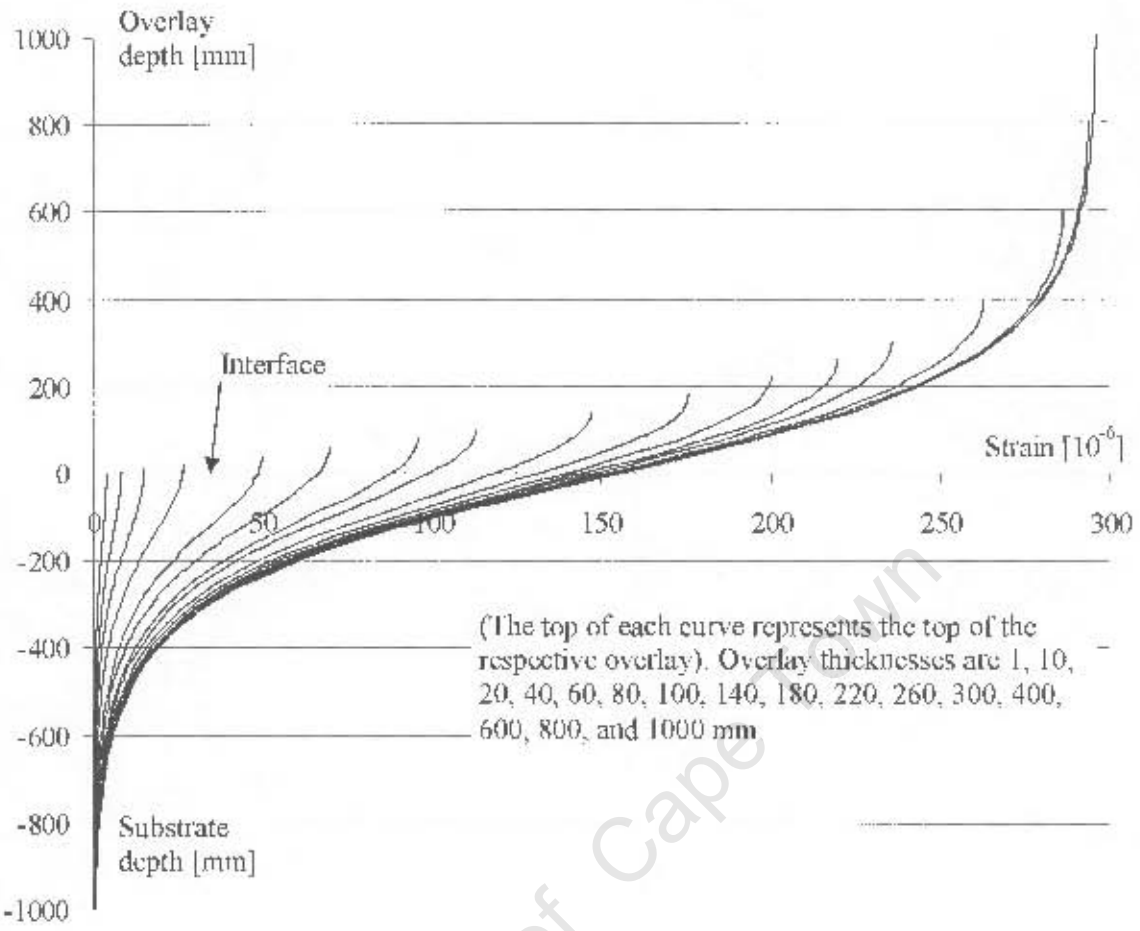

Figure 5.7: Strains across the member depth in relation to overlay thickness

The basic shape of strain profiles across the member depth was the same for all simulated members, with strain magnitudes depending on the overlay thickness. The zone in which the substrate experienced strain due to its restraining action was virtually the same in all specimens, independent of overlay thickness. This zone, which can be termed the depth of strain decay, was approximately 800 mm from the interface.

The above results indicate that restraint of overlay shrinkage is a localised phenomenon at the interface. If the overlay has a thickness greater than a certain limit, in the above simulation approximately 300 mm, relative member dimensions do not have a significant influence on interface strain. **Figure 5.8** shows interface strain values as a function of overlay thickness.

For the computation of interface strains it is important to have information on the limiting overlay thickness for interface restraint, i.e. the overlay thickness above which an increase in thickness does not influence interface strains. As stated above, in the numerical simulation this limiting overlay thickness was approximately 300 mm.

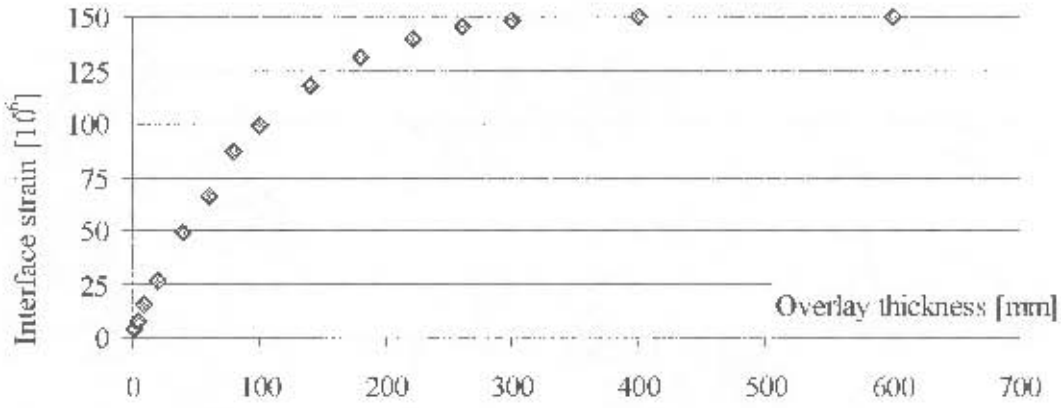

Figure 5.8: Interface strains in relation to overlay thickness

In the experimental research programme discussed in Section 4 overlays of 20, 40 and 80 mm were found to result in very similar interface strain values. Therefore, it seems that, in the tested composite specimens, the limiting overlay thickness for interface restraint lay below 20 mm. More experimental research is necessary to identify this limiting overlay thickness for common overlay materials under characteristic conditions.

5.3.4 Interface strains in relation to elastic overlay properties

The influence of elastic overlay properties was simulated on members with overlays of 20, 40 and 80 mm. Substrate and overlay were defined as concrete sections. The elastic modulus of the substrate was 35 GPa. Different elastic moduli for the overlay were 20, 25 and 35 MPa (**Figure 5.9**).

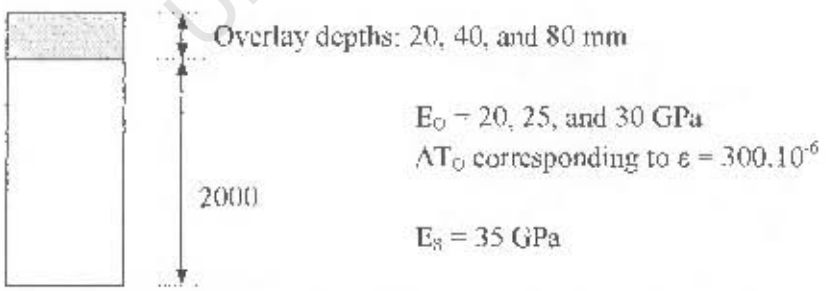

Figure 5.9: Simulation of overlays with different elastic moduli: member dimensions and properties

As shown in **Figure 5.10**, interface strains are related to the elastic modulus of the overlay. An increase in elastic modulus of the overlay results in an increase in interface strains. A stiffer overlay has more "power" to cause contraction at the interface. The difference between interface strains resulting from different elastic moduli increases with overlay depth.

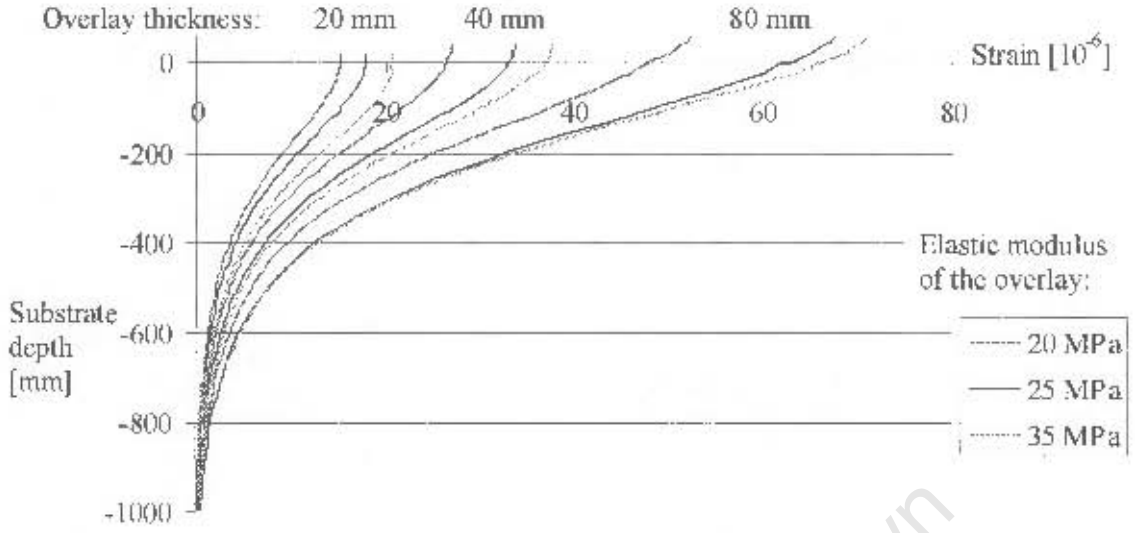

Figure 5.10: Strains across the member section in relation to overlay thickness and elastic modulus

A detailed analysis of strains was not carried out as the above results are merely used to identify fundamental characteristics. The most important information that can be drawn from the above results is that interface strains are related to the relative elastic moduli of overlay and substrate.

5.4 Summary and conclusions

The results of the numerical simulation of strains in composite members allow conclusions on fundamental strain characteristics of bonded overlays. The following aspects are considered as important in the correct modelling of bonded overlays:

- Bernoulli's hypothesis that plane sections remain plane after being stresses does not apply to bonded overlays.
- Overlay shrinkage restraint is a localised phenomenon at the interface.
- The overlay thickness influences interface strains when it does not exceed a certain limit. If the overlay is thicker than this limiting value, shrinkage restraint at the interface is independent of overlay dimensions.
- Interface strains are related to the relative elastic properties of substrate and overlay. An increase in elastic modulus of the overlay results in an increase in interface strains.

The numerical simulation confirmed aspects from the experimental research, most important of which are the non-applicability of Bernoulli's principle and the aspect of localised effects

at the interface. These issues indicate that existing analytical models, as discussed in Section 3, fail to model bonded concrete overlays correctly.

The above aspects were used to support assumptions made for the development of an analytical model for strains and stresses in bonded concrete overlays, as discussed in the following Chapter 6.

CHAPTER 6

MODELLING COMPOSITE MEMBERS BASED ON LOCALISED STRAIN AND STRESS CONDITIONS

6.1 Introduction

This chapter presents the development of an analytical model for the analysis of restrained overlay shrinkage stresses based on localised strain conditions inside the composite member. Reference is made to the literature wherever appropriate. The development of the theoretical approach was accompanied by extensive practical research (Chapter 4). Selected parameters were further verified using the Finite Element Method of analysis (Chapter 5). For verification of chosen parameter values, reference will be made to these sections where necessary (**Figure 6.1**).

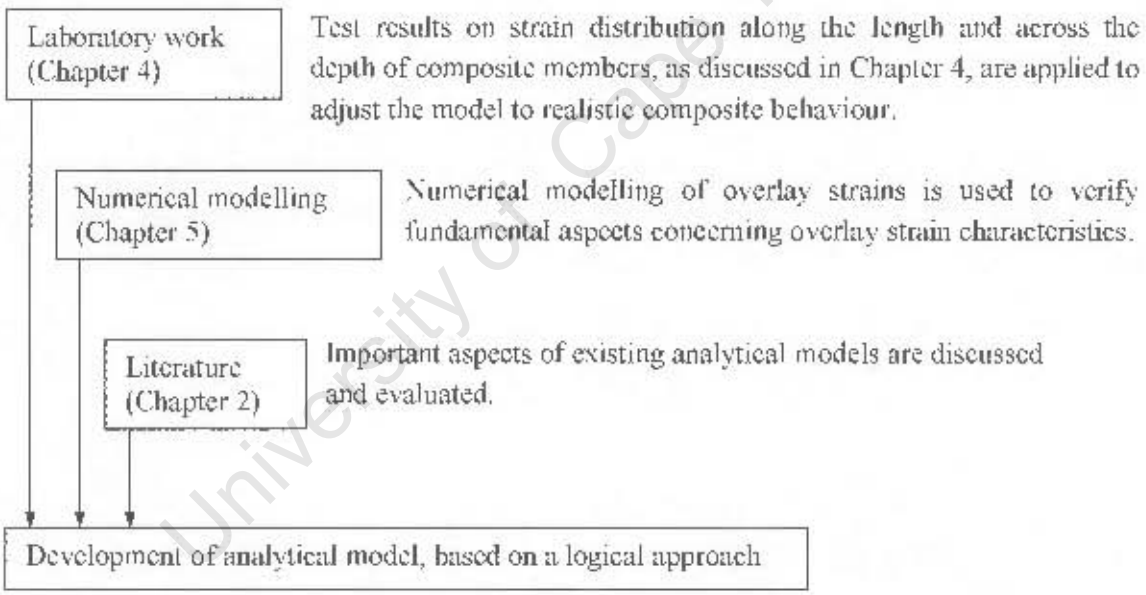

Figure 6.1: Schematic of the development of the analytical model, based on literature research, strain measurements on composite members, and numerical modelling

Differential shrinkage between overlay and substrate is related to internal material properties and external influences resulting from the environment. Due to the complex nature of concrete material properties under time-dependent influences, any analytical model for restrained overlay shrinkage can only present an estimation of actual strains and stresses. The model should therefore be simple and logical and based on reasonable assumptions that can be verified through practical research.

The analytical model presented in the following sections considers elastic strains and stresses at an isolated time increment. However, the development of actual stresses in the member will be strongly influenced by time-dependent material properties, especially by the interaction between the varying influences of shrinkage, creep, and elastic modulus. These time-dependent material properties will be discussed in Section 6.9.

6.2 Basic philosophy of the analytical model

The perspective from which this problem is observed depends on the philosophy of analysis and it is crucial to define perspective and philosophy before the analytical model is developed. There are three possible levels of analysis, namely the global level, the local level, and the micro level, as discussed below.

6.2.1 Global level of analysis

The common approach using conventional linear analysis can be described as a global analytical perspective that looks at the member as a whole, modelling internal strain and stress through externally applied forces without consideration of local influences (**Figure 6.2**).

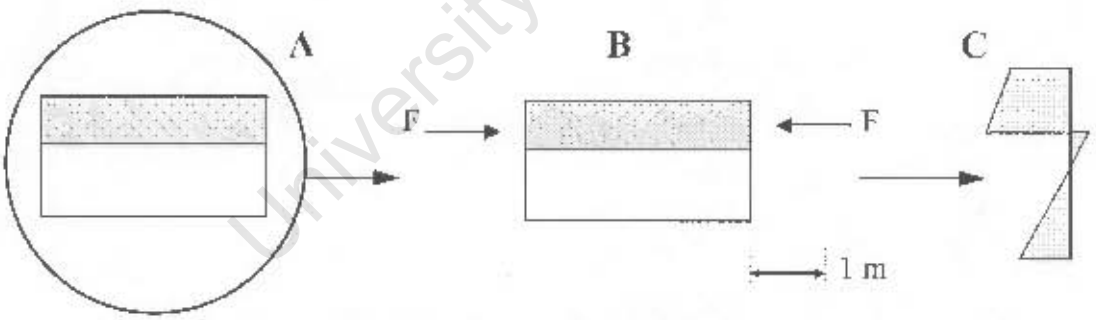

A: Considering the whole member on a global scale
B: Modelling stresses through external forces acting on the member ends
C: Calculation of strains and stresses using conventional solid mechanics

Figure 6.2: Modelling stresses due to differential shrinkage on a global scale

Curvature, bending moments, shear and direct stresses, and stress distribution depend on each other in the conventional way and can be calculated for any part of the member fairly simply with common theories. However, the shortcoming of analytical models that are based on a global level alone is that they tend to oversimplify the problem to an extent where linear solid

analysis can no longer express what happens locally inside the member. It is crucial to consider local parts of the beam, as it is here where stress is initiated.

All existing analytical models operate on a global scale, considering the composite member as a whole and calculating stresses and strains through externally applied forces (see Section 3). The test results obtained during the experimental research as well as the FEM model show that the existing analytical approaches fail to correctly model strains in composite members, which highlights the problem of the global perspective.

6.2.2 Local level of analysis

The main shortcoming of the global level of analysis is that it fails to acknowledge that differential shrinkage stresses are initiated in the interface plane between substrate and overlay. By contrast to the global approach, the local level of analysis attempts to explain strain and stress distribution in composite members rationally on the basis of localised conditions across the composite section (**Figure 6.3**).

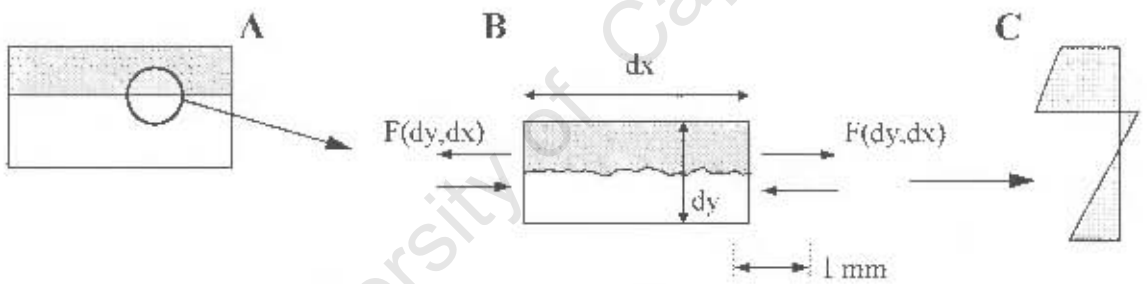

A: Considering stress initiation locally at the interface
B: Modelling restraint, strain and stress at the location of their origin
C: Calculating strain and stress across the member section on a rational basis

Figure 6.3: Modelling stresses due to differential shrinkage considering localised conditions across the member depth

The local level of analysis offers the advantage of taking into account the following aspects in the modelling of differential shrinkage stresses:

- Stress initiation at the interface between substrate and overlay, as opposed to existing analytical models that model stresses through forces applied at the member ends
- Localised, i.e. non-linear, strain distribution across the section

The strain measurements on composite members, as described in Chapter 4, showed the need to model strains and stresses on a local level with consideration of the above parameters.

6.2.3 Micro level of analysis

The micro level of analysis could be used to express what actually happens at a microscopic scale (**Figure 6.4**).

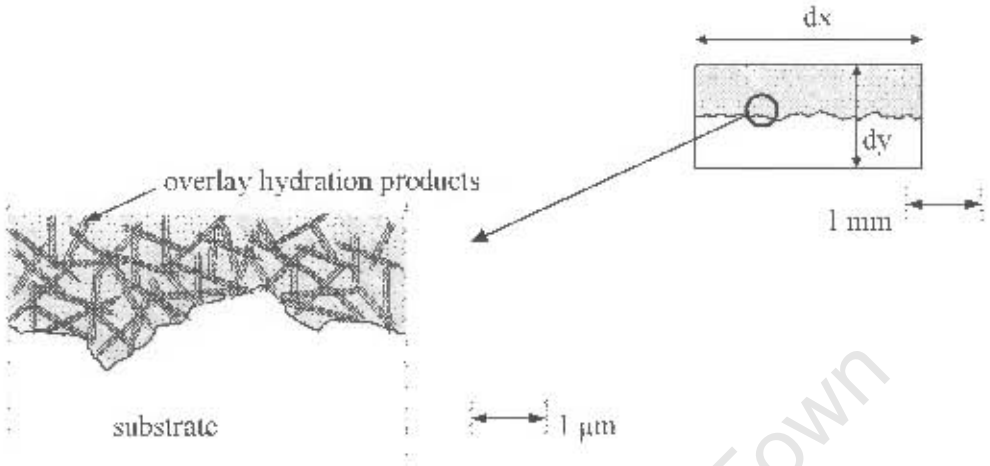

Figure 6.4: Consideration of material parameters on a microscopic scale

Microscopic aspects that may be of value for the analysis of composite members are:

- Microscopic mechanisms of shrinkage and creep, which help to identify the location of stress origin and the resulting characteristic of stress development and stress distribution
- Assessment of partial or full bond failure. Definition of the actual location of fracture after overlay failure (i.e. interface or material failure on a microscopic scale)

Aspects relating to the micro level of analysis are commonly not considered in existing models for bonded concrete overlays.

6.2.4 Combination of the 3 different levels of analysis

As stated previously, most existing models are based solely on global analysis even though phenomena occur on a microscopic scale. To model composite behaviour of overlay and substrate on a microscopic scale alone is, however, not practical. In this thesis, the micro scale is used to logically explain stress initiation at the interface between substrate and overlay.

The local level of analysis proved to be the most appropriate tool for the modelling of stresses and strains in bonded concrete overlays. It facilitated the interpretation of strain measurements in composite specimens and provided a rational basis for the development of

an analytical model. The strategy adopted in this thesis is therefore to commence the analysis on a local level, based on an understanding of material characteristics on a microscopic scale. From that starting point, conclusions on the global level can be drawn for the prediction of the behaviour of the whole member (**Figure 6.5**).

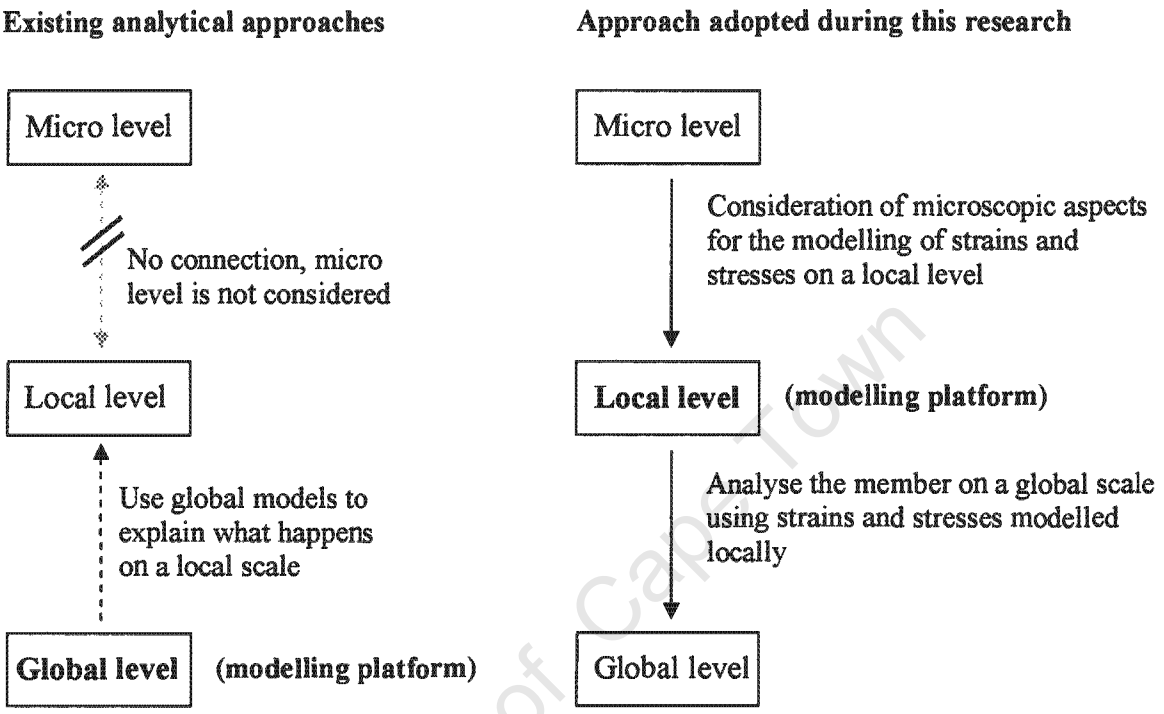

Figure 6.5: Different analytical perspectives for the modelling of stresses and strains resulting from restrained overlay shrinkage

6.3 The degree of bond between substrate and overlay

As outlined in Section 2.3.2, adhesion between substrate and overlay can be divided mainly into mechanical interaction and chemical bonding. Overlay shrinkage might cause interface stress that leads to partial or full loss of any of the above bonding mechanisms. Once partial bond failure has occurred, mechanical friction may be activated to prevent further debonding. Partial debonding might cause interface slip, which would result in a relaxation of overlay tensile stress.

The definition of the degree of bond is an important factor for the analysis of composite members and must be defined before any other assumptions are made. Silfwerbrand (1997) models bond between substrate and overlay through mechanical friction and relates tensile overlay stresses to interface slip (compare Section 3.8). By contrast, all other existing approaches that were investigated assume full bonding. Interface slip corresponds to a certain degree of debonding. As such, it does not correspond to what should be expected in sound

composite specimens. The model described herein assumes perfect bond without interface slip. Overlay and substrate, therefore, undergo the same deformations at the interface:

$$\varepsilon_{O,I} = \varepsilon_{S,I} \qquad [6.1]$$

The validity of Equation 6.1 was confirmed through strain measurement across the interface between substrate and overlay as discussed in Section 4.8.

6.4 Strain gradient across the overlay depth

Because drying takes place at the surface exposed to the environment, monolithic concrete members commonly experience shrinkage gradients throughout their thickness, with maximum strains in the surface region. However, depending on the substrate pore structure and moisture condition, drying of concrete overlays might also take place at the interface. A relatively dry and porous substrate concrete may generate considerable capillary suction, possibly resulting in even higher drying shrinkage at the interface than that experienced at the surface exposed to the environment. For simplicity, analytical models usually assume a constant shrinkage profile throughout the overlay depth.

Another influence on strain gradients across the overlay depth is that of the decay of shrinkage restraint towards the overlay surface. The overlay at the interface, being in full contact with the substrate, experiences the largest restraint. Succeeding layers are subjected to the decay of restraining action (**Figure 6.6**).

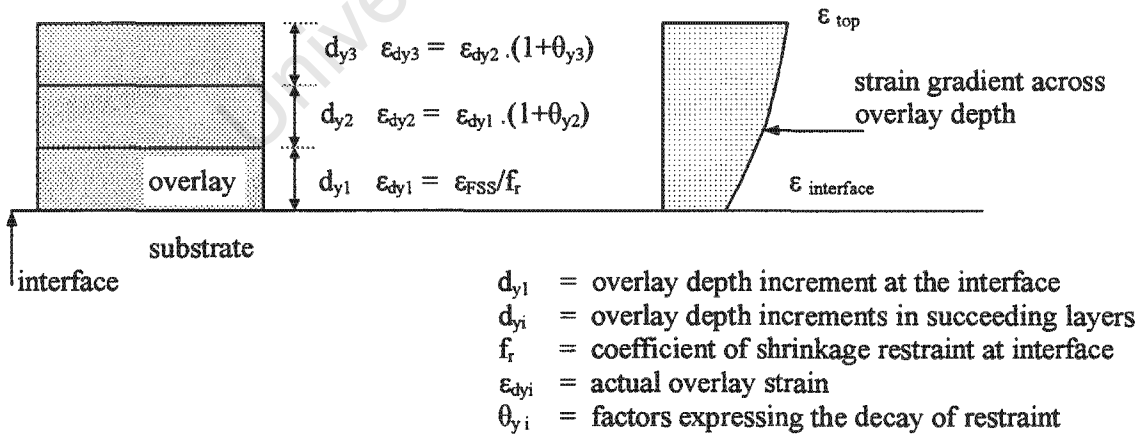

Figure 6.6: Principle of shrinkage restraint decay throughout the overlay depth

The above can best be visualised on an overlay of infinite thickness, where the surface of the member is so far removed from the substrate that the restraining action does not influence the

surface fibre of the overlay. The decay of restraining action across the overlay depth was demonstrated using FEM analysis as discussed in Chapter 5 (compare Figures 5.4 and 5.7).

Existing analytical models link overlay strain and stress distribution directly to the combined influences of relative cross-sectional areas and elastic properties of substrate and overlay. Shrinkage restraint decay across the overlay depth is therefore not considered in these models.

Shrinkage distribution and decay of restraint throughout the overlay depth have the practical implication that they define the magnitude of restrained overlay shrinkage. The latter directly corresponds to tensile stress in the overlay and thus to the magnitude of the actual load applied to the composite section.

Strain measurements on composite members with overlay depths up to 40 mm indicated relatively constant strain, and hence constant restraint, across the overlay depth, as discussed in Section 4.6. Strain gradients across the overlay depth were generally small and were believed to mainly result from curvature. Modelling relatively thin bonded overlays ($d \leq 40$ mm) with the assumption of constant free shrinkage strain as well as constant restraint across the overlay depth therefore seems appropriate from a practical point of view. However, for the analysis of strains and stresses in thicker overlays, strain gradients might have to be considered.

For simplicity, the analytical model developed in the following sections assumes both constant free shrinkage and constant shrinkage restraint across the overlay depth.

6.5 Degree of restraint from the substrate, and stress initiation at the interface

6.5.1 Review of existing analytical approaches

In the estimation of shrinkage restraint, all existing analytical models consider the relative member dimensions of substrate and overlay and the partial restraint resulting therefrom (compare Chapter 3). Haardt (1991) carried out a detailed investigation on the degree of substrate restraint using the FEM method of analysis. He concluded that even if the substrate section is relatively large, overlay shrinkage is not completely restrained (compare Section 3.6). By contrast, all other existing analytical models agree in the point that substrates with infinite depths results in complete restraint of overlay shrinkage, i.e. the complete absence of overlay strain in connection with maximum overlay tensile stress.

The assumption that the degree of overlay shrinkage restraint depends on the relative overlay and substrate dimensions is based on Bernoulli's Principle which states that plane sections remain plane after being stressed, i.e. in the presence of bending and axial forces, strains are

proportional to the distance from the neutral axis of the composite section. In connection with Hooke's Law, i.e. stress is proportional to strain, this leads to a linear stress distribution across each section (**Figures 6.7 and 6.8**).

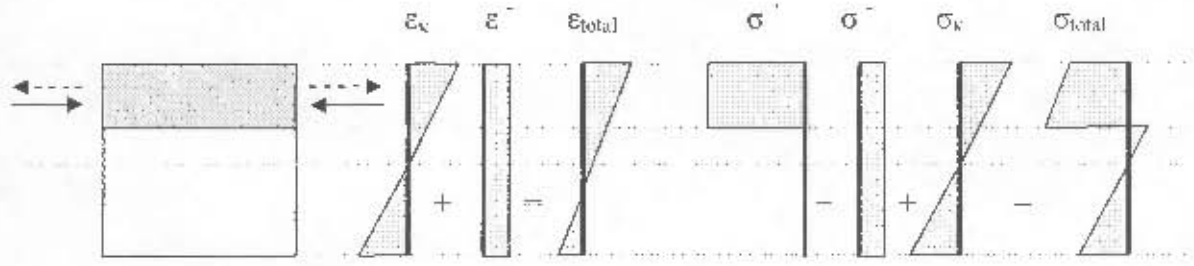

Figure 6.7: Application of Bernoulli's Principle: Strain and stress distribution across the composite member (model introduced by Birkeland, 1960) (compare Section 3.3).

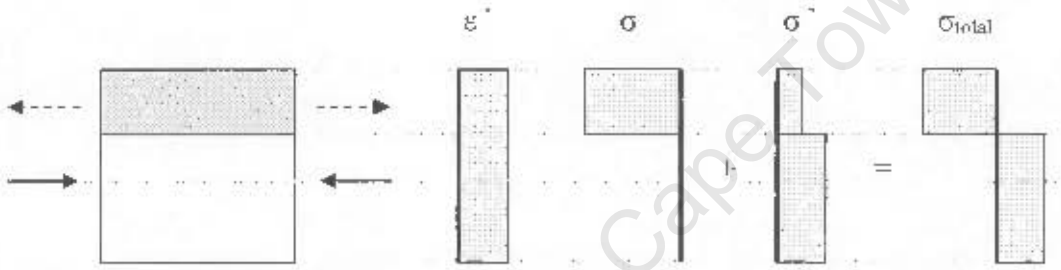

Figure 6.8: Application of Bernoulli's Principle: Strain and stress distribution across the composite member (Alonso Junghanns, 1997) (compare Section 3.4).

The analytical approaches discussed in Sections 3.2 to 3.8 model differential shrinkage stresses through external forces applied to the vertical boundary of the composite section. These forces are either applied at centre line of the overlay (Figure 6.7) or the neutral axis of the whole section (Figure 6.8). Stresses and strains can then be calculated according to Bernoulli's Principle. Sato et al (1994) measured strains on composite means subjected to differential shrinkage and concluded that Bernoulli's principle is "not necessarily" applicable, however without incorporating this issue in an analytical approach. The assumption that plane sections remain plane after being stressed is one of the most common prerequisites in the structural analysis of concrete members and at first sight it seems appropriate to apply this principle to the case of differential shrinkage. However, the application of this principle in the present case corresponds to a misconception of actual stress transfer between overlay and substrate, which will be discussed in detail in the following sections.

The analytical model developed in this thesis is based on the assumption that local strain conditions result in cross-sections that do not remain plane after being stressed. The assumption of non-linear strain and stress distribution was verified by strain measurements across the substrate, as discussed in Section 4.9 (compare Figure 4.47), and FEM analysis of bonded overlays, as discussed in Section 5 (compare Figures 5.4, 5.7 and 5.10).

6.5.2 Stress initiation at the interface between overlay and substrate

6.5.2.1 Characteristics of restraint along the interface

One of the key issues in modelling stresses due to differential shrinkage is the correct understanding of bond mechanisms in the interface plane between overlay and substrate, and the stress initiation resulting therefrom.

The characteristics of free shrinkage strain help illustrate the mechanisms of interface bond. All length increments of a concrete overlay, if they were free to deform, would experience the same linear shrinkage strain. The accumulation of deformations along the overlay would cause the whole member to shrink symmetrically towards its centre line (**Figure 6.9**).

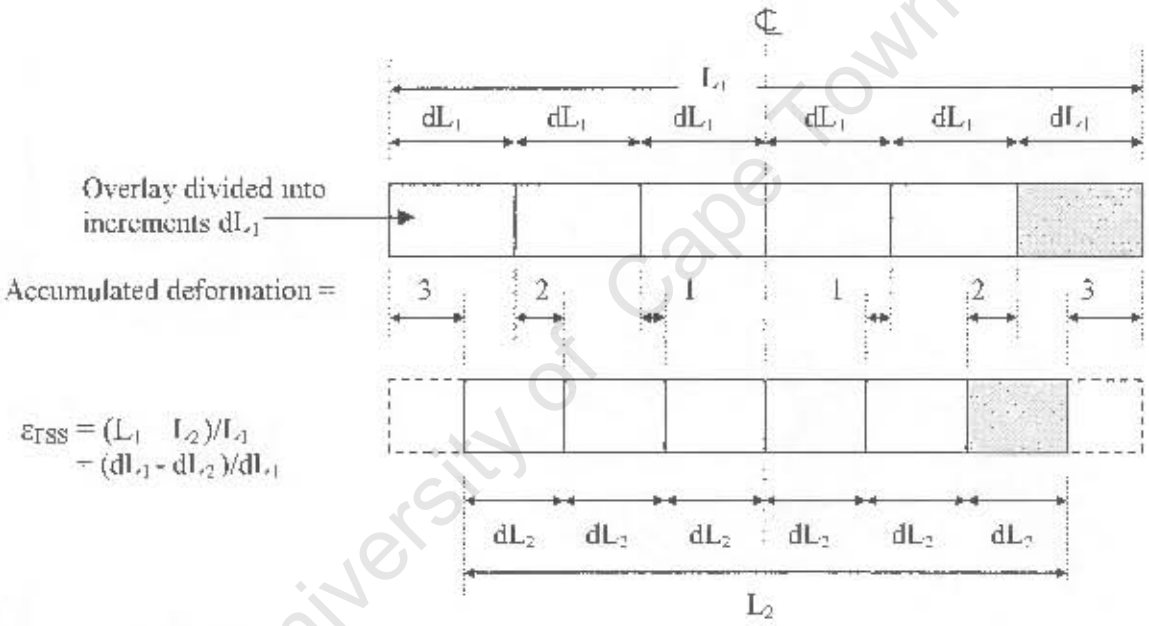

Figure 6.9: Schematic of deformations due to free shrinkage strain ε_{rss}, assuming no restraint of the overlay

As indicated in Figure 6.9, the accumulation of deformations of the single length increments leads to a maximum displacement of the member end boundaries. It is important to note that this maximum displacement is not connected to maximum strain at the member ends. The length increments at the centre line experience minimum displacement but the same strain as the member end increments.

It was stated earlier that substrate and overlay are assumed to be completely bonded. Existing analytical models assume stress transfer only at the boundaries of the composite member. However, linear free shrinkage strain as illustrated in Figure 6.9 and complete bond between overlay and substrate results in constant overlay shrinkage restraint along the whole length of

the interface. This can at best be demonstrated by comparing microscopic and global perspectives (**Figure 6.10**).

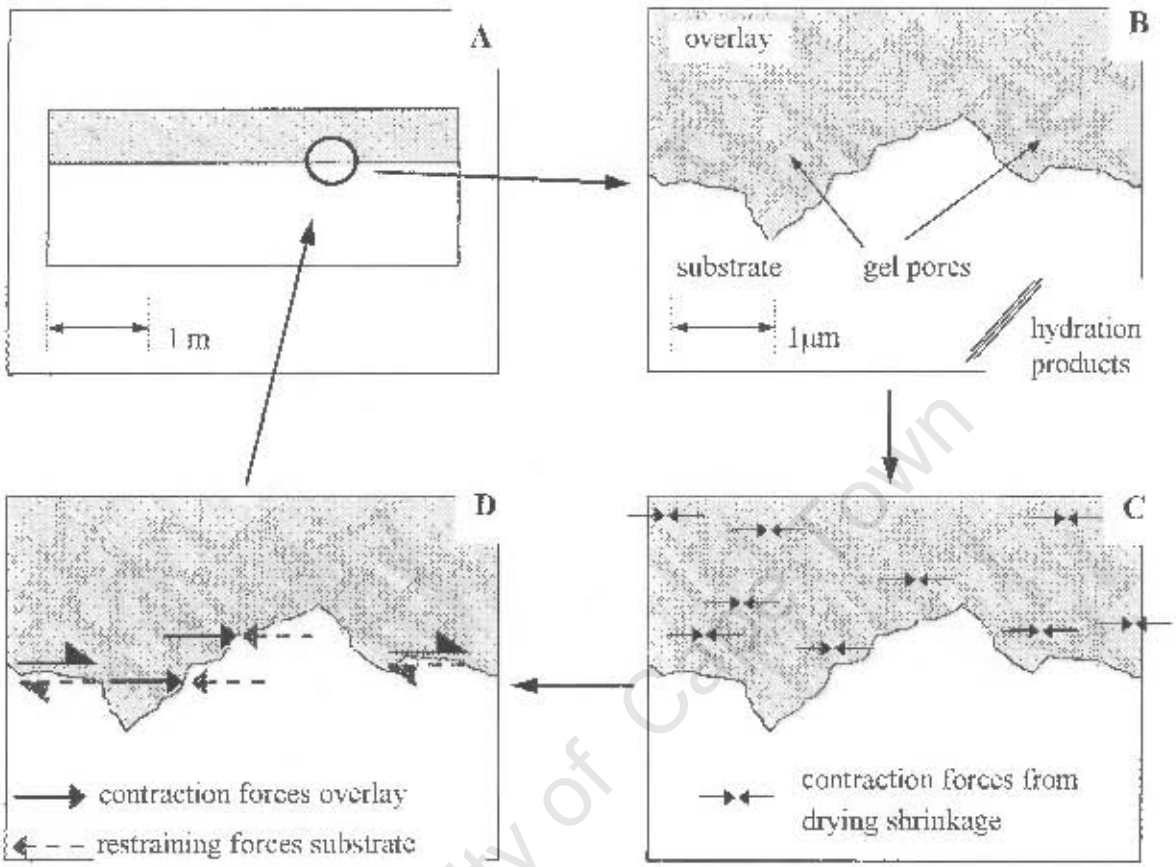

Figure 6.10: Illustration of local restraint of overlay shrinkage along the interface

Figure 6.10A shows a composite beam on a global scale. On a microscopic level, the interface between substrate and overlay may be considered to have an arbitrary shape as illustrated in **Figure 6.10B**. Shrinkage is a phenomenon that includes the deformation of the concrete matrix on a microscopic scale and what is commonly measured as shrinkage strain is the sum of microscopic deformations. This deformation is caused by contraction forces that are generated mainly as water is removed from the gel pores (compare Section 2.4.5.2). Since each increment of the overlay experiences the same drying mechanisms, contraction forces exist inside the overlay along the whole length of the member (**Figure 6.10C**). At the interface, the counteraction of contraction forces, i.e. the restraint of overlay shrinkage, occurs locally along the bond line between overlay hydration products and substrate (**Figure 6.10D**). This is best visualized by projecting the picture back onto the global scale presented in Figure 6.10A. At this scale, inner regions of the beam would be far removed from the beam ends, which illustrates that member end conditions would not influence overlay shrinkage restraint in inner regions of the member.

On a microscopic scale it appears logical that overlay shrinkage is restrained at the location of its origin, i.e. at every increment along the interface. This consequently leads to constant shear stress initiation due to restrained shrinkage along the interface.

6.5.2.2 Prestress analogy versus thermal contraction analogy

The theory on which most analytical models are based is that originally introduced by Birkeland (1960) who used a prestress analogy to model strains and stresses in bonded concrete overlays and assumed stress initiation only at the member ends (compare Section 3.3). The characteristics of shrinkage restraint along the interface outlined in the previous section, as well as the practical work discussed in Chapter 4, demonstrate that this analogy is not applicable for the characterisation of differential shrinkage stresses.

To help visualize the principle of overlay shrinkage restraint, an analogy may be made with bonded thermal contraction, e.g. the hypothetical case where a heated steel bar is embedded in cold concrete. Assuming complete bond between steel and concrete, the thermal contraction of the steel bar is restrained along its whole length and the assumption that forces are only generated at the member ends would be not correct. **Figure 6.11** illustrates the differences between the two analogies.

A concrete overlay, fully bonded to the substrate, can be compared to the case of thermal contraction. In both cases, the contracting member (cooling steel bar, shrinking overlay) would undergo the same linear deformation along its whole length if it was free to deform. Restraint of that deformation takes place along the whole area along which it is bonded to the restraining member. The end of the member experiences the initiation of restraint at the same moment as the inner parts. The end of the members can therefore not influence the restraining action in inner parts. By contrast, a prestressed strand has from the beginning only been restrained at its ends. The cause of restraint changes from the clamps holding the bar at the beam ends to the concrete holding the bar at the beam ends. Inner regions are not affected by the change of one restraining mechanism to the other. Hence, they do not experience any restraint themselves once the clamps are cut off. It appears logical that an analogy to prestressed strand is not applicable to bonded overlays.

A: Prestress analogy

- Expansion of steel:

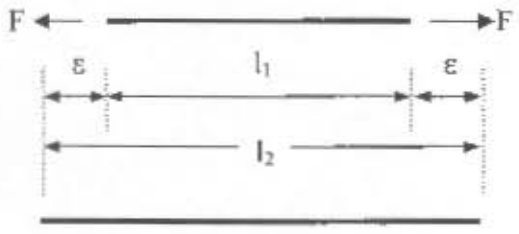

$\varepsilon = F / (A_{steel} \cdot E_{steel})$

- Steel bonded to concrete: Force transmission through cutting of steel:

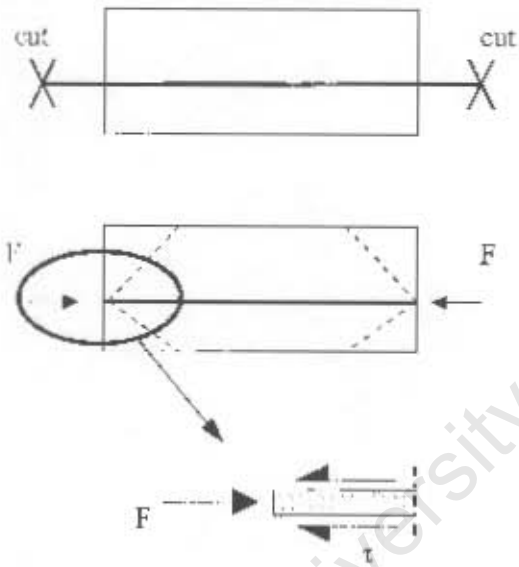

Shear stress τ only develops at the member ends to transfer the force F. Outside the transfer length, contraction of steel is restrained through the member end shear forces, hence inside shear is zero.

Interface shear between substrate and bonded overlay when prestress analogy is applied:

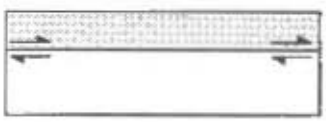

B: Thermal contraction analogy

- Expansion of steel:

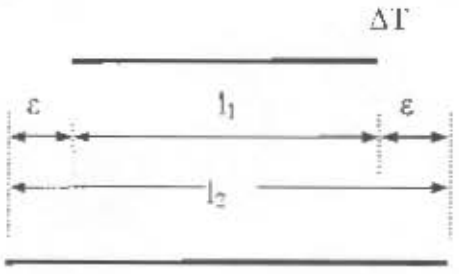

$\varepsilon = \alpha_T \cdot \Delta T$

- Steel bonded to concrete: Force transmission through cooling of steel

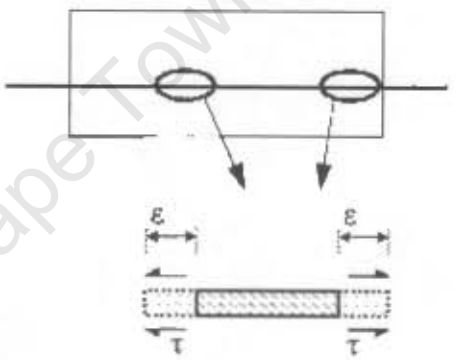

Along its whole length the steel bar tends to contract. Each length increment is restrained locally through shear forces that are generated at the interface between steel and concrete. Member end conditions do not influence the generation of interface shear inside the member as all parts of the steel bar experience the restraint at the same moment.

Interface shear between substrate and bonded overlay when thermal contraction analogy is applied:

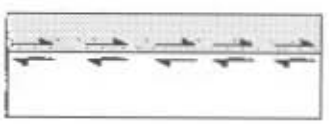

Figure 6.11: Schematics of the prestress analogy (A) and the bonded thermal contraction analogy (B)

6.5.2.3 Summary and main conclusions from practical research

Strain measurements along the interface of composite members showed that, in regions removed from the member ends, overlay and substrate strains developed independently from the location along the member (Section 4.5). It was further shown that, in the substrate, localised maximum strains occurred at the interface along the whole length of the member, indicating localised interaction between overlay and substrate at the interface (Section 4.9). These observations confirm the assumption of local shrinkage restraint at the interface in connection with constant stress initiation along the member.

However, strain and stress differences along the overlay may result from different boundary conditions. At the member ends, measured strains were higher than in inner regions of the members, indicating that a certain length exists, over which the restraint of overlay shrinkage must be developed. The analytical model developed in this section only considers the inner regions of the composite section, i.e. the regions of uniform strain, restraint and stress. This region is commonly subjected to the highest tensile overlay stresses and is therefore the most critical region for the development of cracks.

Overlay and substrate stresses due to restrained shrinkage have their origin at the interface. To directly model these stresses on a global scale with an outside force acting at any location other than the interface plane is, therefore, incorrect and unrealistic. The analysis of strain and stress must start with an understanding of what happens at the interface.

6.6 Strains and stresses in a very thin composite section

The characteristics of strain and stress development in composite members subjected to differential shrinkage can best be identified by first considering a very thin section with equal substrate and overlay depths (**Figure 6.12**).

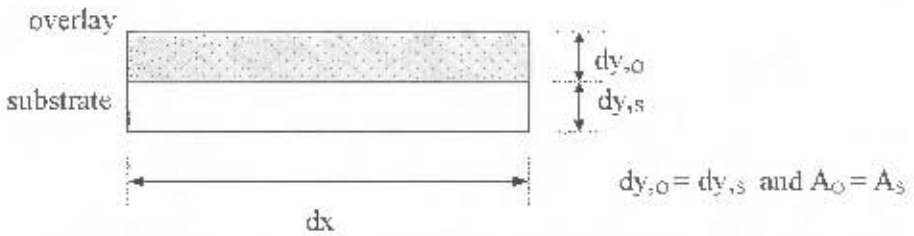

Figure 6.12: Sketch of a thin composite section with equal substrate and overlay depths

Due to the small stiffness (resulting from the small thickness) of the member sketched in Figure 6.12, differential shrinkage between overlay and substrate would cause the whole

member to curve considerably. However, the focus of this section lies on the identification of direct strains and stresses in overlay and substrate. Curvature will therefore not be considered in the modelling of the above member. The effects of curvature in composite members is discussed in Section 6.9.3.

The whole member experiences shortening as the free overlay shrinkage generates contraction forces in the substrate. Overlay shrinkage is restrained at the interface to the substrate, with the maximum restraint being experienced at the interface. The characteristics of restraint decay throughout the overlay depth were discussed in Section 6.4. However, due to the small depths of overlay and substrate of the above member it may be assumed that strains are constant throughout the member depth. Since the bond between substrate and overlay is assumed to be perfect, both substrate and overlay undergo the same linear contraction. Linear strain leads to linear stress in each section (**Figure 6.13**).

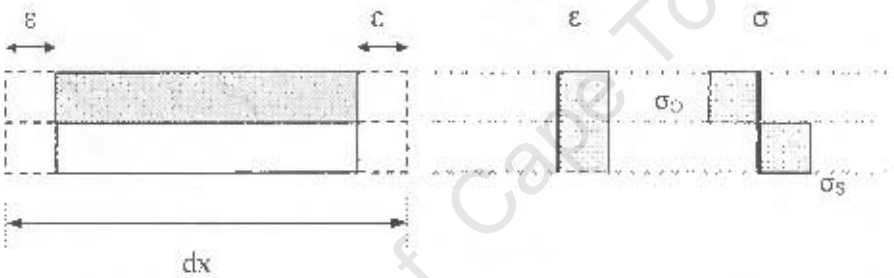

Figure 6.13: Schematics of strains and stresses in a thin composite section (ignoring curvature)

The overlay experiences tensile stress as a portion of its free shrinkage deformation ε_{FSS} is restrained. This stress can be written as:

$$\sigma_O = (\varepsilon_{FSS} \quad \varepsilon) \cdot E_O \qquad [6.2]$$

Compressive substrate stress due to the actual strain can be written as:

$$\sigma_S = \varepsilon \cdot E_S \qquad [6.3]$$

The forces of the system must be in equilibrium:

$$A_O \cdot (\varepsilon_{FSS} - \varepsilon) \cdot E_O = A_S \cdot \varepsilon \cdot E_S \qquad [6.4]$$

From $A_O = A_S$ follows:

$$(\varepsilon_{FSS} - \varepsilon) \cdot E_O = \varepsilon \cdot E_S \qquad [6.5]$$

Solving equation [6.5] for the strain ε:

$$\varepsilon = \varepsilon_O = \varepsilon_S = \frac{\varepsilon_{FSS}}{1 + \frac{E_S}{E_O}} \qquad [6.6]$$

From substituting equation [6.6] in equations [6.2] and [6.3] it follows that the magnitude of tensile stress in the overlay equals the magnitude of compressive stress in the substrate:

$$|\sigma_O| = |\sigma_S| \qquad [6.7]$$

6.7 Localised interface strain in a member of infinite depth

The formulae developed in the previous section refer to very thin composite sections. In composite members of larger thickness, substrate and overlay dimensions must necessarily influence strain and stress distribution across the member. In order to facilitate the understanding of strains and stresses in composite members of common dimensions, reference will first be made to the other extreme, i.e. to a member with infinite substrate and overlay depths (**Figure 6.14**).

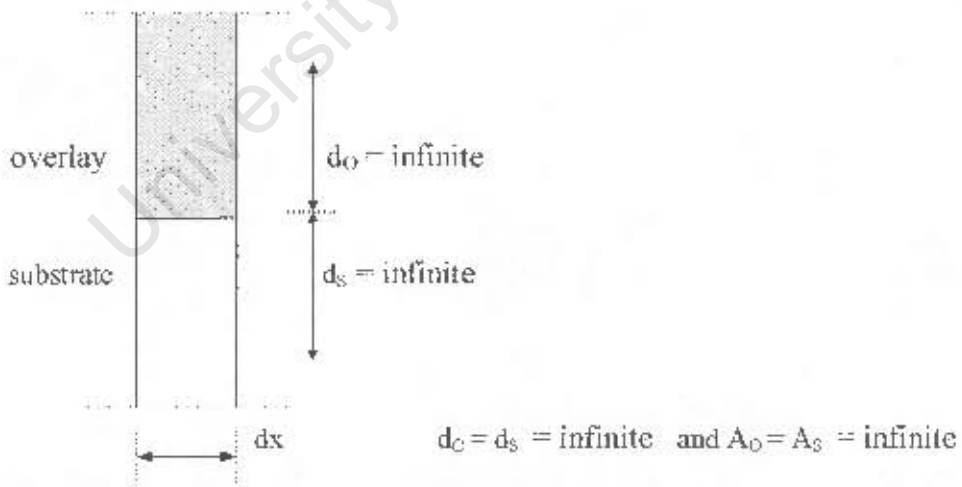

Figure 6.14: Sketch of a composite section with infinite substrate and overlay depths

In the analysis of the member sketched in Figure 6.14, only direct strains will be considered. The influence of curvature on strains and stresses in composite specimens is discussed separately in Section 6.9.3.

In Section 6.4 it was argued that on an overlay of infinite thickness, the surface of the overlay is so far removed from the substrate that the restraining action practically does not influence the surface fibre of the overlay. This phenomenon, termed *decay of restraining action*, was demonstrated using FEM analysis as discussed in Chapter 5. It was shown that local strain conditions result in cross-sections that do not remain plane after being stressed, which illustrates the non-applicability of Bernoulli's principle for the case of differential shrinkage in bonded concrete overlays. It follows that the part of the overlay that lies outside the zone of restraint decay virtually does not experience any restraint and can shrink freely. Similarly, there is a zone of strain decay in the substrate and outside this zone, the substrate does not undergo any appreciable deformation (**Figure 6.15**).

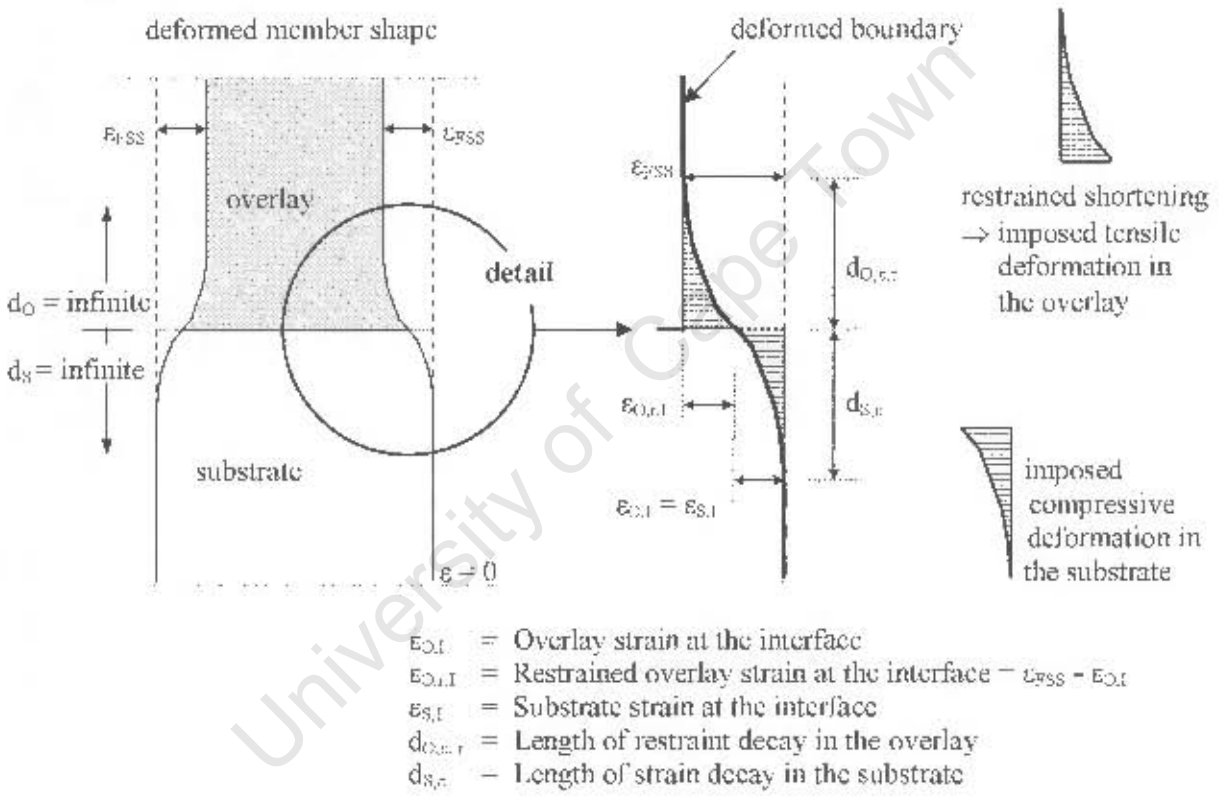

$\varepsilon_{O,I}$ = Overlay strain at the interface
$\varepsilon_{O,I,I}$ = Restrained overlay strain at the interface = $\varepsilon_{FSS} - \varepsilon_{O,I}$
$\varepsilon_{S,I}$ = Substrate strain at the interface
$d_{O,e,r}$ = Length of restraint decay in the overlay
$d_{S,e}$ = Length of strain decay in the substrate

Figure 6.15: Schematic of interface strain, restraint decay in the overlay, and strain decay in the substrate in a member with infinite substrate and overlay depths, ignoring curvature

In Figure 6.15, strains in the regions of substrate strain decay and overlay restraint decay are illustrated as to follow parabolic gradients.

The parts of the member that lie outside the regions of restraint and strain decay do not influence the degree of shrinkage restraint at the interface. If these parts were cut off from the member, strain patterns at the interface would virtually still be the same. The influence of the relative member dimensions is thus eliminated. In terms of the influence of sectional

dimensions, interface strains ε_i depend solely on the strain patterns in overlay and substrate, i.e. the depths and shapes of restraint decay and strain decay. The following 5 unknowns determine the magnitudes of strains and stresses in overlay and substrate:

- Interface strain (equal in overlay and substrate)
- Shape of restraint decay in overlay
- Depth of restraint decay in overlay
- Shape of strain decay in substrate
- Depth of strain decay in substrate

Strain patterns in overlay and substrate must adhere to two prerequisites:

- Interface strains of overlay and substrate are equal
- The sum of tensile overlay forces and compressive substrate forces must be zero

Overlay and substrate forces depend on the respective shapes and depths of restraint and strain decay. Of the 5 variables 4 are independents. If any of the 4 variables are known the 5th can be determined.

For the analysis of strains in the member sketched in Figure 6.15, it is assumed that overlay and substrate are made of the same material compositions. In general, tensile and compressive strain characteristics of concrete in medium stress conditions may be considered to be similar (compare Sections 2.5.2 and 4.3.3). For simplicity, it is therefore assumed that in the above member tensile strain characteristics in the overlay are similar to compressive strain characteristics in the substrate, i.e. the restraint decay in the overlay is assumed to have the same shape and depth as the strain decay in the substrate. With this assumption, overlay and substrate shape patterns have the same influence on interface strain and thus their influences cancel out each other. The restraint of overlay shrinkage at the interface becomes a localised phenomenon that is not influenced by section dimensions of overlay and substrate. As such, interface strains and stresses can be obtained following the same equations as those developed in Section 6.6:

$$\varepsilon_I = \varepsilon_{O,I} = \varepsilon_{S,I} = \frac{\varepsilon_{free}}{1+\frac{E_S}{E_C}} \qquad [6.8]$$

$$\text{and } |\sigma_{O,I}| = |\sigma_{S,I}| \qquad [6.9]$$

Both overlay and substrate experience a stress maximum at the interface. In regions distant from the interface, stresses in overlay and substrate will decrease according to the shape and length of restraint decay and strain decay respectively. **Figure 6.16** presents the schematic of strains and stresses across the member, assuming parabolic strain and stress gradients.

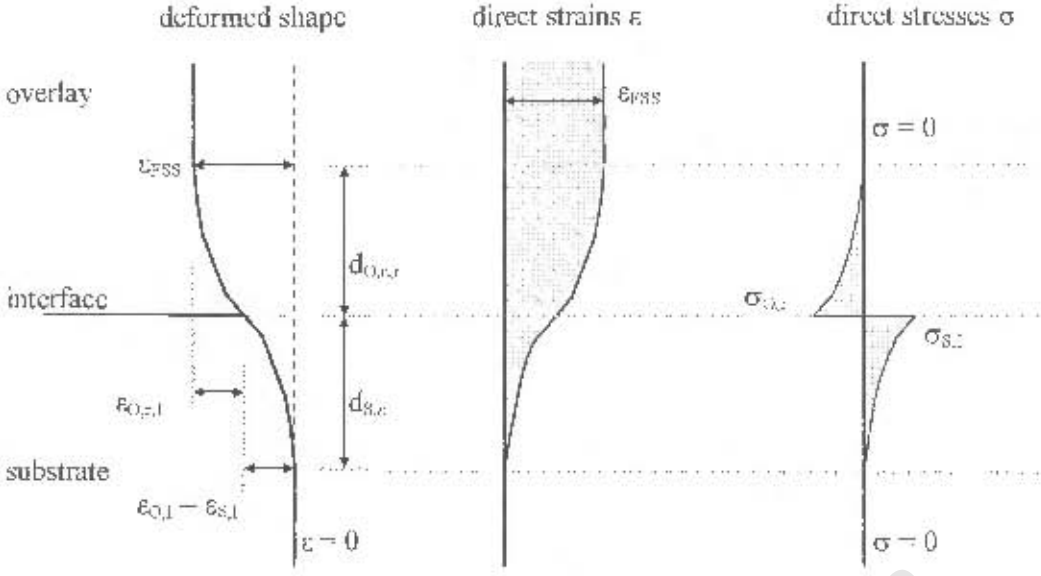

$\sigma_{O,I}$ = Overlay stress at the interface due to $\varepsilon_{O,I}$ (tension)
$\sigma_{S,I}$ = Substrate stress at the interface due to $\varepsilon_{S,I}$ (compression)

Figure 6.16: Schematic of strains and stresses across a member of infinite depth, subjected to differential shrinkage

However, in members with different strain shape profiles in overlay and substrate, the determination of interface strains becomes more complicated. A typical case where overlay and substrate strain patterns are different is a composite member of common dimensions. This case is discussed in the following section.

6.8 Localised restraint in members of finite dimensions

6.8.1 General

In the previous section, interface strains were evaluated for a member of infinite dimensions with the assumption that overlay and substrate have the same material compositions and hence the same strain characteristics. The relation between member dimensions and interface strain appears more complicated with common members of finite dimensions, i.e. for members in which the point of zero restraint in the overlay is not reached and in which substrate and overlay are made of different materials. A crucial aspect for the modelling of interface restraint, and therefore interface strain and stress, are the assumed lengths and shapes of strain decay in both overlay and substrate. This section investigates the case of relatively thin overlays on thick substrates.

6.8.2 Review of existing analytical models

As discussed in Chapter 3, existing analytical models use member end forces to model strains and stresses in overlay and substrate. Stresses applied at the ends spread into the member and cause constant direct stress over the section depth in inner regions of the member. Strains and stresses caused by differential shrinkage are therefore related to the relative member dimensions of overlay and substrate, which is a direct consequence of Bernoulli's principle of plane sections remaining plane. The relation between relative overlay and substrate dimensions and direct strains in the member based on the above principle was expressed in the equation presented by Alonso Junghanns (compare Section 3.4) (**Figure 6.17**).

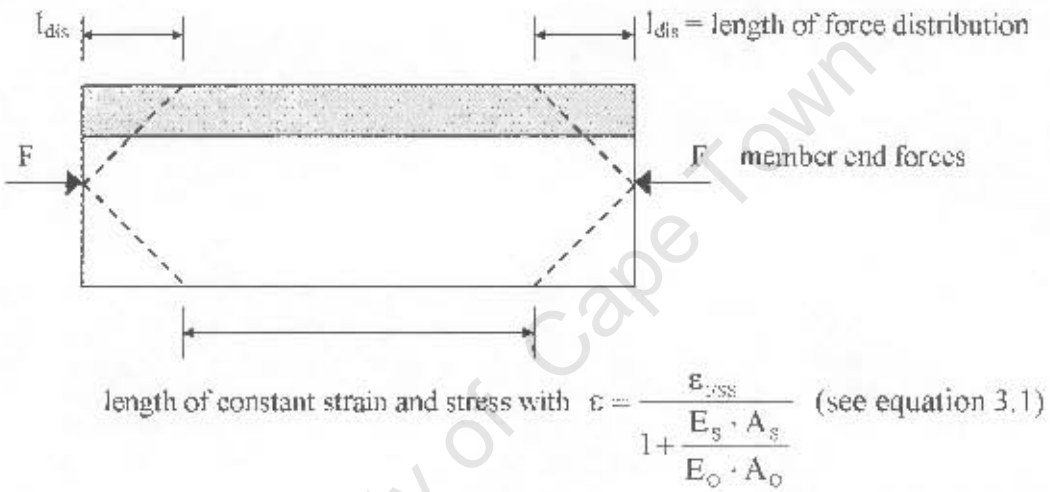

Figure 6.17: Principle of force application and spread of stresses into the member, based on existing analytical theories as presented by Alonso Junghanns (1997).

The principle illustrated in Figure 6.17, which considers direct strains to be constant throughout the member depth, represents the global level of analysis that uses the whole member to model strains and stresses without consideration of localised effects across the member depth. As stated earlier, existing analytical approaches generally operate on the global level.

6.8.3 Results of the numerical simulation

According to the numerical simulation described in Chapter 5, interface strain values are closely related to the depth of the overlay. The magnitude of interface strains decreases with decreasing overlay depth, corresponding to increasing degree of restraint. As such, interface strain values can be determined by the characteristics of strain decay in the substrate and restraint decay in the overlay. Through the FEM modelling a relatively constant depth was

computed of strain decay in the substrate $d_{s,\varepsilon}$, i.e. the depth over which the substrate experiences imposed strain is independent of the overlay depth. Similarly, the basic shape of the deformed member is always the same. The only variables are the strain values across the member depth. The strain values must adhere to the prerequisite that the sum of tensile and compressive forces in the member is zero. Interface strains are thus determined by the strain functions of overlay and substrate, which in turn depend on the overlay depth (**Figure 6.18**).

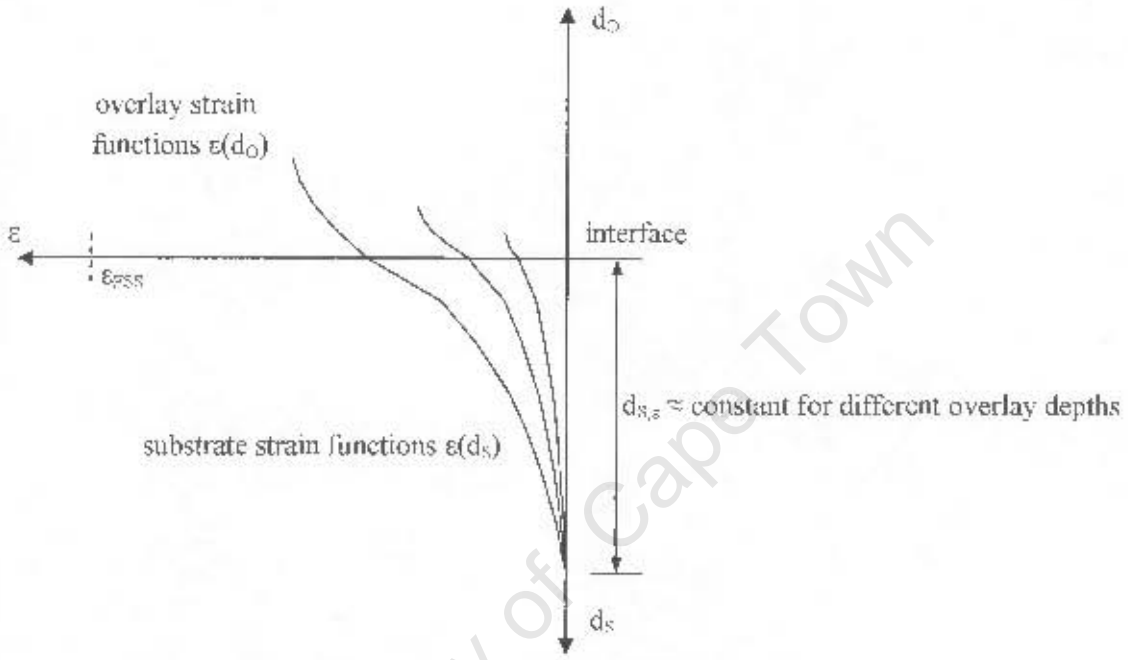

Figure 6.18: Principles of strain distribution across the member depth, assuming perfectly elastic conditions, based on FEM analysis

However, the results of the above numerical simulation indicate trends under elastic conditions, but they do not represent real strain values in actual concrete members. In order to model interface strain values, assumptions must be made for the strain patterns in overlay and substrate. This is explained in the following Section, using a simple example.

6.8.4 Modelling interface strain values in relation to strain profiles

As stated in Section 6.7, the magnitudes of strains and stresses in the composite member relate to strain characteristics, i.e. depths and patterns of strain decay, in substrate and overlay. The basic relation between interface strains and strain characteristics in substrate and overlay will first be demonstrated using the following simplifying assumptions, which roughly correspond to results from the experimental research discussed in Chapter 4:

- The overlay has constant strain throughout its depth
- The strain decay in the substrate is linear (**Figure 6.19**)

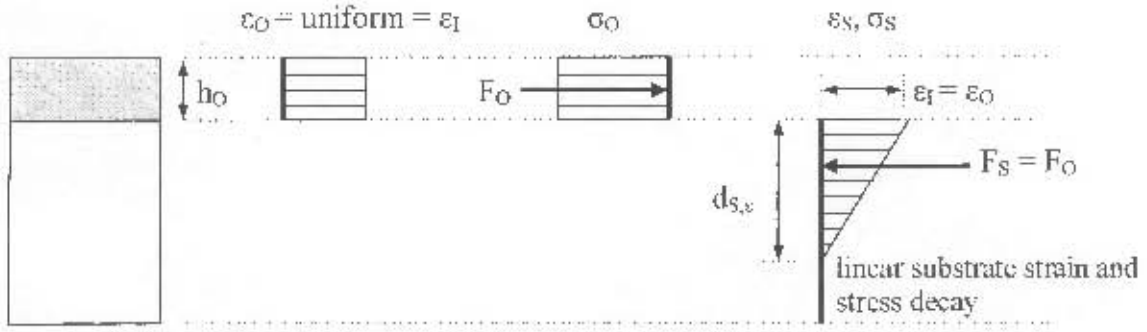

Figure 6.19: Schematic of assumed overlay and substrate strain and resulting direct stresses, using the simplifying assumption of linear strain patterns in overlay and substrate

The only 2 unknowns in the system are the magnitude of interface strain and the depth of strain decay in the substrate. Interface strain can be calculated in terms of the depth of substrate strain decay with the prerequisite that the sum of forces in the member must be zero:

$$F_O = \sigma_O \cdot h_O = E_O \cdot (\varepsilon_{rss} - \varepsilon_I) \cdot h_O \qquad [6.10]$$

$$F_S = \sigma_{S,I} \cdot 0.5\, d_{S,\varepsilon} = E_S \cdot \varepsilon_I \cdot 0.5\, d_{S,\varepsilon} \qquad [6.11]$$

$$\Sigma F = 0 \quad \therefore \quad F_O = F_S \qquad [6.12]$$

Substituting equations [6.10] and [6.11] in [6.12]:

$$\varepsilon_I = \frac{\varepsilon_{rss}}{1 + \frac{E_S}{E_O}\left(\frac{d_{S,\varepsilon}}{2h_O}\right)} \qquad [6.13]$$

Therefore, interface strains are a function of the depth of strain decay in the substrate. It is apparent that the basic form of the equation used by Alonso Junghanns (compare equation 3.1 in Figure 6.17) can be maintained if interface strains are expressed in terms of strain characteristics in overlay and substrate. It was previously argued that the relative member dimensions, in equation 3.1 expressed as the ratio between the areas of substrate and overlay (A_S/A_O), are not appropriate parameters for the prediction of interface strain. The term (A_S/A_O) should thus be exchanged by a term that accounts for the combined influences of

member dimensions and strain decay characteristics. In equation 6.13, this is the term in (brackets).

Equation 6.13 is based on the simplifying assumption that strains in overlay are constant and strains in the substrate follow a linear profile. In actual concrete members, this may not be the case. **Figure 6.20** shows a typical schematic of a strain profile in the composite member.

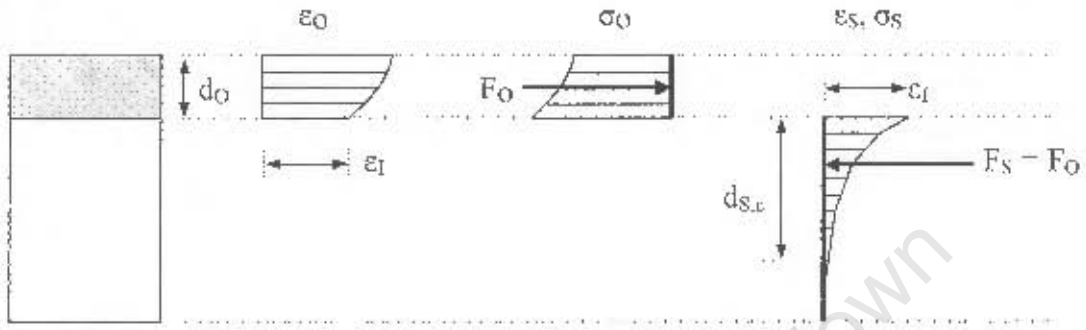

Figure 6.20: Schematic of non-linear overlay and substrate strain and resulting direct stresses

For the above member, the tensile force in the overlay can be computed as:

$$F_O = \int_{interface}^{\varepsilon_{overlay}} F_O \cdot (\varepsilon_{FSS} \cdot \varepsilon(d_O))\, dd_O \qquad [6.14]$$

The compressive force in the substrate can be computed as:

$$F_S = \int_{d_{S,c}}^{interface} F_S \cdot \varepsilon(d_S)\, dd_S \qquad [6.15]$$

The sum of forces in the above member must be zero ($F_O = F_S$, compare equation 6.12). Similarly to equation 6.13, interface strains can be expressed as a function of the remaining unknowns. In the above case of schematic strain patterns, these unknowns denote the strain patterns in substrate and overlay ($\varepsilon(d_S)$ and $\varepsilon(d_O)$), and the depth of strain decay in the substrate ($d_{S,c}$). For the general case, i.e. for arbitrary strain patterns in overlay and substrate, equation 6.13 can thus be transformed to:

$$\varepsilon_I = \frac{\varepsilon_{FSS}}{1 + \dfrac{E_S \cdot f(\varepsilon(d_S), d_{S,S})}{E_O \cdot f(\varepsilon(d_O))}} \qquad [6.16]$$

where $f(\varepsilon(d_S), d_{\varepsilon,S})$ is a function accounting for the strain characteristics in the substrate and $f(\varepsilon(d_O)$ is a function accounting for the strain pattern in the overlay for a given overlay depth. These 2 functions combine the influences of member dimensions and strain patterns.

The literature does not provide information on strain decay characteristics in composite members. In order to solve equation 6.16, strain patterns in overlay and substrate, as well as the depth of strain decay in the substrate, have to be determined empirically for a range of different overlay and substrate materials. This can be done through strain measurements in composite concrete members as discussed in Chapter 4. Strain profiles of specimens tested during this research were discussed in Section 4.9. However, analysis of strain measurements in bonded concrete overlays and substrates is difficult as measured strains are a combination of elastic and visco-elastic components. Visco-elastic strain components relate to imposed stress and hence to elastic strain components. An estimation of visco-elastic effects such as substrate creep strain and overlay relaxation requires an estimate of elastic strains and stresses. It is therefore difficult to use strain measurements for the estimation of elastic strain and stress components (**Figure 6.21**).

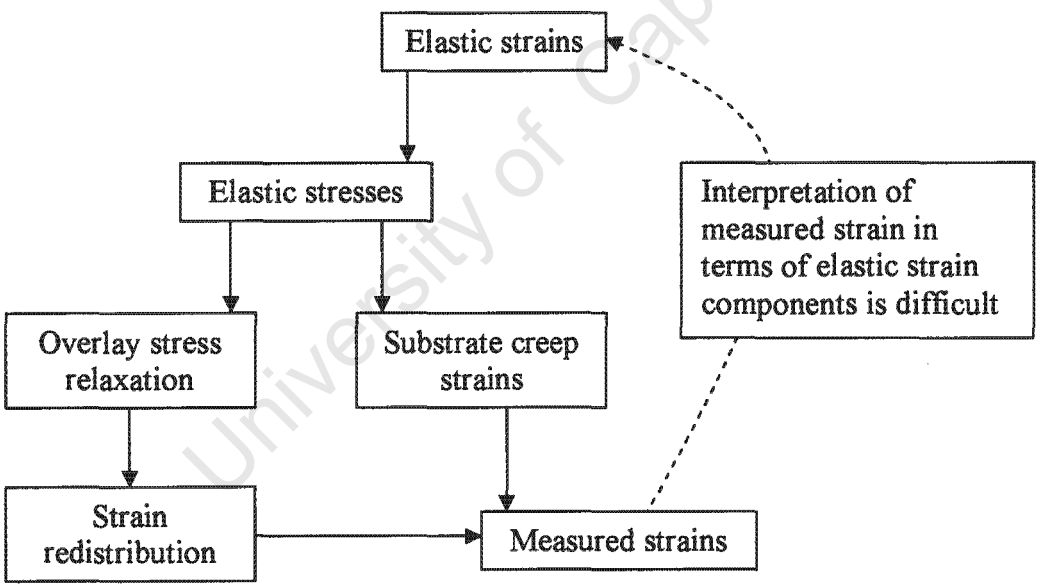

Figure 6.21: Schematic of strain components in bonded overlays

In order to use equation 6.16 as an engineering tool for the analysis of bonded concrete overlays, it therefore appears appropriate to account for the influence of these parameters in a simplified way. The basic form of equations 3.1, 6.13 and 6.16 can be maintained while the influences of strain pattern characteristics are combined in a single parameter. For facilitation of strain computation and in absence of contradicting experimental results, basic strain characteristics, i.e. strain patterns and length of strain decay, may be assumed to be time-independent variables for given substrate and overlay materials. The ratio between the

functions accounting for substrate and overlay strain characteristics can therefore be considered a constant parameter:

$$\varepsilon_I = \frac{\varepsilon_{FSS}}{1 + \frac{E_S \cdot f(\varepsilon(d_S), d_{\varepsilon,S})}{E_O \cdot f(\varepsilon(d_O))}} = \frac{\varepsilon_{FSS}}{1 + \frac{E_S}{E_O} \cdot C_\varepsilon} \qquad [6.17]$$

where C_ε denotes the combined influences of member dimensions and strain patterns in substrate and overlay. For practical use, the parameter C_ε has to be determined empirically for different materials and structural systems. Strain measurements on composite beam specimens were discussed in Chapter 4. Test results were analysed using equations for visco-elastic effects developed in the following sections. Elastic strains were estimated using equation 6.17, which allowed an estimation of the factor C_ε for the specimens used in this research. Section 6.10 discusses these issues in detail.

6.8.5 Simplified assumptions for computing interface strains

Equation 6.17 in Section 6.8.4 refers to arbitrary overlay and substrate strain patterns. In absence of detailed information on overlay and substrate strain characteristics it appears appropriate to account for simplified strain patterns in the composite member to facilitate the computation of interface strains. During the experimental research, strains were found to be relatively constant throughout the overlay depth. Strains in substrates were found to follow relatively linear patterns (compare Section 4.9). Therefore, for the computation of stresses in relatively thin bonded overlays, i.e. overlays with depths of up to 40 mm, the following assumptions are made:

- Overlay strains are constant throughout the overlay depth (compare Section 6.4)
- Substrate strains follow a linear profile

The above assumptions are illustrated in Figure 6.19. Interface strains can thus be computed as a function of the depth of substrate strain decay using equation 6.13.

6.8.6 Summary

The test results obtained during the experimental research do not correspond to existing analytical models that operate on the macro level of analysis, applying Bernoulli's principle of plane sections remaining plane. Existing analytical models are therefore unsuccessful in realistically modelling strains and stresses in composite sections subjected to differential shrinkage.

In general, strains and stresses due to differential shrinkage can possibly most accurately be modelled through numerical analysis, using a FEM programme that can take all significant time-depended factors into account. However, as an engineering tool, analytical formulae are generally more useful as they provide instant results without the need for special computer programmes. In the previous sections, simple analytical equations were developed for the estimation of interface strains in composite sections subjected to differential shrinkage. The equations are based on the principle of localised restraint at the interface between substrate and overlay. With these equations, interface strains are computed in relation to the combined influences of member dimensions and strain characteristics of overlay and substrate.

Future research is necessary to gain information on strain characteristics for different overlay and substrate materials. Based on experimental findings discussed in Chapter 3, a simplified equation for the computation of interface strains, using constant strain throughout the overlay depth and linear strain decay in the substrate, was proposed (equation 6.13).

Equations for the estimation of visco-elastic effects are developed in the following sections, based on elastic strains computed with the general equation 6.17.

6.9 Elastic and visco-elastic strains and stresses in substrate and overlay

6.9.1 Introduction

Direct and bending stresses in overlay and substrate can be computed from the degree of overlay shrinkage restraint, expressed through actual interface strain, and strain patterns in overlay and substrate. The following sections discuss the computation of elastic stresses, i.e. theoretical stresses without consideration of visco-elastic effects, as well as the computation of substrate creep strains and overlay creep relaxation. For clarity, the different strain and stress components are discussed separately and subsequently summarized in Section 6.9.6.

Theories for the computation of interface strains were discussed in previous sections. For the development of elastic and visco-elastic stress components, the general equation for elastic interface strains (equation 6.17) is used, as discussed in Section 6.8.4. For clarity, elastic interface strains are marked with the subscript "elastic" in the following sections:

$$\varepsilon_{I,elastic} = \frac{\varepsilon_{FSS}}{1 + \frac{E_S}{E_O} \cdot C_\varepsilon} \qquad \text{[compare equation 6.17]}$$

6.9.2 Direct elastic stresses

As shown earlier, direct overlay and substrate stresses can be derived from the degree of interface restraint. Elastic substrate stress corresponds to elastic substrate strain, whereas elastic overlay stress corresponds to elastic restraint of free shrinkage. The schematics of direct overlay and substrate stresses were presented in Figure 6.20.

Direct interface stresses in the overlay follow from the restrained portion of overlay shrinkage by combining Equations [6.2] and [6.17]:

$$\sigma_{O,I,direct,elastic} = \left(\varepsilon_{FSS} - \frac{\varepsilon_{FSS}}{1 + \frac{E_S}{E_O} \cdot C_\varepsilon} \right) \cdot E_O \qquad \text{(Tension)} \qquad [6.18]$$

Direct stresses in the substrate result from elastic strain and have a maximum at the interface:

$$\sigma_{S,I,direct,elastic} = \frac{\varepsilon_{FSS}}{1 + \frac{E_S}{E_O} \cdot C_\varepsilon} \cdot E_S \qquad \text{(Compression)} \qquad [6.19]$$

Equations 6.18 and 6.19 express overlay and substrate stresses in perfectly elastic conditions. The actual stresses in the composite member are influenced by the time-dependent properties of both substrate and overlay. Next to the development of overlay material parameters such as shrinkage strain and elastic modulus, the most important influences on stress development are those of substrate creep strain and overlay stress relaxation. Elastic stress and creep in bonded overlays depend on each other and the numerical estimation of the sum of all influences is difficult. For clarity, the influences of curvature, substrate creep, and overlay relaxation will be dealt with individually in the following sections. Subsequently, the different influences on strain and stress development are summarized in 6.9.6.

6.9.3 Curvature

Restrained shrinkage causes tensile overlay stress. The resulting force in the overlay produces secondary effects, i.e. bending stresses in the composite section. Bending stresses due to differential shrinkage commonly have the beneficial effect that they relieve a portion of the tensile overlay stress. However, for concrete repairs of common dimensions, i.e. thin overlays on stiff substrates, the effect of bending moments can usually be neglected. Conversely, in members with relatively low substrate stiffness, e.g. structural overlays on concrete slabs,

bending moments due to differential shrinkage might cause considerable curvature, resulting in compressive strain in the overlay and hence in partial relief of tensile overlay stress.

To compute bending moments, strain patterns in overlay and substrate are needed since they determine the lever arm of internal forces (**Figure 6.22**).

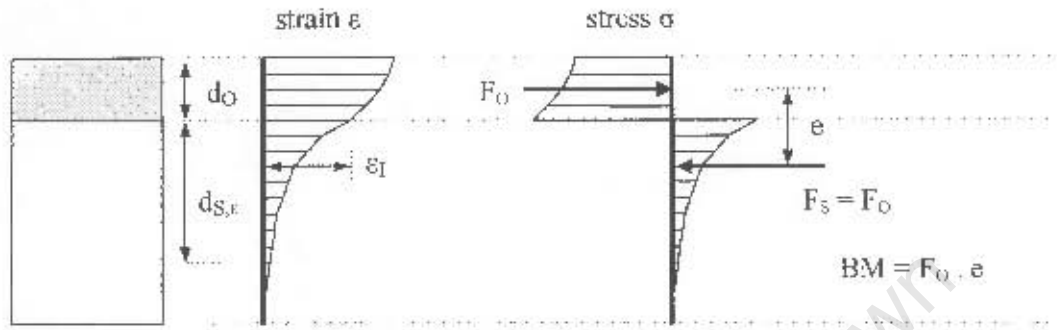

Figure 6.22: Schematic of stresses, resulting forces and internal lever arm

In absence of detailed information on overlay and substrate strain patterns, simplified assumptions need to be made to compute the internal lever arm e. As discussed in Section 6.8.5, for relatively thin overlays it appears appropriate to assume constant strain throughout the overlay depth and linear strain decay in the substrate. The schematics of direct strain and stress, bending moment, curvature κ, and total elastic strain and stress, using simplifying assumptions for strain patterns, are presented in **Figure 6.23**.

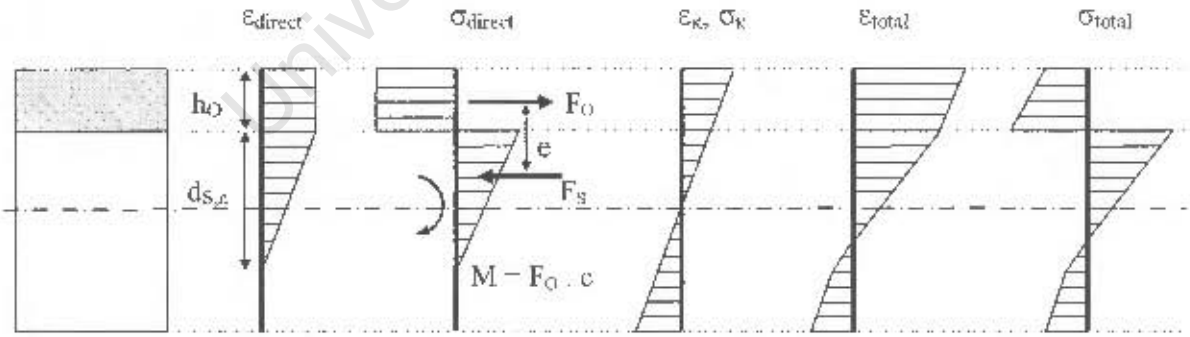

Figure 6.23: Schematics of direct elastic strain, stress, bending moment and curvature, assuming simplified strain patterns

The lever arm e between F_O and F_S can be computed as:

$$e = 0.5\, h_O + 0.33\, d_{s,\varepsilon} \qquad [6.20]$$

The above formula for the internal lever arm relates to the simplified assumption that strains are linear in the substrate and overlay strains are constant. If direct interface strains are computed with equation 6.17, the relating internal lever arm, using the above simplifying assumptions for curvature strain, can be computed as:

$$d_{s,\varepsilon} = C_\varepsilon \cdot 2h_O \qquad [6.21]$$

The bending stress initiation is analogous to the case of prestressing. The tensile prestress force in the steel is counteracted by compression in the concrete and the resulting elastic strain in the concrete leads to a partial loss of prestress. In the case of eccentricity, the remaining tensile force in the steel, i.e. the force that corresponds to the restrained shortening of the steel, causes bending stresses in the member. In the same manner it is only the restrained part of overlay shrinkage that induces stresses in the section.

Direct and bending stresses in concrete members are commonly calculated individually and subsequently superimposed to compute total stress. However, simple superimposition of direct and bending stresses caused by differential shrinkage would lead to an overestimation of the beneficial effects of curvature. Moments induced by restrained shrinkage are internal moments and as such they depend on internal deformations. The force that produces bending moments and thus curvature in the composite section results from restrained overlay shrinkage, i.e. it results from restrained shortening of the overlay. Curvature causes compressive strain, i.e. additional shortening in the overlay and thus reduces the force that initially caused the curvature. Bending moments and curvature must, therefore, be computed with the total overlay stress resulting from elastic strain including curvature (**Figure 6.24**).

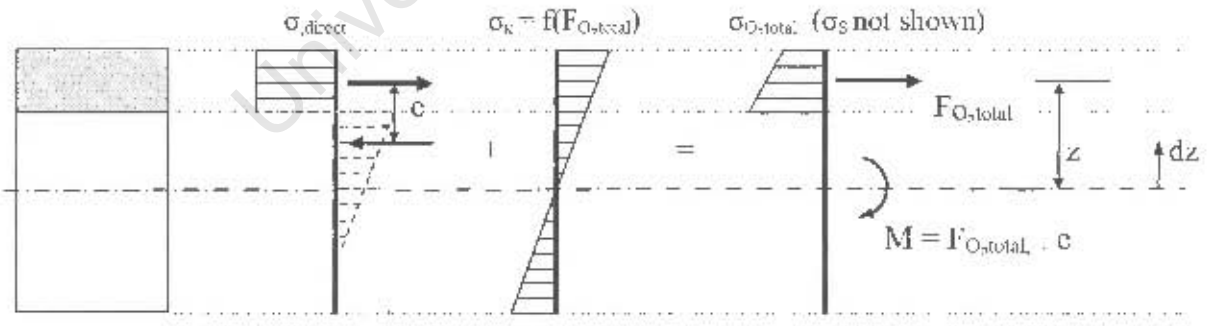

Figure 6.24: The interaction between direct overlay stress and curvature

The resulting overlay force $F_{O,total}$ that produces bending moment and curvature can be computed from the average stress in the centre of the overlay at distance z from the centroidal axis of the composite section. $F_{O,total}$ per mm width can thus be expressed as:

$$F_{O,total} = \left(\varepsilon_{FSS} - \frac{\varepsilon_{FSS}}{1 - \frac{E_S}{E_O} \cdot C_\varepsilon} \cdot \varepsilon_{\kappa,z} \right) \cdot E_O \cdot h_O \qquad [6.22]$$

$$\text{where } \varepsilon_{\kappa,z} = \frac{M}{E_C \cdot I_C} \cdot z = \frac{F_{O,total} \cdot e}{E_C \cdot I_C} \cdot z \qquad [6.23]$$

where $\varepsilon_{\kappa,z}$ is the curvature strain in the centre of the overlay, E_c the elastic modulus of the composite section, and I_c the transformed second moment of area accounting for different elastic properties of the composites.

Substituting equation [6.22] in equation [6.23] results in:

$$\varepsilon_{\kappa,z} = \left(\varepsilon_{FSS} - \frac{\varepsilon_{FSS}}{1 - \frac{E_S}{E_O} \cdot C_\varepsilon} \right) \cdot E_O \cdot h_O \cdot e \cdot z \cdot \frac{1}{E_C \cdot I_C} \left\{ \frac{1}{1 + \frac{E_O \cdot h_O \cdot e \cdot z}{E_C \cdot I_C}} \right\} \qquad [6.24]$$

where the term in front of the{brackets}is the curvature computed directly from elastic overlay stress and the term in the{brackets}is a correction factor accounting for the interaction between curvature and internal forces. For the specimens tested during the experimental research the correction factor computed with equation 6.24 was approximately 0.90 and hence for these specimens the above effect could in practice be neglected. However, specimens with relatively thin substrates might experience considerable curvature and neglecting the above mechanisms would result in an overestimation of curvature strain.

For any fibre at a distance dz from the centroidal axis of the composite member, the curvature can be computed as:

$$\varepsilon_{\kappa,dz} = \left(\varepsilon_{FSS} - \frac{\varepsilon_{FSS}}{1 - \frac{E_S}{E_O} \cdot C_\varepsilon} \right) \cdot E_O \cdot h_O \cdot e \cdot dz \cdot \frac{1}{E_C \cdot I_C} \left\{ \frac{1}{1 + \frac{E_O \cdot h_O \cdot e \cdot z}{E_C \cdot I_C}} \right\} \qquad [6.25]$$

where $e = 0.5\, h_O + 0.33\, d_{S,c}$ (see equation 6.20).

6.9.4 Substrate creep strain

As a result of its restraining action, the substrate undergoes considerable deformation at the interface. Imposed elastic strain and stress consequently cause creep deformations. Since bond between substrate and overlay is assumed to be perfect, this leads to additional shortening of the overlay and hence to loss of shrinkage restraint and the associated relaxation of tensile overlay stresses (**Figure 6.25**).

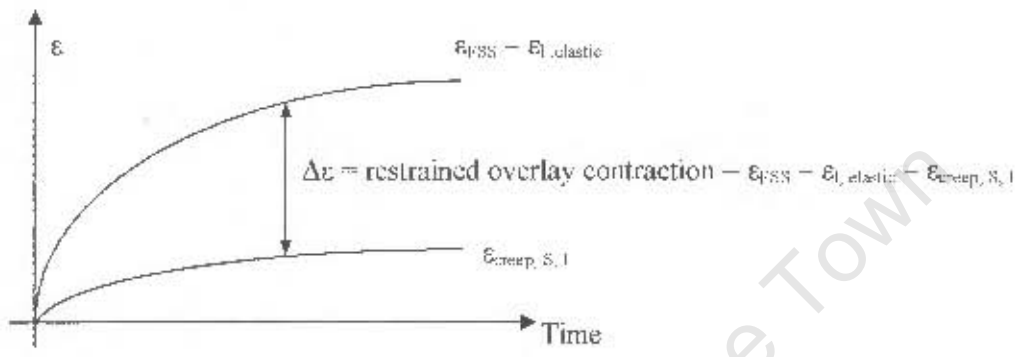

Figure 6.25: Schematic of overlay stress relaxation at the interface through substrate creep strain

The relation between substrate creep at the interface and direct elastic interface strain due to restrained shrinkage is complex. The stress-producing interface strain at any time t, which is a combination of direct elastic strains and creep strains, may be called *instantaneous interface strain* ($\varepsilon_{inst,I}(t)$). It is influenced by the substrate creep that took place between the time of stress initiation t_0 and t. Therefore, the general equation for interface strain (equation 6.17) can be extended to:

$$\varepsilon_{inst.,I}(t) = (\varepsilon_{FSS}(t) - \varepsilon_{creep,S,I}(t,t_0)) \cdot \frac{1}{1 + \frac{E_S}{E_O} \cdot C_2} \qquad [6.26]$$

Substrate creep in turn depends on the imposed instantaneous strain and stress:

$$\varepsilon_{creep,S,I}(t) = f\left(\sigma_{inst.,I}(t,t_0)\right) - f\left(\varepsilon_{inst.,I}(t,t_0), E_S\right) \qquad [6.27]$$

The characteristics of creep under incremental loading were discussed in Section 2.5.3. The *Boltzmann* superposition principle will be adopted to express substrate creep strain under increasing stress due to overlay shrinkage. Using a stepwise approach of the *Boltzmann*

principle, i.e. considering stress increments for the calculation of creep, 2 different simplified approaches can be applied as presented in **Figure 6.26**.

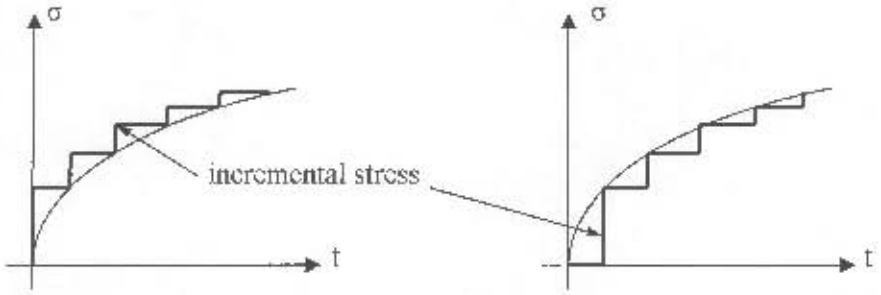

Figure 6.26: Schematic of possible approaches for the application of the *Boltzmann* principle

The first approach (Figure 6.26, left) is based on the concept that the total stress during a certain time increment was present from the beginning of that time increment. The second approach (Figure 6.26, right) accounts for the total incremental stress only at the end of the particular time increment. The first approach leads to an overestimation and the second approach to an underestimation of creep strains. Over- and underestimation may be neglected if small time increments are used. For practical purposes, an aging coefficient ρ of 0.8, as proposed by Walraven and Shkoukani (1993) (compare Section 2.5), can be applied in connection with the first of the above two approaches. Creep strains are calculated with the simplifying assumption that 80% of the incremental stress was present from the beginning of the particular time increment. Consequently, the interaction between substrate creep strain and instantaneous strain at the interface may be expressed as follows:

at $t = t_0$:

$$\varepsilon_{creep,S,1}(t_0) = 0 \qquad [6.28]$$

$$\varepsilon_{inst.,1}(t_0) = \varepsilon_{elastic,1}(t_0) - \varepsilon_{FSS}(t_0) \cdot \frac{1}{1 + \frac{E_S}{E_O(t_0)} \cdot C_s} \qquad [6.29]$$

$$\varepsilon_{total,2}(t_0) = \varepsilon_{inst.,2}(t_0) \qquad [6.30]$$

at $t = t_1$:

$$\varepsilon_{creep,S,1}(t_1) = \varepsilon_{inst.,1}(t_0) \cdot \varphi_S(t_1, t_0) + (\varepsilon_{inst.,1}(t_1) - \varepsilon_{inst.,1}(t_0)) \cdot 0.8 \cdot \varphi_S(t_1, t_0) \qquad [6.31]$$

$$\varepsilon_{inst.,1}(t_1) = (\varepsilon_{FSS}(t_1) - \varepsilon_{creep,S,1}(t_1)) \cdot \frac{1}{1 + \frac{E_S}{E_O(t_1)} \cdot C_s} \qquad [6.32]$$

$$\varepsilon_{total,1}(t_1) = \varepsilon_{inst.,1}(t_1) - \varepsilon_{creep,S,1}(t_1) \qquad [6.33]$$

at $t = t_2$:

$$\varepsilon_{creep,S,I}(t_2) = \varepsilon_{inst.,1}(t_0)\cdot\varphi_S(t_2,t_0) + (\varepsilon_{inst.,2}(t_1) - \varepsilon_{inst.,1}(t_0))\cdot\varphi_S(t_2,t_1) + \\ + (\varepsilon_{inst.,2}(t_2) - \varepsilon_{inst.,1}(t_1))\cdot 0.8\cdot\varphi_S(t_2,t_1) \quad [6.34]$$

$$\varepsilon_{inst.,I}(t_2) = (\varepsilon_{FSS}(t_2) - \varepsilon_{creep,S,I}(t_2))\cdot\frac{1}{1-\frac{E_S}{E_O(t_2)}\cdot C_\varepsilon} \quad [6.35]$$

$$\varepsilon_{total,I}(t_2) = \varepsilon_{inst.,I}(t_2) + \varepsilon_{creep,S,I}(t_2) \quad [6.36]$$

at $t = t_i$:

$$\varepsilon_{creep,S,I}(t_i) = \sum_{n=1}^{i}\left[(\varepsilon_{inst.,2}(t_{i-n}) - \varepsilon_{inst.,2}(t_{i-(n+1)}))\cdot\varphi_S(t_i,t_{i-n})\right] + \\ + (\varepsilon_{inst.,2}(t_i) - \varepsilon_{inst.,I}(t_{i-1}))\cdot 0.8\cdot\varphi_S(t_i,t_{i-1}) \quad [6.37]$$

$$\varepsilon_{inst.,I}(t_i) = (\varepsilon_{FSS}(t_i) - \varepsilon_{creep,S,I}(t_i))\cdot\frac{1}{1+\frac{E_S}{E_O(t_i)}\cdot C_\varepsilon} \quad [6.38]$$

$$\varepsilon_{total,I}(t_i) = \varepsilon_{inst.,I}(t_i) + \varepsilon_{creep,S,I}(t_i) \quad [6.39]$$

Substituting equation [6.37] in equation [6.38] results in

$$\varepsilon_{inst.,I}(t_i) = \left(\varepsilon_{FSS}(t_i) + \varepsilon_{inst.,I}(t_{i-1})\cdot 0.8\cdot\varphi_S(t_i,t_{i-1}) - \sum_{n=1}^{i}\left[(\varepsilon_{inst.,I}(t_{i-1}) - \varepsilon_{inst.,I}(t_{i-(n+1)}))\cdot\varphi_S(t_i,t_{i-n})\right]\right)\cdot \\ \cdot\left(1+\frac{E_S}{E_O(t_i)}\cdot C_\varepsilon + 0.8\cdot\varphi_S(t_i,t_{i-1})\right)^{-1} \quad [6.40]$$

When the whole period since commencement of overlay shrinkage is considered in a one-step-analysis, equation [6.37] can be written in a simple manner:

$$\varepsilon_{creep,S,I}(t_i) = \varepsilon_{inst.,I}(t_0)\cdot\varphi_S(t_i,t_0) + (\varepsilon_{inst.,2}(t_i) - \varepsilon_{inst.,I}(t_0))\cdot 0.8\cdot\varphi_S(t_i,t_0) \quad [6.41]$$

Since instantaneous strain at $t_0 = 0$ is zero, equation [6.41] can be written as:

$$\varepsilon_{creep,S,I}(t_i) = \varepsilon_{inst.,I}(t_i)\cdot 0.8\cdot\varphi_S(t_i,t_0) \quad [6.42]$$

Substituting equation [6.42] into equation [6.38] results in:

$$\varepsilon_{inst.,I}(t_i) = \varepsilon_{FSS}\cdot\frac{1}{1+\frac{E_S}{E_O(t_i)}\cdot C_\varepsilon + 0.8\cdot\varphi_S(t_i,t_0)} \quad [6.43]$$

The outcome of equations 6.40 and 6.43 were compared for a range of different substrate ages at the time of first loading. If substrates are subjected to differential shrinkage at early ages (e.g. 10 days), instantaneous strains computed with equation 6.43 over a period of 150 days are approximately 10 to 15% less than those computed with equation 6.40. The difference increases with increasing age of the composite member. With an increase in the substrate age at first loading, the difference between equations 6.40 and 6.43 becomes less pronounced (**Figure 6.27**).

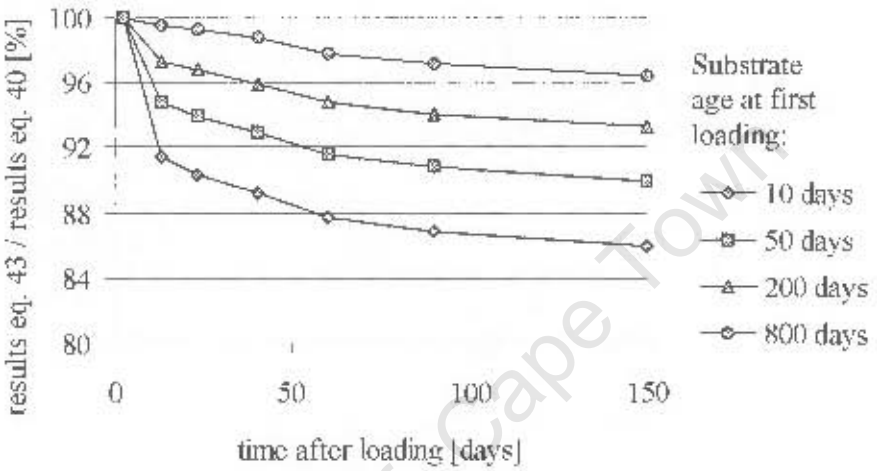

Figure 6.27: Comparison of test results computed with equations 6.40 and 6.43

For concrete repairs, substrates are usually relatively old at the time of overlay application. Equations 6.40 and 6.43 would therefore give very similar results. In order to facilitate the computation of differential shrinkage stresses in bonded concrete overlays, it therefore appears appropriate to use the simplified equation (equation 6.43) for the calculation of instantaneous interface strains. The total interface strain at any time t can thus be computed by combining equations 6.39, 6.42 and 6.43 to:

$$\varepsilon_{total,I}(t) = \varepsilon_{inst.,I}(t) + \varepsilon_{creep,S,I}(t) - \varepsilon_{inst.,I}(t) \cdot (1 + 0.8 \cdot \varphi_S(t, t_0)) - \varepsilon_{FSS} \cdot \frac{1}{1 + \frac{E_S}{E_C(t)} \cdot C_c + 0.8 \cdot \varphi_S(t, t_c)} \cdot (1 + 0.8 \cdot \varphi_S(t, t_c)) \quad [6.44]$$

Research on concrete creep strain generally refers to uniformly loaded members, i.e. members that experience uniform stress over their cross-section. In the above case of differential shrinkage stresses, the substrate is subjected to non-uniform stress conditions. In that respect, substrate creep strains calculated with the above formulae might be overestimated. However, strain measurements on composite specimens indicated a

considerable amount of substrate creep (compare Section 4.9). The practical applicability of the above equations will be discussed in Section 6.10.

6.9.5 Overlay stress relaxation

Tensile overlay stress is partly relieved through relaxation. The characteristics of stress relaxation were discussed in Section 2.5.2. As stated earlier, elastic interface strain caused by differential shrinkage corresponds directly to overlay stress. Relaxation of tensile overlay stress, therefore, results in a reduction of interface strain. However, the actual interaction between overlay relaxation and elastic interface strain is complex. At the time of loading, overlay and substrate undergo the same elastic deformation at the interface. Subsequently, the overlay experiences relaxation, and the remaining stress can be written as:

$$\sigma_O = \psi_O \cdot \left(\varepsilon_{FSS} - \frac{\varepsilon_{FSS}}{1 + \frac{E_S}{E_O} \cdot C_\varepsilon} \right) \cdot E_O \qquad [6.45]$$

where ψ_O is the relaxation coefficient of the overlay. Since the relaxation of overlay stress is not directly coupled with a reduction of overlay strain, the substrate still experiences the same strain and hence the same stress as at the time of loading. This leads to a redistribution of stress in the member since tension and compression must be in equilibrium. Overlay stress relaxation influences interface strain therefore indirectly through the reduction in the actual shrinkage force acting on the composite section and hence through the reduction in instantaneous strain.

Strain measurements on cracked specimens (Section 4.11) led to the conclusion that a large amount of tensile stress relaxation takes place in the early ages of loading. This was confirmed in the literature as Horimoto and Koyangani (1994), Gutsch and Rostasy (1994), and Kordina et al (2000) found tensile stress relaxation to develop rapidly after loading (compare Section 2.5.2). As such, stress relaxation develops at a much faster rate than stresses resulting from ongoing overlay shrinkage. In order to facilitate analytical modelling of overlay and substrate stresses, it therefore appears appropriate to account for overlay stress relaxation in a simple manner. For the analysis of stresses it is assumed that tensile stress relaxation occurs instantaneously after loading (**Figure 6.28**).

Consequently, it is not overlay shrinkage that causes interface strain but overlay shrinkage strain adjusted to the overlay relaxation coefficient $\psi_O(t, t_0)$:

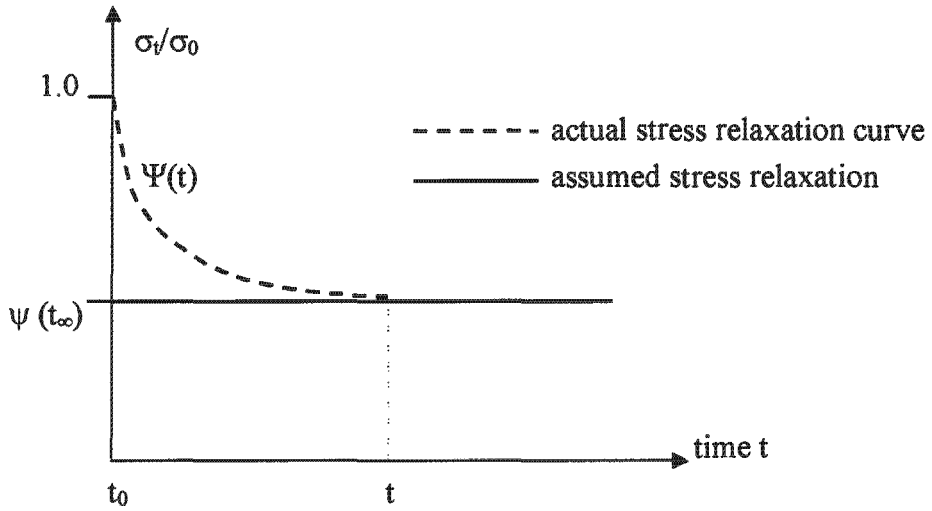

Figure 6.28: Schematic of simplified approach for the consideration of overlay stress relaxation

$$\varepsilon_I(t) = \frac{\psi_O(t,t_o)\cdot\varepsilon_{FSS}(t)}{1+\frac{E_S}{E_O(t)}\cdot C_\varepsilon} \qquad [6.46]$$

where $\psi(t, t_0)$ is the relaxation coefficient at time t, accounting for the total relaxation of incremental stresses since the time of first loading t_0. The relaxation coefficient depends on the age of the overlay since stress relaxation generally decreases with age, i.e. overlay shrinkage at a later age will cause less stress relaxation. The substrate and overlay stresses corresponding to interface strains calculated with equation 6.46 are:

$$\sigma_{S,I}(t) = \varepsilon_I(t)\cdot E_S = \frac{\psi_O(t,t_o)\cdot\varepsilon_{FSS}(t)}{1+\frac{E_S}{E_O(t)}\cdot C_\varepsilon}\cdot E_S \qquad \text{(compression)} \qquad [6.47]$$

$$\sigma_{O,I}(t) = (\psi_O(t,t_0)\cdot\varepsilon_{FSS}(t) - \varepsilon_I(t))\cdot E_O(t) =$$

$$= \left(\psi_O(t,t_0)\cdot\varepsilon_{FSS}(t) - \frac{\psi_O(t,t_0)\cdot\varepsilon_{FSS}(t)}{1+\frac{E_S}{E_O(t)}\cdot C_\varepsilon}\right)\cdot E_O(t) = \qquad [6.48]$$

$$= \psi_O(t,t_0)\cdot\left(\varepsilon_{FSS}(t) - \frac{\varepsilon_{FSS}(t)}{1+\frac{E_S}{E_O(t)}\cdot C_\varepsilon}\right)\cdot E_O(t) \qquad \text{(tension)}$$

If the overlay relaxation function $\Psi_O(t)$ is known, $\psi_O(t, t_0)$ may be expressed with the *Boltzmann* principle:

$$\psi_O(t,t_0) = \left(\sum_{t_i=0}^{t} (\varepsilon_{FSS}(t_i) - \varepsilon_{FSS}(t_i - 1)) \cdot \Psi_O(t_i - t_{i-1}) \right) \cdot \frac{1}{\varepsilon_{FSS}(t)} \quad [6.49]$$

A relaxation function $\Psi(t, t_0)$ for tensile creep was introduced by Gutsch and Rostásy (1994) (compare Section 2.5.2). In general, information on stress relaxation functions in the literature is scarce and practical research would be required for an accurate estimation of $\Psi(t, t_0)$ for different overlay compositions.

6.9.6 Summary

Actual overlay strains are a result of all different strain components discussed in the previous sections. The interaction between the different strain components is complex. Overlay stress relaxation depends on the loading history and hence on substrate creep strain. The latter in turn depends on the imposed load and hence on overlay stress relaxation. To facilitate the computation of overlay strains, overlay stress relaxation and substrate creep strains are simply superimposed by combining equations 6.44 and 6.46. Overlay strains combining the influences of overlay stress relaxation and substrate creep strains are termed $\varepsilon_{O,vis\text{-}el}$ ("vis-el" = "visco-elastic"):

$$\varepsilon_{I,vis-elc}(t) = \psi(t,t_0) \cdot \varepsilon_{FSS}(t) \cdot \frac{1}{1 + \frac{E_S}{E_O(t)} \cdot C_\varepsilon + 0.8 \cdot \varphi_S(t,t_0)} \cdot (1 + 0.8 \cdot \varphi_S(t,t_0)) \quad [6.50]$$

As discussed in Section 6.9.5, the overlay stress relaxation factor ψ (t, t_0) accounts for the total relaxation of incremental stresses since the time of first loading t_0. The relaxation at different time increments depends on the age of the overlay since overlays tend to have less relaxation when loaded at later ages (**Figure 6.29**).

With a simple computer programme, e.g. written in *Microsoft Excel*, the time dependent relaxation of overlay stress can easily be modelled if the time-dependent relaxation function $\Psi(t)$ is known. Appendix 8 contains such a programme. Strains at any time t can thus be computed. If the time-dependent relaxation factor is not known, a simplified approach may be used, estimating total stress relaxation at time t. This can, for example, be done by estimating a relaxation factor $\psi(t)$, based on creep tests for a given overlay composition.

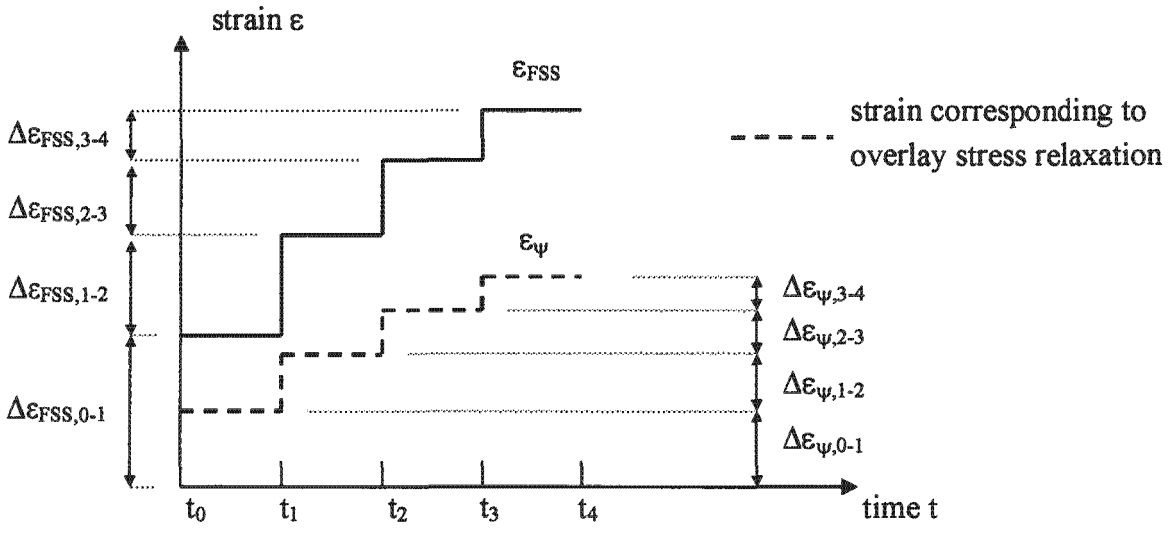

$$\Delta\varepsilon_{\psi,3\text{-}4} / \Delta\varepsilon_{FSS,3\text{-}4} < \Delta\varepsilon_{\psi,2\text{-}3} / \Delta\varepsilon_{FSS,2\text{-}3} < \Delta\varepsilon_{\psi,1\text{-}2} / \Delta\varepsilon_{FSS,1\text{-}2} < \Delta\varepsilon_{\psi,0\text{-}1} / \Delta\varepsilon_{FSS,0\text{-}1}$$

Figure 6.29: Schematic of overlay stress relaxation as a function of the time of loading

As discussed in Section 4.7.9, overlay relaxation in the composite specimens examined at different ages during the experimental research was found to be approximately 40-60% of the total tensile stress. Based on these values, the relaxation factor ψ(t) in equation 6.50 for the tested specimens may be estimated as 0.50. In absence of time-dependent relaxation values, a constant relaxation factor may be used for an approximation of overlay stresses at any time t. Considering the complexity of strains and stresses in bonded concrete overlays, such an approximation appears appropriate for design purposes if it leads to a conservative estimation of overlay stress. In general, a relation between basic tensile creep and shrinkage strain, as suggested by Pigeon and Bissonnette (1999) (compare Section 2.5.2), can be considered as a useful tool for the estimation of the relaxation factor ψ(t). Further research is necessary to establish such relationships for different overlay materials.

Curvature is an elastic strain component that depends on the magnitude of overlay stress. Curvature strain usually releases overlay tensile stress and therefore indirectly influences overlay stress relaxation and substrate creep strains. For simplicity, curvature can be calculated using the total overlay strain calculated with equation 6.50. Equation 6.25 can thus be written as:

$$\varepsilon_{\kappa,dz}(t) = \left(\varepsilon_{O,vis-el}(t) - \frac{\varepsilon_{O,vis-el}(t)}{1 + \frac{E_S}{E_O} \cdot C_\varepsilon} \right) \cdot E_O \cdot e \cdot h_O \cdot dz \cdot \frac{1}{E_C \cdot I_C} \cdot \left\{ \frac{1}{1 + \frac{E_O \cdot h_O \cdot e \cdot z}{E_C \cdot I_C}} \right\} \qquad [6.51]$$

Total overlay strains at any time t can be computed as:

$$\varepsilon_{O,total}(t) = \varepsilon_{O,vis-el}(t) + \varepsilon_{\kappa}(t) \qquad [6.52]$$

The above equations for the calculation of total overlay strains assume simple superposition of different strain components. As such, they represent a simplified approach, as the actual interaction between different strain components is complex. However, the exact estimation of all combined influences on overlay strain is virtually impossible as the factors that need to be considered are numerous and often uncertain, ranging from different strain components, environmental conditions, interface conditions, workmanship, etc. The simplified approach presented in this section is therefore a practical tool for the estimation of overlay strains due to differential shrinkage. Strains predicted with the above equations coincided reasonably closely to measured strains on composite specimens, as discussed in Section 6.10.

With the above equations, overlay stress at the interface can be calculated to be:

$$\sigma_{I,O}(t) = (\psi(t,t_0)\cdot\varepsilon_{FSS}(t) - \varepsilon_{I,O,total}(t))\cdot E_O(t) \qquad [6.53]$$

Neglecting curvature, tensile overlay stress at the interface can be obtained by substituting equation 6.50 in equation 6.53:

$$\sigma_{I,O}(t) = \psi(t,t_0)\cdot\varepsilon_{FSS}(t)\cdot E_O(t)\cdot\left(1 - \frac{1}{1 + \frac{E_S\cdot C_\varepsilon}{E_O(t)\cdot(1+0.8\cdot\varphi_S(t,t_0))}}\right) \qquad [6.54]$$

6.10 Comparison of experimental research and analytical model

6.10.1 Introduction

The strain development in bonded overlays was investigated through experimental research, using different overlay materials and different interface textures, as discussed in Chapter 4. Fundamental characteristics of composite behaviour identified in the experimental research were used for the development of an analytical model for the prediction of strains and stresses in bonded overlays, as discussed in Sections 6.1 to 6.9. This model combines the influences of elastic interface strain, overlay relaxation, substrate creep strain, and curvature.

It must be noted that any analytical model for the behaviour of bonded overlays can only present an approximation of overlay strain values. The precise prediction of overlay strains is

practically difficult as many time-dependent variables influence the behaviour of the composite specimen.

In the following sections, overlay strains measured on specimens tested during the experimental research are compared to the analytical model. It is anticipated to show that the analytical model is able to predict strain development in bonded concrete overlays both in terms of fundamental strain characteristics and numerical strain values (compare Figure 4.1, page 69).

The analytical model is based on the following input parameters:

1. Material properties of the overlay:
   - Shrinkage strain development $\varepsilon_{FSS}(t)$
   - Elastic properties $E_O(t)$
   - Time-dependent relaxation factor $\psi(t,t_0)$

2. Material properties of the substrate:
   - Properties needed to estimate substrate creep strains (mix design, age, environmental influences, etc)
   - Elastic modulus E_S

3. System characteristics:
   - Member dimensions d_O and d_S (for estimation of curvature strain)

4. Empirical factor accounting for the combined influences of relative member dimensions and strain characteristics of substrate and overlay (C_ε)

During the experimental research, information on all parameters mentioned under 1-3 in the above list was obtained. These parameters can therefore be modelled appropriately for the tested specimens. However, the empirical factor C_ε must be estimated. This poses a challenge as C_ε can only be found empirically by interpreting experimental work with the analytical model. The model, in turn, can only be verified against the experimental work if values for C_ε are available. In the model, C_ε is used to compute elastic strains and stresses. The interpretation of measured strain values, which include visco-elastic components, in terms of elastic strain components is difficult, as discussed in Section 6.8.4 (compare Figure 6.21). The approach used is to first estimate the factor C_ε from test results obtained on Specimens C, which is discussed in Section 6.10.2. With this factor, overlay strains are computed and compared to the experimental results (**Figure 6.30**).

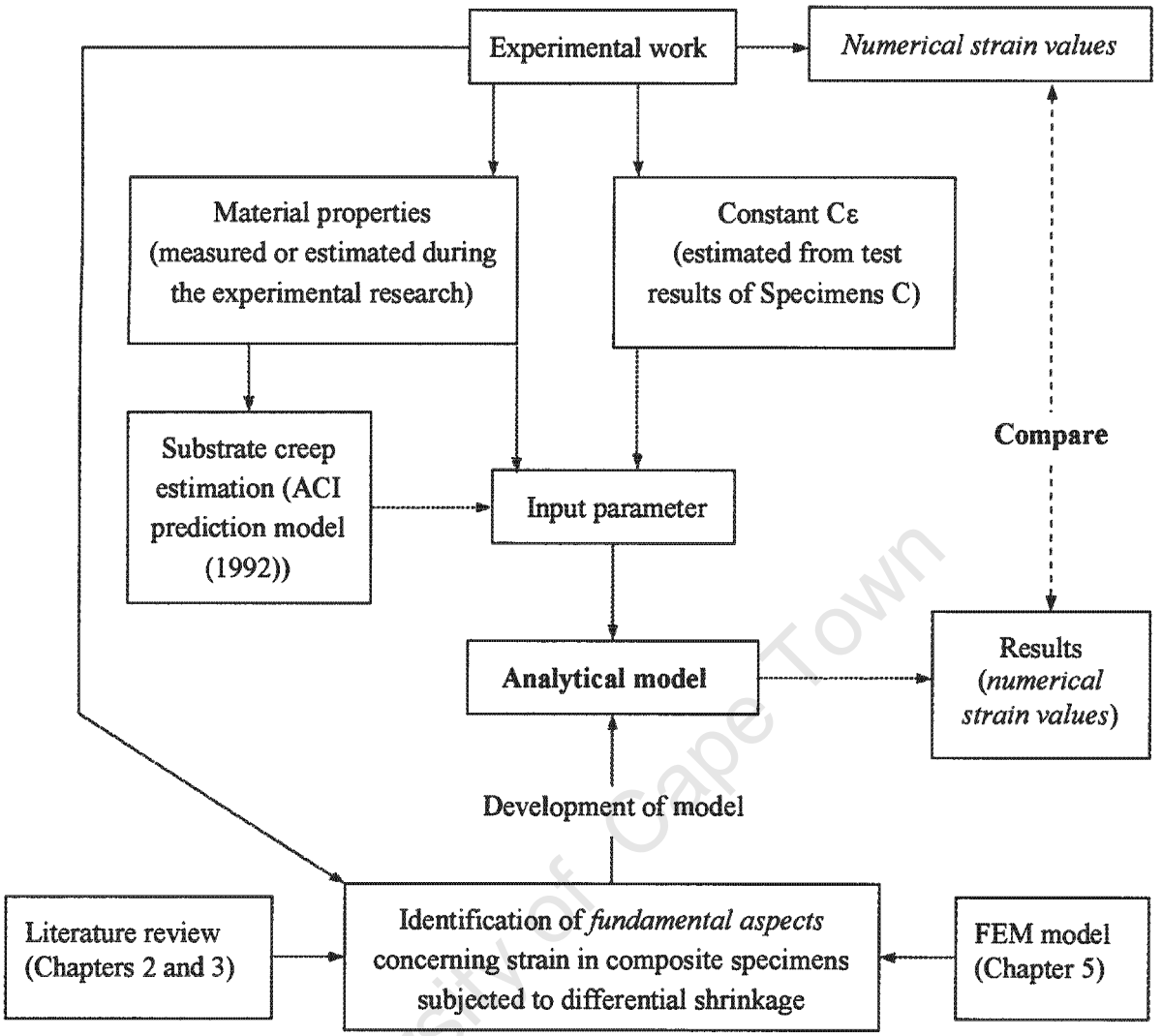

Figure 6.30: Strategy adopted for the comparison of experimental results and analytical model

Using the above approach, the influence of the factor C_ε on the computational results is discussed.

The computation of overlay strains is based on the equations developed in Sections 6.8 and 6.9. A simple computer programme was developed in *Microsoft Office – Excel* to facilitate the step-wise computation of time-dependent strains and stresses. Input and output user interfaces are presented in the following sections. Appendix 8 contains an electronic version of the programme.

6.10.2 Estimation of the empirical constant C_ε

The empirical constant C_ε estimates the combined influences that relative member dimensions and strain characteristics of substrate and overlay have on interface strain values (compare Section 6.8.4, equation 6.17). It is believed that in relatively thin overlays C_ε increases, i.e. the degree of overlay shrinkage restraint increases, with decreasing overlay depth.

Section 4.9.2 discusses strains across members that are not free to curve (Specimens C). Substrate strains at the interface were measured using overlays of 20, 40, and 80 mm depth. Substrate strain values could be related to the respective free shrinkage strains of the different overlays. It appeared that substrate interface strains developed independently from the relative cross-sectional dimensions of substrate and overlay and that the strains measured were simply a function of free shrinkage strains. This phenomenon could in theory be related to either of the two following explanations:

- For the tested specimens, elastic interface strains occurred independently from relative member dimensions of substrate and overlay. With the given materials, an overlay depth of 20 mm was sufficient to cause maximum possible interface strains. The measured strains, which include visco-elastic components, were therefore equal for specimens with different overlay depths

- The observed phenomenon describes the apparent effect of similar elastic strains. Actual elastic strains were different for different overlay depths. However, the combined influences of elastic and visco-elastic components led to similar interface strain values

It is not possible to draw final conclusions on the above from the limited test results available. However, from a logical point of view, the apparent effect of equal elastic strains could not have resulted from the influences of visco-elastic mechanisms. As outlined previously, strains measured are a combination mainly of elastic strains, substrate creep strains, and strain-redistribution resulting from overlay relaxation. A thin overlay, should it cause less elastic interface strain compared to a thick overlay, would also cause less creep strain in the substrate. Further, less elastic strain would be related to higher overlay stress and hence higher overlay relaxation. Less substrate creep strain and higher overlay relaxation both have the effect that they reduce total strain measured (**Figure 6.31**).

Similar total strain measured with different overlay depths can therefore not be related to visco-elastic effects. It appears that the tested specimens experienced similar elastic interface strain and that, therefore, the overlay thickness had no practical influence on the degree of shrinkage restraint. However, this effect should be investigated further, using a range of different overlay materials, to draw final conclusions on the above for practical application of the analytical model.

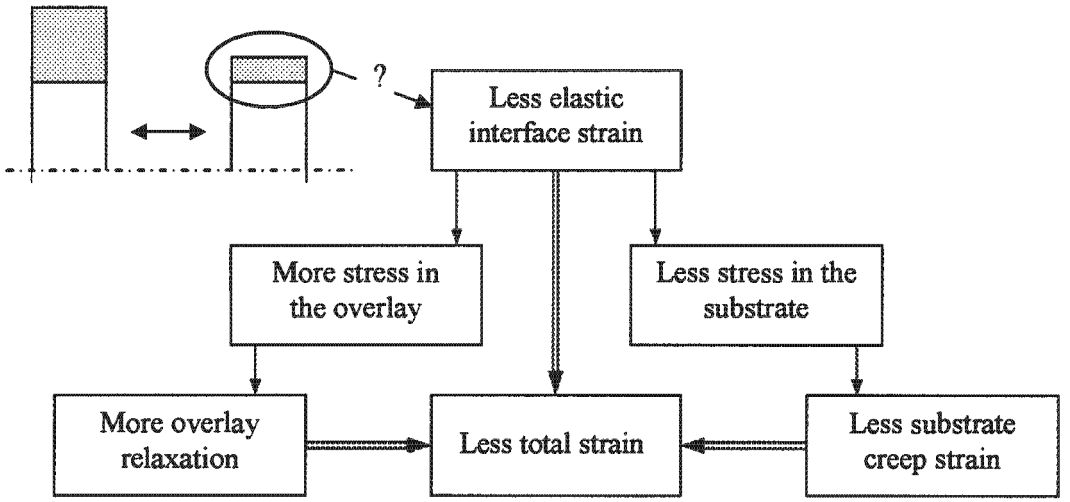

Figure 6.31: Schematic of strain components influencing measured strain, assuming lesser elastic strain resulting from lesser overlay depth

In general, the parameter C_ε must be quantified for a range of different overlay materials and overlay depths. Assuming that relative overlay and substrate dimensions have to practical influence on interface strains, the parameter C_ε takes a value of 1. For computation of interface strains with the analytical model, using the specimens tested during the experimental research, a value of $C_\varepsilon = 1$ is therefore used in the following sections.

The influence of the numerical magnitude of C_ε on computed interface strains is discussed in more detail in Section 6.10.4.4.

6.10.3 Input parameters for the computation of interface strains

During the experimental research, 3 different overlays were tested. To not exceed the scope of this section, only specimens with sandblasted interfaces are discussed (Specimens A1 (Overlay 1), Specimens A2 (Overlay 2), and Specimens B1 (Overlay 3)). These specimens were free to curve. Specimens that were not free to curve (Specimens C (Overlay 3)) showed very similar strain values to Specimens B1 and are therefore not discussed.

Overlay and substrate material properties of the tested specimens were discussed in Section 4.3 and 4.4. Substrate creep strains are estimated using the ACI method (ACI, 1992, compare Section 2.5.1). Overlay relaxation properties were discussed in Sections 4.7.9 and 4.11.4. Overlay strains and stresses were computed using the computer programme mentioned earlier. An overview of all input parameters for the computer programme is presented in **Figure 6.32**, using Specimens B1 as an example.

Overlay parameters			
t (day)	ε_{FSS}*	ψ_O **	E_O ***
6	160	0.55	31.0
13	173	0.55	31.0
20	235	0.55	31.0
34	313	0.55	31.0
50	333	0.55	31.0
67	330	0.55	31.0
81	388	0.55	31.0
102	428	0.55	31.0
130	480	0.55	31.0
310	598	0.55	31.0
Overlay depth d_O (mm)			40

Substrate parameters	
Elastic modulus E_S (GPa)	32
Substrate depth d_S (mm)	200
Parameters for substrate creep strain	
Age of concrete at first loading (days)	720
Variation in RH (%)	20
Slump (mm)	90
Coarse aggregate (kg/m^3)	985
Fine aggregate (kg/m^3)	750

Constant Cε	1

Include curvature in calculation? (yes: 1, no: 0)	1

* Values for ε_{FSS}: Compare Figure 4.17, page 85

** Values for ψ_O: estimated, compare Section 4.11.4.2, page 132. In absence of detailed information, ψ_O is assumed constant

*** Values for E_O: Compare Figure 4.14, page 83. E_O was measured to be relatively constant during the first 28 days. Long-term values of E_O were not measured. E_O is thus assumed constant for the computation of strains and stresses

Figure 6.32: Computer programme for the computation of overlay strains, user interface for input parameters, Specimen B1

Appendix 5 contains the computations of strains for all specimens discussed in this section. Information on the input parameters of all specimens can be taken from this Appendix.

6.10.4 Computational results and comparison to experimental research

6.10.4.1 Specimens B1

Figure 6.33 (on the following page) shows the numerical test results computed with the programme. Measured overlay interface strains of Specimen B1 and interface strains computed with the programme are presented in **Figure 6.34**.

For the first approximately 150 days, the analytical model was able to relatively accurate estimate both overlay strain development and numerical strain values. In general, the prediction model led to an underestimation of overlay strains. Possible reasons for differences between computed results and actual measurements are numerous. The underestimation of substrate creep strains is one of the possible explanations. As indicated in Section 4.9.4 (compare Figure 4.51 on page 117), measured substrate creep appeared to be higher than creep predicted using the ACI (1992) method.

Considering that time-dependent influences on actual overlay strain had to be estimated and simplified approaches were used for the estimation of overlay relaxation and substrate creep in the computation, the model can be considered to have predicted overlay strains of Specimens B1 reasonably well.

It is also interesting to compare the ratio between interface strains and free shrinkage strains (**Figure 6.35**).

The effects of increasing ratios between interface strains and free shrinkage strains ($\varepsilon_O/\varepsilon_{FSS}$) with time were discussed in Section 4.7.5. The prediction of the development of $\varepsilon_O/\varepsilon_{FSS}$ with time shows similar pattern as those observed on Specimens A1-5 and B1. To not exceed the scope of this section, only results obtained with Specimen B1 are presented in the above figure. The increase in $\varepsilon_O/\varepsilon_{FSS}$ with time mainly relates to the mechanisms of substrate creep. It appears that these mechanisms can be modelled reasonably well with the prediction model.

The main objective of the prediction model is to assess the risk of overlay cracking by comparing tensile overlay strength with computed tensile stress. Computed values for tensile overlay stress can be found in Figure 6.33 in column "J". Measured 28-day tensile strength of Overlay 3 was approximately 3 MPa (compare Figure 4.12, page 82). Computed tensile stress never exceeded the tensile strength, which explains the absence of cracks on Specimens B1.

	Interface strains (10^{-6})								Interface stress (MPa)	
	A	B	C	D	E	F	G	H	I	J
t_i	excl. substrate creep		including substrate creep and ψ_O			curvature κ	Σ	ratio	substrate	overlay
(day)	$\varepsilon_{elastic}$	$\varepsilon_{ipd,\psi O}$	$\varepsilon_{rel,\psi}$	$\varepsilon_{creep,S,I}$	$\varepsilon_{total,I}$	ε_K	$\varepsilon_{total,1\,inch}$	ε_{total} / ε_{gross}	$\sigma_{S,I}$ (-)	$\sigma_{O,I}$ (+)
6	79	43	37	12	49	3	53	0.33	1.20	1.09
13	85	47	38	17	55	4	59	0.34	1.22	1.10
20	116	64	50	27	77	5	83	0.35	1.61	1.45
34	154	85	64	41	106	7	113	0.36	2.06	1.83
50	164	90	66	48	114	8	122	0.37	2.12	1.88
81	191	105	75	62	136	9	146	0.38	2.39	2.09
130	236	130	89	82	172	12	184	0.38	2.86	2.49
310	294	162	106	114	219	15	235	0.39	3.38	2.92
	eq. 6.17	eq. 6.46	eq. 6.43, incl. ψ_O	eq. 6.42, incl. ψ_C	eq. 6.50 (= C+D)	eq. 6.51	eq. 6.52 (= E+F)		= C . E_S	eq. 6.53

Computation of substrate creep coefficients (ACI 1992) (compare Section 2.5.1)										
day:	0	6	13	20	34	50	81	130	310	
$\varphi(t, t_i)$	0	0.40	0.56	0.67	0.80	0.91	1.03	1.15	1.34	

Creep parameter	
$\gamma 1$	0.58
$\gamma 2$	1.14
$\gamma 3$	1.11
$\gamma 4$	1.06
$\gamma 5$	0.98
$\gamma 6$	1.00
$\varphi_C(t,\tau)$	1.77

Parameter for computation of curvature strain (equation 6.51)		
dS,e (mm)	80	(equation 6.21)
e (mm)	47	(equation 6.20)
$d_{s,i}$	80	(per mm width)
z (mm)	100	
I_c (mm^3)	1152000	

Figure 6.33: Computation of strains and stresses: Specimens B1 (Overlay 3 (MS))

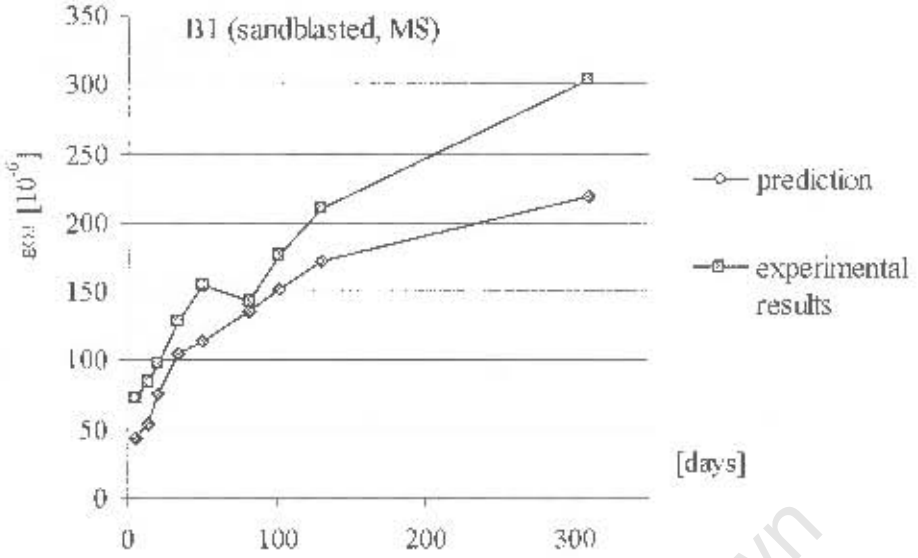

Figure 6.34: Specimens B1, overlay strains at the interface, comparison between experimental research and prediction model

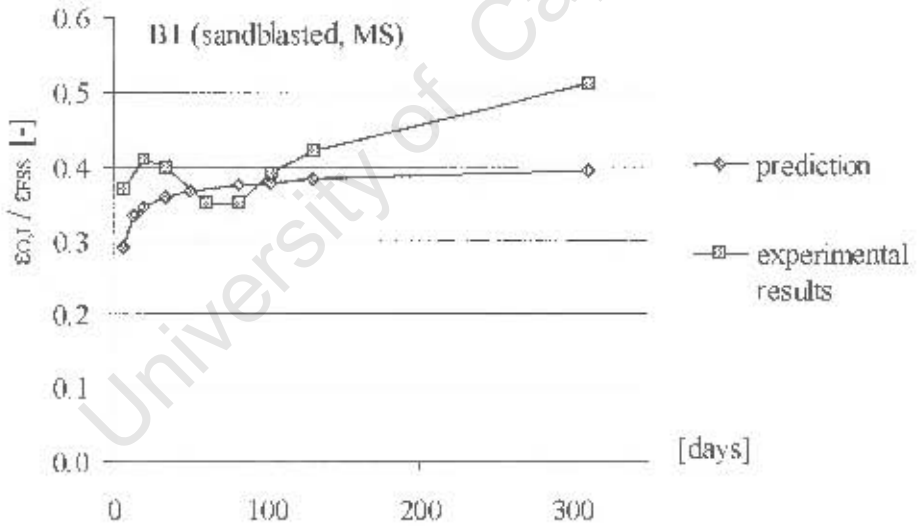

Figure 6.35: Specimens B1, strain ratios $\varepsilon_{O,I}/\varepsilon_{FSS}$, comparison between experimental research and prediction model

6.10.4.2 Specimens A1

Computing strains for Specimens A1 led to a substantial underestimation of overlay strain values (**Figure 6.36**). The unusually high magnitudes of overlay strains of Specimens A1 are discussed in Section 4.7.5.2 and could not fully be explained as all other specimens had much lower relative overlay strain values. It can however be seen that the analytical model was able

to predict basic characteristics of overlay strain development, even though the predicted strain rate was too low.

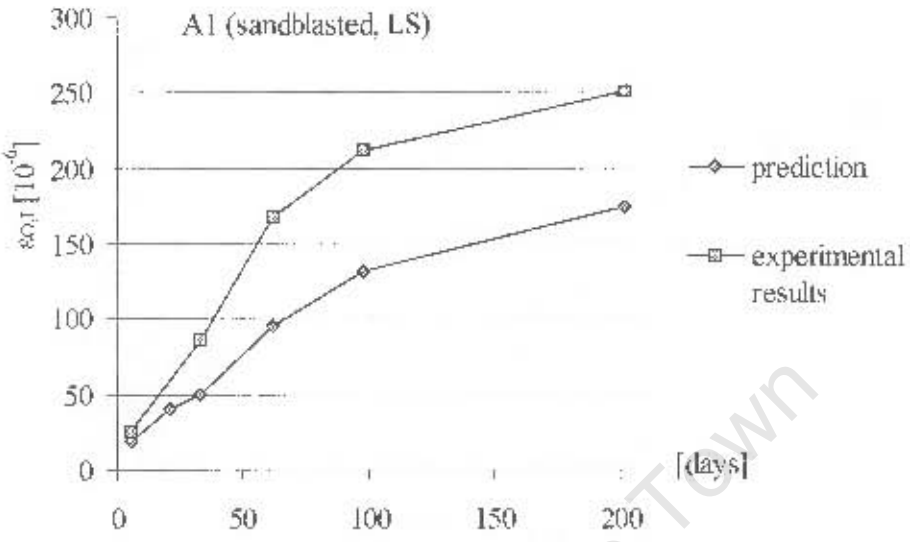

Figure 6.36: Specimens A1, overlay strains at the interface, comparison between experimental research and prediction model

Computed tensile overlay stress was always lower than tensile strength. Also, considering the difference between computed and measured overlay strains, tensile stress was overestimated with the analytical model. This explains the absence of cracks on Specimens A1.

6.10.4.3 Specimens A2

Specimens with Overlay 2 (HS) showed extensive cracking during the first weeks after the onset of drying shrinkage (compare Section 4.11). The analytical model was able to reasonably well predict overlay strains during this period, especially in the critical first week (**Figure 6.37**).

Tensile strength of Overlay 2 was measured to be approximately 1.8 MPa between 7 and 14 days (compare Figure 4.12, page 82). Cracks were identified visually after 7 days. The analytical model computes tensile overlay stress of 1.8 MPa at 9 days and was thus able to predict the time of overlay failure reasonably accurately.

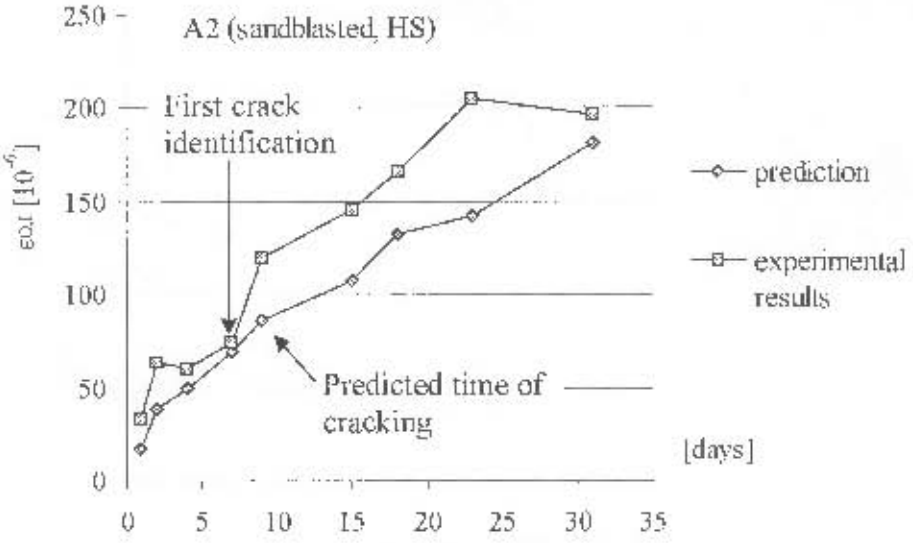

Figure 6.37: Specimens A2, overlay strains at the interface at early ages, comparison between experimental research and prediction model

6.10.4.4 The influence of C_ε on the computation of interface strains

The computation of elastic strains in the analytical model developed in Sections 6.1 to 6.9 depends on the constant C_ε that estimates the combined influences of relative cross-sectional areas and strain characteristics of substrate and overlay on the degree of overlay shrinkage restraint. In Sections 6.10.4.1 to 6.10.4.3, a value of $C_\varepsilon = 1.0$ was used for the comparison of the analytical model with experimental results, i.e. it was assumed that relative cross-sectional dimensions had no influence on overlay shrinkage restraint. This section examines the influence of the magnitude of C_ε on total overlay strain, including time-dependent visco-elastic components, using Specimens B1 as an example.

It must be noted that C_ε cannot take a value smaller than 1.0 as this would correspond to decreasing restraint with decreasing overlay thickness, which appears illogical.

Computed overlay strains using different values for C_ε, and measured strains of Specimens B1 are presented in **Figure 6.38**. Overlay strains of Specimens B1 could at best be predicted using a value of $C_\varepsilon = 1$. Increasing values of C_ε, i.e. increasing degrees of restraint, resulted in lesser comparability between experimental results and predicted strains. However, as stated previously, C_ε should be tested for a range of different overlay materials to confirm the above observation for practical application of the prediction model.

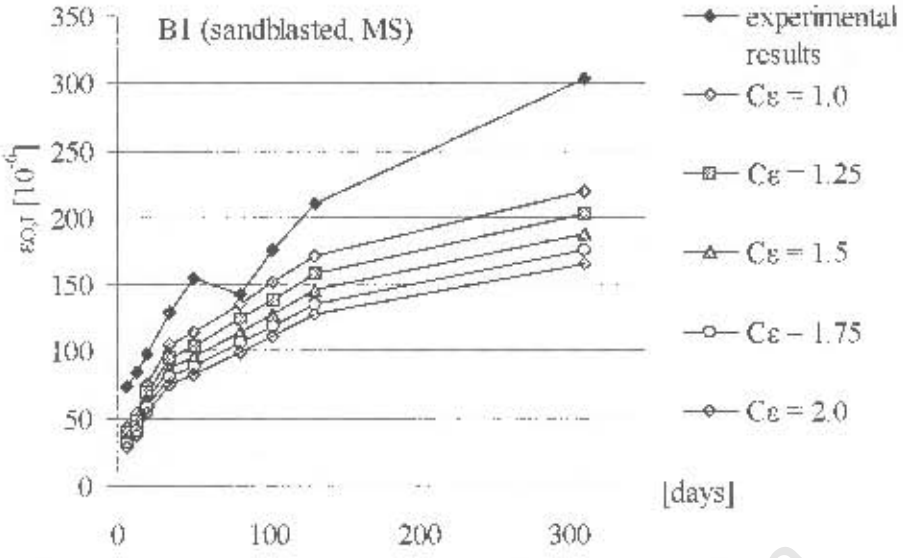

Figure 6.38: Specimens B1, computed overlay strains in relation to the constant C_ε

6.10.5 Conclusions

In general, the analytical model led to an underestimation of overlay strains in the tested specimens. As stated previously, possible reasons for this are numerous. The influences of substrate creep and overlay relaxation were estimated using simplified approaches. Accounting for more substrate creep and/or less overlay relaxation, for example, would result in computation of strain values that are closer to strains measured on the test specimens. However, exact prediction of overlay strains is practically difficult as discussed previously. The computed strain values therefore appear to predict overlay strains reasonably well. Underestimation of overlay strains generally leads to conservative computational results of tensile overlay stress, which is acceptable.

The main intention of the analytical model is to compute tensile stress and predict crack development in the overlay. Modelling Specimens A2-A5 (Overlay 2 (HS)) led to the prediction that cracks would occur after approximately 9 days. Most cracks on Specimens A2-A5 were identified after 7 days (compare Section 4.11). By contrast, Specimens A1 (Overlay 1(LS)) and B (Overlay 3 (MS)) did not crack during the test period. For these specimens the analytical model predicts tensile stress to not exceed tensile strength. The above indicates that the analytical model was successful in predicting cracking in the tested specimens.

The influence of the empirical constant C_ε on the prediction of overlay strains of was tested. The best agreement between experimental and computed strains were obtained for $C_\varepsilon = 1$ and therefore appeared to develop independently of relative sectional dimensions of substrate and overlay. However, this phenomenon should be tested with a range of common overlay

materials, including concrete repair mortars, to draw final conclusions on the influence of relative cross-sectional dimensions of substrate and overlay.

6.11 Influence of individual material parameter on direct overlay tensile stress

Direct tensile overlay stress at the interface can be computed with equation 6.54 (page 185). A range of material parameters influence overlay stress values (ε_{Fss}, ψ_O, E_O, E_S, C_u, and φ_S (as a function of substrate age)). The influence of each of these parameters on tensile overlay stress is discussed in the following, neglecting the effects of curvature. Overlay stresses were computed with varying material parameters and compared to a reference stress value. The latter was computed with the material parameters listed in **Table 6.1**.

Table 6.1: Reference input parameters for the computation of tensile overlay stress*

Overlay parameters				
t_i (day)	ε_{Fss}	ψ_O	E_O	$\sigma_{O,i}$ (+)
0	0		0.0	0.00
28	***300***	***0.60***	***25.0***	2.02
Overlay depth d_O (mm)			40	

Substrate parameters		
Elastic modulus E_S (GPa)	***30***	
Substrate depth d_S (mm)	200	
Parameters for substrate creep strain		
Age of concrete at first loading (days)	***5475***	***(15 years)***
Variation in RH (%)	20	
Slump (mm)	90	
Coarse aggregate (kg/m^3)	985	
Fine aggregate (kg/m^3)	750	

Constant Cu	***1.0***	
Include curvature in calculation? (yes: 1, no: 0)		0

* Values in ***italics***: parameters that were varied for the evaluation of their influence on overlay tensile stress

From equation 6.54 (page 185) it is immediately apparent that tensile overlay stress is proportional to free shrinkage strain $\varepsilon_{FSS}(t)$ and overlay relaxation factor $\psi(t,t_0)$.

The influences of elastic moduli of overlay E_O and substrate E_S are presented in **Figure 6.39**.

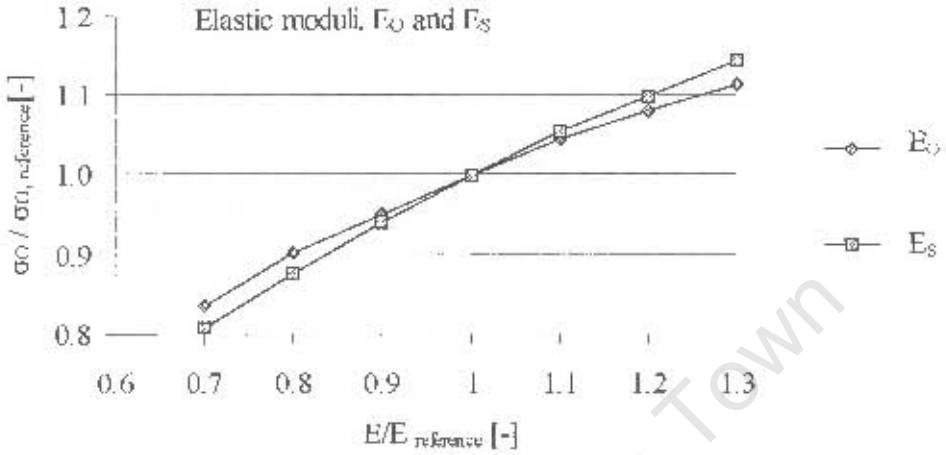

Figure 6.39: Tensile overlay stress in relation to elastic moduli of overlay and substrate

Increasing values for E_S result in increasing restraint and hence increasing overlay stress. Increasing values of E_O result in decreasing restraint but also in increasing stress, as the latter is a product of restrained strain and E_O. The relationships between elastic moduli (E_O and E_S) and overlay stress are virtually linear.

An increasing value of C_s results in increasing restraint and hence increasing overlay stress. Similarly to the influences of elastic moduli of overlay and substrate, there is a nearly linear relationship between the parameter C_s and tensile overlay stress (**Figure 6.40**). As can be seen from the figure, the influence of C_s on overlay stress is relatively significant.

An increase in substrate age results in a decrease of substrate creep strains and hence in an increase of overlay stress. However, the influence of the substrate's age on overlay stress, when creep is computed with the ACI method (ACI, 1992), is only noteworthy if the substrate is fairly young, i.e younger than 5 years (**Figure 6.41**). However, it should be noted that even relatively old substrates, i.e. substrates older than 30 years, have noteworthy creep deformations.

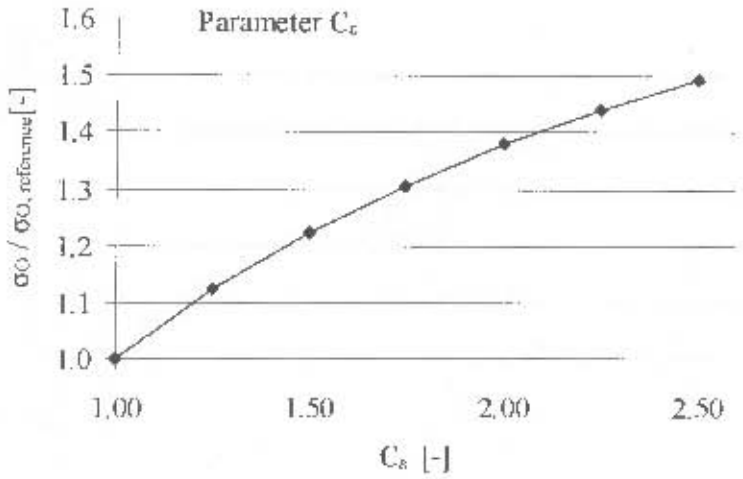

Figure 6.40: Tensile overlay stress in relation to the parameter C_s

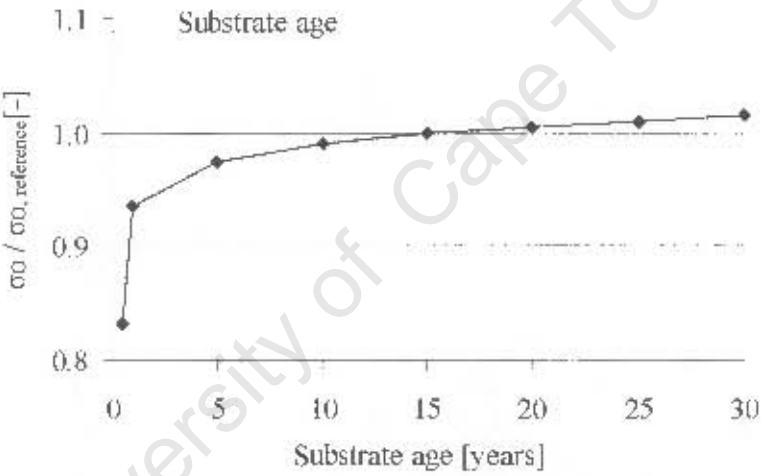

Figure 6.41: Tensile overlay stress in relation to the age of the substrate

6.12 Summary

Results from experimental research and numerical simulation indicate that existing analytical approaches do not model the behaviour of bonded concrete overlays in a realistic way. A new analytical model was developed, based on localised strain conditions at the interface between substrate and overlay.

Elastic and visco-elastic strain mechanisms were discussed individually. Equations for the prediction of different strain and stress components were developed. The following main assumptions were made and incorporated in the analytical model:

- Overlay and substrate are fully bonded

- Shrinkage is constant throughout the overlay depth

- The restraint of overlay shrinkage is a localised phenomenon at the interface, Bernoulli's hypothesis of plane sections remaining plane does not apply

- Overlay shrinkage restraint can at best be modelled through the prediction of interface strains

- Elastic interface strains can be computed in relation to an empirical constant C_ε that describes the combined influences of relative substrate and overlay dimensions and strain characteristics

- Substrate creep strains are an important component for the behaviour of bonded concrete overlays. The effects of substrate creep can be estimated using a simplified approach that accounts for creep in a one-step analysis

- A significant part of overlay relaxation occurs shortly after stress induction. Relaxation therefore develops at a considerably higher rate than stress related to continuous overlay shrinkage. The effects of overlay relaxation can therefore be considered in a simplified way, assuming full relaxation to occur simultaneously with stress induction.

Existing analytical models relate overlay shrinkage restraint to the relative member dimensions of substrate and overlay. The basic form of the generally accepted equation resulting from the above assumption was kept for the new analytical model. However, the term that accounts for the direct influences of relative member dimensions was exchanged against the factor C_ε.

Curvature in composite specimens commonly causes overlay contraction and hence partial release of tensile overlay stress. In existing analytical approaches, direct strains and curvature are generally computed individually and simply added up to obtain total strains. This however leads to an overestimation of the beneficial effects of curvature as discussed in Section 6.9.3. The analytical model developed in the previous sections computes curvature strain with consideration of a correction factor. This factor accounts for the circumstance that a portion of direct overlay stress is released through curvature.

Substrate creep strains can be estimated using creep prediction models presented in the literature. For the analysis of test specimens, the ACI prediction model for creep (1992) was used.

Information on tensile stress relaxation is scarce and more research is necessary to find time-dependent relaxation functions for different concretes. In absence of more detailed information it appears appropriate to account for overlay stress relaxation in the simplified way mentioned above.

Any analytical model can merely present an approximation of overlay strains and stresses. Numerous visco-elastic influences and time-dependent material parameters make it practically impossible to predict overlay strains exactly. However, the comparison of the analytical model with results obtained during the experimental research revealed that the model is able to reasonably closely predict overlay strain development. The prediction of tensile overlay stress conformed to experimental test results. The analytical model can therefore facilitate the design of bonded concrete overlays.

CHAPTER 7

INTERFACE BOND STRENGTH

7.1 Introduction

The bond between substrate and overlay is often the main aspect concerning durability of a concrete repair project and hence its success. Fundamental mechanisms of adhesion between concretes of different ages and factors affecting short- and long-term bond development are discussed in Section 2.3. From the literature review, 2 parameters were identified for experimental research (compare Section 2.3.8):

- Short-term bond strength development in relation to mechanical overlay strength and the location of failure
- Long-term bond properties in relation to different overlay materials, environmental conditions and interface textures

Bond mechanisms, discussed in Section 2.3, indicate that overlay mechanical strength might have a significant influence on bond strength. The relation between overlay strength and bond has however not yet fully been examined. In relation to bond mechanisms it appears important to identify the actual location of fracture, which, in connection with mechanical material strength, can help identify fundamental bond mechanisms.

Factors concerning the long-term performance of bonded concrete overlays relate mainly to cracking and debonding. The characteristics of overlay cracking in relation to overlay shrinkage were discussed in Chapter 4. The testing of bond durability was carried out in conjunction with the measurements of strains on composite members, using the same materials and interface textures. The long-term bond specimens were thus designed to estimate the influence of shrinkage restraint on bond durability.

7.2 Test methods

7.2.1 General

Bond strength was measured as the stress required for separating substrate and overlay. In general, bond tests are designed to apply tensile, shear, or torsional stress to the interface of the member. The most common test method is the tensile pull-off test on cores. The popularity of the tensile test relates mainly to the circumstance that it can be carried out on-site on an existing structure as well as in the laboratory. By contrast, interface shear tests can commonly only be carried out in the laboratory and can thus not be used for characterisation

of bond strength in existing structures. Torsional tests may be applied on site and in the laboratory, but are very seldom used.

For this research project, shear and tensile tests were initially used for the identification of interface bond strength. However, several difficulties were encountered with the tensile pull-off test, which made this method unfavourable for the characterisation of interface bond characteristics, as discussed.

For the identification of tensile interface strength, a force must be applied perpendicular to the interface plane. Any misalignment of the pull-off force leads to stress peaks in the member, which might have a significant influence on measured strength values. Misalignments might be induced by the core drilling process, an uneven substrate surface, and the test equipment and are generally difficult to avoid. A combination of misalignments from different sources might intensify the problem so that the measured stress at failure does not represent actual tensile interface strength. Some of these problems might be eliminated when the core is isolated from the structure and both ends carefully ground to be parallel before the member is tested. This, however, is a cumbersome procedure if a large number of tests have to be conducted.

A second problem that is commonly encountered with tensile pull-off tests is that only seldom does failure take place in the interface plane. Reports on pull-off strengths in the literature often relate to material failure in either substrate or overlay. This problem was also extensively encountered during this research as cores under pull-off stress mainly failed in the substrate or overlay but seldom at the interface. If material failure occurs, the measured failure stress merely represents a lower bound value for interface strength. For practical purposes, this may be sufficient to prove that required minimum strength has been achieved, which makes the pull-off test a valuable tool for in-situ control of concrete overlays. However, for the identification of actual interface strength in relation to different test parameters, the tensile-pull of test is of little value. A third problem encountered with pull-off tests is that the coring procedure might damage the bond between substrate and overlay, which could result in premature failure when the pull-off force is applied.

For this research, interface bond was characterised with shear test methods. Tensile test results are not considered, as they were inconclusive due to the above reasons.

7.2.2 Interface shear bond tests

The shear bond specimens consisted of a 150 x 150 x 75 mm concrete substrate body which received overlays of 75 or 40 mm thickness, depending on the test method described below.

Two different interface shear bond tests were designed to suit different test parameters. Method A (**Figure 7.1**) is a modification of the FIP test for direct interface shear (FIP, 1978) and was applied where the overlay thickness was thought to have no influence on the test parameter, which was the case with specimens fully cured in water.

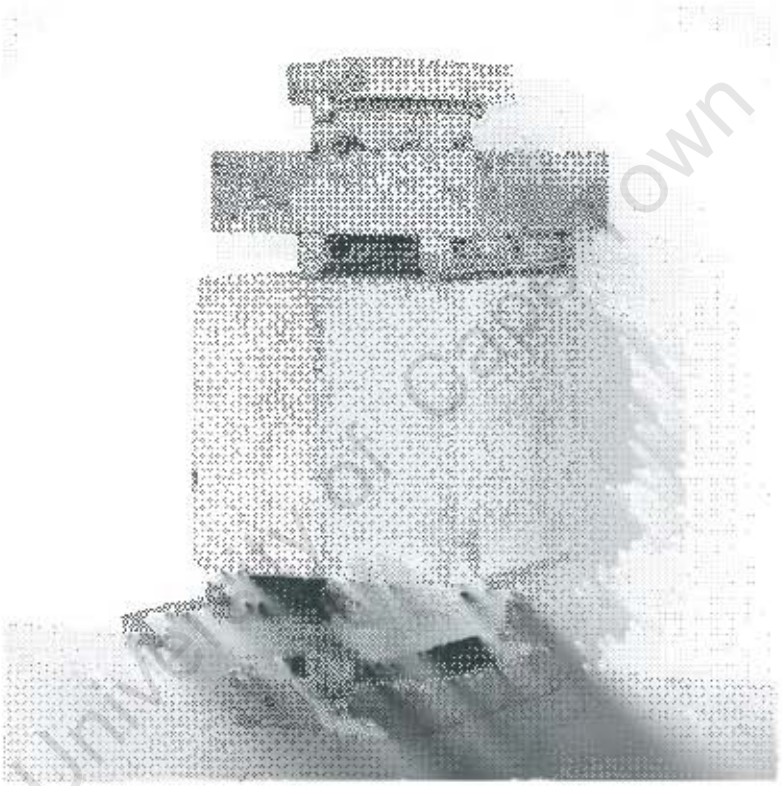

Figure 7.1: Photograph of interface shear bond test method A – direct shear

For specimens that concerned the influence of curing and environmental conditions, a modified guillotine test, method B, was utilised as shown in **Figure 7.2**. Method B allowed an overlay thickness representing common repair patch dimensions. An overlay thickness of 40 mm was chosen for specimens tested with method B.

Details of the dimensions of the test equipments are given in Appendix 6. The schematics of load application and interface stresses resulting from both methods are presented in **Figure 7.3**.

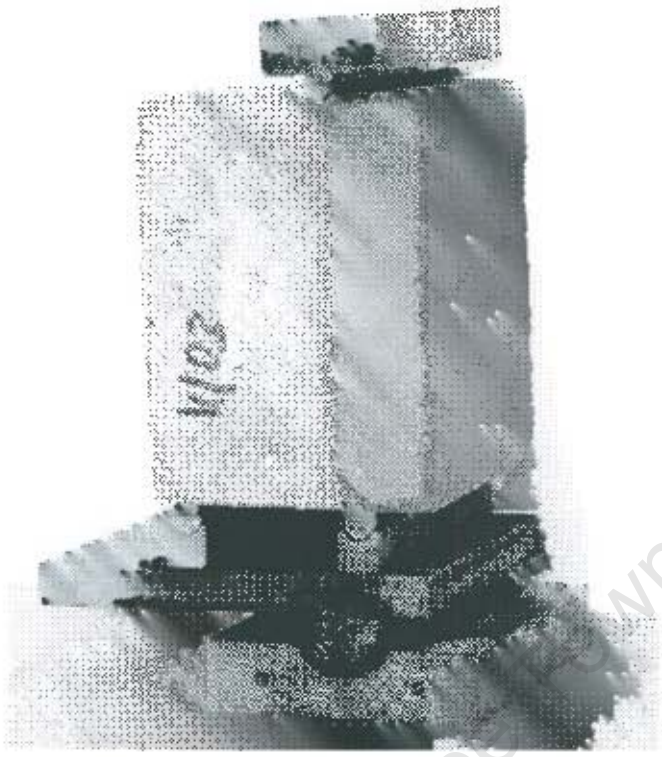

Figure 7.2: Photograph of interface shear bond test method B – Guillotine test

With method A, a force was applied in the interface plane of the specimens. This, in theory, led to pure shear stress at the interface. Method B applied the force with a small eccentricity and therefore caused shear and bending stresses at the interface. The calculation of direct stresses at the interface, resulting from the bending moment induced by method B, is given in Appendix 6.

Comparison of test results was always done between specimens that had been tested with the same method, i.e. test results obtained with method A were not compared to those obtained with method B. Therefore, direct stresses at the interface were neglected for the analysis. Test results of both methods A and B are expressed as interface shear stress.

The size of test specimens was chosen following two main reasons. Firstly, common cube moulds could be used for the fabrication of specimens (150 x 150 mm), which makes this test suitable for practical repetition in future research projects. Secondly, the relatively small interface area facilitates the investigation of the influences of differential shrinkage. Interface stresses resulting from restrained overlay volume changes are highest at the boundaries of the overlay, such as free member ends, joints and cracks. The size of test specimens therefore allowed the development of relevant shear stresses over the test area.

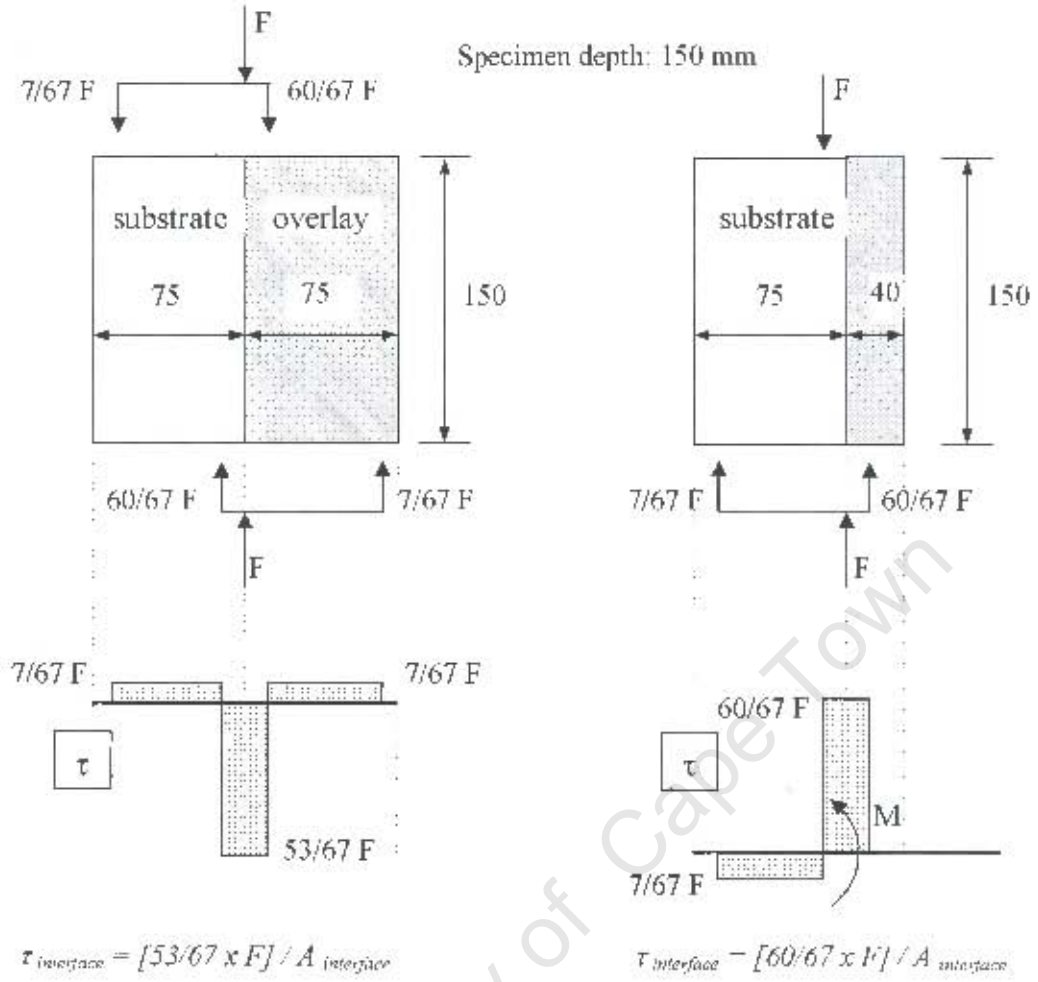

Figure 7.3: Schematics of load application and interface shear stresses resulting from Test methods A (left) and B (right). (*Applied forces and stresses result from the dimensions of the test equipment, as discussed in Appendix 6*)

7.3 Test specimens

7.3.1 Short-term bond strength development (Specimens S1-4)

The mechanisms of concrete compressive and tensile strength development with time are well known. By contrast, little work has been done on the mechanisms that influence bond strength development between concrete of different ages. The test series described in this section aimed at establishing a direct relation between the developments of compressive overlay strength and interface bond strength. Short-term shear bond strength development was tested using specimens with sandblasted interfaces and overlays of different compressive strengths. Sandblasted interfaces were chosen since they were shown to provide good bond strength and relatively consistent results during previous tests. Substrate bodies with sandblasted interfaces are presented in **Figure 7.4**.

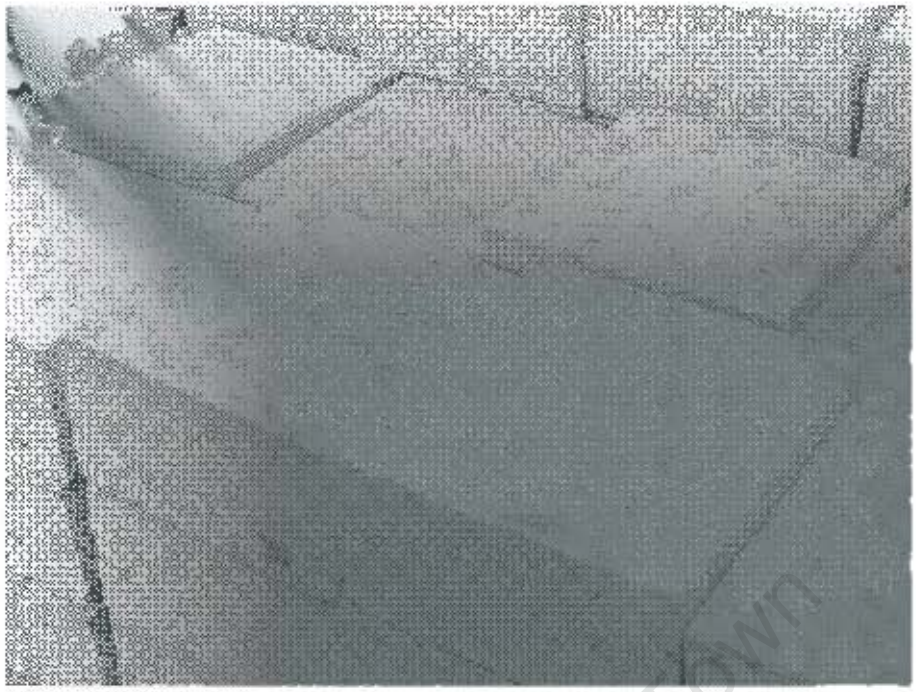

Figure 7.4: Substrate bodies for interface shear bond tests, with sandblasted interfaces

Prior to overlay application, the substrate bodies were wetted with moist sheets for 24 hours and subsequently exposed to the laboratory for approximately 30-45 minutes to dry until the moisture surface shine disappeared. Overlays were compacted using a poker vibrator and smoothened with a trowel. Curing was done with wet burlap for 24 hours. Subsequently, specimens were cured in water at 23°C until testing. Test method A (direct shear test) was used for determination of bond strength. Therefore, the overlay thickness was 75 mm.

Overlays were designed with constant water content to achieve similar workability. Mix designs are presented in **Table 7.1**. Shear test specimens were denoted Specimens S1, S2, etc (Specimens Shear 1, 2, etc).

The overlays were designed for 28-day compressive strengths of 10, 20, 30, and 50 MPa. Due to insufficient numbers of samples, interface shear tests of Specimens S1 and S2 were completed at 14 days. For comparison of overlay strengths, 14-day compressive strength values are therefore given in Table 7.1.

Table 7.1: Overlay mix designs and material properties for Specimens S1 – S4

Specimen		S1	S2	S3	S4
Cement CEM I	[kg/m^3]	510	392	294	235
Water	[kg/m^3]	235	235	235	235
9 mm Greywacke	[kg/m^3]	940	940	940	940
Klipheuwel sand	[kg/m^3]	660	758	840	890
W/C ratio	[-]	0.46	0.60	0.80	1.00
Slump	[mm]	100	90	90	80
28-d design strength	[MPa]	50	30	20	10
14-d compr. Strength	[MPa]	42.7	28.7	17.1	9.7

7.3.2 Long-term bond strength in different and changing environments

7.3.2.1 General

Different factors influence long-term bond properties and compatibility between concretes of different ages. The overlay undergoes volume changes due to temperature cycles and shrinkage, which can be very different from those of the substrate. These differential movements may weaken interface bond strength and result in partial or full debonding. Previous research on bond durability was discussed in Section 2.3.6.

To date, data on the direct influence of overlay shrinkage on interface bond strength is not available. The tests described in this section aimed at investigating the influence of long-term shrinkage on bond durability with respect to different interface textures, different overlay materials, and different curing conditions. To test the direct influence of overlay shrinkage on bond strength, specimens were cured in the laboratory for a period of approximately 2 years. Specimens used for these tests were cast in connection with the beam specimens described in Section 4.2, having the same interface textures, material properties, and curing conditions.

The influences of different and changing environments on bond strength were tested on specimens that were stored for 2 years in different outdoor locations in the Western Cape. In addition, temperature- and moisture cycles were simulated in the laboratory.

The procedures for the control of substrate moisture condition and overlay application were the same as those described in Section 7.3.1 for Specimens S1-4.

All long-term bond specimens were tested with interface shear test method B (Guillotine test).

7.3.2.2 Long-term shrinkage under laboratory conditions (Specimens S5-8)

The long-term bond strength tests on specimens cured in the laboratory were designed to supplement the shrinkage measurements described in Sections 4.5 to 4.7. They were further used as a reference in comparison to the site-cured specimens.

All substrate bodies had an age of at least 8 months at the time of overlay placing to ensure that most of the substrate shrinkage had taken place. Interface textures comprised sandblasted (compare Figure 7.4), smooth, and notched interfaces (**Figures 7.5 and 7.6**).

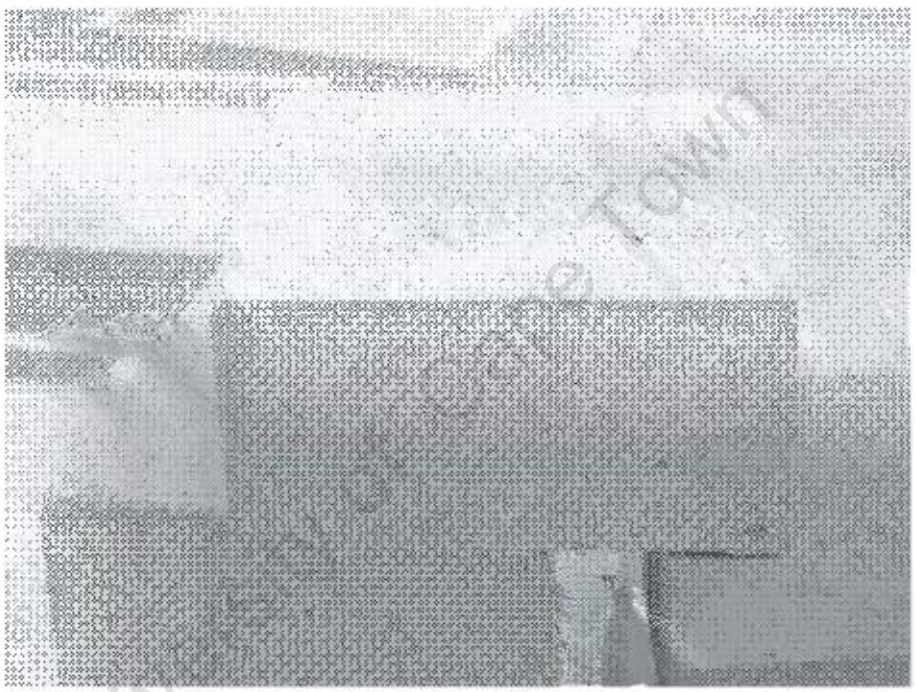

Figure 7.5: Substrate bodies with smooth surfaces

The preparation of interface textures was done in the same way as discussed for the beam specimens (compare Section 4.2.3).

Overlays were moist cured for a period of 7 days after casting, using wet burlap and plastic sheets. Subsequently, the test specimens were left uncovered in the laboratory where they were exposed to seasonal changes in temperature and relative humidity ranging from 16 to 23 °C and 55 to 80 % RH respectively. All overlays were cast in autumn or winter in order to prevent rapid shrinkage development.

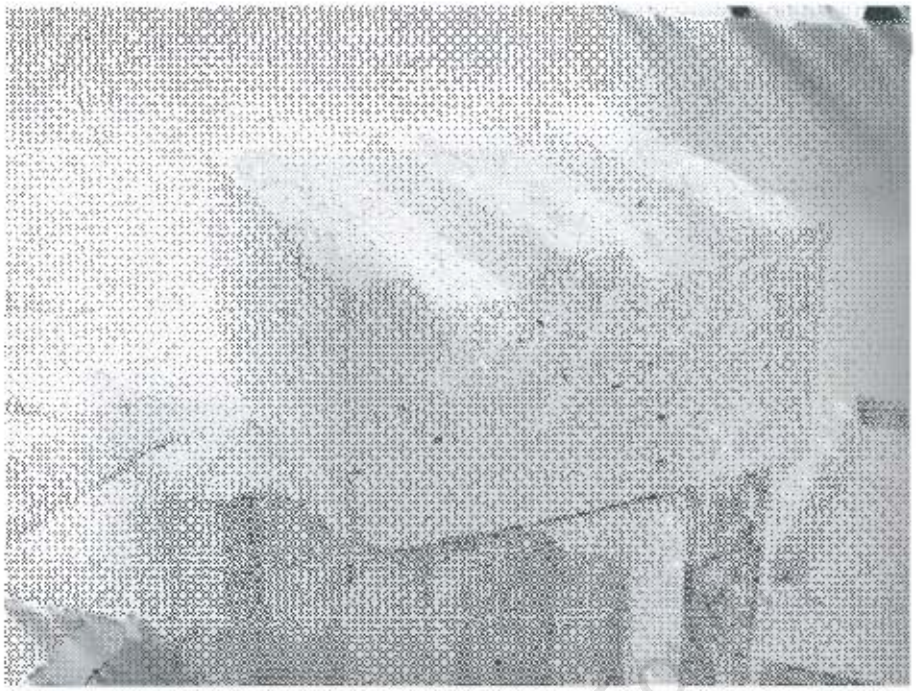

Figure 7.6: Substrate bodies with notched surfaces

Two overlays with different shrinkage characteristics were used, namely Overlays 1 ("Low-Shrink, LS") and 2 ("High-Shrink, HS") as discussed in Section 4.2.4. Mix design and material properties of Overlays 1 and 2 are presented in Table 4.2 on page 73.

The influence of different interface textures was only tested with Overlay 2 (HS). The influence of different overlay shrinkage characteristics, using Overlays 1 and 2, was tested on sandblasted interfaces only. Specimens are summarized in **Table 7.3** (page 213).

Specimens were tested after 28 days for short-term bond strength, and after approximately 26 months for long-term bond strength.

7.3.2.3 Site conditions (Specimens S9-14)

To evaluate long-term bond strength in realistic environmental conditions, different sites were chosen for the exposure of specimens. Specimens on all sites were placed such that the overlay was exposed to the environment without protection against sunlight or rain. An overview on the location of the sites is presented in **Figure 7.7**. **Table 7.2** summarizes the environmental conditions encountered on the sites.

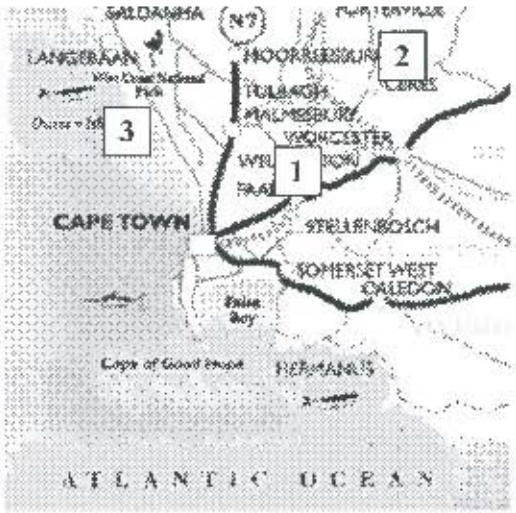

Figure 7.7: Overview on site locations for the curing of shear test specimens

Table 7.2: Environmental conditions encountered at the site locations for the curing of shear test specimens

no.	Location	Conditions
1	Wellington	Winter: rainy, T > +3°C; Summer: dry and sunny, T< +35°C *
2	Cedar Mountains / Tulbagh	Winter: rainy, T > -5°C; Summer: dry and sunny, T< −35°C; RH 25 - 90% **
3	West Coast / Koeberg	Winter: rainy, T > +3°C; Summer: sunny, T< +35°C; RH ; stored on a breakwater damn, regularly exposed to splashing sea water. Average RH 70% ***

* No data on RH is available for this site
** Data on RH supplied by South African Weather Service
*** Data on RH supplied by the weather station at Koeberg Nuclear Power Plant

All specimens were prepared with sandblasted interfaces. Overlays consisted of Overlays 1 (LS) and 2 (HS) (compare Section 7.3.2.2).

The test specimens were moist cured for a period of 1 day after casting, using wet burlap and plastic sheets, and transported to site and exposed to the environment the next day. A curing period of one day was considered to represent common conditions encountered on site during concrete repair projects. All specimens were stored on site for 26 months and subsequently tested in the laboratory.

7.3.2.4 Temperature and moisture cycles (Specimens S15-18)

Temperature and moisture cycles were simulated in the laboratory, using the same types of specimens as described in Section 7.3.2.2 (Specimens S1-5). For this, the specimens were cured for approximately 23 months under the same conditions as Specimens S1-5 and subsequently exposed to a total of 40 temperature and moisture cycles comprising the following:

- 4-5 hours oven drying at 40- 45°C
- 25-30 minutes rain simulation, using tap water (typically 12-14°C)
- Period between cycles: 20 hours minimum

Specimens were placed in such a manner that the water came in contact with the overlay surface only. All other faces of the specimens were sealed with silicon (**Figure 7.8**).

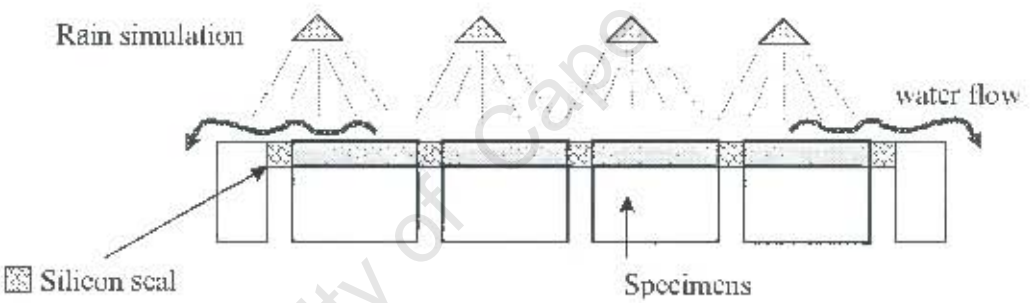

Figure 7.8: Arrangement of specimens for the simulation of temperature and moisture cycles

The duration from the first to the last cycle was approximately 3 months. Specimens were tested on completion of 40 cycles at an age of approximately 26 months.

7.3.3 Summary of test specimens

Table 7.3 summarizes the shear test specimens.

Table 7.3: Summary of shear test specimens

Specimen	Curing condition	Interface	Overlay	Test age
S1	Water cured	Sandblasted	50 MPa	1 - 14 days*
S2			30 MPa	
S3			20 MPa	3 - 28 days**
S4			10 MPa	
S5	Laboratory environment	Sandblasted	Overlay 1 (LS)	1 month and 30months
S6			Overlay 2 (HS)	
S7		Smooth		
S8		Notched		
S9	Site 1	Sandblasted	Overlay 1 (LS)	30 months
S10	Site 2			
S11	Site 3			
S12	Site 1		Overlay 2 (HS)	
S13	Site 2			
S14	Site 3			
S15	Temperature and moisture cycles in the laboratory	Sandblasted	Overlay 1 (LS)	
S16			Overlay 2 (HS)	
S17		Smooth		
S18		Notched		

* Specimens S1 and S2 were tested at 1, 2, 3, 7, and 14 days as the first 2 weeks are considered important for strength development

** Specimens S3 and S4 were of too low strength to be tested before day 3 and were therefore at day 3, 7, 14, and 28 days

7.4 Test results

7.4.1 Statistical evaluation

Per test parameter and test age, between 4 and 10 specimens, depending on availability, were tested for interface shear strength. Analysis of test results and comparison between different parameters was done using the mean values of all tests after exclusion of outliers.

Outliers were detected using a method described by Montgomery and Runger (2003), which is shortly described. Results obtained for a certain test parameter at a certain age are listed in ascending order. Quartiles are the three values of such a set of results that partition it into four equal parts. The centre value is called the median, and the upper and lower values are called lower and upper quartiles, respectively. The interquartile range is defined as the data range

between lower and upper quartile. An outlier was defined as a data point that lies outside a region of 1.5 times the interquartile range from the lower or upper quartile. The method is illustrated in **Figure 7.9**, using test results of Specimens S9.

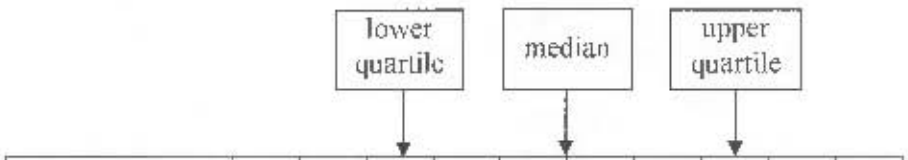

number	1	2	3	4	5	6	7	8	9	10
test value [kN]	68	75	88	88	93	97	100	105	110	113

Interquartile range IQR = 105 – 88 = 17
Outliers: values below 88 - 1.5x17 = 63; and values above 105 + 1.5x17 = 131

Figure 7.9: Method of determination of outlying values, exemplified using test results of Specimens S9

As shown in Figure 7.9, test results of Specimens S9 did not have any outlying values. Due to the relatively small number of test results for each parameter from a statistical point of view, outlier were found in a few instances only. Statistical evaluation of all test results is given in Appendix 7.

A statistical analysis on the *significance* of differences between test results obtained on different sets of samples was not carried out. Sets of samples were compared on the basis of engineering judgement, using mean values determined as discussed above.

7.4.2 Short-term bond strength development

7.4.2.1 Location of bond failure

Specimens S1 and S2 were tested at 1, 2, 3, 7, and 14 days. Specimens S3 and S4 were tested at 3, 7, 14 and 28 days (compare footnotes Table 7.3).

Practically all specimens failed in the interface plane, with very little failure occurring in the overlay or substrate. However, the term "interface failure" used for the description of shear failure in this project in actual fact refers to material failure very close to the interface. Failure truly along the interface would refer to separation of overlay and substrate without leaving overlay material attached to the substrate or vice versa. Substrate concrete surfaces always have a certain roughness, provided by open pores and cavities (micro roughness), and

surface texture (macro roughness). Mechanical keys are formed between the two composites when the overlay flows into the interface texture and fills open pores and cavities on the substrate surface. Interface failure as such could only occur if these mechanical keys are pulled out of their anchored position, which is virtually impossible. Therefore, failure mostly occurs inside the materials. At most instances it was clearly visible that a very thin layer of overlay material remained on the interface, even if, at first sight, the failure seemed to have happened at the interface plane as such. The overlay layer remaining on the interface usually appeared to be of an estimated thickness of up to approximately 0.5 mm (**Figure 7.10**).

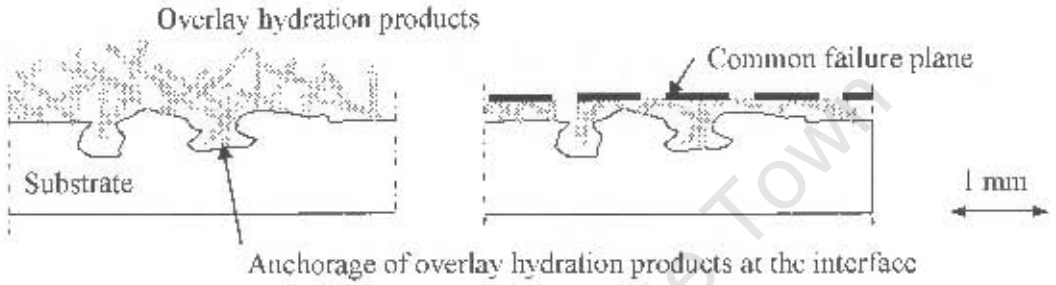

Figure 7.10: Schematics of "interface failure"

In some instances, "interface failure" was also observed to refer to substrate failure very close to the interface. The above observations point out that, for well prepared substrate surfaces, the weakest part of the bond line between substrate and overlay is not the interface as such but the material very close to the interface. This shows that overlay and substrate material strengths are significant factors for interface bond strength. Therefore, for stresses induced by overlay shrinkage, overlay strength might be a critical factor for bond durability. This observation relates to the assumption that a transition zone exists at the interface between concretes of different ages, similar to the transition zone between aggregate and cement paste, as discussed in Section 2.3.2

Significant material failure occurred only in Specimens S4 at a test age of 7 and 14 days. In these specimens, failure occurred to approximately 70% and 30% at the interface and in the overlay respectively, with overlay failure reaching a depth of up to 10 mm from the interface. The reason for this lies in the low strength of the overlay of Specimens S4.

In general, the appearance of failure very close to the interface showed that the test method successfully induced shear stress in the interface.

7.4.2.2 Interface shear bond strength in relation to overlay compressive strength

Overlay compressive strength was found to have a significant influence on interface shear bond strength (**Figure 7.11**). Individual test results of groups of samples, indicating the scatter of results, are presented in Appendix 7.

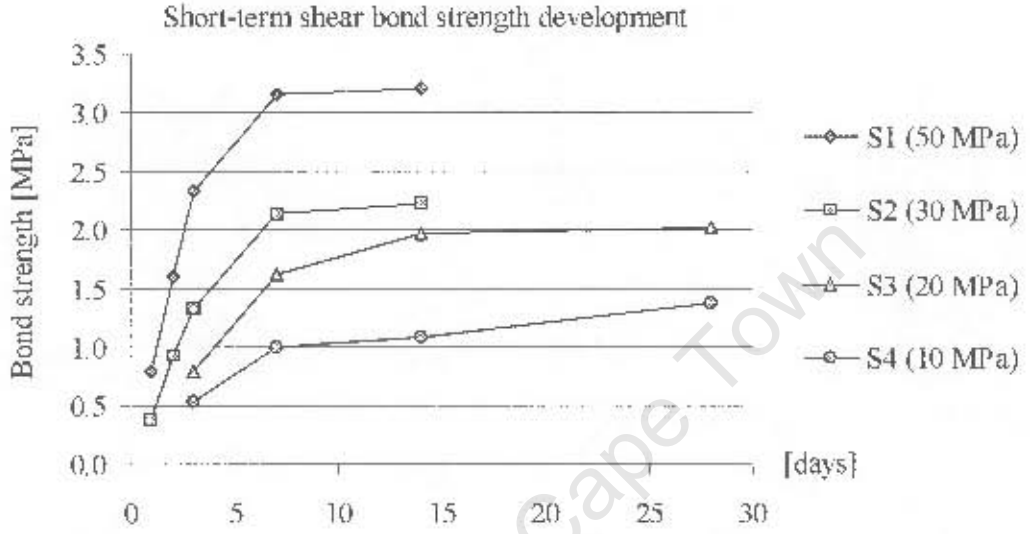

Figure 7.11: Short-term bond strength development of Specimens S1-4. Strength values in (brackets) refer to overlay design compressive strength.

Bond strength development was found to correlate consistently to overlay compressive strength development. **Table 7.4** summarizes the ratios between interface shear bond strength and overlay compressive strength.

Table 7.4: Ratio between interface shear bond strength and overlay compressive strength (in %).

Specimen \ day	1	2	3	7	14	28
S1	7	8	9	9	7	
S2	9	9	10	9	8	
S3			10	11	12	10
S4			12	12	11	11

For all specimens, the ratio between interface shear bond and overlay compressive strength was relatively constant during the test period within any one group. Interface shear bond strength in all specimens was measured to be approximately 10% of overlay compressive strength, independent of the test age. This consistent correlation indicates that overlay

compressive strength can be used as an indicator for bond strength development, assuming proper bond is provided. This observation relates to the existence of an interface transition zone, in which mechanical material strength determines bond properties, as discussed previously.

With the observation that in most cases bond failure occurs in the overlay very close to the interface, it is apparent that shear bond strength correlates to the shear strength of the overlay paste at the interface. Decreasing overlay compressive strength led to an increasing ratio between interface shear bond strength and overlay strength as shown in Table 7.4. Shear failure in concrete is generally considered to be initiated by tensile-type stress. Shear strength of concrete can thus be related to its tensile strength, which in turn relates to compressive strength. However, there is no direct proportionality between compressive and tensile strength as the ratio between the two depends on the general level of strength of the concrete (Neville 2002). As the compressive strength increases, tensile strength also increases but at a decreasing rate. This was believed to be the explanation for the slightly decreasing ratio between interface shear bond strength and overlay compressive strength as overlay strength increased.

7.4.3 Long-term bond strength development in different environments

7.4.3.1 Specimens cured in the laboratory

Specimens S5-8 were cured in the laboratory and tested at 28 days and 26 months for short- and long-term interface shear bond strength respectively. Test results are summarized in **Figure 7.12**.

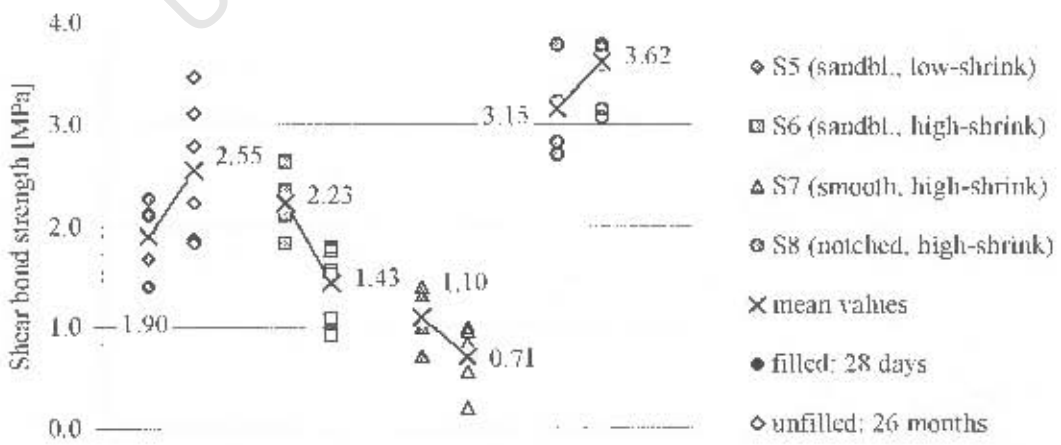

Figure 7.12: Development of interface shear strength under laboratory conditions. Comparison between values at 28-days and 26-months.

Specimens S5 (sandblasted interface, LS) and S8 (notched interface, HS) showed higher interface shear bond strength after 26 months, compared to the 28-day value. By contrast, Specimens S6 and S7 (sandblasted and smooth interfaces respectively, HS) showed a decrease in bond strength after 26 months.

Specimens S5-7 failed mainly at the interface, with very little material failure in overlay or substrate. However, it should be noted, as stated in Section 7.4.2, that "interface failure" mainly refers to failure in the overlay very close to the interface. Specimens S8 (notched interface) generally showed a mixed mode of failure, as illustrated in **Figure 7.13**. Short-term and long-term specimens failed in the same mode.

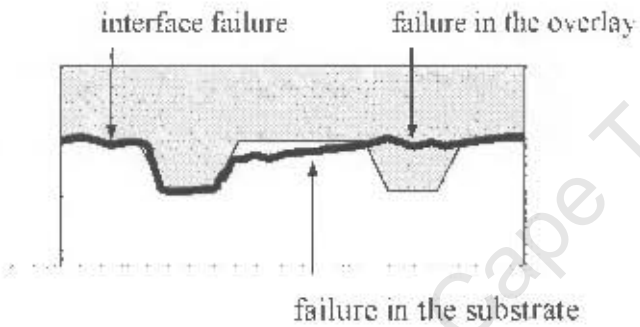

Figure 7.13: Typical modes of failure in specimens with notched interfaces

Specimens S6 and S7 (sandblasted and smooth interfaces respectively) both had interfaces with very little macro-roughness. For such interfaces, the test results show that high overlay shrinkage can result in a noteworthy decrease in long-term bond strength. By contrast, Specimens S8 (notched interface), having the same overlay shrinkage characteristics as Specimens S6 and S7, showed an increase in bond strength with time. The mechanical keys provided by the notched interface often led to material failure in overlay or substrate before the interface was affected. In Specimens S8, a major part of the shear strength between substrate and overlay therefore related to material strength of substrate and overlay rather than "interface strength". This explains that the bond strength of these specimens was not affected by overlay shrinkage.

Shear stresses in specimens with smooth and sandblasted interfaces were mainly transferred along the interface, leading to failure in the "weak link", i.e. in the overlay at the interface. By contrast, in specimens with notched interfaces, stresses were to a large extent transferred inside the overlay, distant from the weak link at the interface (**Figure 7.14**).

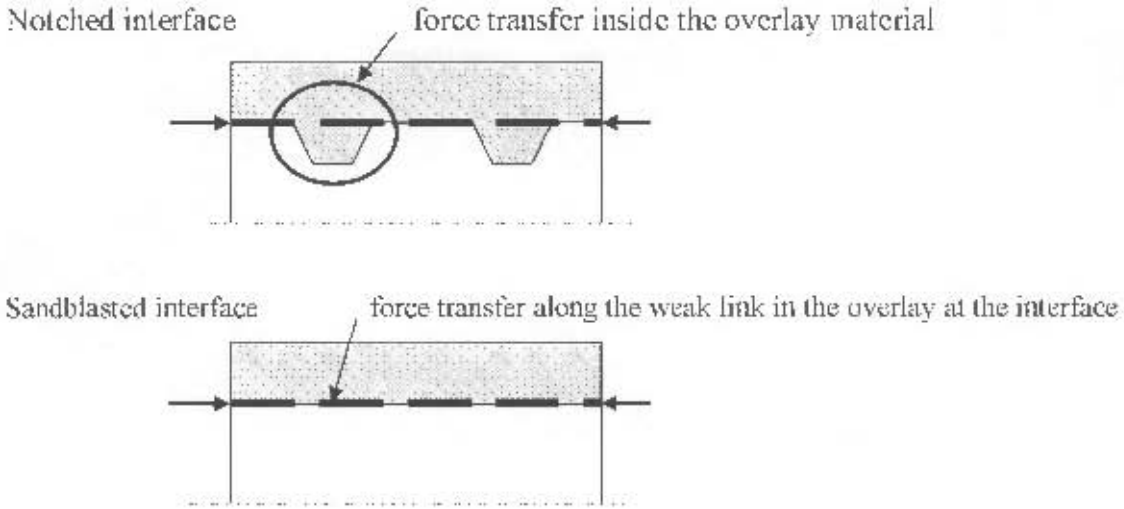

Figure 7.14: Shear force transfer in specimens with notched and sandblasted interfaces

The practical significance of this observation is that interfaces with a high macro-roughness can be expected to have a more durable shear bond strength compared to interfaces with a low macro-roughness.

The influence of overlay shrinkage on long-term bond strength can be estimated by comparing Specimens S5 and S6, both of which had sandblasted interfaces but different overlay shrinkage values. In contrast to Specimens S6, Specimens S5, having "low-shrink" overlay, showed increasing shear bond strength with time, despite the low interface macro-roughness. The mechanisms of bond deterioration therefore appear to be related to the magnitude of overlay shrinkage. In future studies it should be investigated as to how far overlay shrinkage values relate to bond deterioration. With only 2 overlays tested, it could not be established if there is a threshold value for overlay shrinkage, below which bond strength is not affected.

7.4.3.2 Specimens cured in different environments

Long-term shear bond strength test results of Specimens with "low-shrink" (S5, S9-11) and "high-shrink" (S6, S12-14) overlays in relation to exposure conditions are presented in **Figures 7.15** and **7.16** respectively.

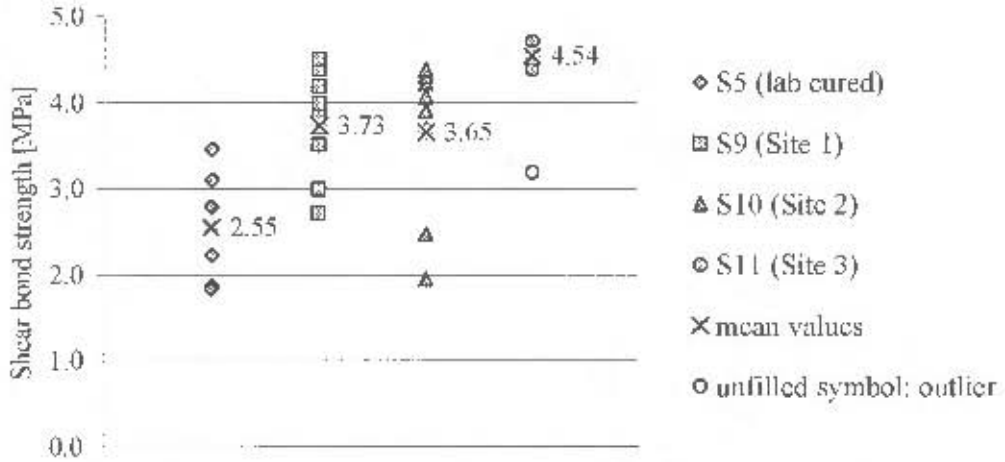

Figure 7.15: Long-term shear bond strength of Specimens with "low-shrink" overlays in relation to curing environment

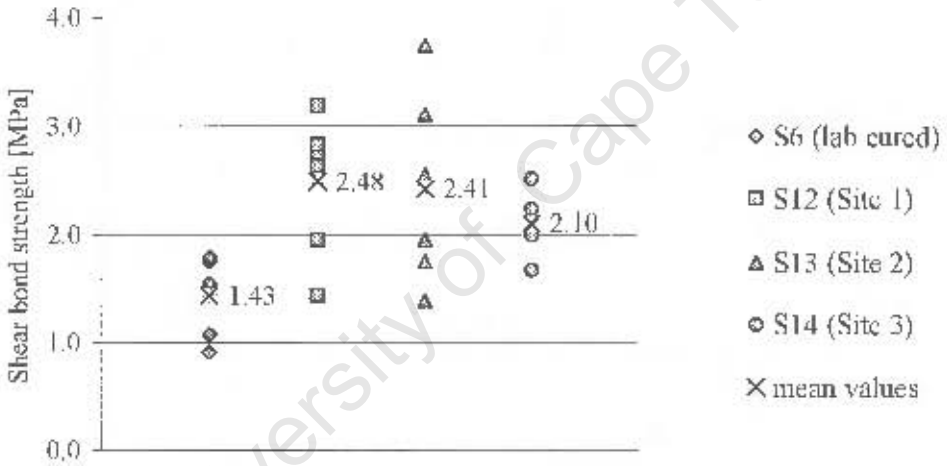

Figure 7.16: Long-term shear bond strength of Specimens with "high-shrink" overlays in relation to curing environment

In comparison with laboratory-cured specimens, all site-cured specimens showed noteworthy higher long-term shear bond strength. The difference in bond strength resulting from different site conditions was, with exception of Specimens S11 which showed comparatively high bond strength, insignificant. On average, site cured specimens with "low-shrink" and "high-shrink" overlays respectively showed 55% and 63% higher bond strength compared to laboratory-cured specimens.

As mentioned earlier, most laboratory-cured specimens failed along the interface. By contrast, site-cured specimens showed comparatively high material failure in overlay or substrate (**Figures 7.17** and **7.18**), with most material failures occurring at a distance from the

interface of no more than 5 mm. The relatively high material failure in the site-cured specimens supported the observation of high interface bond strength.

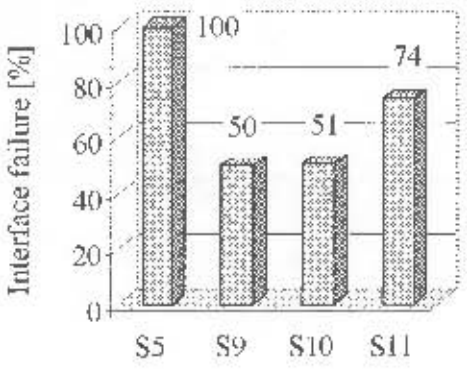

Figure 7.17: Proportion of interface failure, specimens with "low-shrink" overlays

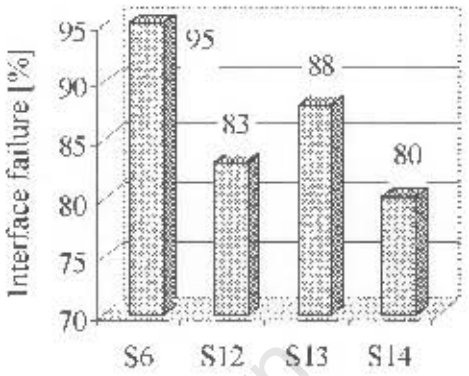

Figure 7.18: Proportion of interface failure, specimens with "high-shrink" overlays

The comparatively high bond strength that was measured on site-cured specimens is believed to relate to ongoing curing as sporadic rain and dew continuously provided moisture. However, compressive strengths measured on site-cured specimens were only slightly higher than those measured on laboratory-cured specimens. This indicates that the higher bond strength of the site-cured specimens did not only relate to the common mechanisms ongoing cement hydration.

As mentioned earlier, bond strength in the laboratory-cured specimens was mainly governed by overlay strength at the interface. In comparison, site-cured specimens showed less interface failure and higher bond strength values (**Figure 7.19**).

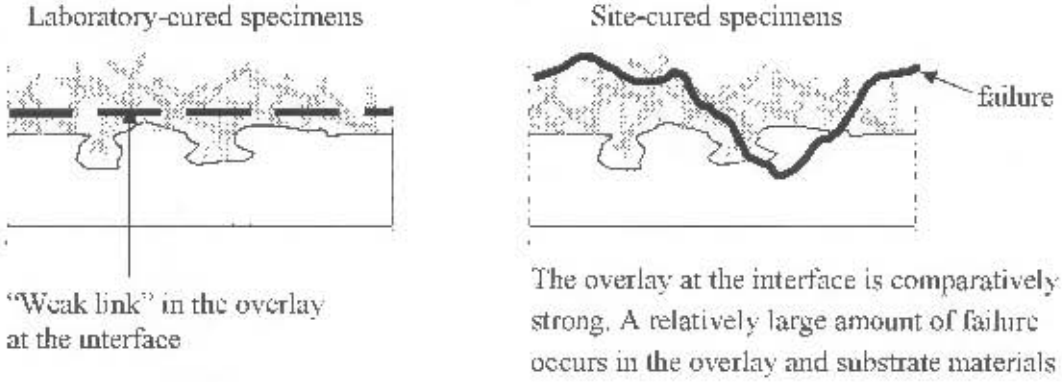

Figure 7.19: Schematic of different failure patterns in laboratory-cured and site-cured specimens

The site conditions therefore had a much more significant influence on overlay properties at the interface, compared to the influence on the overlay material in general, the latter being expressed by compressive strength values.

Alexander (1995) made similar observations when he investigated the effects of ageing on elastic properties of concrete. For certain concretes, unexpectedly high increases in elastic moduli with time were observed. This was ascribed to the mechanisms of densifying the initially porous interface transition zone between aggregates and cement paste. The mechanisms in the transition zone between substrate and overlay appear to adhere to similar principles. This is a further indication that the bond mechanisms between aggregates and cement paste can be compared to those between concretes of different ages.

With the above observations, overlay strength at the interface proved to be a significant factor for long-term bond strength.

7.4.3.3 Specimens subjected to temperature and moisture cycles

For approximately 27 months, Specimens S1-5 and S15-18 were cured under the same laboratory conditions. Subsequently, Specimens S15-18 were exposed to 40 temperature and moisture cycles as described in Section 7.3.2.4. All specimens were tested at the same age of approximately 30 months. The comparison between shear bond strengths of specimens with and without exposure to temperature and moisture cycles is presented in **Figure 7.20**.

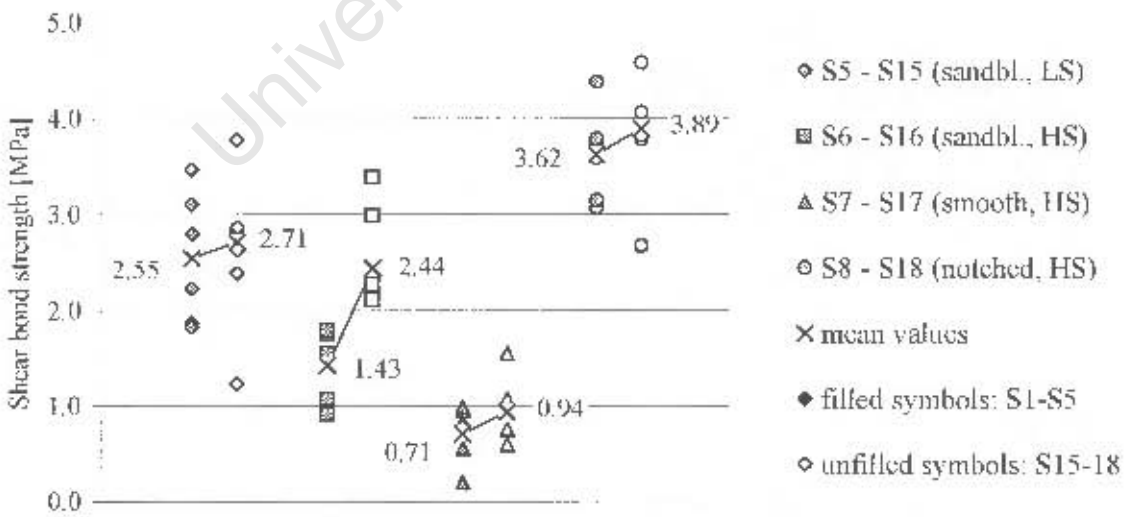

Figure 7.20: Comparison between shear bond strength test results of Specimens S5-8 (laboratory cured) and Specimens S15-18 (exposed to temperature and moisture cycles in the laboratory)

All specimens showed higher interface shear bond strength after exposure to temperature and humidity cycles. However, except for specimens with sandblasted interfaces and Overlay 2 ("high-shrink"), the increase in strength was a result of normal variation of test results. The relatively large increase in bond strength between Specimens S6 and S16 could not be explained.

The test results indicate that, for the tested overlays, temperature and moisture cycles did not have a detrimental influence on interface bond strength, irrespective of the interface texture. This observation correlates to test results on site-cured specimens, which also did not show any signs of bond deterioration despite exposure to environmental cycles.

As discussed in Section 2.4.4, temperature gradients through the overlay depth, e.g. those caused by a sudden rainfall on a hot concrete surface, as simulated in the laboratory, are expected to mainly cause tensile interface stresses related to the restraint of curling deformations (compare Figures 2.11, page 29). Figure 2.13 (page 33) however shows that significant temperature gradients possibly occur only up to a depth of approximately 20 mm. It appears that the overlay thickness of 40 mm resulted in tensile interface stress too low to affect bond strength when the surface was subjected to sudden temperature changes. This could be taken as an indicator that sudden temperature changes caused by rainfalls on hot summer days only affect interface bond strength in specimens with relatively thin overlays. This conclusion however should be tested with specimens having various overlay thicknesses.

7.5 Summary and conclusions

The shear bond strength test results were conclusive for the identification of fundamental bond mechanisms and factors influencing bond durability. However, in the scope of this research, only a relatively small number of parameters were tested. The test results therefore cannot be used for a comprehensive model on the influence of shrinkage strain on bond durability.

An important aspect concerning "interface bond" strength is that the interface as such is usually not the weak link in the composite member. The main aspect for bond strength and bond durability is the overlay material at the interface as it is here where most of the "bond failure" occurs. On well-prepared substrate surfaces, overlay strength is therefore one of the decisive factors for bond strength and bond durability. This was also confirmed in the observation that in fully bonded specimens bond strength development related closely to the development of overlay compressive strength.

The interface texture was found to have no significant influence on short- and long-term strain development of bonded concrete overlays (compare Sections 4.5 and 4.7). By contrast,

bond strength values, as well as bond durability, was closely related to interface texture. This shows that, on fully bonded overlays, overlay strains, and thus direct overlay stresses, do not depend on interface bond strength. The restraint of overlay shrinkage at the interface exists independently from interface bond strength.

The durability of bonded concrete overlays mainly refers to cracking and debonding. As discussed in Section 4.11.2, high overlay shrinkage was found to cause extensive cracking, irrespective of the interface texture. By contrast, bond durability was affected by interface texture, with interfaces of low macro-roughness leading to a loss of bond strength with time. The observed influences of interface texture on bond durability confirm observations made by Talbot et al (1994) (compare Section 2.3.6).

High overlay shrinkage caused cracking on beam specimens and, depending on interface texture, loss of bond strength with time. By contrast, overlays with low shrinkage strains showed neither cracking nor bond deterioration, despite the low macro-roughness of the sandblasted interface. This points out that overlay shrinkage strain values have a significant influence on the durability of composite sections both in terms of cracking and debonding. Further research should aim at identification of a "threshold" value for overlay shrinkage in terms of bond durability.

All site-cured specimens showed a noteworthy increase in bond strength with time, irrespective of the exposure conditions encountered on the sites, which included high temperatures, exposure to direct sunlight and rain, and daily and seasonal temperature cycles. Similarly, the simulation of environmental cycles in the laboratory did not lead to any bond deterioration. However, practical experience shows that bond failure is a phenomenon occasionally observed in concrete overlays such as patch repairs, floors, and bridge decks. This indicates that bond durability in real structures probably mainly refers to the quality of workmanship, i.e. preparation of the substrate concrete, rather than environmental influences. In future research it should be investigated in how far overlay thickness influences interface stresses caused by sudden temperature changes.

The relation between "interface" bond strength and overlay compressive strength, as well as the typical location of bond fracture, i.e. the overlay close to the interface, and the bond strength gain with time observed in specimens exposed to continuous moisture supply (Specimens exposed to outdoor conditions) indicate that a transition zone exists at the interface between substrate and overlay, similar to the transition zone between aggregate and cement paste. This phenomenon can be used to identify fundamental bond mechanisms.

CHAPTER 8

SUMMARY, CONCLUSIONS, AND RECOMMENSATIONS

8.1 Summary of main conclusions

Differential shrinkage between substrate and overlay was identified as the parameter of main concern for the durability of bonded concrete overlays. The influences of differential shrinkage on composite behaviour were examined through strain measurements on composite beam specimens and the testing of interface shear bond strength development. Various interface textures and overlay materials were examined. Detailed conclusions on all relevant test parameters investigated were provided at the end of each section. A summary of the main conclusions is presented in the following. Fundamental characteristics of bonded concrete overlays concerning bond strength development and mechanisms of overlay shrinkage restraint are discussed.

Bond mechanisms between substrate and overlay

Interface shear tests, as opposed to tensile pull-off tests, appear appropriate for the evaluation of long-term bond strength in composite members, as they represent the main stress condition caused by differential shrinkage. The method developed for the testing of interface shear strength proved to be practical as standard moulds (150mm cube moulds) could be used for the fabrication of specimens. Interface stresses resulting from restrained overlay volume changes are highest at the boundaries of the overlay, such as free member ends, joints and cracks. The size of test specimens therefore allowed the development of relevant shear stresses over the test area (interface dimensions 150 x 150 mm). The mode of failure observed on the majority of test specimens was shear at the interface, corresponding to the parameter anticipated for investigation.

On the contrary, the use of pull-off tests for the characterisation of interface bond strength was found to be unsatisfactory, as consistent results could not be obtained with this method. Pull-off tests often lead to failure inside substrate or overlay materials and therefore only indicate a lower bound of actual interface bond strength. This seems appropriate for testing if bond strength requirements are adhered to in actual structures, but appears to be unsatisfactory for the identification of fundamental bond mechanisms. In general, results obtained with tensile bond tests should be interpreted more critically as is commonly done in the literature.

Shear bond strength between substrate and overlay is largely characterised by mechanical material properties of the overlay close to the interface. Bond strength development during 28 days could be linked to the development of compressive overlay strength. This was established on fully water-cured specimens with sandblasted interfaces and different overlay strengths. All specimens showed a shear bond strength / compressive overlay strength ratio of approximately 10%, irrespective of overlay strength and test age. "Interface bond failure" could in most instances visually be identified to have occurred in the overlay close to the interface. The term "interface failure" commonly used for the discussion of bond characteristics therefore appears ambiguous. It is important to identify the actual location of fracture in order to conclude on fundamental bond mechanisms. In contrast to adhesion between substrate and overlay, bond mechanisms between aggregates and cement paste have been extensively investigated in previous research, concluding that an interface transition zone exists which is characterised by high porosity and low strength. The comparison between aggregate - cement paste and concrete - concrete bond mechanisms was found to be useful for the characterisation of interface shear strength in composite specimens.

Interface texture and overlay shrinkage were found to have notable influences on the durability of bond strength. Under laboratory conditions, specimens with low macro roughness at the interface, i.e. specimens with smooth and sandblasted interfaces, and high overlay shrinkage strains showed a reduction of bond strength of approximately 40% after 2 years exposure, compared to the 28-day value. By contrast, specimens with notched interfaces or low-shrink overlays experienced an increase in bond strength of between 10% and 30% in the same time. Only 2 overlays with different shrinkage strains were tested (with 28-day shrinkage values of 140.10^{-6} and 540.10^{-6}). It could not be established if there is a "threshold" value for shrinkage, below which bond durability is not affected. This should be investigated in further research.

Exposure to 40 temperature and moisture cycles did not have a detrimental influence on bond strength, indicating that overlay shrinkage is of greater concern for bond durability than environmental cycles. This however should be verified for thinner overlays which can be expected to be more affected by sudden temperature changes.

All specimens exposed to site conditions showed notable increase in bond strength after 2 years exposure, independent of interface texture, overlay shrinkage, and environmental site conditions which included direct sunlight, wind, cyclic temperature changes, and exposure to rainfalls. In general, site-cured specimens had approximately 60% higher bond strength, compared to laboratory-cured specimens. This indicated ongoing hydration at the porous interface transition zone facilitated by environmental moisture including sporadic rainfalls.

Providing adhesion is adequate and no deteriorating influences exist, short-term bond strength development can be linked to the development of mechanical overlay strength. Long-term bond properties appear to mainly be related to the influences of workmanship and

overlay shrinkage. Detrimental effects caused by high shrinkage can partly be counteracted by provision of good macro-roughness at the interface.

Strains and stresses in composite members subjected to differential shrinkage

Overlay shrinkage is restrained at the interface to the substrate, mobilizing interface shear as the restraining mechanism. In this research, the degree of overlay shrinkage restraint was characterised by the magnitudes of interface strain. Independent of overlay materials and interface textures it was found that substantial strains occur along the whole length of the interface. The member ends commonly experienced notably higher strains than inner regions along the interface, which can be accounted to the effects of a missing restraining "neighbour" and the resulting freedom to deform. High member end strains are however no indication for interface shear stresses only occurring at member ends, as is commonly assumed in existing analytical models. With respect to this aspect it was crucial to obtain information on strain distribution across the depth of the whole member in order to identify fundamental mechanisms of restraint. Measurements across the substrate depth of members that were not free to curve clearly indicated that substrate strains have a maximum value at the interface and fade out to reach zero strain in regions away from the interface. Restraint of overlay shrinkage is a localised phenomenon at the interface, occurring along the whole length of the member and consequently producing interface shear stresses along the whole member.

In terms of bond durability it is of no significance from a practical point of view if interface stresses occur only at member ends or along the whole length of the member. Debonding is commonly connected to overlay slip at the interface, which can only occur at overlay boundaries such as member ends, joints, and cracks, irrespective of stresses in regions remote from such boundaries. However, for the correct modelling of direct overlay stresses it is crucial to understand the mechanisms of localised shrinkage restraint along the whole interface. In this respect, the most important conclusion that can be drawn from experimental research and numerical modelling is that Bernoulli's hypothesis of strain sections remaining plane, which is commonly used for analysis of bonded concrete overlays subjected to differential shrinkage, does not apply. Analytical approaches based on Bernoulli's principle do not succeed in modelling strains and stresses in a realistic way.

An analytical model was developed that is based on localised strain conditions at the interface. The degree of overlay shrinkage restraint is expressed as a function that combines the influences of relative member dimensions, elastic properties, and strain characteristics of overlay and substrate. Assuming that fundamental strain characteristics, i.e. shape and depth of strain profiles in substrate and overlay, are time-independent parameters, the influences of strain profiles and member dimensions can be combined in a single constant, termed C_ε.

Based on the above, a simple equation was developed for the computation of direct elastic interface strains:

$$\varepsilon_I = \frac{\varepsilon_{FSS}}{1 + \frac{E_S}{E_O} \cdot C_\varepsilon} \qquad [6.17]$$

For practical application of the above equation, the constant C_ε has to be determined empirically for different overlay and substrate materials. For the specimens investigated during this research, C_ε sensibly took a value of approximately 1, i.e. relative overlay and substrate dimensions appeared to not have an influence on the degree of overlay shrinkage restraint. In general it was shown that relative member dimensions of substrate and overlay have a far lesser influence on overlay restraint than commonly assumed.

The development of overlay stresses is governed by a number of different strain and stress components. Substrate creep, which is not considered in existing analytical approaches, was found to be an important mechanism for overlay and substrate strain development, leading to a decreasing degree of overlay restraint with time. Next to the development of shrinkage, the most important influence on overlay durability is that of tensile stress relaxation. For the test specimens, relaxation could be estimated to reduce tensile overlay stress by approximately 50%, which corresponds to values given in the literature. Curvature was found to be of minor significance for the performance of the test specimens.

Substrate creep and overlay relaxation are time-dependent variables. However, it was shown that it is practical to account for substrate creep in a one-step analysis.

In the literature, tensile stress relaxation in concrete is reported to develop rapidly after loading. To facilitate the estimation of overlay stresses it is therefore suggested to account for stress relaxation in a simple way. This is done in the analytical model by adjusting the stress inducing shrinkage strains $\varepsilon_{FSS}(t)$ with a factor accounting for total relaxation that took place between t and t_0:

$$\varepsilon_{\text{stress inducing}}(t) = \varepsilon_{FSS}(t)\ \psi(t,t_0) \qquad [8.1]$$

The relaxation factor $\psi(t,t_0)$ is dependent on age and material characteristics of the concrete. It can be expressed by the relaxation function $\Psi(t)$. However, information on tensile relaxation in concrete is rare and for practical application, $\psi(t,t_0)$ has to be estimated for the overlay under investigation. This can be done using common relaxation tests for restrained specimens.

With the above simplifying assumptions, the influences of elastic strains, substrate creep and overlay relaxation were combined in a single equation which can be used for the estimation of time-dependent direct overlay stress:

$$\sigma_{I,O}(t) = \psi(t,t_0)\cdot\varepsilon_{FSS}(t)\cdot E_O(t)\cdot\left(1-\frac{1}{1+\frac{E_S\cdot C_\varepsilon}{E_O(t)\cdot(1+0.8\cdot\varphi_S(t,t_0))}}\right) \qquad [6.54]$$

The crack resistance of the overlay can be estimated using simple stress-strength comparison. Considering that the estimation of time-dependent stresses and strains in bonded concrete overlays is complex, the comparison between experimental results and strains and stresses computed with the analytical model shows reasonably good correlations. Equation 6.54 can therefore assist in designing bonded concrete overlays for long-term performance. For practical use of equation 6.54, future research is however necessary to gain further information on the parameter C_ε and on stress relaxation functions $\Psi(t)$ for a range of overlay materials.

For most specimens, measured overlay strains on composite members were approximately 35% (between 30% and 40%) of free overlay shrinkage strains. Tensile relaxation of the overlays was found to be roughly 50%, conforming to results given in the literature. Therefore, stress-producing strain ε_σ could be estimated to be approximately:

$$\varepsilon_\sigma = (1-0.35)\cdot 0.5\cdot\varepsilon_{FSS} = 0.33\varepsilon_{FSS} \qquad [8.2]$$

This corresponds to overlay tensile stress of:

$$\sigma_O = 0.33\varepsilon_{FSS}\cdot E_O \qquad [8.3]$$

For the tested overlays it appears appropriate to assume as a "rule of thumb" that one third of free overlay shrinkage caused tensile stress. In general, "rule of thumb" values can assist design procedures as a practical tool for estimation of overlay stresses.

Existing design recommendations for bonded concrete overlays appear inadequate, as they do not include important overlay material parameters such as shrinkage and relaxation

properties. In general it is more practical to move away from prescriptive design recommendations and provide design methods, i.e. analytical tools, which take account of the interaction between material properties, environmental influences, and the structural system.

8.2 Recommendations for future work

Fundamental aspects concerning bond mechanisms and the characteristics of strain development in composite members were identified in this research, though many questions still remain. The following aspects appear most significant for a deeper understanding of the structural behaviour of bonded concrete overlays:

- Localised restraint conditions at the interface should be further investigated to find practical values for the parameter C_ε which describes the combined influences of relative section dimensions and strain profiles of substrate and overlay on interface strains. With this, the general validity of equations 6.17 and 6.54 should be verified for a range of overlay materials

- Time-dependent tensile relaxation functions under relevant stress conditions should be identified for common overlay materials

- Research should be carried out to assess how far existing knowledge on aggregate-paste interfaces can be applied to the characterisation of bond between substrate and overlay, which could help identify important mechanisms influencing the durability of composite members

- The influences of overlay shrinkage on interface bond strength should be further investigated to establish if a threshold value for shrinkage exists, under which bond durability is not affected. This should be done in conjunction with tests on the influences of overlay relaxation properties on bond strength.

- The influence of overlay thickness on interface stresses caused by sudden temperature changes needs to be established

REFERENCES

Alexander, M.G. (1991), 'Fracture energies of interfaces between cement paste and rock, application to the engineering behaviour of concrete', Proceedings: Fracture Process in Brittle Disordered Materials (editors J. Van Mier et al.), Noordwijk, Netherlands, E&FN Spon, London, pp. 333-346.

Alexander, M.G. (1995), 'The effects of ageing on the interfacial zone in concrete', in 'Interfacial Transition zone in Concrete', Edited by J.C. Maso, RILEM Report 11, London, 1995, pp.151-174.

Alexander, M.G. (2001), 'Deformation and volume change of hardened concrete', in 'Fulton's Concrete Technology', 8th Edn 2001, Midrand, South Africa.

Alonso Junghanns, M.T (1997), 'Zur Rissicherheit zementgebundener dehnungsbehinderter Schichten unter Berücksichtigung von Dauereinflüssen', PhD thesis, Universität Hamburg-Harburg, Shaker Verlag, Aachen, Germany, 1997.

Ambroise, J., Georgin, J. F., Pera, J., and Reynouard, J. M. (2002), 'Curling of cement-based screeds', Concrete Science and Engineering, Vol.4, No.14, 2002, pp.114-120.

American Concrete Institute (ACI), Committee 209 (1992), 'Prediction of creep, shrinkage and temperature effects in concrete structures', 209R-92, ACI, Detroit, USA, 1992.

American Concrete Institute (ACI) (1999), 'ACI 318 (1999). Building Code Requirements for Structural Concrete (ACI 318-99) and Commentary (ACI 318R-99)', Farmington Hills, Michigan, USA, 1999.

American Society for Testing Materials (2003), 'Standard Test Method for determining age at cracking and induced tensile stress characteristics of mortar and concrete under restrained shrinkage', ASTM draft 02/04/03, Philadelphia, 2003.

Asad, M., Baluch, M. H., and Al-Gadhib, A. H. (1997), 'Drying shrinkage stresses in concrete patch repair systems', Magazine of Concrete Research, Vol.49, No.181, 1997, pp.283-293.

Atzeni, C., Massidda, L., and Sanna, U. (1993), 'Dimensional variations, capillary absorption and freeze-thaw resistance of repair mortars admixed with polymers', Cement and Concrete Research, Vol. 23, 1993, pp.301-308.

Austin, S., Robins, P., and Pan, Y. (1999), 'Shear bond testing of concrete repairs', Cement and Concrete Research, 29, 1999, pp 1067-1076.

Bangash, M. Y. H. (1999), 'Manual of numerical methods in concrete', published by Thomas Telford Publishing, London, 1999.

Banthia, N., and Bindiganavile, V. (2001), 'Repairing with hybrid-fiber-reinforced concrete', Concrete International, June 2001, pp. 29-32.

Banthia, N., Azzabi, M., and Pigeon, M. (1993), 'Restrained shrinkage cracking in fibre-reinforced cementitious composites', Materials and Structures, Vol.26, 1993, pp.405-413.

Baroghel-Bouny, V., and Godin, J. (2001), 'Experimental study on drying shrinkage of ordinary and high-performance cementitious materials', Concrete Science and Engineering, Vol.3, No.9, March 2001, pp.13-22.

Baroghel-Bouny, V., and Kheirbek, A. (2001), 'Effect of mix-parameters on autogenous deformations of cement pastes-microstructural interpretations', Concrete Science and Engineering, Vol.3, March 2001, pp.23-38.

Bernard, O. (2000), 'Comportement à long termedes elements de structure formés de bétons d'âges différents', Doctoral thesis, swiss Federal Institute of Technology no 2283, Lausanne, Switzerland, 2000.

Bentur, A. (2001), 'Early-age shrinkage and cracking in cementitious systems', Concrete Science and Engineering, Vol.3, March 2001, pp.3-12.

Birkeland, H. W. (1960), 'Differential shrinkage in composite beams', Journal of the American Concrete Institute, May 1960, pp.1123 – 1136.

Bisschop, J., and van Mier, J. G. M. (1999), 'Quantification of shrinkage microcracking in toung mortar with fluorescence light microscopy and ESEM', HERON, Vol.44, No.4, 1999, pp.245-255.

Bissonette, B., and Pigeon, M. (1995), 'Tensile creep at early ages of ordinary, silica fume and fiber reinforced concretes', Cement and Concrete Research, Vol.25, No.5, 1995, pp.1075-1085.

Block, K. and Porth, M. (1989), 'Spritzbeton auf carbonatisiertem Beton – Haftzugfestigkeit bei nachträglichem Aufspritzen', Beton 7/89, pp.299-302.

Brameshuber, W. (1988), ‚Bruchmechanische Eigenschaften von jungem Beton', Massivbau Baustofftechnologie Karlsruhe, Heft 5, Karlsruhe, Germany, 1988.

Brühwiler, E., Bernard, O., Wolf, S. (2000), 'Beton-Beton Verbundbauteil bei der Verbreiterung eines Brückenüberbaus', Beton- und Stahlbetonbau 95, 2000, Heft 3, pp.158-166.

British Standards BS 1881-115 (1983), 'Testing concrete, Part 115. Method for determination of compressive strength', British Standard Institution BSI, London, 1983.

British Standards BS 1881-117 (1983), 'Testing concrete, Part 117. Method for determination of tensile splitting strength', British Standard Institution BSI, London, 1983.

British Standards BS 1881-102 (1983), 'Method for determination of slump', British Standard Institution BSI, London, 1983.

British Standards BS 6319 (1984), 'Part 4, Slant shear test method for evaluating bond strength of epoxy systems', British Standard Institution BSI, London, 1984

Bungey, J.H. and Madandoust, R. (1992), "Factors influencing pull-off tests on concrete", Magazine of concrete Research, 1992, 44, no, 158, Mar., pp 21-30.

Cao, J., and Chung, D. D. L. (2001), 'Degradation of the bond between old and new mortar under cyclic shear loading, monitored by contact electrical resistance measurement', Cement and Concrete Research, Vol.31, 2001, pp.1647-1651.

Carter, P., Gurjar, s., and Wong, J. (2002), 'Debonding of highway bridge deck overlays', Concrete International, July 2002, pp. 51-58.

Charron, J. P., Marchand, J., and Bissonnette, B. (2001), 'Early-age deformations of hydrating cement systems: comparison of linear and volumetric shrinkage measurements', Concrete Science and Engineering, Vol.3, No.11, September 2001, pp.168-173.

Chen, P., Fu, X., and Chung, D.D.L. (1995), 'Improving the bonding between old and new concrete by adding carbon fibres to the new concrete', Cement and Concrete Research, Vol. 25, No. 3, 1995, pp. 491-496.

Climaco, J. C. T. S., and Regan, P. E. (2001), 'Evaluation of bond strength between old and new concrete in structural repairs', Magazine of Concrete Research, Vol.53, No.6, 2001, pp.377-390.

Comitè Euro-International du Bèton (CEB) (1990), 'Evaluation of time depended behaviour of concrete. CEB Bulletin d'information, no. 199, Lausanne, Switzerland, 1990.

Comité Euro-International du Béton & Federation Internationale de la Precontrainte, (1993), 'CEB-FIP Model Code 1990', Thomas Telford Services Ltd, London, 1993.

Comitè Euro-International du Bèton (CEB) (1993a), 'CEB-FIP Model Code for Concrete Structures, 1990 (MC-90)', CEB Bulletin d'information, No. 213/214, Lausanne, Switzerland, 1993.

Comitè Euro-International du Bèton (CEB) (1993b), 'Structural effects of time-dependent behaviour of concrete', CEB Bulletin d'information, No. 215, Lausanne, Switzerland, 1993.
Corinaldesi, V., Moriconi, G., Leoni, G., and Dezi, L. (2003), 'Evaluation of cracking tendency due to early-age concrete shrinkage', ICPCM Proceedings, Cairo, Egypt, February 2003, pp.2-9.

Courard, L. (1998), 'Parametric definition of sandblasted and polished concrete surfaces', IX ICPIC 98 Proceedings, Bologna, Italy, September 14-18th, 1998, pp.771-778.

Courard, L. (1999), 'How to analyse thermodynamic properties of solids and liquids in relation with adhesion?' Proceedings of the 2nd International RILEM Symposium ISAP '99, pp.9-19.

Courard, L. (2000), 'Parametric study for the creation of the interface between concrete and repair products', Materials and Structures, Vol. 33, January-February 2000, pp. 65-72.

Cusson, D., and Mailvaganam, N. (1996), 'Durability of repair materials', Concrete International, March 1996, pp. 34-38.

Daschner, F., and Kupfer, H. (1986), 'Literaturstudie zur Schubsicherung bei nachträglich ergänzten Querschnitten', DAfStb Heft 372, Berlin, Germany, 1986.

Delatte, N.J., Williamson, M.S., and Fowler, D.W. (2000) (a), 'Bond strength development of high-early-strength bonded concrete overlays', ACI Materials Journal, no.97-M27, March-April 2000, pp. 201-207.

Delatte, N.J., Wade, D.M., and Fowler, D.W. (2000) (b), 'Laboratory and field testing of concrete bond development for expedited bonded concrete overlays', ACI Materials Journal, no.97-M33, May-June 2000, pp.272-280.

Denarié, E., and Silfwerbrand, J. (2004), 'Structural behaviour of bonded concrete overlays', Proceedings, International RILEM Workshop on 'Bonded Concrete Overlays', June 7-8 2004, Stockholm, Sweden, pp. 37-45.

Denarié, E., Habel, K, Charron, J.P., Wuest, J., Kamen, A., and Brühwiler, E. (2004), 'Ultra High Performance Fibre Reinforced Concretes for rehabilitation', Proceedings, International RILEM Workshop on 'Bonded Concrete Overlays', June 7-8 2004, Stockholm, Sweden, pp. 37-45.

Deutscher Ausschuss für Stahlbeton, DAfStb (1990-1992), 'Richtlinie für Schutz und Instandsetzung von Betonbauteilen', part 1 – 4, Berlin 1990-1992.

Dilger, W.H., Wang, C. and Niitani, K. (1996), 'Experimental study on shrinkage and creep of high-performance concrete', 4th International Symposium on Utilization of high-strength/high-performance concrete, Paris, 1996, conference proceedings, pp.311-319.

Eurocode No. 2 (EC 2) (1991), 'ENV 1992-1, Design of Concrete Structures. Part 1: General rules and rules for buildings', European Committee for Standardisation (CEN), 1991.

Eierle, B., Schikora, K. (2000), 'Bodenplatten unter frühem Temperaturzwang – Rechenmodelle und Tragverhalten', Bauingenieur, Band 75, Oktober 2000, pp.671-678.

El-Rakib, T.M., Farahat, A.M., El-Degwy, W.M., and Shaheen, H.H. 'Shear transfer parameters at the interface between old and new concrete', ICPCM Proceedings, Cairo, Egypt, February 2003, pp.

Emberson, N.K. and Mays, G.C. (1990), 'Significance of property mismatch in the patch repair of structural concrete. Part 1: Properties of repair systems', Magazine of Concrete Research, 1990, 42, No. 152, Sept., pp.147-160.

Emmons, P.H., McDonald, J.E. and Vaysburd, A.M. (1983), 'Some compatability problems in repair of concrete structures – a fresh look', in 'Proceedings of the third international colloqium on materials science and restauration', Technische Akademie Esslingen (1983) pp.837-853.

Emmons, P.H. and Vaysburd, A.M. (1994), 'Factors affecting the durability of concrete repair: the contractor's viewpoint', Construction and Building Materials, Vol 8, no. 1, 1994, pp.5-16.

Emmons, H. and Vaysburd, A. M. (1995), 'Performance criteria for concrete repair material, phase 1', Technical Report REMR-CS-47, US Army Corps of Engineers, April 1995.

Emmons, P.H., Vaysburd, A.M, McDonald, J.E., Poston, R.W. and Kesner, K.E. (2000), 'Selecting durable repair materials: performance criteria', Concrete International, March 2000, pp.38-45.

European Committee for Standardization (2001), 'Eurocode 2. Design of Concrete Structures', 2nd draft, Brussels, Belgium, January 2001.

Evans, R.H., Parker, A.S. (1955), 'Behaviour of prestressed concrete composite beams', Journal of the American Concrete Institute, Title No. 51-43, May 1955, pp.861-878.

Evans, R.H., and Chung, H.W. (1967), 'Shrinkage and deflection of composite prestressed concrete beams', Concrete, May 1967, pp. 157-166.

Fiebrich, M. (1994), 'Grundlagen der Adhäsionskunde', Deutscher Ausschuss für Stahlbeton, Heft 334, Beuth Verlag, Berlin 1994, pp. 75-90.

FIP Federation Internationale de la Prècontrainte (1978), "Shear at the interface of precast and in-situ concrete", Technical report, August, 1978.

Ghali, A., and Favre, R. (1994), ' Concrete structures – Stresses and deformations', second edition, published by E&FN Spon, London, 1994.

Geissert, D. G., Li, S. E., Frantz, G. C., and Stephens, J. E. (1999), 'Splitting prism test method to evaluate concrete-to-concrete bond strength', ACI Materials Journal, Vol.96, No.3, May-June 1999, pp.359-366.

Granju, J.L. (1996), 'Thin bonded overlays – About the role of fibre reinforcement on the limitation of their debonding', Advanced cement based materials, 1996, 4, pp.21-27.

Granju, J.L. (2004), '193-RLS RILEM TC Bonded cement-based material overlays for the repair, the lining or the strengthening of slabs or pavements' State of the Art report (draft), France, August 2004.

Granju, J.L., Sabathier, V., Turatsinze, A. and Bissonnette, B. (2004), 'Shrinkage and fatique of cement-based bonded overlays: about its modelling', Proceedings, Internaional RILEM Workshop on Bonded Concrete Overlays, June 7-8 2004, Stockholm, Sweden, pp. 61-67.

Gulyas, R. J., Wirthlin, G. J. and Champa, J. T. (1995), 'Evaluation of Keyway grout test methods for precast concrete bridges', PCI Journal, January-February 1995, pp.44-57.

Gutsch, A., and Rostásy, F.S. (1994), 'Young concrete under high tensile stresses - creep relaxation and cracking', Proceedings: RILEM Symposium 'Thermal Cracking in Concrete at early ages', edited by R. Springenschmidt, Chapman & Hall, London 1995, pp.111 - 116.

Haardt, P. (1991), 'Zementgebundene und kunststoffvergütete Beschichtungen auf Beton', Massivbau Baustofftechnologie Karlsruhe, Heft 13, TH Karlsruhe, 1991.

Haardt, P., and Hilsdorf, H. K. (1988), 'Ausbesserung beschädigter Oberflächen bewehrter und unbewehrter Betonkonstruktionen', Forschungsbericht der Universität Karlsruhe, Abteilung Baustofftechnologie, Karlsruhe, 1988.

Hartl, G. (1983), 'Kraftverlauf in Beschichtungen', Zement und Beton, 28. Jahrgang, Heft 2, 1983, pp. 45-51.

Hartl, G. (2000), 'Materialtechnologische Beurteilung von Verstaerkungsmassnahmen', Beton- und Stahlbetonbau 95, 2000, Heft 12, pp.707-712.

Hilsdorf, H. K. (1995), 'Beton', Betonkalender 1995, Teil 1, Ernst und Sohn Verlag, Berlin, 1995, p. 67.

Holl, C.H., and O'Connor, S.A. (1997), 'Cleaning and preparing concrete before repair', Concrete International, March 1997, pp.60-63.

Horimoto, H., and Koyanagi, W. (1994), 'Estimation of stress relaxation in concrete at early ages', Proceedings: RILEM Symposium 'Thermal Cracking in Concrete at early ages', edited by R. Springenschmidt, Chapman & Hall, London 1995, pp.95 - 102.

Illston, J.M., Dinwoodie, J.M., and Smith, A.A. (1979), 'Concrete, timber and metals', Van Nostrand Reinhold, London, 1979.

Karihaloo, B.L. (1995), 'Fracture mechanics and structural concrete', Longman Scientific & Technical, Essex, England, 1995.

Kauw, V, Dornbusch, J. (1997), 'Optimierung der Verwendung von Hochdruck-Wasserstarhlsystemen (HDWS) bei der Betonuntergrund-Vorbereitung', Beton und Stahlbetonbau 92 (1997), Heft 6, pp.149-155.

Kaufmann, N. (1971), 'Das Sandflächenverfahren', Strassenbau Technik , 24, no.3, 1971, pp. 31-50.

Klopfer, H. (1987), 'Spannungen und Verformungen von Industrie-Estrichen'. Technische Akademie Esslingen, International Colloquium: Industry Floors, January 1987.

Knutson, M. (1990), 'Fast-track bonded overlays', Concrete Construction, December 1990, pp. 979-990.

Kordina, K., Schubert, L., and Troitzsch, U. (2000), 'Kriechen von Beton unter Zugbeanspruchung (Creep of concrete subjected to tensile stress)', Deutscher Ausschiss für Stahlbeton, Heft 498, Beuth Verlag, Berlin, Germany, 2000.

Kuroda, M., Watanabe, T., and Terashi, N. (2000), 'Increase of bond strength at interfacial transition zone by the use of fly ash', Cement and Concrete Research, Vol.30, 2000, pp.253-258.

Lacombe, P., Beauprè, D., and Pouliot, N. (1999), 'Rheology and bonding characteristics of self-leveling concrete as a repair material', Materials and Structures, Vol. 32, October 1999, pp. 593-600.

Lange, D. A., and Shin, H. C. (2001), 'A computer-based design tool for analysis of bonded concrete overlays', Concrete Science and Engineering, Vol.3, No.12, December 2001, pp.189-194.

Langlais, M., Pigeon, M., Bissonnette, B., and Allard, D. (1994), 'Durability of pavement repairs: A field experiment', Concrete International, August 1994, pp.39-43.

Larralde, J., Elpert, M. S., and Weckermann, D. (2001), 'A simplified shear test for the sdhesion of FRP composites to concrete', cement, Concrete and Aggregates, Vol.23, No.1, June 2001, pp.66-70.

Laurence, O., Bissonnette, B., Pigeon, M., and Rossi, P. (2001), 'Concrete repairs subjected to hygrothermal loading: in situ experiments', Concrete Science and Engineering, Vol.3, June 2001, pp.92-99.

Letsch, R. (1995), 'Spannungen in polymermodifizierten Zementmörteln (PCC) unter Verformungsbehinderung beim Aushärten und wechselnden Temperaturen', Technische Universität München, Abschlussbericht zum Forschungsvorhaben "Spannungen im PCC", München, Germany, April, 1995.

Letsch, R. H. (1991), 'Shrinkage and temperature stresses in PC and PCC due to hindered deformation', International Symposium on Concrete Polymer Composites, Bochum, Germany, 1991, Conference proceedings, pp.53-62.

Li, G. (2003), 'A new way to increase the long term bond strength of new-to-old concrete by the use of fly ash', Cement and Concrete Research, Vol.33, 2003, pp.799-806.

Li. S.L., Frantz, G.C., and Stephens, J.E. (1997), "Application of pull-off test to assess the durability of bond between new and old concrete subjected to deicer salts", Innovations in non-destructive testing of concrete, ACI International, SP-168, 1997, pp 267-294.

Li, S.E., Geissert, D.G., Frantz, G.C., and Stephens, J.E. (1999), 'Freeze-thaw bond durability of rapid-setting concrete repair materials', ACI Materials Journal, Title no. 96-M31, March/April 1999, pp.241-249.

Loov, R.E., and Patnaik, A.K. (1994), 'Horizontal shear strength of composite concrete beams with a rough interface', PCI Journal, January-February 1994, Vol. 39, no.1, pp.48-69.

Mainz, J. and Zilch, K. (1998), 'Schubtragfähigkeit von Betonergänzungen an nachträglich aufgerauhten Betonoberflächen bei Sanierungs- und Ertüchtigungsmassnahmen', Research report, Technical University Munich, Germany, February 1998.

Zilch, K., and Mainz, J. (2002), 'Schubtragfähigkeit von Betonergänzungen an nachträglich aufgerauten Betonoberflächen bei Sanierungs- und Ertüchtigungsmaßnahmen', DAfStb, Heft 528, Beuth Verlag, Berlin, 2002.

Marsszeky, M. and Yuan, Y. (1994), 'Restrained shrinkage in repaired reinforced concrete elements'. Materials and Structures, 1994, 27, pp. 375-382.

Mindess, S., Alexander, M.G. (1995), 'Mechanical Phenomena at Cement/Aggregate Interfaces', in Material Science of Concrete IV, Ed J.P. Skalny, American Concrete Society, 1995, pp. 263-282.

Misra, A., Cleland, D. J., and Basheer, P. A. M. (2001), 'Effect of different substrate and overlay concretes on bond strength and interfacial permeability', Concrete Science and Engineering, Vol.3, No.10, 2001, pp.73-77.

Miyazawa, S., and Tazawa, E. (2001), 'Influence of specimen size and relative humidity on shrinkage of high-strength concrete', Concrete Science and Engineering, Vol.3, March 2001, pp.39-46.

Momayez, A., Ramezanianpour, A. A., Rajaie, H., and Ehsani, M. R. (2004), 'Bi-surface shear test for evaluating bond between existing and new concrete', ACI Materials Journal, March-April 2004, pp.99-106.

Montani, R. (1995), 'In defence of bonding agents', Concrete Repair Digest, April/May 1995, pp.135-138.

Montgomery, D. C., and Runger, G.C. (2003), 'Applied statistics and probability for engineers', John Wiley & Sons, Inc., USA, 2003.

Mueller, H. S., Kvitsel, V. (2002), 'Kriechen und Schwinden von Beton - Grundlagen der neuen DIN 1045 und Ansaetze fuer die Praxis', Beton- und Stahlbetonbau 97, 2002, Heft 1, pp.8-19.

Murrey, M.A. (1989), 'Surface preparation for adhesives', Concrete International, September 1989, pp. 69-71.

Neville, A.M (2002), 'Properties of Concrete', 4th Edition, Pearson Education Limited, England, 2002.

Okada, K., Koyanagi, W., and Yoshioka, Y. (1970), 'Study on the differential shrinkage of composite concrete beam', Symposium on design of concrete structures for creep, shrinkage and temperature changes, Madrid, 1970, Reports of the working commissions, Vol. 5, pp.46-54.

Onken, P. and Rostásy, F. S. (1995), 'Wirksame Betonzugfestigkeit im Bauwerk bei früh einsetzendem Temperaturzwang', Deutscher Ausschuss für Stahlbeton, Heft 449, Berlin 1995.

Paulsson, J., and Silfwerbrand, J. (1998), ' Durability of repaired bridge deck overlays', Concrete International, February 1998, pp. 76-82.

Pigeon, M. and Bissonette, B. (1999), 'Bonded concrete repairs - Tensile creep and cracking potential', Concrete International, November 1999, pp.31-35.

Pigeon, M. and Saucier, F. (1992), 'Durability of repaired concrete structures', Proceedings, International Symposium on Advances in Concrete Technology, Athens, 11-12 May, October 1992, pp.741-773.

Radocea, A. (1994), 'A model of plastic shrinkage', Magazine of Concrete Research, 1994, 46, No. 167, June, pp.125-132.

Reinhard, H.W. (1977), 'Rechnerische Behandlung der Wärmespannungen in Betonfahrbahnen mit mehrschichtigem Aufbau', Strassen- und Tiefbau 31, 1977, 2, pp. 25-28.

Reinhard, H.W., and Walraven, J. C. (1982), 'Cracks in concrete subject to shear', Journal of the Structural Division, Vol.108, January 1982, pp.207-224.

RILEM Recommendation MDT.D.3, 'Determination "in-situ" of the adhesive strength of rendering and plastering mortars to their substrate', Materials and Structures, Vol.37, August-September 2004, pp.488-490.

Rizzo, E. M., and Sobelman, M. B. (1989), 'Selection criteria for concrete repair materials', Concrete International, September 1989, pp. 46-49.

Robins, P.J. and Austin, S.A. (1995), 'A unified failure envelope from the evaluation of concrete repair bond test', Magazine of Concrete Research, 1995, 47, No. 170, pp. 57-68.

Rostàsy, F.S., Krauss, M., and Budelmann, H. (2002), 'Planungswerkzeug zur Kontrolle der frühen Rissbildung in massigen Betonbauteilen', Teil 1-7, Bautechnik 79 (2002), Hefte 7-12, Berlin, Germany, 2002.

Saha, G.P. (1998), 'Differential shrinkage stresses in concrete structures', Proceedings from the International Symposium on 'Innovative World of Concrete-98', Calcutta, India, pp.3.113-3.120.

Sato, R., Dilger, W. H., and Ujike, I. (1994), 'Deformations and thermal stresses of concrete beams constructed in two stages', in 'Thermal Cracking in Concrete at early Ages', published by E&FN Spon, London, 1994, pp.313-320.

Schäfer, H.G., Block, K., and Drell, R. (1996), 'Oberflächenrauheit und Haftverbund', Deutscher Ausschuss für Stahlbeton DafStb, Heft 456, Berlin 1996, pp. 75-94.

Schrader, E.K. (1992), 'Mistakes, Misconceptions, and controversial issues concerning concrete and concrete repairs, Part 1, 2, and 3', Concrete International September, October, November 1992.

Silfwerbrand, J. (1986), 'Bonding between old and new concrete in structures loaded by static and time-depended load', Proceedings, Adhesion between polymers and concrete, Aix-en-Provence, France, September 16-19, 1986, pp. 309-319.

Silfwerbrand, J. (1990), 'Improving concrete bond in repaired bridge decks', Concrete International, September 1990, pp.61-66.

Silfwerbrand, J., (1992), 'The Influence of Traffic-Induced Vibrations on the Bond between Old and New Concrete', Bulletin No. 158, Dept. of Structural Mechanics and Engineering, Royal Institute of Technology, Stockholm, 1992.

Silfwerbrand, J. (1997), 'Stresses and strains in composite concrete beams subjected to differential shrinkage', ACI Structural journal, V.94, No. 4, July-August 1997.

Silfwerbrand, J. (1998), 'Concrete repair with shotcrete', IABSE Symposium on durability of structures, Proceedings, Lisbon, September 1989, pp. 785-790.

Silfwerbrand, J. and Paulsson, J. (1998), 'Better bonding of bridge deck overlays', Concrete International, October 1998.

Silfwerbrand, J. (2000), 'Evaluation of tests on water-jet equipment', BHR Group 2000 Jetting Technology, pp.113-119.

Silfwerbrand, J. (2003), 'Shear Bond Strength in Repaired Concrete Structures', Materials & Structures, Vol. 36, July 2003, pp. 419-424.

Smithson, L.D., and Whiting, J.E. (1992), 'Rebonding delaminated bridge deck overlays', Concrete Repair Digest, June/July 1992, pp.100-101.

Sodeikat, C. (2002), 'Beanspruchung von Betonfahrbahnen mit sehr unterschiedlichen Eigenschaften von Ober- und Unterbeton durch Feuchte- und Temperaturänderungen', Beton- und Stahlbetonbau 97, 2002, Heft 1, pp.20-35.

Souza, R.F.F. de, and Silva Appleton, J.A. da (2003), 'Assessing the structural performance of repaired reinforced concrete members', ICPCM Proceedings, Cairo, Egypt, February 2003.

Springenschmidt, R., Wagner-Grey, U. and Schwarzkopf, M. (1978), 'Temperaturspannungen in Beton bei sommerlicher Erwärmung', Bauingenieur 53, 1978, pp. 265-267.

Springenschmidt, R. (1984), 'Die Ermittlung der Spannungen infolge von Schwinden und Hydratationswärme im Beton', Beton- und Stahlbetonbau 10, 1984, pp.263-269.

Springenschmidt, R., Breitenbücher, R., Ballardini, P. (1988), 'Vergleich zwischen Berechnungen und Messungen von Zwangspannungen in jungem Beton', Beton- und Stahlbetonbau 83, Berlin, Germany, 1988, Heft 4, pp.93-97.

Springenschmidt, R., and Breitenbücher, R. (1990), 'Beurteiling der Rissneigung anhand der Risstemperatur von jungem Beton bei Zwang', Beton und Stahlbetonbau 85, 1990, H.2, Berlin, Germany, 1990, pp.29-33..

Springenschmidt, R., Fleischer, W. (1993), 'Ueber das Schwinden von Beton, Schwindmessungen und Schwindrisse', Beton- und Stahlbetonbau 88, Berlin, Germany, 1993, part 1: Heft 11, 297-301, part 2: Heft 12, pp.329-332.

Talbot, C., Pigeon, M., Beauprè, and Morgan, D.R. (1994), 'Influence of surface preparation on long-term bonding of shotcrete', ACI Materials Journal, Title no. 91-M56, Vol. 91, No. 6, November-December 1994, pp. 560-566.

Tassios, T. P., and Vintzeleou, E. N. (1987), 'Concrete to concrete friction', Journal of Structural Engineering, Vol.113, No.4, April 1987, pp.832-849.

Taylor, P. C., Addis, B. J. (1994), 'Concrete at early ages', in 'Fulton's Concrete Technology', 7th Edn 1994, Midrand, South Africa.

Thomsing, M. (1998), 'Spannbeton (Prestressed concrete)', B.G. Teubner Stuttgart, Leipzig, Germany, 1998.

Timoshenko, S. (1941), 'Strength of materials, Part II: Advanced theory and problems', D. Van Nostrand Company, USA, 1941.

Trost, H. (1991), 'Auswirkungen des Superpositionsprinzips auf Kriech- und Relaxationsprobleme bei Beton und Spannbeton', Beton- und Stahlbetonbau 62, Berlin, Germay 1967, Heft 10, pp 230-238 und Heft 11, pp. 261-269.

Tschegg, E.K., Ingruber, M., Surberg, C.H.,and Münger, F. (2000), 'Factors influencing fracture behaviour of old-new concrete bonds', ACI Materials Journal, Title no. 97-M52, V.97, No.4, July-August 2000, pp.447-453.

Tuartsinze, A., Farhat, H. and Granju, J.L. (2003), 'Influence of autogenous cracking on the durability of repairs by cement-based overlays reinforced with metal fibres', Materials and Structures 36 (264), 2003, pp. 673-677.

USDT – United States Department of Transportation (2000), 'Tensile bond strength of a high performance concrete bridge deck overlay', Field Test Report, Federal Highway Administration MCL Project 9904, Washington, USA, February 2000.

Van Mier, J.G.M., Nooru-Mohammed, M.B., and Timmers, G. (1991), "Experimental study of shear fracture and aggregate interlock in cement-based composites", Heron, Vol. 36, No. 4, Delft, Netherlands, 1991, pp.8-30.

Van Mier, J. G. M. (1997), 'Fracture processes of concrete', published by CRC Press Inc, USA, 1997.

Vaysburd, A.M., and McDonald, J.E. (1999), 'An Evaluation of Equipment and Procedures for Tensile Bond Testing of Concrete Repairs'. Technical Report REMR-CS-61, US Army Corps of Engineers, Waterways Experiment Station, Vicksburg, Mississippi USA, 75 pp.

Vaysburd, A.M., Emmons, P.H., McDonald, J.E., Poston, R.W. and Kesner, K.E. (2000), 'Selecting durable repair materials: performance criteria – field studies', Concrete International, December 2000, pp.39-45.

Vaysburd, A.M., Emmons, P.H., Mailvaganam, N.P., McDonald, J.E., and Bissonette, B. (2004), 'Concrete Repair Technology – A revised approach is needed', Concrete International, January 2004, pp. 59-65.

Wagner, W., and Erlhof, G. (1991), 'Praktische Baustatik', B.G. Teubner Stuttgart, Germany, 1991.

Walraven, J. (1993), 'Shear Friction in High-strength Concrete', Proceedings ACI Conference on High Strength Concrete, Singapore, 1993, pp.57-65.

Walraven, J. and Shkoukani, H. (1993), 'Kriechen und Relaxation des Betons bei Temperatur-Zwangsbeanspruchung', Beton- und Stahlbetonbau 88 (1993), Heft 1, p. 10-15.

Walraven, J., Frenay, J., and Pruijssers, A. (1987), 'Influence of concrete strength and load history on the shear friction capacity of concrete materials', PCI Journal, Vol.32, No.1, January-February 1987, pp.69-83.

Warner, J., Bhuyan, S., Smoak, W.G., Hindo, K.R., and Sprinkel, M.M. (1998), 'Surface preparation for overlays', Concrete International, May 1998, pp. 43-46.

Weber, M. (1971), 'Mechanischer Verbund zwischen Beton verschiedenen Alters mittels Kunststoffen', Dissertation, Fakultaet fuer Bauingenieur- und Vermessungswesen der Universitaet Karlsruhe, Karlsruhe, 1971.

Wells, J.A., Stark, R.D., and Polyzois, D. (1999), 'Getting better bond in concrete overlays', Concrete International, March 1999, pp.49-52.

Yoon, W.H. (1989), 'Untersuchung der temperatur- und feuchtebedingten Spannungsverhältnisse im Bereich non Instandsetzungen bei massiven Betonbauten', Dissertation, RWTH Aachen, Germany, 1989.

Yuan, Y., and Marsszeky, M. (1994), 'Restrained shrinkage in repaired reinforced concrete elements', Materials and Structures, 1994, 27, pp. 375-382.

Yuan, Y., Li, G., and Cai, Y. (2003), 'Modeling for prediction of restrained shrinkage effect in concrete repair', Cement and Concrete Research, Vol.33, 2003, pp.347-352.

Zhu, Y. (1992), 'Effect of surface moisture condition on bond strength between new and old concrete', Bulletin No. 159, Department of Structural Mechanics and Engineering, Royal Institute of Technology, Stockholm, 1992.

Žnidaric, A., Piau, J.M., and Woodward, R. (2003), 'SAMARIS (Sustainable and Advanced Materials for Road Intrastructure), Inception Report', 2003, 87 pp.

APPENDICES

A1 DESIGN RECOMMENDATIONS FOR CONCRETE REPAIR (DAfStb, 1992)

A number of standards and recommendations for concrete repair were examined, of which the German design code presented by the DAfStb (Deutscher Ausschuss für Stahlbeton, 1992) was found to be the most detailed one. The document is divided into 4 parts. In the following, design recommendations relevant to this research are summarized.

German Committee of Reinforced Concrete (1990-1992): "Guidelines for protection and repair of concrete elements"
Part 2: Construction planning and application (1990)

(…)

1.2 Requirements (in the following, only the requirements for cement-bonded repair systems, with or without addition of polymers, are listed)

(...)

- Surface wetness: substrate "may or must" be wet, without having a glossy film of water on the surface. The pores of the substrate must not be saturated.
- Temperature of substrate and surrounding air: 5 – 30 ^{o}C
- Environmental conditions: humidity (no restriction), rain (no rain), wind (= approximately 5 m/s), sun (direct sunlight must be avoided)
- Surface pull-off strength: average =1.5 N/mm^2, smallest single value =1.0 N/mm^2

(…)

3.2 Loading classes

For every repair project, the consultant engineer has to decide which of the following classes is applicable for the repair:

- M1: Local surface repair, non-structural
- M2: Realkalinisation. Dynamic loading (e.g. traffic) during and after application of material. Durability requirements.
- M3: Like M2, with some additions: Structural repair. Dynamic loading during and after application of material. Additional requirements for strength etc
- M4: Industrial floors, high wear resistance. Dynamic loading during and after application of material

Table A1-1 presents selected requirements for repair materials.

Table A1-2 gives requirements for overlay thickness for big repair areas

Table A1-2: Selected requirements for repair mortars (DAfStb,1992)

Parameter	Class of mortar / concrete					
	M1		M2	M3	M4	
	cementitious	resinious	cementitious	cementitious	cementitious	resinious
2 Strength						
2a Curing condition: 23 °C / 50% RH						
Compressive strength $\beta_{D,age}$ (min)	$\beta_{D,28} \geq 10$ MPa	x	$\beta_{D,28} \geq 10$ MPa	$\beta_{D,28} \geq 30$ MPa 1)	$\beta_{D,28} \geq 30$ Mpa	$\beta_{D,7} \geq 45$ Mpa
Flexural tensile strength $\beta_{BZ,age}$	-	-	-	-	-	$\beta_{BZ,7} \geq 15$ Mpa
2b Curing condition: in water, 20 °C						
Δ Compressive strength $\Delta\beta_{D,age}$ 2)	-	-	-	$\Delta\beta_{D,90} \leq 30\%$	$\Delta\beta_{D,90} \leq 30\%$	-
Δ Flexural tensile strength $\Delta\beta_{BZ,age}$ 2)	-	-	-	$\Delta\beta_{BZ,90} \leq 30\%$	$\Delta\beta_{BZ,90} \leq 30\%$	-
3 Deformation characteristics						
3a Shrinkage $\varepsilon_{s,90}$ (90 days) (max)	-	-	≤ 1.2 ‰	≤ 1.0 ‰	≤ 1.0 ‰	-
3b Shrinkage $\varepsilon_{s,7}$ (7 days) (max)	-	≤ 0.5 ‰	-	-	-	≤ 0.5 ‰
3c Swelling $\varepsilon_{q,90}$ (90 days) (max)	-	-	≤ 0.3 ‰	≤ 0.3 ‰	≤ 0.3 ‰	-
3d Thermal coefficient (max)	-	x	-	1)	1)	≤ 25 x 10^{-6} K^{-1}
3e Elastic modulus, compression (min)	-	-	-	$E_D \geq 30$ Gpa, 1)	-	-
3f Creep	-	-	-	1)	-	-

x The parameter has to be identified, but there are no quantitative requirements

\- No specific requirement

1) Has to be judged by the design engineer 2) maximum difference in strength, compared to dry curing

Detailed description of specimens, equipment, and procedures for testing the above requirements is given in Part 4 of the design code

Table A1-2: Requirements for overlay thicknesses for large repair areas (DAfStb, 1992)

	Concrete or mortar	largest aggregate	overlay thickness	
			minimum	maximum
		mm	mm	mm
1	Concrete according DIN 1045	> 4	30	-
2	Cementitious mortar	<= 4	20	40
3	Polymer modified concrete	> 4	30	-
4	Polymer modified mortar	<= 4	10	40
5	Resinious concrete	> 4	15	40
6	Resinious mortar	<= 4	5	15

Summary of important aspects

- Basically, the design of the repair, according to DAfStb 1990-92, includes the following: Investigation of the deteriorated structure, decision of the design engineer, which repair class is applicable (M1 – M4), substrate preparation following conventional rules, and application of a repair material of the required class.
- Only very basic requirements for shrinkage strains of the repair material are given.
- Control of crack width is tested on restrained shrinkage specimens
- No requirements for thermal coefficients of cementitious repair mortar
- No requirements for creep or relaxation
- No requirements for tensile strength and elastic modulus for non-structural mortars
- Fibre reinforcement is not covered
- Curing procedures are not covered, except a comment in the introduction that the curing procedures of conventional concrete constructions also apply for concrete repair

A2 SHRINKAGE VALUES OF COMMON SOUTH AFRICAN REPAIR MORTARS

South Africa's concrete repair industry experiences problems similar to those reported in the literature (compare Sections 2.3 and 2.4). Patch repairs often show extensive surface cracking, delamination and spalling. Most of these problems can be related to the quality of workmanship and issues like substrate surface preparation, choice and application of materials, and curing procedures. However, during experimental research, failure of common concrete repair materials was encountered even under controlled laboratory conditions with careful workmanship and proper curing. Poor material performance included excessive surface cracking on concrete patch specimens, as well as poor tensile and shear bond strength.

Common South African concrete repair products, obtained from 3 different suppliers, were tested for selected material properties and volume changes. To simulate normal drying conditions, the test specimens were moist-cured for one day after casting and subsequently exposed to laboratory conditions with temperatures and relative humidity ranging between 16 and 23°C and 55 and 75% respectively. Selected material properties are presented in **Table A2-1**.

Table A2-1: Selected material properties of tested repair mortars

Material	Type of repair mortar	Water content[1] [kg/m^3]	Density[2] [kg/m^3]	Porosity[3] [%]
RM 1	Patch repair, cement based	307	2015	20.88
RM 2	Patch repair, polymer modified, silica fume	209	1621	9.63
RM 3	Grout, cementitious, "non-shrink"	246	2215	10.82
RM 4	Expanding grout, cementitious	256	2086	13.81
RM 5	Structural concrete, "non-shrink"	226	1989	13.58
RM 6	Epoxy quartz filled mortar for flooring	236	1925	16.52
RM 7	Grout, non-shrink	255	1852	15.00
RM 8	Patch repair, polymer modified	192	2112	6.48
RM 9	Patch repair, polymer mod., fibres, "non-shrink"	307	2136	14.27
RM 10	Patch repair, cement based	250	1648	12.05

[1] The maximum water content specified by the material supplier was used.
[2] Density was measured at 28 days on cubes 100x100x100 mm. The presented values are the mean of 3 samples per material.
[3] Porosity was measured at 28 days on specimens 100x100x30 mm. The presented values are the mean of 2 samples per material

While strength test results generally conformed to the material suppliers specification, often little or no data was available on material properties such as drying shrinkage, thermal coefficients or creep. Probably one of the main shortcomings of the repair material industry is the underestimation of time dependent volume changes and the primary focus on material strength.

Shrinkage was measured on prisms 100x100x200 mm, using a BAM Strain-measuring extensometer (compare Figure 4.7) with measuring length 100 mm. Per material, 2 specimens with 2 measurement locations each were tested. Test results were therefore obtained as the mean of 4 measurements. Short-term shrinkage strains are presented in **Figure A2-1**.

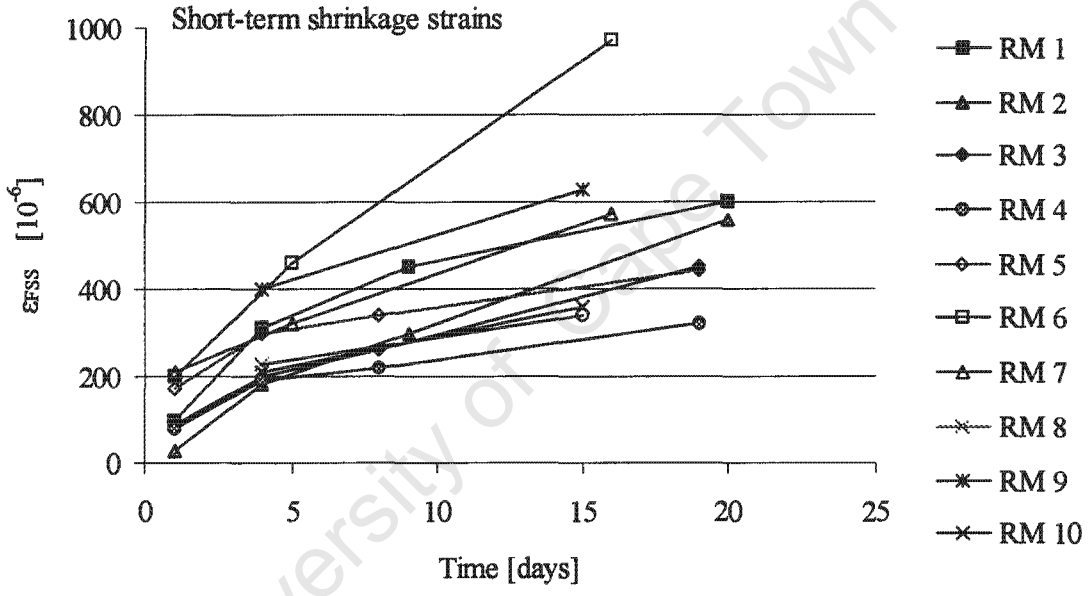

Figure A2-1: Short-term shrinkage of South African repair materials

The notably high early strain values explain the early age cracking that is often experienced in concrete repairs during the first few weeks of service life. Long-term results indicate that ε_{FSS} continue to increase considerably for more than 3 months, with approximately 40% to 60% of the total strain occurring in the first 4 weeks (**Figure A2-2**).

Type and composition of the repair mortars did not have a significant influence on ε_{FSS} values, which corresponds to observations made by Emberson (1990), Emmons et al (1993), and Chen et al (1995). In general, free shrinkage values of South African repair materials are very similar to those reported by Emmons and Vaysburd (1995), who found that a minority of repair materials tested could be labelled as low shrinkage, despite the fact that manufacturers classify them as expansive, non-shrinking or shrinkage compensating.

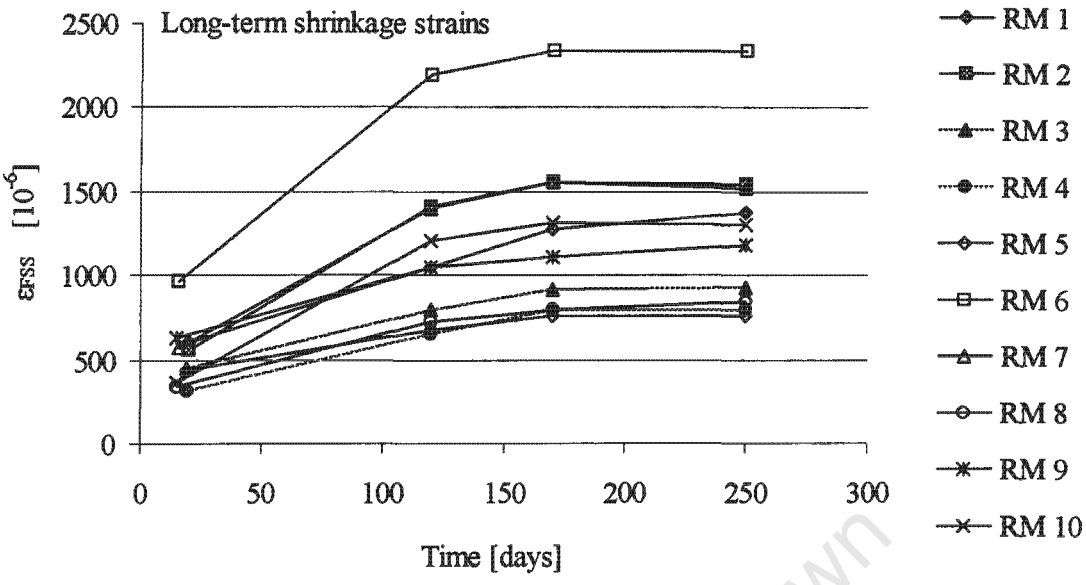

Figure A2-2: Long-term drying shrinkage of South African repair materials

A3 EXPERIMENTAL RESULTS: MATERIAL PARAMETERS, SPECIMENS USED FOR STRAIN MEASUREMENTS

A3.1 Compressive strength

Table A3.1-1: 28-day compressive strength test results

Specimen	Density [kg/m^3]	f_c [MPa] single	mean
Substrate	2315	48.0	48.4
	2360	49.6	
	2351	47.5	
Overlay 1	2370	53.9	54.1
	2360	53.5	
	2410	54.8	
Overlay 2	2153	49.7	50.9
	2155	52.0	
	2168	51.1	
Overlay 3	2350	53.6	53.3
	2383	54.2	
	2368	52.0	

A3.2 Tensile strength

Table A3.2-1: Tensile strength Overlay 1

Age [days]	no.	f_t (MPa) single	mean
7	1	2.7	2.8
	2	2.8	
	3	3.0	
14	1	3.0	3.2
	2	3.5	
	3	3.2	
28	1	3.6	3.4
	2	3.1	
	3	3.5	

Table A3.2-2: Tensile strength Overlay 2

Age [days]	no.	f_t (MPa) single	mean
7	1	2.0	1.9
	2	1.7	
	3	1.9	
14	1	1.6	1.8
	2	1.9	
	3	2.0	
28	1	2.2	2.1
	2	2.2	
	3	2.0	

Table A3.2-3: Tensile strength Overlay 3

Age [days]	no.	f_t (MPa) single	mean
7	1	2.6	2.8
	2	3.0	
	3	2.9	
14	1	2.7	2.9
	2	2.6	
		3.1	
28	1	3.0	3.0
	2	2.8	
		3.2	

A3.3 Elastic modulus

Table A3.3-1: Elastic modulus Substrate

Age [days]	no.	E-modulus (GPa) single	mean
7	1	26.5	25.3
	2	24.4	
	3		
14	1	25.1	27.7
	2	26.8	
	3		
28	1	28.3	28.1
	2	28.0	
	3		

Table A3.3-2: Elastic modulus Overlay 1

Age [days]	no.	E-modulus (GPa) single	mean
7	1	21.2	21.9
	2	22.2	
	3	22.4	
14	1	23.9	23.6
	2	22.9	
	3	24.0	
28	1	25.3	25.1
	2	25.3	
	3	24.7	

Table A3.3-3: Elastic modulus Overlay 2

Age [days]	no.	E-modulus (GPa) single	mean
7	1	20.1	19.5
	2	19.2	
	3	19.2	
14	1	20.4	21.0
	2	20.5	
28	1	22.2	22.0
	2	22.0	

Table A3.3-4: Elastic modulus Overlay 3

Age [days]	no.	E-modulus (GPa) single	mean
7	1	29.8	30.2
	2	30.5	
	3	30.1	
14	1	30.9	31.1
	2	31.4	
	3	31.0	
28	1	30.1	29.6
	2	30.0	
	3	28.8	

A4 TEST RESULTS: STRAIN MEASUREMENTS ON COMPOSITE MEMBERS

Due to the large number of test values, detailed results of all strain measurements of Specimens A, B, C, and D are provided in electronic format on CD (see attachment "CD 1").

On the CD, experimental data of Specimens A1-5, B1 and B2, C1-3, and D1-3 are presented in separate folders. These folders contain contain the following:

- Time-dependent strain data (obtained from the "raw" measurements) at all locations along the specimens
- Mean strain values, calculated for locations where more than one specimen was available for a certain measurement location (highlighted in bold font)
- Free shrinkage strain values for all overlays used
- A summary of strains on top of the member of Specimens A
- A summary of interface strains of Specimens A
- A summary of member end strain values for Specimens A
- A summary of strain values at cracked locations for Specimens A and B (highlighted in green)
- Statistical evaluation of test data (highlighted in blue)
- A reference to Figures illustrating the specimen under consideration in the thesis document. This is intended to facilitate the identification of strain locations used for the processing of the data.

A5 STRAINS AND STRESSES IN SPECIMENS A1, A2, AND B1, USING THE PREDICTION MODEL

Material parameter of Specimens A1, A2, and B1 were used for the computation of strains and stresses. Computation was done using the prediction model presented electronically in Appendix 8 (see attachment "CD 2"). Input parameters not measured were estimated. Input parameter and computed strain and stress values are presented in **Tables A5-1 to A5-6**.

Table A5-1: Input parameter Specimens A1 (Overlay 1 (LS)

Overlay parameters			
t_i (day)	ε_{FSS}	ψ_O	E_O
6	80	0.55	21.9
21	130	0.55	23.0
33	150	0.55	25.1
62	270	0.55	26.0
98	360	0.55	26.5
202	463	0.55	27.0
Overlay depth d_O (mm)			40
Substrate parameters			
Elastic modulus E_S (GPa)			32
Substrate depth d_S (mm)			200
Parameters for substrate creep strain			
Age of concrete at first loading (days)			240
Variation in RH (%)			20
Slump (mm)			90
Coarse aggregate (kg/m^3)			985
Fine aggregate (kg/m^3)			750
Constant $C\varepsilon$		1	
Include curvature in calculation? (yes: 1, no: 0)			1

	Interface strains (10^{-6})								Interface stress (MPa)	
	A	B	C	D	E	F	G	H	I	J
t_i	excl. substrate creep		including substrate creep and ψ_O			curvature κ	Σ	ratio	substrate	overlay
(day)	$\varepsilon_{elastic}$	$\varepsilon_{incl.\ \psi O}$	$\varepsilon_{inst.,I}$	$\varepsilon_{creep,S,I}$	$\varepsilon_{total,I}$	ε_κ	$\varepsilon_{total,I,incl.\kappa}$	ε_{total} / ε_{FSS}	$\sigma_{S,I}$ (-)	$\sigma_{O,I}$ (+)
6	33	18	18		18	1	19	0.24	0.57	0.55
21	54	30	24	13	38	2	40	0.31	0.78	0.73
33	66	36	28	19	47	3	50	0.33	0.89	0.82
62	121	67	48	41	89	6	95	0.35	1.54	1.39
98	163	90	62	60	123	8	131	0.36	1.99	1.78
202	212	117	77	87	164	11	174	0.38	2.45	2.17
	eq. 6.17	eq. 6.46	eq. 6.43, incl. ψ_O	eq. 6.42, incl. ψ_O	eq. 6.50 (= C+D)	eq. 6.51	eq. 6.52 (= E+F)		= C . E_S	eq. 6.54

Computation of substrate creep coefficients (ACI 1992) (compare Section 2.5.1)										
day:	6	21	33	62	98	202				
$\theta(t, t_0)$	0	0.68	0.85	1.07	1.21	1.42				

Creep parameter	
$\gamma 1$	0.65
$\gamma 2$	1.14
$\gamma 3$	1.11
$\gamma 4$	1.06
$\gamma 5$	0.98
$\gamma 6$	1.00
$\Phi(t,\tau)$	2.02

Parameter for computation of curvature strain (equation 6.51)		
$d_{S,\varepsilon}$ (mm)	80	(equation 6.21)
e (mm)	47	(equation 6.20)
$d_{z,I}$	80	(per mm width)
z (mm)	100	
I_C (mm^4)	1152000	

Table A5-2: Computation of strains and stresses: Specimens A1 (Overlay 1 (LS))

Table A5 -3: Input parameter Specimens A2 (Overlay 2 (HS)

Overlay parameters			
t_i (day)	ε_{FSS}	ψ_O	E_O
1	86	0.55	17.0
2	173	0.55	18.0
4	200	0.55	19.0
7	262	0.55	19.5
9	316	0.55	20.0
15	374	0.55	20.4
18	448	0.55	21.0
23	466	0.55	21.5
31	574	0.55	22.1
Overlay depth d_O (mm)			40

Substrate parameters	
Elastic modulus E_S (GPa)	32
Substrate depth d_S (mm)	200
Parameters for substrate creep strain	
Age of concrete at first loading (days)	240
Variation in RH (%)	20
Slump (mm)	90
Coarse aggregate (kg/m^3)	985
Fine aggregate (kg/m^3)	750

Constant Cε	1

Include curvature in calculation? (yes: 1, no: 0)	1

	Interface strains (10^{-6})								Interface stress (MPa)	
	A	B	C	D	E	F	G	H	I	J
t_i	excl. substrate creep		including substrate creep and ψ_O			curvature κ	Σ	ratio	substrate	overlay
(day)	$\varepsilon_{elastic}$	$\varepsilon_{incl.\ \psi O}$	$\varepsilon_{inst.,I}$	$\varepsilon_{creep,S,I}$	$\varepsilon_{total,I}$	ε_κ	$\varepsilon_{total,I,incl.\kappa}$	ε_{total} / ε_{FSS}	$\sigma_{S,I}$ (-)	$\sigma_{O,I}$ (+)
2	62	34	33	5	37	2	39	0.23	1.04	1.01
4	75	41	37	10	47	3	50	0.25	1.19	1.15
7	99	55	48	18	65	4	69	0.26	1.53	1.46
9	122	67	58	24	82	5	86	0.27	1.84	1.75
15	146	80	66	35	102	6	107	0.29	2.13	2.01
18	178	98	80	45	125	7	132	0.30	2.55	2.40
23	187	103	82	52	134	8	142	0.30	2.63	2.46
31	234	129	100	70	171	10	181	0.31	3.21	2.98
	eq. 6.17	eq. 6.46	eq. 6.43, incl. ψ_O	eq. 6.42, incl. ψ_O	eq. 6.50 (= C+D)	eq. 6.51	eq. 6.52 (= E+F)		= C . E_S	eq. 6.54

Computation of substrate creep coefficients (ACI 1992) (compare Section 2.5.1)										
day:	1	2	4	7	9	15	18	23	31	
$\theta(t, t_0)$	0	0.18	0.33	0.46	0.52	0.66	0.71	0.79	0.88	

Creep parameter	
$\gamma 1$	0.65
$\gamma 2$	1.14
$\gamma 3$	1.11
$\gamma 4$	1.06
$\gamma 5$	0.98
$\gamma 6$	1.00
$\Phi(t,\tau)$	2.02

Parameter for computation of curvature strain (equation 6.51)		
$d_{S,\varepsilon}$ (mm)	80	(equation 6.21)
e (mm)	47	(equation 6.20)
$d_{z,I}$	80	(per mm width)
z (mm)	100	
I_C (mm^4)	1152000	

Table A5-4: Computation of strains and stresses: Specimens A2 (Overlay 2 (HS))

Table A5-5: Input parameter Specimens B1 (Overlay 3 (LS)

Overlay parameters			
t_i (day)	ε_{FSS}	ψ_O	E_O
0	0	0.55	31.0
6	160	0.55	31.0
13	173	0.55	31.0
20	235	0.55	31.0
34	313	0.55	31.0
50	333	0.55	31.0
81	388	0.55	31.0
102	428	0.55	31.0
130	480	0.55	31.0
310	598	0.55	31.0
Overlay depth d_O (mm)			40

Substrate parameters	
Elastic modulus E_S (GPa)	32
Substrate depth d_S (mm)	200
Parameters for substrate creep strain	
Age of concrete at first loading (days)	720
Variation in RH (%)	20
Slump (mm)	90
Coarse aggregate (kg/m^3)	985
Fine aggregate (kg/m^3)	750

Constant Cε	1

Include curvature in calculation? (yes: 1, no: 0)	1

	Interface strains (10^{-6})								Interface stress (MPa)	
	A	B	C	D	E	F	G	H	I	J
t_i	excl. substrate creep		including substrate creep and ψ_O			curvature κ	Σ	ratio	substrate	overlay
(day)	$\varepsilon_{elastic}$	$\varepsilon_{incl.\ \psi O}$	$\varepsilon_{inst.,I}$	$\varepsilon_{creep,S,I}$	$\varepsilon_{total,I}$	ε_κ	$\varepsilon_{total,I,incl.\kappa}$	ε_{total} / ε_{FSS}	$\sigma_{S,I}$ (-)	$\sigma_{O,I}$ (+)
6	79	43	37	12	49	3	53	0.33	1.20	1.09
13	85	47	38	17	55	4	59	0.34	1.22	1.10
20	116	64	50	27	77	5	83	0.35	1.61	1.45
34	154	85	64	41	106	7	113	0.36	2.06	1.83
50	164	90	66	48	114	8	122	0.37	2.12	1.88
81	191	105	75	62	136	9	146	0.38	2.39	2.09
130	236	130	89	82	172	12	184	0.38	2.86	2.49
310	294	162	106	114	219	15	235	0.39	3.38	2.92
	eq. 6.17	eq. 6.46	eq. 6.43, incl. ψ_O	eq. 6.42, incl. ψ_O	eq. 6.50 (= C+D)	eq. 6.51	eq. 6.52 (= E+F)		= C . E_S	eq. 6.54

Computation of substrate creep coefficients (ACI 1992) (compare Section 2.5.1)										
day:	0	6	13	20	34	50	81	130	310	
$\varphi(t, t_0)$	0	0.40	0.56	0.67	0.80	0.91	1.03	1.15	1.34	

Creep parameter	
$\gamma 1$	0.58
$\gamma 2$	1.14
$\gamma 3$	1.11
$\gamma 4$	1.06
$\gamma 5$	0.98
$\gamma 6$	1.00
$\varphi_U(t,\tau)$	1.77

Parameter for computation of curvature strain (equation 6.51)		
dS,ε (mm)	80	(equation 6.21)
e (mm)	47	(equation 6.20)
$d_{z,I}$	80	(per mm width)
z (mm)	100	
I_C (mm^4)	1152000	

Table A5-6: Computation of strains and stresses: Specimens B1 (Overlay 3 (MS))

A6 SHEAR TEST EQUIPMENT

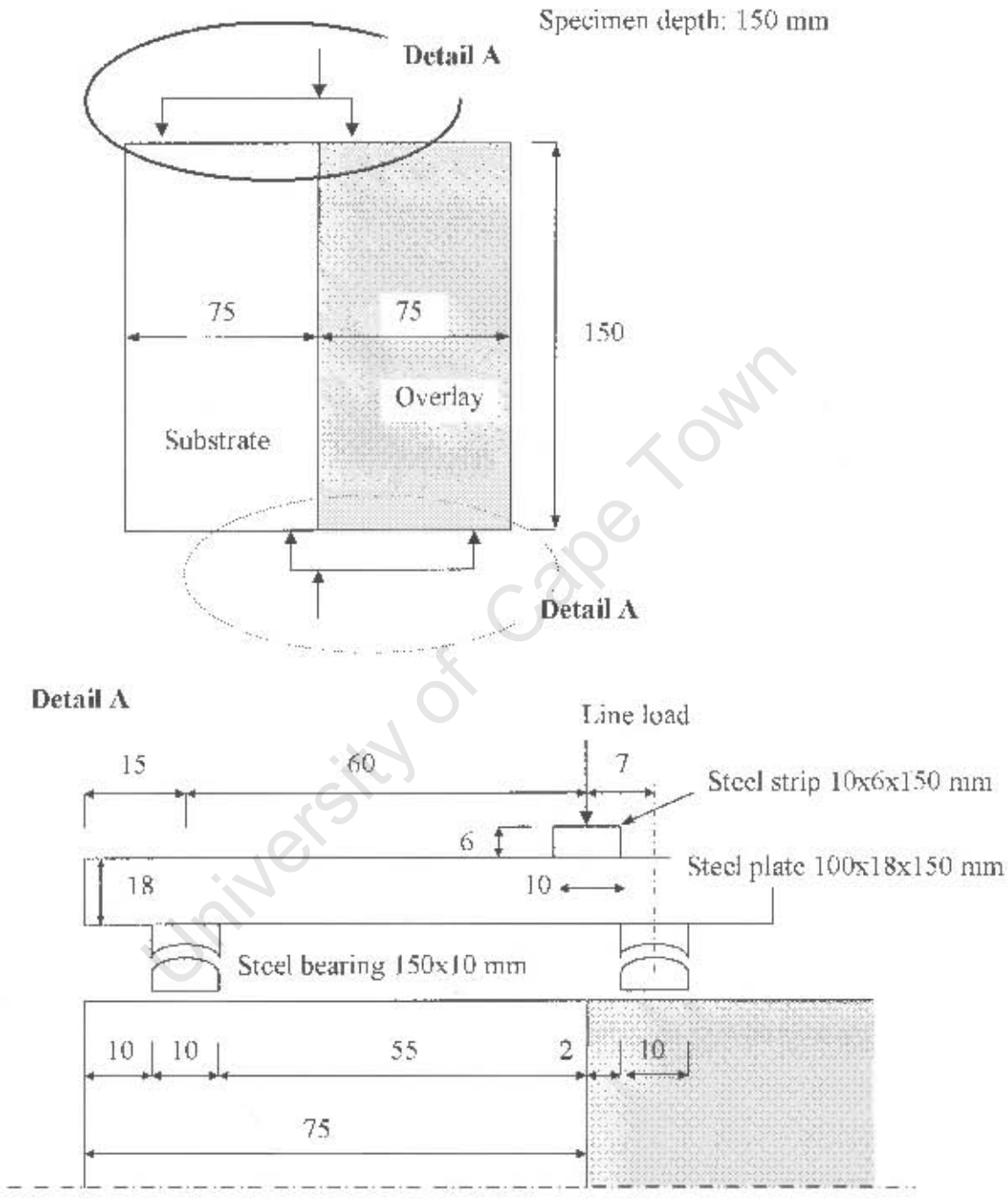

Figure A6-1: Schematic of test equipment Interface shear test method A

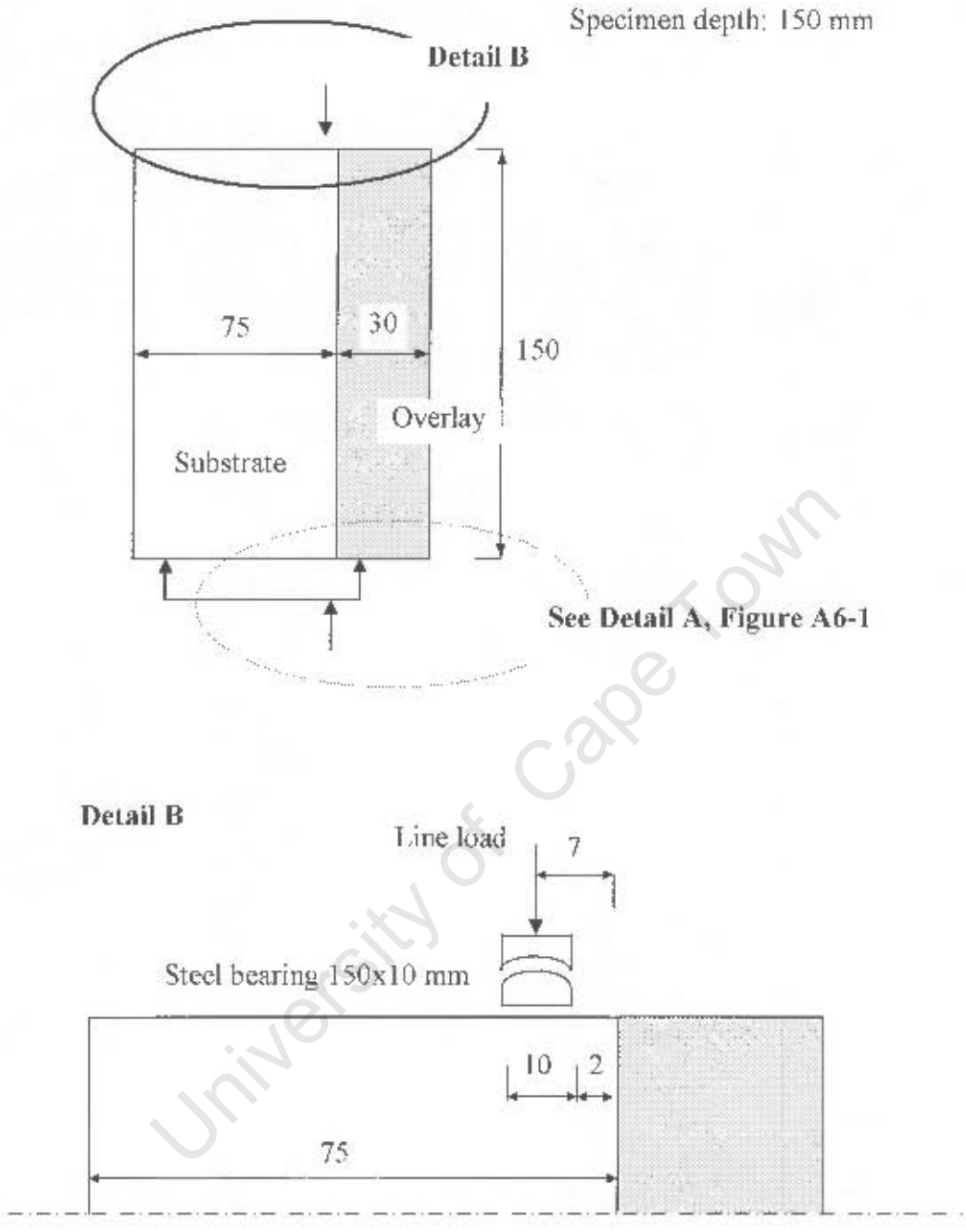

Figure A6-2: Schematic of test equipment – Interface shear test method B

A7 SHEAR TEST RESULTS

Table A7-1: Specimens S1

Age at test (days):	1	2	3	7	14
Test values [kN]	*19*	35	58	80	*76*
	22	38	69	88	88
	22	45	72	93	90
	23	52		97	95
	39	58			*108*
Statistical analysis					
1.5 IQR low	20.5	17		67.5	77.5
1st Quartile	22	38		84	88
Median	22	45		90.5	90
3rd Quartile	23	52		95	95
1.5 IQR high	24.5	73		111.5	105.5
IQR	1	14		11	7
Outlier (yes/no)	y	n	n	n	y
Strength values					
Shear (mean) [MPa]	0.79	1.60	2.33	3.15	3.20
f_c [MPa]	10.6	20.2	25.7	37	42.7
Ratio: shear / f_c (%)	7.4	7.9	9.1	8.5	7.5

Table A7-2: Specimens S2

Age at test (days):	1	2	3	7	14
Test values [kN]	10	23	32	43	42
	11	25	33	49	48
	12	28	40	57	67
		29	41	65	77
		39	44	70	82
				80	
Statistical analysis					
1.5 IQR low		19	21	17.5	4.5
1st Quartile		25	33	49	48
Median		28	40	61	72
3rd Quartile		29	41	70	77
1.5 IQR high		35	53	101.5	120.5
IQR		4	8	21	29
Outlier (yes/no)	n	y	n	n	n
Strength values					
Shear (mean) [MPa]	0.39	0.92	1.34	2.13	2.22
f_c [MPa]	4.1	9.9	13.8	22.9	28.7
Ratio: shear / f_c (%)	9.4	9.3	9.7	9.3	7.7

Table A7-3: Specimens S3

Age at test (days):	3	7	14	28
Test values [kN]	17	42	52	48
	22	44	53	54
	23	47	58	56
	29	51	61	64
				65
Stanstical analysis				
1.5 IQR low	9.75	34	42	39
1st Quartile	19.5	43	52.5	54
Median	22.5	45.5	55.5	55
3rd Quartile	26	49	59.5	64
1.5 IQR high	35.75	58	70	79
IQR	6.5	6	7	10
Outlier (yes/no)	n	n	n	n
Strength values				
Shear (mean) [MPa]	0.80	1.62	1.97	2.02
f_c [MPa]	7.9	14.4	17.1	20.8
Ratio: shear / f_c (%)	10.1	11.2	11.5	9.7

Table A7-4: Specimens S4

Age at test (days):	3	7	14	28
Test values [kN]	12	25	26	35
	14	27	28	37
	16	30	31	39
	18	32	38	40
				44
Statistical analysis				
1.5 IQR low	7	18.5	15.75	32.5
1st Quartile	13	26	27	37
Median	15	28.5	29.5	38
3rd Quartile	17	31	34.5	40
1.5 IQR high	23	38.5	45.75	44.5
IQR	4	5	7.5	3
Outlier (yes/no)	n	n	n	n
Strength values				
Shear (mean) [MPa]	0.53	1.00	1.08	1.37
f_c [MPa]	4.5	8.3	9.7	12.2
Ratio: shear / f_c (%)	11.7	12.1	11.1	11.2

Table A7-5: Specimens S5-8

Specimen	S5		S6		S7		S8	
Age at test (months):	1	32	1	32	1	32	1	32
Test values [kN]	35	46	46	23	18	5	68	77
	42	47	53	27	25	14	71	79
	42	56	56	36	27	21	81	90
	53	70	59	38	33	24	81	94
	57	78	66	39	35	25	95	95
	57	87		44				110
				45				
Statistical analysis								
1.5 IQR low	22.5	0.5	44	1.5	13	-1	56	55
1st Quartile	42	47	53	27	25	14	71	79
Median	48.5	63	56	38	27	21	81	92
3rd Quartile	55	78	59	44	33	24	81	95
1.5 IQR high	74.5	124.5	68	69.5	45	39	96	119
IQR	13	31	6	17	8	10	10	16
Outlier (yes/no)	n	n	n	n	n	n	n	n
Strength values								
Shear (mean) [MPa]	1.90	2.55	2.23	1.43	1.10	0.71	3.15	3.62

Table A7-6: Specimens S9-14

Specimen	S9	S10	S11	S12	S13	S14
Site	1	2	3	1	2	3
Age at test (months):	30	30	30	30	30	30
Overlay	1	1	1	2	2	2
Test values [kN]	68	49	80	36	35	42
	75	62	110	49	44	50
	88	93	113	65	49	56
	88	98	115	66	64	63
	93	98	118	69	78	
	97	102		71	94	
	100	106		80		
	105	108				
	110	110				
	113					
Statistical analysis						
1.5 IQR low	62.5	33.25	102.5	16	-7	40.75
1st Quartile	88	77.5	110	49	44	46
Median	95	98	113	66	56.5	53
3rd Quartile	105	107	115	71	78	49.5
1.5 IQR high	130.5	151.25	122.5	104	129	54.75
IQR	17	29.5	5	22	34	3.5
Outlier (yes/no)	n	n	y	n	n	n
Strength values						
Shear (mean) [MPa]	3.73	3.65	4.54	2.48	2.41	2.10

Table A7-7: Specimens S15-18

Specimen	S15	S16	S17	S18
Age at test (months):	30	30	30	30
Test values [kN]	*31*	53	*15*	*67*
	60	57	19	95
	66	58	27	96
	71	60	39	102
	72	75		*115*
	72	85		
	95			
Statistical analysis				
1.5 IQR low	42	30	-7	84.5
1st Quartile	60	57	17	95
Median	71	59	23	96
3rd Quartile	72	75	33	102
1.5 IQR high	90	102	57	112.5
IQR	12	18	16	7
Outlier (yes/no)	y	n	n	y
Strength values				
Shear (mean) [MPa]	2.71	2.44	0.94	3.89